INTERACTIONS OF DOLOMITIC LIME WITH IRON SILICATE MELTS.

BY

PAUL WILLIAMS

A THESIS SUBMITTED TO THE COUNCIL FOR NATIONAL ACADEMIC AWARDS IN PARTIAL FULFILMENT FOR THE DEGREE OF

DOCTOR OF PHILOSOPHY
IN INDUSTRIAL METALLURGY

COLLABORATING ESTABLISHMENT:-

Steetley Minerals Ltd.,
P.O. Box 2,
Carlton Road,
WORKSOP,
S81 7QG,
Nottinghamshire.

SPONSORING ESTABLISHMENT:-

Department of Metallurgy,
Sheffield City Polytechnic,
Pond Street,
SHEFFIELD,
August,1980.

PREFACE

The work reported in this thesis was carried out during the period for which the candidate was registered for a higher degree.

In accordance with the regulations for PhD in Industrial Metallurgy, a full course in Metallurgical Process Management was successfully completed. The details of the courses are given below.

MODULE 1.

Process Metallurgy
Mechanical Metallurgy
Advanced Thermodynamics

MODULE 2.

Accountancy
Economics and Financial control
Computational methods and Operation Research

MODULE 3.

Arc Furnace Steelmaking
Oxygen Steelmaking
High Strength Steels
Refractories
Metals and Competitive Materials
Quality Assurance

MODULE 4.

3 Industrial Case Studies

One of the case studies is attached at the rear of the thesis on page 359 and is related to the current research investigation.

The Candidate's performance during the formal coursework was assessed by means of written examinations and continuous assessment of specific assignments.

The work described in the thesis is, to the best of my knowledge, original except where reference is made to others, and no part of it has been submitted for an award at any College or University.

Paul Williams.

Acknowledgements

The author would like to express his gratitude to Dr G. Briggs and Dr M. Sunderland for their guidance and advice during the supervision of this work.

My thanks are also given to Dr J. Quin and Dr J. Green of Steetley Minerals for their helpful advice and criticism. The use of the SEM facilities at Steetley Refractories, under the guidance of Mr C. Nutt, is gratefully acknowledged.

I am grateful to Mr D. Latimer and Mr G. Gregory for their co-operation, technical assistance and expertise in the construction of various pieces of experimental apparatus, and to members of the Metallurgy Department Workshop, in particular Mr P. Fletcher.

I would also like to express my gratitude to all my fellow post graduates, noteably Steve Horne, Jess Cawley and Godwin Ekebuisi for their interest, help and enthusiasm.

Special thanks to my wife Julie, for her considerable patience and skill in the typing of this thesis.

Acknowledgement is made to the Science Research Council for providing the financial support during the three year period spent at Sheffield City Polytechnic.

Interactions of dolomitic lime with iron silicate melts.

by

Paul Williams

Abstract.

An investigation has been made of the dissolution of dolomitic lime in iron silicate (fayalite) melts at temperatures corresponding to those obtained during the early stages of an LD blow (1300°C). The melts were contained in iron crucibles and held in a furnace under an argon atmosphere. Cylinders of dolomitic lime, prepared from dolomitic limestone, were preheated to the temperature of the melt and immersed for times ranging from 15 to 540 seconds. The reacted cylinders were withdrawn, and quenched under an argon jet for microscopic examination and scanning electron microscope analysis. Equivalent experiments were undertaken with calcitic lime cylinders prepared from limestone. A rotating bob-fixed crucible viscometer technique has been established, and viscosities of synthetic slags within the system CaO - 'FeO' - SiO_2 - MgO, were measured. Cone fusion studies were used to determine the melting behaviour of the slag system.

Dolomitic lime and iron silicate (fayalite) melt reacted to form magnesiowüstite and dicalcium silicate, and a globular wüstite and forsterite - fayalite olivine series was established at the melt - cylinder interface region. The dissolution of dolomitic lime was controlled by the transport of magnesia into the melt, by diffusion, from the forsterite - fayalite zone. Corresponding iron silicate - calcitic lime reactions produced a liquid calciowüstite phase contained within a continuous envelope of dicalcium silicate, surrounding the lime sample, which assumed a granular morphology when a 5 mass % MgO addition was made to the melt. Magnesia levels up to 7.5 mass % MgO raised the viscosity of fayalite by 250 mPa.s at 1300°C. Magnesia increased the liquidus temperature and melting range of synthetic CaO - 'FeO' - SiO_2 melts at all levels of addition. A modified film theory approach has been used to calculate the experimental mass transfer coefficients for CaO and MgO.

The relative rates of calcitic and dolomitic lime solution have been assessed and the results evaluated in relation to the industrial situation. It has been shown that dolomitic lime does not represent a replacement for calcitic lime. However, it is essential for reducing refractory wear rates and enhancing the formation of a basic early formed slag, when used in conjunction with calcitic lime, provided it is added at the commencement of the blow.

Table of Contents.

		Page
Preface		1
Acknowledgements		2
Abstract		3
Table of Contents		4
Glossary of terms		11
1. Introduction		14
2. Literature Survey		17
2.1	Introduction to oxygen steelmaking	17
2.1.1	Alternative oxygen steelmaking processes	18
2.1.2	Rotating vessels	18
2.1.3	Oxygen-Lime Powder (OLP-LD AC) and bottom blown processes (OBM, Q-BOP, VLN)	20
2.2	Refining reactions within the LD	21
2.2.1	Silicon	23
2.2.2	Manganese	23
2.2.3	Phosphorus	24
2.2.4	Sulphur	26
2.2.5	Carbon	28
2.3	Decarburisation mechanisms within the LD	30
2.4	Reaction kinetics	34
2.5	Physical aspects of steelmaking slags	36
2.5.1	The structure of liquid slags	37
2.5.2	The viscosity of LD-type slags	38
2.5.3	The density and surface tension of LD-type melts	40
2.6	Constitutional and Structural slag models	42
2.7	LD steelmaking slags	47

		Page
2.7.1	The lime charge	47
2.7.2	The CaO-Iron Oxide-SiO_2 system	48
2.7.3	The system CaO-'FeO'-SiO_2 in contact with metallic iron	49
2.7.4	The dissolution kinetics of lime	
2.7.5	Flux practices	50
2.8	LD refractory linings	56
2.9	Dolomitic lime and LD steelmaking slags	60
2.9.1	The system CaO-MgO-'FeO'-SiO_2	62
2.9.2	Dolomitic lime quality	62
2.9.2.1	Factors that lead to increased lining life	63
2.9.2.2	Factors that affect the refining character of LD slags	68
2.9.2.3	Factors that lead to savings in lime fluxes	70
2.10	Conclusion	70
3.	Experimental Work.	72
3.1	Starting Materials	72
3.1.1	Dolomitic limestone	72
3.1.2	Limestone	73
3.1.3	Sample collection	73
3.1.4	Sample preparation	73
3.2	Synthetic slag preparation	75
3.3	Experimental equipment	76
3.3.1	The furnace used in viscosity and rotary dissolution experiments	77
3.3.2	The furnace used in the static immersion experiments	78
3.3.3	The cone fusion furnace	78
3.3.4	The viscometer	79
3.3.4.1	Outline of viscometer theory	79
3.3.4.2	Units of viscosity	81
3.3.4.3	The commercial Viscometer	82
3.3.5	Crucibles	84

		Page
3.3.5.1	Crucibles used in immersion tests	84
3.3.5.2	Crucibles used in viscosity determinations	84
3.4	Experimental Procedures	85
3.4.1	Temperature Profiles	85
3.4.2	Viscometer component materials	86
3.4.3	Choice of crucible dimensions	87
3.4.4	The viscometer shaft and air bearing	88
3.4.5	Crucible support stand	90
3.4.6	'Melt' temperature measurement	91
3.4.7	Compressed air supply	91
3.5	Determination of the Calibration constant (K)	92
3.5.1	Re-determination of the calibration constant	94
3.5.2	Determination of the zirconia crucible constant	95
3.6	Viscosity measurement procedure	96
3.6.1	Introduction of the viscometer shaft	96
3.6.2	Furnace heating sequence	96
3.6.3	Alignment of the viscometer measuring bob	97
3.6.4	Alignment problems	99
3.7	Immersion experiments	99
3.7.1	Calcination of dolomitic limestone and limestone cylinders	100
3.7.2	Cylinder properties	100
3.7.3	Density and porosity determinations	101
3.7.4	Differential thermal analysis	102
3.7.5	Immersion tests	103
3.7.6	Quenching of reacted cylinders	106
3.7.7	Pill tests	106
3.7.8	Cylinder examination procedure	107
3.7.9	Polished section preparation	108
3.8	Scanning Electron Microscope Studies	108
3.8.1	Qualitative studies	108
3.8.2	Quantitative studies	109

		Page
3.9	The melting behaviour of synthetic slags	111
3.9.1	Cone preparation	112
4.	Experimental Results and their interpretation.	115
4.1	The viscosity of some synthetic slags in the system CaO-'FeO'-SiO_2-MgO	116
4.1.1	The viscosity of an iron silicate melt	116
4.1.2	Viscosity relationships of lime-iron silicate melts	118
4.1.2.1	The addition of 10 mass % CaO	118
4.1.2.2	The addition of 32 mass % CaO	118
4.1.3	Viscosity relationships of magnesia-iron silicate melts	120
4.1.3.1	The addition of 2 mass % MgO	120
4.1.3.2	The addition of 5 mass % MgO	121
4.1.3.3	The addition of 7.5 mass % MgO	122
4.1.4	The viscosity of a lime-magnesia-iron silicate melt	123
4.1.5	The effect of crucible component materials	124
4.1.5.1	Iron components	124
4.1.5.2	Zirconia components	127
4.1.5.3	The influence of zirconia on viscosity values and melting temperatures	129
4.1.6	Liquidus temperature determination extrapolated from temperature - viscosity curves	131
4.2	Cylinder properties and reaction parameters	133
4.2.1	Differential thermal analysis (D.T.A.) measurement	133
4.2.2	Porosity relationships	134
4.2.3	Reheat effects on cylinder properties	137
4.2.4	The hydration of calcined cylinders	138

		Page
4.3	Immersion experiments	141
4.3.1	Static isothermal immersion studies on dolomitic lime	141
4.3.1.1	Rotational isothermal immersion studies on dolomitic lime	149
4.3.1.2	The addition of 5 mass % MgO to the synthetic slag bulk	150
4.3.1.3	The pill test	151
4.3.1.4	The iron silicate - "Dolomet" reaction	152
4.3.2	Static isothermal immersion studies on lime	152
4.3.2.1	"Hard" burnt lime	153
4.3.2.2	"Soft" burnt lime	155
4.3.2.3	The addition of 5 mass % MgO to the synthetic slag bulk	157
4.3.3	Quantitative SEM studies	159
4.3.3.1	Dolomitic lime	159
4.3.3.2	Lime	163
4.3.4	Dissolution experiments	165
4.3.4.1	Dolomitic lime cylinders	165
4.3.4.2	Lime cylinders	166
4.4	Cone fusion studies	167
4.4.1	The effect of magnesia on the melting range of iron silicate melts	169
4.4.2	The effect of magnesia on the melting range of a 10 mass % CaO - iron silicate melt	169
4.4.3	The effect of magnesia on the melting range of a 15 mass % CaO - iron silicate melt	170
4.4.4	The effect of magnesia on the melting range of a 20 mass % CaO - iron silicate melt	170
4.4.5	The effect of magnesia on the melting range of a 30 mass % CaO - iron silicate melt	170

		Page
4.4.6	The effect of magnesia on the melting range of a 35 mass % CaO - iron silicate melt	171
4.4.7	Polished section examination of melts used in cone fusion studies	171
5.	Discussion.	173
5.1	Assessment of Experimental techniques	173
5.1.1	Viscosity studies	173
5.1.1.1	The thermal expansion of components	174
5.1.1.2	The geometrical arrangement of the crucible and measuring bob	175
5.1.1.3	Errors due to the temperature measurement	175
5.1.1.4	Composition changes within the melt	176
5.1.1.5	Factors affecting the calibration constant	176
5.1.2	Cone fusion studies	178
5.1.3	Cylinder immersion studies	180
5.1.3.1	Duration of immersion	180
5.1.3.2	Cylinder submergence	181
5.1.3.3	Quantitative results	181
5.2	Kinetics and phase relationships	184
5.2.1	The dissolution of dolomitic lime in iron silicate melts	184
5.2.2	The estimation of experimental mass transfer coefficients	189
5.2.3	The effect of magnesia on lime dissolution	200
5.2.4	The rate controlling mechanism	203
5.3	Relevance to the LD or basic oxygen steelmaking process	204
6.	Conclusions.	208
7.	Suggestions for further work.	212
Appendix 1		215
Appendix 2		216
Appendix 3		218

		Pages
References		219 - 230
Tables	1 to 42	231 - 262
Figures	1 to 65	263 - 306
Plates	1 to 89	307 - 358
8. The Case Study in Industrial Metallurgy.		359 - 410

Glossary of terms.

[ ]	species in metal phase
( )	species in slag phase
P_{O_2}	oxygen partial pressure
a	activity
γ	Raoultian activity coefficient
ΔG^M	free energy of mixing
x	mole fraction of species
$K^\dagger$	equilibrium quotient
k	equilibrium constant for Toop and Samis slag model
k_{11}	equilibrium ratio for silicate polymer reaction where n = 1 (Masson slag model)
N	Temkin ionic fraction
T	temperature
mm	millimetre
cm	centimetre
m	metre
μ m	micrometre (10^{-6} m)
Å	Angstrom unit (10^{-10} m)
A	area
ℓ	length
g	gram
kg	kilogram
ℓ	litre
d	diameter
s	second
cP	centipoise
mPa	millipascal (pressure)
MPa	megapascal (pressure)
lb/in^2	pounds per square inch
μ or μ_N	Newtonian viscosity
ρ	density
ν	kinematic viscosity ($\frac{\mu}{\rho}$)
Bd	bulk density
Papp%	apparent porosity (percent)

Das	apparent solid density
K	calibration constant for viscometer apparatus
U	reciprocal speed factor
S	scale factor
M	torque
Ω	angular velocity
Rb	radius of measuring bob
Rc	internal radius of crucible
h	height of bob
$\dot{n}$	mass rate or slope value
$\dot{n}''$	mass flux
D or Di	diffusivity, diffusion coefficient, self diffusion coefficient
m	slope value derived from least squares regression
x,y(xj,yi)	variables used in least squares regression method
$\bar{x}$, $\bar{y}$	average values of variables used in least squares method
k or k_M	mass transfer coefficient
δ	effective boundary layer thickness
U	peripheral velocity
Cb	concentration of species in bulk phase
Ci	concentration of species at equilibrium saturated interface
Re	Reynolds number $\left(\frac{U \rho d}{\mu}\right)$
Sc	Schmidt number $\left(\frac{\mu}{\rho Di}\right)$
K α	x-ray emission line
K β	x-ray emission line

Phase notation

F_2S	iron silicate (fayalite)	$2FeO.SiO_2$
C_2S	dicalcium silicate	$2CaO.SiO_2$
C_3S	tricalcium silicate	$3CaO.SiO_2$

MF'	magnesiowüstite	MgO.FeO
F'	wüstite (iron oxide)	FeO
M	magnesia	MgO
C	lime	CaO
CM	dolomitic lime	CaO.MgO
C-F-S	calcic olivines	CaO-'FeO'-SiO_2
M-F-S	magnesian olivines	MgO-'FeO'-SiO_2
ol	olivine	
Fo	forsterite	$2MgO.SiO_2$
Fa	fayalite	$2FeO.SiO_2$
Fo-Fa	forsterite-fayalite olivine series	
CF'	calciowüstite	CaO.FeO
Fe	metallic iron	
(s)	solid	
(ℓ)	liquid	
(ss)	solid solution	
α', β, γ	temperature dependent, crystalline modifications of dicalcium silicate	

1. Introduction.

The top blown oxygen or LD steelmaking process has been developed extensively over the past decade to provide the bulk of the United Kingdom's steel requirements. The viability of the process is achieved by rapid tap to tap times (35 to 40 minutes) in vessels capable of containing between 150 and 350 tonnes of steel. A fluid, highly basic slag must be produced early in the blow to meet not only the thermodynamic prerequisites for the efficient removal of carbon, phosphorus and sulphur, but also for reduction of the refractory lining wear rate.

Calcitic lime is charged to the hot metal and scrap contents of the vessel at the commencement of the blow, and the silica (SiO_2) and ferrous oxide (FeO), from the metal bath, produce the major slagmaking components. The rapid oxidation of silicon from the bath into the slag during the first 6 to 7 minutes of the blow, results in the formation of a siliceous slag. The dissolution of calcitic lime in the early part of the blow is retarded in a siliceous slag by the development of a continuous dicalcium silicate barrier on the surface of the lump lime. The formation of dicalcium silicate exacerbates the aggression of early formed siliceous slags on the lining (doloma or magnesia), and the rate of MgO loss from the refractory becomes correspondingly high during this period. Over the past decade, dolomitic lime additions, averaging 20kg/tonne steel, have been made with the calcitic lime charge as a means of extending lining life by reducing the degree of refractory MgO solution in early

formed, siliceous slags.

Important economic consequences of dolomitic lime usage have arisen with the reduction in output of LD steelmaking shops. Dolomitic lime practices, although variable, have created increased vessel availability, and consequently, fewer relines and reduced manning levels. Tempered doloma and magnesia enriched linings have been utilised successfully with slag practices involving dolomitic lime in conjunction with vessels operating at low production levels. The current U.K. trend has been to line LD vessels with magnesia bricks which involves a four to five-fold increase in lining costs. Although the high cost magnesia lining practice has reduced the number of relines and vessel downtime periods, dolomitic lime slag practices are continuing to make these linings more cost effective under the current low levels of steel production. Magnesia linings are particularly susceptible to large temperature fluctuations within the vessel which can lead to spalling and, in extreme cases, slabbing of the brickwork.

A review of the Literature has confirmed that magnesia, derived from dolomitic lime additions and present at saturation levels of 6 to 7 mass % in the turndown slag, has a substantial influence in reducing the refractory wear rate, without seriously affecting the refining properties of the slag. Physical factors such as the control of slag viscosity and fusion temperatures also play an important role in extending the life of the lining and creating optimum conditions for refining. The precise

mechanism(s) by which the lining life is increased in the presence of magnesia - rich slags is not fully understood, nor is the effect of magnesia on steelmaking reactions by the changes in slag chemistry. Particularly lacking is fundamental information on the chemistry and kinetics of dolomitic lime solution in early formed LD slags and the manner by which this may influence the overall rate of slag formation.

There is clearly a need to identify the effects of magnesia and dolomitic lime additions on LD-type slag forming systems. To establish a basis for a study of the mechanisms which account for the interactions occurring during early slag formation, both physical and chemical investigations were envisaged. To accomplish this aim, data on both viscosity and melting relationships as well as reaction studies were considered necessary. The programme of work therefore included:-

1) The development of a viscometer technique to study the effect of magnesia levels on the fluidity of liquid slags.

2) High temperature crucible techniques were to be used to study the rates of dolomitic lime reactions with other slag forming oxides.

3) Compositional changes and mechanisms of dissolution were to be established by optical microscopy, scanning electron microscopy and chemical analysis.

It was anticipated that these results when considered as a whole would identify the effects of magnesia and dolomitic lime on LD slagmaking systems. The combined experimental results and their interpretation should allow extrapolation to the industrial situation.

2. Literature Survey

2.1 Introduction to oxygen steelmaking.

The majority of economically viable iron bearing formations are linked to a sedimentary or igneous origin. High quality imported iron ores contain on average 62% iron, while local sedimentary ores contain up to 25% iron [1]. After ore dressing and reduction within the blast furnace, the processed iron will contain unwanted metalloids such as silicon (Si), phosphorus (P), sulphur (S) and, perhaps, manganese (Mn). In addition, the pig iron becomes saturated with carbon (approximately 4%) from the coke to produce a low melting point liquid ($<1150^{o}C$). The essential features of conventional steelmaking are the partial oxidation of the carbon along with Si, P, Mn and the accompanying reduction in sulphur level.

The development of steelmaking processes throughout the 19th and 20th Century has recently been reviewed by Michaelis [2] and others [3, 4]. The air blown Bessemer and Thomas Converters and externally heated open hearth processes of steel production have declined with the advent of tonnage oxygen which was produced on a commercial scale by Fränkl (1928). Oxygen was used in early steelmaking trials to initiate and control exothermic oxidation reactions of carbon and metalloids within a hot metal bath. In 1952 the first industrial plants at Linz and Donawitz in Austria manufactured steel from low phosphorus pig iron in 35 ton vessels lined with basic (magnesia) refractories. Oxygen was top blown at high velocity onto the surface of the hot metal by a water cooled lance. This process has

been extensively developed and is known as the Linz-Donawitz (LD) process in Britain and Europe, and as Basic Oxygen Steelmaking (BOS) in North America. In the context of this thesis the term LD will apply to the furnace as well as the process. In its prevailing present form the LD furnace is a pear-shaped, tiltable vessel ranging in size from 5 to 350 tonnes. The engineering problems of supporting and manoeuvering large LD vessels have been discussed by Langmead [5]. Oxygen consumption in large (>300 ton) vessels is in the region of 50 Nm^3 per ton of blown metal for the average 20 minute blowing period. The LD process now accounts for 53% of the World's total steel production [2].

2.1.1 Alternative oxygen steelmaking processes.

Industrial practice with the LD produced a series of offshoot processes with respect to oxygen steelmaking "reactors". This was largely due to European innovators attempting to overcome problems with high phosphate bearing ores and the need for "clean" steels. The principal variants are listed below for comparison with the LD process.

2.1.2 Rotating vessels.

The Swedish Kaldo (1956) developed by Kalling at Domnarvet consisted of a rotating vessel with two running rings mounted on four support wheels which allowed the vessel to be tilted on trunnions. The furnace had a capacity of 25 to 30 tonnes, an outside diameter of 3.5m and a length of 5.5m. The vessel could be rotated at 30 r.p.m.

whilst inclined at an angle of 17° to the horizontal axis, during blowing. Oxygen was blown through a lance at a low velocity and at a flat angle to the bath; the blowing period lasting for 35 - 40 minutes. The conversion of CO to CO_2 within the vessel increased the heat to the bath during rotation. Due to the heat economy of the Kaldo process, up to 50% scrap could be melted as opposed to 25 to 30% in the LD. Kaldo vessels became largely inoperational due to (i) excessive lining costs; (ii) costly maintainance of rotary equipment; (iii) production per furnace was about half that of coexisting LD vessels. Pearson et al [6] have made a critical comparison between slag-metal reactions in the LD and Kaldo processes.

The German designed Graef-Rotor (1957) used two water cooled lances one of which was submerged in the bath and the other used to burn CO to CO_2. The furnace was essentially a 14.6m long cylindrical vessel with an internal diameter of 2.7m. Rotational speed was limited to about 2 r.p.m. with rotation about a horizontal axis. The blowing time was approximately 2 hours. Although designed to combine advantages of open hearth and pneumatic steelmaking, similar high cost problems were encountered as with the Kaldo. A vertical LD-type vessel called a Rotovert was developed around the same period which could operate at a rotation speed of 85 r.p.m. Slag was retained in a "well" of metal formed by the spinning action of the vessel which was claimed to reduce refractory wear rates. The vessel size was restricted to 6 ton capacity.

2.1.3 Oxygen-Lime Powder (OLP - LD AC) and bottom blown processes (OBM, Q-BOP, VLN).

With high phosphorus iron ores problems were encountered in end point P targets when using the LD process. The Oxygen - Lime Powder (OLP or LD AC) process was developed by IRSID of France to achieve better dephosphorisation. Powdered lime was blown simultaneously with oxygen through the lance system to bring about a controlled foaming of the slag. On a series of 30 ton heats, high quality steels low in phosphorus, sulphur and nitrogen were produced [7]. Very high reaction temperatures were reached at a so-called "hot spot" where the $CaO-O_2$ jet impinged upon the metal bath.

Bottom air blown Bessemer and Thomas converter processes often introduced high concentrations of nitrogen into the steel which affected its cold workability and weldability. Since all pneumatic processes for phosphoric pig iron are characterised by the fact that carbon elimination precedes phosphorus elimination, methods of bringing about earlier dephosphorisation reactions were tried. One such bottom blowing method was tried at Port Talbot in Wales by blowing oxygen and steam. This was termed the Very Low Nitrogen (VLN) process [2]. However, difficulties arose through tuyere and bottom wear as well as hydrogen pick up in the steel. The innovation of the bottom blown oxygen converter was the Maxheutte tuyere, developed by Savard and Lee of L'Air Liquide in Canada in conjunction with Maximilliansh"utte of West Germany.

The Maxheutte tuyere consists of two concentric

pipes. The inner pipe delivers oxygen through the base of the furnace and the outer delivers a shielding gaseous or liquid hydrocarbon. Decomposition of the hydrocarbon at the mouth of the tuyere brings about an endothermic reaction which provides a means of cooling the tuyere. Besides moderating the temperature, the endothermic dissociation reduces chemical attack and wear upon the bottom and the tuyeres. Modification of Thomas converters became possible by replacing the whole bottom of the converter and the process has become known as the Oxygen Blown Maxheutte (OBM) in Europe and the Quick or Quiet Blown process (Q-BOP) in North America. Promoters of this basic oxygen process [8-11] claim many advantages over the LD including smoother blowing; a higher metallic yield; an ability to melt 5 - 8% more scrap; easier attainment of lower carbon levels; shorter blowing times (12 minutes) and, perhaps equally important, the lower cost of installation on "greenfield" or "brownfield" sites. Only one LD shop at Gary in Indiana (U.S. Steel) has been converted to a Q-BOP. Table 1 (p. 231) gives an indication of the development of basic oxygen steelmaking processes in Britain and their standing at the present time.[12] The limited investment programme of BSC suggests that LD plants will remain the major bulk producers of steel in Britain for all the 1980's.

2.2 Refining reactions within the LD.

The objective of the LD process is to convert blast furnace metal (pig iron) into steel by the partial oxidation of carbon (C), silicon (Si), phosphorus (P), and

manganese (Mn) and to reduce the sulphur level. Blast furnace hot metal ideally contains about 4 mass% C; 0.7 to 0.8 mass% Si; 0.7 to 0.8 mass% Mn; 0.04 mass% S (max); and 0.15 mass% P [13]. These solute elements may be diluted to some extent by a scrap addition which can form 20 to 30% of the metallic charge.

To facilitate charging, the mouth of the LD is tilted downwards towards the charging section, hot metal being added after the scrap basket charge. The vessel is rotated back to the vertical and the lance lowered to the first blowing position. Slag-making additions are generally made at the start of the blow and enter the mouth of the vessel through chutes fed from overhead charging bins. A hood envelopes the mouth of the converter during the blowing period and is connected to a fume extraction system.

Examination of oxide stabilities illustrated on the modified Ellingham diagram in Fig. 1 (p.263) reveals that at steel making temperatures (1300 - 1650°C), carbon, silicon and manganese will be oxidised in preference to iron, but that phosphorus and sulphur cannot be removed by oxidation unless the activities of their oxides are lowered, or in the case of sulphur a stable sulphide is formed [3]. The oxidation of silicon and manganese is also enhanced by the presence of a slag because the activities of silica and manganese oxide in slag are less than unity [13]. The slag phase fulfills a number of roles. It acts as a sink and fluxing media for the oxidised metalloids and is easily discarded at the end of the refining process.

At the zone of impingement below the lance, oxygen goes into solution in the hot metal charge and iron oxides form. The excess of iron in the impingement zone enables iron oxide to transfer to the slag so that both metal and slag are initially oxidised as follows:-

$$\tfrac{1}{2}O_2 \rightleftharpoons [O] \qquad (2.1)$$

$$Fe + [O] \rightleftharpoons (FeO) \qquad (2.2)$$

$$2FeO + \tfrac{1}{2}O_2 \rightleftharpoons (Fe_2O_3) \qquad (2.3)$$

[ ] in hot metal

( ) in slag phase.

In actual LD practice the removal of impurity elements does not proceed in the thermodynamic sequence described above. Instead, oxidation of the metalloids takes place simultaneously. This is clearly illustrated in the change of bath composition during an idealized blow in Fig. 2 (p. 264) The refining reactions are briefly outlined as follows:-(3, 13, 14, 15)

2.2.1 Silicon.

Silicon is rapidly oxidised into the slag by the following reaction mechanism and within 6 to 7 minutes of blowing oxygen. The silica formed is acidic and viscous in nature.

$$[Si] + 2[O] \rightleftharpoons (SiO_2) \qquad (2.4)$$

$$[Si] + 2FeO \rightleftharpoons (SiO_2) + 2Fe \qquad (2.5)$$

2.2.2 Manganese.

Manganese is removed in a similar fashion.

$$[Mn] + [O] \rightleftharpoons (MnO) \qquad (2.6)$$

$$[Mn] + [FeO] \rightleftharpoons (MnO) + Fe \qquad (2.7)$$

Initially, the manganese content of the metal phase drops rapidly as a result of oxidation, but later a slight reversion occurs followed by a second fall near the end of the blow, Fig. 2 (p.264). The increase in manganese during the middle part of the blow has been attributed to two causes

(a) the melting of scrap.

(b) the reduction of manganese oxides from the slag, as a result of temperature changes and variations in slag composition which affect the activity of MnO.

2.2.3 Phosphorus.

The factors controlling the partition of phosphorus between slag and metal are known only empirically and both the element P and its oxide P_2O_5 are gaseous at steelmaking temperatures (Fig. 1 p.263). The very low values of the equilibrium constant in liquid iron, 4×10^{-10} at 1600°C, precludes the possibility of oxidising phosphorus to P_2O_5 in the metal [4, 16]. The necessary low activities of the reaction product can only be obtained when it is dissolved in the slag. The phosphorus oxidation reaction takes place at the slag-metal interface. Phosphorus may exist as phosphorus pentoxide (P_2O_5) or as the oxy-anion radical PO_4^{3-} in a basic slag, the activity coefficient (γP_2O_5) being lowered with increasing basicity. The concept of slag basicity has been reviewed by Ward [3] and may generally be expressed in two ways;

(a) $$\text{Basicity} = \frac{CaO + MgO}{SiO_2 + P_2O_5}$$

(b) "V"ratio $$= \frac{\text{wt\%}CaO + \text{wt\%}MgO}{\text{wt\%}\ SiO_2}$$

A more convenient general form of ($_b$) which can be used to follow the course of the blow in practice is:-

$$(_c)\ V\ \text{ratio} = \frac{\text{wt\% CaO}}{\text{wt\% } SiO_2}$$

By far the most important basic oxide is lime (CaO) but other basic oxides such as magnesia (MgO) and MnO used to be believed to exhibit the same basic behaviour as CaO towards dephosphorisation reactions [17]. However, Bookey [18] in determining the free energy of formation of magnesium phosphate ($Mg_3P_2O_{8\ solid}$) found that magnesia had a negligible effect compared with lime in dephosphorisation. Calculated activity coefficients for P_2O_5 covering a wide range of slag compositions were found to vary from 10^{-14} to 10^{-18} and were temperature dependent [16].

The slag - metal reaction is written in ionic form and is best explained by a modified version of the ionic theory first proposed by Flood and Grjotheim [19] (Sect. 2.6 p. 42).

$$2[P] + 5[O] + 3(O^{2-}) \rightleftharpoons 2(PO_4^{3-}) \qquad (2.8)$$

In the $CaO-SiO_2$ - "FeO" system, the equilibrium distribution of phosphorus has been equated to specific concentration ranges of CaO by Healy [20].

$$\log\frac{(\%P)}{[\%P]} = \frac{22350}{T} - 23{\cdot}7 + 7\log\%CaO + 2{\cdot}5\log\%{}^{*}Fe_t \qquad (2.9)$$

and

$$\log\frac{(\%P)}{[\%P]} = \frac{22350}{T} - 16\,0 + 0{\cdot}08\times\%CaO + 2{\cdot}5\log\%{}^{*}Fe_t \qquad (2.10)$$

$^{*}Fe_t$ = % total iron.

Equation (2·9) was found to be applicable to slags containing over 24% CaO, whilst equation (2.10) was valid from zero% CaO to saturation. Equation (2.10) was found to

fit the experimental results obtained by Mori et al [21]. In practice, the phosphorus partition ratios (%P)/[%P] are far from values calculated for equilibrium with carbon-free iron, because the oxygen potential ($RT \ln p_{O_2}$) of the slag/metal is influenced by decarburisation [13]. The main points for successful dephosphorisation are high slag basicities, high FeO contents and low temperatures i.e. low compared to the steelmaking range. However, at higher slag basicities of 3 to 4, the optimum phosphorus partition between slag and metal was found to occur at 15 - 17 wt% FeO, after which the partition ratio decreased dramatically [3].

2.2.4 Sulphur.

The sulphur equilibrium between slag and metal may be expressed by molecular equations but arbitary assumptions have to be made concerning the molecular species involved. A more general ionic form of reaction between sulphur in the bath and cations in the slag involves no assumptions concerning the cations coordinating with oxygen and sulphur in the slag [3].

$$[S] + (O^{2-}) \rightleftharpoons (S^{2-}) + [O] \qquad (2.11)$$

The basic oxides CaO, MgO, MnO are all capable of influencing desulphurisation by contributing oxygen anions. If Henrian behaviour for all components is assumed, Ward [3] has indicated that the sulphur partition between slag and metal is;

$$\frac{(wt\%S)}{[wt\%S]} = K' \frac{(NO^{2-})}{[wt\%O]} \qquad (2.12)$$

where K^{+} is an equilibrium quotient and NO^{2-} is the Temkin ionic fraction (sect. 2.6, p. 42). In the mixing of anions only, the ionic fraction NO^{2-} is equivalent to the activity of oxygen after the oxygen requirements for the SiO_4^{4-}, PO_4^{3-} and AlO_3^{3-} ions have been satisfied. The value of NO^{2-} can also be regarded as a measure of the basicity of the slag, the desulphurising power of basic oxides following the descending order CaO, FeO, MnO and MgO. Lime has been estimated to be 1000 times more powerful than MgO for holding sulphur in a basic slag (4). High FeO contents although highly desirable in facilitating rapid lime solution, will effectively increase the [wt%O] values in the metal and reduce the sulphur partition as indicated in equation (2.12). Ward and Salmon(22) found that blast furnace slags favoured an increase in the rate of sulphur transfer from metal to slag through increased temperature and calcium fluoride additions, suggesting that slag fluidity was an important feature in the partition of sulphur. Only about half of the sulphur present within the charge can be removed during the course of an LD blow, indicating the necessity for careful control over the materials charged to the furnace. Ward (23) has suggested that within the blast furnace there should be a critical low sulphur level that is economically attainable and that below this level some other method of sulphur control could be more economical. At Appleby-Frodingham, the maximum economical sulphur level was found to be 0.042 mass% and to achieve a final LD sulphur level of below 0.02 mass%, external desulphurisation was required.

Various methods of external desulphurisation have been discussed for use in torpedo cars and transfer ladles [24,25], principally through the use of calcium carbide injection and magnesium impregnated coke. External desulphurisation has largely removed the problems of sulphur removal in the LD process.

2.2.5 Carbon.

The principal refining reaction is the removal of carbon in the form of gaseous carbon monoxide.

$$[C] + [O] \rightleftharpoons CO \qquad (2.13)$$

$$[C] + (FeO) \rightleftharpoons CO + Fe \qquad (2.14)$$

The thermodynamic equilibrium relationships between the carbon and oxygen contents in the metal are well established. The oxygen content of the bath increases in the early stage of the blow, reaching values in excess of that in equilibrium with the carbon present. As the oxygen content of the bath decreases, the oxygen content approaches its equilibrium value, becoming very close at <0.5 mass% C [4].

The variation in decarburisation rate throughout a typical blow is illustrated in Fig. 3 (p. 264) for a single lance practice [26]. The idealised form of the blowing curve is shown in Fig. 4 (p. 264) and can be divided into three stages or periods.

Stage I Decarburisation:

The rate of decarburisation initially increases until a steady state value is attained, the slow rate of decarburisation being due to slag formation and oxidation

of Si and Mn from the bath. Preformed slags have been found to increase the rate of decarburisation [26]. Oxidation reactions increase the slag temperature from around 1300°C to 1420°C during the first third of the blow [27]; the bath temperature increasing from 1280 to 1380°C. Bardenheuer et al [28] have suggested that slag temperatures may in fact reach temperatures in excess of 1550°C during the first quarter of the blow, the metal bath temperature being some 250 - 300°C lower.

Stage II Decarburisation:

During stage II a steady state rate of decarburisation is achieved although abrupt fluctuations may occur. The plateau decarburisation rate is believed to be controlled by the maximum rate of introduction of oxygen into the system. Introduction of more oxygen through multinozzle lances or increased blowing rates can reduce the plateau period of decarburisation and lead to shorter refining times.

Stage III Decarburisation:

The carbon concentrations in the bath decrease until the transport of this species in the metal phase becomes rate controlling and the decarburisation rate decreases. Carbon transport control becomes dominant at compositions ranging from 1.2 down to 0.2 mass% C. Slag temperatures reach 1630 to 1650°C and the metal bath temperatures of 1610 to 1620°C may be attained at turndown, depending upon the aim carbon required.

2.3 Decarburisation mechanisms within the LD.

Early explanations of refining mechanisms in the LD were based on the existence of a localised high temperature reaction zone under the lance. This gave rise to the "Hot spot theory" and temperatures of 2400 to 2600°C were suggested to be responsible for decarburisation through gas-metal and slag-metal reactions [27][29]. The concept of decarburisation taking place in such a localised area as the oxygen jet impingement zone was difficult to reconcile with the very high overall decarburisation rates observed to exist during the LD process.

Evidence that most of the refining in the LD process was occurring in a slag-metal-gas system was obtained from sporadic tap hole ejections of converter material collected on metal plates during various timed parts of the blow [30,31]. After separating the slag and metal fractions, the metal droplets were subjected to size analysis and slag and metal droplets chemically analysed. The majority of droplets collected were in the size range 1 - 2mm diameter. The interfacial area available for reaction was calculated to be in excess of 50,000m^2 in a 200 tonne vessel and up to 30% of the total metallic charge could be dispersed within the slag during the blow. Chemical analyses of the metal droplets showed that the carbon and phosphorus contents were much lower than that of the bath. The residence time for droplet retention in the slag was calculated to be 2 to 3 minutes.

The existence of slag-metal-gas systems in steel-

making has been reviewed by Kozakevitch [32] and used in conjunction with Meyer and Trentini's results, it established the concept of foams and emulsions in the LD process as a principal mechanism of decarburisation. The term "emulsion" is applied to a system where two liquid phases are immiscible or partly miscible, and the droplets of the dispersed phase within the continuous phase are sufficiently far apart to permit independent movement. A "foam" is a coarse dispersion of gas in liquid, but since the gas bubbles are separated by thin liquid films, the bubbles cannot move freely [13]. At the height of refining, up to two thirds of the total carbon present can be removed within a slag metal emulsion. Decarburisation involved the unsteady state transfer of oxygen from the slag to metal droplets, which were completely surrounded by slag. Since the metal droplets could exist surrounded by slag for some period of time without contacting a CO gas bubble, a high degree of supersaturation could be achieved with respect to the C - O reaction. CO may be discharged by a number of mechanisms [30]:-

(a) By coming into contact with CO bubbles rising through the slag.

(b) Heterogeneous nucleation at the slag metal interface, especially in the presence of solid particles in the slag.

(c) Homogeneous nucleation - the observed [C] and [O] concentrations were sufficiently high to suggest the possibility of this mode. CO bubbles, once nucleated in this way would grow at an explosive rate, leading to the

destruction of the droplet and creating an even finer dispersion.

Decarburisation studies of single droplets in oxidising slags has indicated that the nucleation of CO bubbles may not be as difficult as once thought [33]. Gas can be continuously evolved from the surface of a reacting droplet suggesting that the transport of oxygen in slag and perhaps in metal, the transfer of carbon in metal, and interface chemical reaction may be all important in determining the decarburisation rate. Transport of oxygen through a gas phase halo may also be important.

The possibility of the decarburisation of droplets as they flew through the air, has been eliminated by sampling within the converter during the blow [34][35]. Price [34] used a "bomb" sampling method to take samples every $1\frac{1}{2}$ to 2 minutes during the blow but only after the first 10 minutes of the blow. Chatterjee [35] took spoon-like samples from a 6 tonne converter during the blow. Droplet sizes were found to range from 0.15 to 1.2mm and many of the droplets contained hollows and blow holes caused by CO evolution. Residence times of 2 to 2.5 minutes were thought likely. Carbon and phosphorus levels were lower in the droplets than in the bath, although Price has suggested that only about one third of the decarburisation occurred in the slag-metal emulsion. Schoop and co-workers [36] found that droplets of 0.05 to 2mm diameter had a phosphorus content one-tenth that of the bath. The importance of droplet residence time in slags has been indicated by Russian workers [37][38] who found

that droplet settling time was dependent upon slag viscosity. This allowed decarburisation and dephosphorisation reactions to proceed for longer periods in viscous slag-metal emulsions. Although Meyer believed that a fluid slag was a prerequisite for rapid decarburisation, Chatterjee found that viscous slags produced higher rates of decarburisation. The argument was that a fluid slag would decrease the residence time of the droplet in the foam-emulsion phases, and impede carbon removal, since mass transfer rates associated with liquid-liquid reactions were generally lower than gas-liquid reactions at corresponding temperatures.

The observations and results on some LD processes outlined above, indicate that from the start of the blow, the refining reactions occur in a heterogeneous mixture of metal, slag and gas which, with increasing decarburisation rate, expands rapidly filling the whole vessel with foam and emulsion. This dispersed system may be arbitarily divided into three overlapping periods; (i) creation; (ii) stabilisation; (iii) destruction [13]. These periods will not only be dependent on the mechanical energy resulting from jet impingement on the surface of the bath, but also on surface tension on the bath surface and in the foam; the viscosity of dissolved slag phases; the amount of solid slag particles within liquid slag and the evolution of CO gas during decarburisation. Many of these factors affect the stability of the foam and therefore successful steel production will depend on a good blowing technique, a good slag practice and a consistent source of hot metal

and scrap charge.

2.4 Reaction Kinetics.

In order that a reaction may proceed, reactants and products must be brought to the reaction site and removed from the site so that reactions involving diffusion and other transport mechanisms are likely to be rate controlling. Reactions that involve more than one phase are heterogeneous reactions and are classified into the following groups: gas-solid; gas-liquid; liquid-solid; liquid-liquid [39]. The study of a heterogeneous system such as that operating in the LD process is more complex than the study of a homogeneous reaction, since it is necessary to examine not only the chemical kinetics of the reactions, but also the mass transfer phenomena which may have a controlling effect on the overall rate.

In the vicinity of an interface, transport of reactants and products may occur under laminar or turbulent flow conditions [39][40]. Under laminar flow conditions "elements" of liquid which arbitarily have dimensions larger than molecules, but smaller than the container or associated parts, move only in the direction of flow in a streamline manner. In the turbulent case, "elements" of liquid may move at many angles to the net direction of flow and produce eddy current effects. In stirred systems the transfer of solutes across a phase boundary is important, and gradients of concentration exist only near the interface because the turbulence keeps the bulk concentration relatively uniform. In the LD process, there is

transport of reactants to a slag-metal-gas interface, chemical reaction at the interface and transport of the products away from the slag-metal-gas interface.

At steelmaking temperatures the [C] - [O] reaction is believed to proceed rapidly and is therefore unlikely to control the rate of the overall process [14]. In the decarburisation of single iron-carbon droplets, Hazeldean and co-workers [33] have shown that the evolution of CO bubbles proceeds rapidly and this is also unlikely to be important in determining reaction rates. Mass transport of the reactants in the slag and metal phases probably controls the rate of the decarburisation reaction. Two rate controlling conditions exist;

(i) Continuous phase control.

For the decarburisation reaction, the rate of transport of the oxidising species through continuous slag phase may control the reaction rate. However, some of the droplet's surface will be effectively masked by CO bubbles [30, 31].

(ii) Dispersed phase control.

The rate of transport of carbon atoms through the dispersed metal phase to the reaction interface may also control the rate of the decarburisation reaction.

In foams and emulsions, decarburisation may occur under oxygen transport control or carbon transport control [30]. Acheson and Hills [41] from model converter studies have suggested that the rate at which CO bubbles escape from the foaming slag is a major factor controlling reaction rates in the process. Mass transfer by natural

diffusion and turbulence mechanisms have been discussed under the surface renewal theories of Higbie, Danckwerts and Machlin [40, 42]. General forms of dimensionless equations or groups have been applied to mass transfer mechanisms in rigid metal drops. Aeron et al [43] have studied the fall of metal droplets through various liquids and concluded that with increasing droplet size, the viscous forces acting at the interface caused circulation to occur within the droplet so that droplets above a certain size cannot be treated as rigid, non-circulating drops. Studies [44] on the rate limiting steps in the decarburisation of iron droplets in an oxidising slag have shown a conflicting mechanism which is consistent with interface chemical reaction control at the metal-gas interface of the slag-metal-gas system. The evidence that a gas-metal contact occurred at the droplet interface in an oxidising slag came from x-ray fluoroscopy studies carried out by Hazeldean and co-workers [33].

There are clearly a number of conflicting theories with regards to the mechanism or mechanisms of decarburisation within the LD-process. In practice it is likely that most of the mechanisms discussed briefly above make some contribution to the overall decarburisation reaction and as Walker and Anderson [13] conclude, estimates of refining rates will necessarily involve some degree of empiricism.

2.5. Physical aspects of steelmaking slags.

Prediction of process rates and heat and mass

transfer coefficients will be dependent to a large extent on the physical properties of slag phases. For example, in LD slags the stability of the foam during blowing will largely be dependent upon slag viscosity, slag density and surface tension properties [32] which in turn would influence thermal conductivity and diffusion of reacting species within the dynamic system. Before considering the nature of the slagmaking additives it is necessary to review briefly the structures and properties of slags and slag models.

2.5.1 The structure of liquid slags.

The understanding of liquid slag structures has partly been derived by extrapolation of solid state structures determined by x-ray or electron diffraction and consideration of coordination number [4]. In the molten state, the regular arrangement of the ions is destroyed. Conductivity measurements have indicated the ionic nature of slags [40], whilst entropies of fusion have suggested that the melting of silicates containing M - O and Si - O bonds involves the breaking of ionic bonds with strongly covalent bonds resisting the melting process [3]. The melts are envisaged as being truly ionic with all entities carrying a charge even though the SiO_4^{4-} anion itself is held together by predominantly covalent bonds. Slags or melts may contain so-called "acid" or "basic" oxides. An acid oxide will absorb oxygen ions when dissolved in a basic melt. A basic oxide will dissociate and release oxygen ions when dissolved in a melt.

Activation energies of viscous flow in the systems $CaO-SiO_2$, Li_2O-SiO_2, $MgO-SiO_2$ etc., have shown that fundamental changes occur in the silicate lattice on the addition of approximately 10 mole% alkali oxide or 20 mole% alkaline earth oxide [45, 46]. The assumption that infinite chains or sheets of silicates existed was not supported on the low experimental values of activation energy for viscous flow determined by Bockris and Lowe[45]. From this and additional work [47], the addition of metal oxides to silica resulted in the breakdown of the three-dimensional silicon-oxygen network, Fig. 5 (p.265) into silicate anions of varying sizes, which can exist as tetrahedral SiO_4^{4-} anions depending upon the proportion of metal oxide added [48].

With increasing silica, simple linear polymerisation occurs first to ions such as $Si_2O_7^{6-}$, with ring ions forming at 50 mole% SiO_2. Polymerisation of silicate melts is an important concept in the thermodynamic treatment of slag model theory. Polymerisation may be defined as the chemical union of two or more molecules of the same compound to form larger molecules of the same empirical formula but of greater molecular weight [49]. Table 2 (p.232) illustrates the structural relationships in basic oxide-silicate melts.

2.5.2 The viscosity of LD-type slags.

From the commencement of the blow, it has been shown in sections 2.2 and 2.2.1 (pages 21 and 23) that 'FeO' and silica are readily generated by oxidation

reactions within the metal bath. The early formed slag will therefore correspond to that of the pseudo binary system 'FeO'-SiO_2 in contact with liquid metallic iron[50]. The lime addition forms the other major slag component and allows LD slags to be represented by the pseudo-ternary CaO-'FeO'-SiO_2 system in contact with liquid metallic iron or the system CaO-Fe_2O_3-SiO_2 in air [28, 50].

A number of studies [51, 52, 53] have been made on the viscosity of the 'FeO'-SiO_2 pseudo binary at varying mole percentages of silica. Fig. 6 (p.265) illustrates the wide range of viscosities exhibited at 1300°C and the notable viscosity maxima reached at 33 mole% SiO_2 which corresponds to the composition of fayalite ($2FeO \cdot SiO_2$). Average values of viscosity range from 45 mPa.s (cP) at 22 mole% SiO_2, to a fayalite maxima of 70 to 200 mPa.s and in excess of 200 mPa.s at 44 mole% SiO_2. The viscosity increases with increasing silica content. Within the system FeO-Fe_2O_3-SiO_2 [50, 54], the phase field covered by fayalite is relatively large, Fig. 7 (p.266), and exists over a range of oxygen partial pressures. Increasing the oxygen partial pressure from 10^{-11} to 10^{-7} reduced the viscosity slightly from 105 mPa.s (cP) to 95 mPa.s at 1300°C and a $^{Fe}/_{Si}$ ratio of 3.09 [54]. At 1300°C and $^{Fe}/_{Si}$ ratios of $^{3.88}/_{1}$ and $^{4.99}/_{1}$, the viscosities fell from 70 to 50 mPa.s and 42 to 38 mPa.s respectively.

Limited studies on the viscosities of the CaO-'FeO'-SiO_2 system have been reported [52, 55]. The viscosity

has been found to decrease steadily towards the 'FeO' corner of the system as illustrated in Fig. 8 (p. 266). With the exception of melts of fayalite composition, the viscosity of the slags along lines of fixed silica content remain relatively constant up to values of 32 mole% lime. The viscosity of slags prepared in a pilot LD furnace and approximating to the CaO-'FeO'-SiO_2 system has been measured over a range of basicities in flux trials [56]. In a flux-free master slag with a V-ratio of 1.4, a viscosity of 200 mPa.s was recorded with molybdenum components at 1450°C, decreasing to 100 mPa.s at 1570°C. Iron components have been used in the majority of viscosity measuring devices due to the aggressive nature of 'FeO'-rich melts towards refractory materials and certain metals. For this reason, viscosity measurements on the CaO-'FeO'-SiO_2 system are restricted by the melting point of iron to temperatures of 1200 to 1450°C.

2.5.3 The density and surface tension of LD-type melts.

Interpretation of density measurements [57, 58], determined by the maximum bubble pressure method, has indicated that ferrous silicate melts are more highly polymerised than corresponding calcium silicate melts. These results were based on the concept of oxygen density, which was taken to be a measure of the efficiency with which oxygen fills a space in the melt structure, and was considered to be a measure of the degree of silicate anion polymerisation. In ternary-type iron-calcium silicates, preferred ionic associations were postulated to

occur between Ca^{2+} and the silicate ions and between Fe^{2+} and free oxygen ions which resulted in a microsegregation of calcium silicate-rich groups and iron oxide-rich groups. Some confirmation of microsegregations were discussed by Shiraishi et al [53] who found that volume changes in fayalite were much smaller than those of ionic crystals in spite of the fact that molten fayalite behaves as an ionic melt. Cluster formation of some type was thought probable and they proposed that the "hump" phenomena, recorded in viscosity measurements, were attributed to fayalite clusters made up of 11 to 12 molecules of fayalite.

The addition of calcium orthosilicate brought about the non-linear depolymerisation of iron orthosilicates and the presence of approximately 42 mole% $2CaO \cdot SiO_2$ in the mixed orthosilicate system was sufficient to bring about complete polymerisation. At mole fractions of 0.67 FeO and 0.33 SiO_2, corresponding to the composition of fayalite, a density of 3.65 gcm^{-3} was recorded at 1315°C. The addition of lime to the melt to yield a composition of 0.369 CaO, 0.296 FeO and 0.335 SiO_2 produced a density of 3.06 gcm^{-3} at 1290°C. Some alternative evidence [59] has suggested that at constant iron oxide content, replacing SiO_2 with CaO raises the density and lowers the molar volume of the melt.

The bonds which make a contribution to surface tension are believed to be ionic bonds of the type $M^{2+}O^{2-}$ and $-O^{-}-M^{2+}-O^{-}-$ [57]. Surface tension will be dependent upon the strength of the bonds $M^{2+}O^{2-}$ etc., which will be determined by cation type; the proportion of bonds which is

dependent on the degree of polymerisation; and the number of bond types present per unit area of surface. The large difference between the surface tensions of calcium and iron orthosilicates, 375 and 352 dynes cm^{-1} respectively at 1450°C, indicates that bonds involving Ca^{2+} ions and oxygen are stronger than bonds involving Fe^{2+} and oxygen. The negative deviation from the "ideal" line of calculated $2FeO.SiO_2$ activities indicated the occurrence of surface segregations of an iron oxygen-rich complex. From studies of calcium-manganese silicate melts, the lowest energy configuration and lowest surface tension values occurred in stoichiometric, vitreous or molten silica [60]. Changes that resulted in destroying the symmetry and decreasing the anion size of the silicate network led to increases in surface tension. This effect was explained by the addition of basic oxides such as CaO or MgO, or by changes in the atmosphere above the melt. Within the context of foam formation, Cooper et al [61] found that foaming only occurred in $CaO-SiO_2$ melts with above 67 mass% SiO_2. Foam formation was enhanced further by the addition of 1 to 2 mass% P_2O_5 at low V-ratios. Surface tension measurements indicated that P_2O_5 was absorbed at the surface, increasing the surface elasticity of the foam. Although FeO or Fe_2O_3 was not taken into account, their presence apparently influenced only the volume and rate at which gas was produced.

2.6 Constitutional and Structural slag models.

The interpretation and prediction of slag-metal distribution equilibria requires detailed knowledge of

activities and chemical compositions of slags to determine equilibrium constants. In multicomponent slags, activity data is often sparse or non-existent so that numerous slag models have been proposed to calculate activities of slag components from chemical analysis. A number of slag model theories have been reviewed by Ward [3] who discusses early molecular theories and the later ionic slag models of Temkin and Flood. The Temkin model is an example of the constitutional theory where structural aspects of the molten slag are ignored. Temkin's model proposed that slags consist only of ions exhibiting ideal behaviour, existing as separately charged entities and that like-charged ions were of equivalent interaction with their nearest neighbours. The activity of an oxide could be represented as follows;

$$aFeO = N_{Fe^{2+}} \; N_{O^{2-}} \qquad (2.15)$$

where N represented the ionic fraction derived from;

$$N_{Fe^{2+}} = \frac{nFe^{2+}}{\Sigma n \text{ cations}} \quad , \quad N_{O^{2-}} = \frac{nO^{2-}}{\Sigma n \text{ anions}} \qquad (2.16)$$

The Temkin model takes no account of the polymerised species which are known to occur from evidence in sections 2.5.2 and 2.5.3 (pages 38 and 40) and assumes silicon exists only as SiO_4^{4-} ions. At compositions above the orthosilicate (>30% SiO_2), activities deviated from the ideal line. The slag model proposed by Flood et al [19] used the concept of electrically equivalent ion fractions which, unlike the Temkin approach, takes into account variation of interaction between different ions. In basic slags all silicon (Si), phosphorus (P) and aluminium (Al)

were present only as SiO_4^{4-}, PO_4^{3-} and AlO_3^{3-} whilst all cations existed as Ca^{2+}, Mn^{2+}, Mg^{2+} and Fe^{2+}.

Liquid silicates are now widely accepted as being polyionic melts with cations, free oxygen ions (O^{2-}), and varying sized silicate ions. Toop and Samis [62] have used a general form of equilibrium reaction proposed by Richardson [63] by which equilibrium polymerisation takes place instead of a specific form of silicate anion reaction. Three forms of oxygen were considered to exist in silicate melts;

Singly bonded Si atoms doubly bonded 2Si atoms free ions

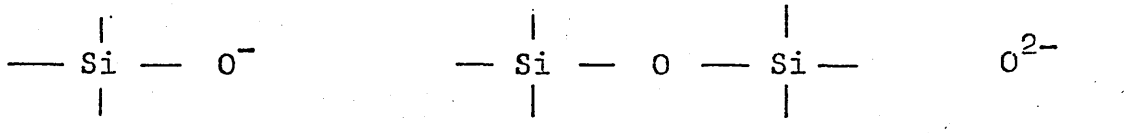

e.g.

$$2SiO_4^{4-} \rightleftharpoons Si_2O_7^{6-} + O^{2-} \qquad (2.17)$$

$$2O^- = O^0 + O^{2-} \qquad (2.18)$$

$$k = \frac{(O^0)(O^{2-})}{(O^-)^2} \qquad (2.19)$$

A high value of k indicated a high degree of polymerisation. The values of O^0, O^- and O^{2-} refer to moles per mole of slag. k is not a true equilibrium constant but assumptions are made that;

(i) It is constant at constant temperature.

(ii) It is a characteristic of cations present in any binary or ternary silicate melt.

(iii) It is independent of composition.

From charge and material balances the following equation was derived:

$$4k = \frac{[4x_{SiO_2} - (O^-)]\,[2 - 2x_{SiO_2} - (O^-)]}{(O^-)^2} \qquad (2.20)$$

For various values of k obtained by curve fitting, values of xO^- were derived as a function of x_{SiO_2} where x represents the mole fraction of the particular species. Curves were produced which resembled free energy of mixing curves for binary silicates(ΔG^M). On this basis the model was extended to an ionic ternary Gibbs-Duhem relationship which correlated qualitatively "ionic activities" $a_{Fe^{2+}}$, $a_{Ca^{2+}}$ and $a_{O''}$ with known activity data for a_{FeO} and a_{CaO}. From reviews of slag models [64, 65, 66] it is suggested that the drawbacks suffered in the Toop and Samis model were as follows. The contribution to the entropy of mixing of the three reaction parameters was not considered in the expression for free energy of mixing; there were difficulties in assigning physical significance to activities of electrically charged particles i.e. Temkin fractions; an unusual standard state for the ternary, $a_{O''} = 1$ along the CaO-'FeO' pseudo binary which can only be true if Ca^{2+}, Fe^{2+} and O^{2-} form ideal solutions.

Masson [65] and Masson et al [67, 68] have proposed two models for the calculations of the activities of basic oxide in a binary silicate melt using a predominantly constitutional slag model approach based on polymer theory. Three main assumptions are made:

(a) The approach is limited to consideration of linear and branched chains of the form $Si_nO_{3n+1}^{2(n+1)-}$ which from stoichiometric reasons restricts the treatment to melts more basic than the metasilicate composition ($<0.5\ SiO_2$).

(b) All O^- groups are chemically equivalent regardless of the size of the polyanion to which they are attached.

(c) The observed activities may be related to calculated ion fractions by the Temkin equation. For example for MO

$$a_{MO} = N_{M^{2+}} \times N_{O^{2-}} \quad (N = \text{ionic fraction}) \qquad (2.21)$$

With these assumptions, the following expressions have been derived for the activity of MO as a function of composition in binary melts $MO\text{-}SiO_2$. For linear chains;

$$\frac{1}{N_{SiO_2}} = 2 + \frac{1}{1 - a_{MO}} - \frac{1}{1 + a_{MO}(\frac{1}{k_{11}} - 1)} \qquad (2.22)$$

k_{11} is the equilibrium ratio when n = 1 i.e.

$$SiO_4^{4-} + SiO_4^{4-} = Si_2O_7^{6-} + O^{2-} \qquad (2.23)$$

For all chain configurations (linear or branched):

$$\frac{1}{N_{SiO_2}} = 2 + \frac{1}{1 - a_{MO}} - \frac{3}{1 + a_{MO}(\frac{3}{k_{11}} - 1)} \qquad (2.24)$$

From the results, SiO_4^{4-} was by far the most abundant species in $CaO\text{-}SiO_4$ melts at all compositions and almost the only one present when $x_{SiO_2} < 0.3$. At silica contents higher than the orthosilicate, $Si_2O_7^{6-}$ and $Si_3O_{10}^{8-}$ ions etc, appeared, especially towards the metasilicate composition. With 'FeO'-SiO_2 melts, the distribution was broader and although SiO_4^{4-} was still the most abundant species, $Si_2O_7^{6-}$ and $Si_3O_{10}^{8-}$ became significant even below the orthosilicate composition.

2.7 LD Steelmaking slags.

2.7.1 The lime charge.

In the LD process, lime is generally the only externally added slagmaking component, the other slag forming phases being generated by oxidation reactions within the bath. The consumption of lime in LD steelmaking has been estimated to be seven times greater than that of the open hearth furnace, while the corresponding ratio of cycle times is some eight times quicker [13]. The production and quality requirements of steelmaking lime have been reviewed [69, 70]. A limestone with a high and uniform calcium carbonate ($CaCO_3$) content is desirable with inherent impurities such as SiO_2, FeO and Al_2O_3 kept as low as possible. Sulphur may be derived from calcium sulphate or from the coal or fuel oils used in the calcination process. Specifications of 0.05 mass%S are quoted [70] but an increase in lime sulphur from 0.05 to 0.1 mass% contributes less than 0.001% increase in final steel sulphur. The rate of lime solution in steelmaking is related to the available surface area of individual lumps, -38 +12mm in size, and apparent density of the material, rather than to a specific reactivity test. Relating water or acid lime reactivity tests to slag-lime reactivities has been the subject of much discussion [71, 72, 73]. Once reactive lime has become hydrated, which apparently can occur over a few hours, the various types of reactivity test become suspect [71]. However, Limes [73] believes that high temperature crucible reactivity tests can be

related to reactivity tests measured by normal ASTM methods. As a consequence of reactivity tests and trials relating temperature and duration of calcination to available surface area, highly porous lime is supplied to the steel industry with a bulk density of 1500 to 1600kgm^{-3}. Under normal steelmaking practice, lime is added at the commencement of the blow and may comprise between 8 and 10 mass% of the total vessel content.

2.7.2. The CaO-Iron Oxide-SiO_2 system.

LD slags form a highly complex multicomponent system and as a first approximation Muan and Osborn (50) consider the system CaO-iron oxide-SiO_2 under two different levels of oxygen pressure. Isothermal sections at 1600°C through the systems in contact with metallic iron or air, Figs. 9a, 9b (p. 267) indicated that the area of the all liquid field was approximately the same under the two extremes of oxygen pressure prevailing i.e. 10^{-8} to 1 atms. The "nose" formed by the dicalcium silicate (C_2S) plus liquid phase field in Figs. 9a and 9b indicates that up to 10 mass% more of lime can be dissolved under conditions of high oxygen pressure (1 atms.) and decreasing iron oxide content. The liquid must also be simultaneously low in silica and saturated with lime so that ideally slag compositions at the end of the blow fall around the dark circles in Figs. 9a and 9b.

With magnesia as a possible exception, it has been suggested (50) that the other oxide constituents will decrease the liquidus temperature further and increase the

area comprising mixtures which are all liquid at a chosen temperature. Of particular importance are regions of the phase diagrams separating the all liquid area from those areas where liquids coexist in equilibrium with either CaO or calcium silicates so that thermodynamic and basicity requirements are met.

In-blow LD converter sampling presents many problems[34] but van Hoorn et al [74] have developed a sampling procedure which allowed the evolution of slag composition to be determined without interruption throughout most of the blowing period. The converter was sampled in an upright position by lowering two saucer-shaped dishes 150mm in diameter attached to a chain, down the side of the lance. Sample masses of between 200 and 500g were collected from 31 heats during three converter campaigns. The development of slag composition is illustrated by reference to Figs. 10 and 11 (p. 268) [74]. In addition, the slag analyses in Tables 3 and 4 (p. 233) allow comparison between some of the results of van Hoorn[74] and Price [4]. A number of features become apparent:

a. The initial slags are siliceous.

b. Lime dissolves only relatively slowly.

c. There is a high concentration of FeO during the early part of the blow.

d. There is an initial high concentration of magnesia, presumably as a result of refractory erosion.

2.7.3 <u>The system CaO-'FeO'-SiO_2 in contact with metallic iron</u>.

The general difficulties associated with obtaining

steelmaking slag samples, particularly in the LD-process, have led to the widespread use of laboratory or pilot plant studies. Simple synthetic slag systems have been used and for studies on the dissolution of lime, the system CaO-'FeO'-SiO_2, illustrated in Fig. 12 (p. 269) has been used, or one of its pseudo-binary edges.

In the dissolution of lump lime in CaO-'FeO' slags, it has been suggested that the pore radius and not the density of lime is the most important factor, the dissolution rate increasing with strongly unsaturated slags[75]. When silica additions were made to the slags, the lump lime was infiltrated by the silicate slags relatively quickly. At slag basicities of 1.8 to 2, lime dissolution became inhibited by the formation of a dicalcium silicate layer. In low 'FeO' slags, the dicalcium silicate layer became very stable and hindered dissolution. The degree of lime dissolution with time of blowing has been studied in a 200 ton and 3 ton pilot furnace by Iyengar and Petrilli [76] and the result is shown in Fig. 13 (p. 270). The retardation in lime dissolution between 20 and 60% of the blow is due to the formation of calcium silicate phases around the particles of lime. The effect of slag basicity on the erosion of LD refractory bricks was also studied and is shown for comparison in Fig. 14 (p. 270). Maximum lining erosion occurred at a CaO/SiO_2 ratio of 0.7 corresponding to 20% of the blow.

2.7.4. <u>The dissolution kinetics of lime</u>.

In a laboratory study of the kinetics of the solution

of lime in LD-type slags, Biochenko et al [77] showed that slag temperature and degree of oxidation were important in the assimilation of lime by slag. Increased FeO and MnO contents exerted a favourable influence on the solution of lime by reducing the viscosity of the slag. These observations tended to support those of Yershov and co-workers [78] who inferred that the dissolution of the dicalcium silicate inhibiting layer was affected by the amount of FeO and MnO present within the slag. Lime samples rotated in slags of high FeO contents brought about the direct solution of CaO through the formation of dicalcium ferrite (C_2F) which formed a eutectic with lime at 1120°C.

Matsushima and co-workers [79] studied the decrease in diameter of a rotating lime specimen in FeO and Al_2O_3 rich slags. The rate of dissolution increased with temperature and rotational speed, supporting the assumption that the diffusion of calcium through a slag phase boundary layer would be a rate determining step. The dissolution rate into slag containing FeO was several times larger than that into slag without FeO due to differences in physical properties of the slags and the morphology of dicalcium silicate formation. Mass transfer coefficient values of 9.7×10^{-4} and 17.1×10^{-4} cms^{-1} were measured at stirring speeds of 200 and 400 rpm respectively in a slag of composition $20FeO - 40CaO - 40SiO_2$ by mass.

From studies on iron silicate melts, Green[80] has suggested that a kinematic model for the dissolution of lime involved the following rate controlling steps.

Initially, the dissolution of lime was controlled by the transport of lime to the liquid-dicalcium silicate interface but at a later time, the rate controlling stage was the transport of the reacting species of the melt (iron oxide and silica) from the bulk melt to the dicalcium silicate-liquid interface. Whilst these reactions were progressing, the fluidity of the slag was decreased through suspensions of dicalcium silicate within the molten slag.

A recent review and study of lime dissolution by Natalie and Evans [81] has suggested that dicalcium silicate dissolves as the lime/melt interface boundary layer, approximately 200 μm thick, moves past the dicalcium silicate layer so that individual fragments are swept into the bulk slag by the motion of the slag during pellet rotation. Fresh dicalcium silicate precipitates within the boundary layer to maintain a steady state quantity. The quantity of dicalcium silicate within the boundary layer, and the resistance it presents to lime dissolution, depends on the nucleation, growth and dissolution of dicalcium silicate; in addition to the velocity of movement of the lime/slag interface. Higher interface velocities occurred with more porous limes and resulted in less dicalcium silicate formation and therefore less resistance to dissolution.

2.7.5 Flux practices.

Apart from vessel availability, one of the most important factors in the economic production of steel

within the LD is time. Therefore, the acceleration of lump lime solution becomes a paramount parameter in achieving the correct slag basicity for dephosphorisation and desulphurisation and the reduction of refractory wear rate. This action may be achieved by using a lime flux which can enhance slag formation by several different mechanisms [82];

(i) Solid dicalcium silicate (C_2S) precipitation may be suppressed thereby limiting shell formation.

(ii) The structure of the C_2S cortex may be modified rendering it more permeable to slag.

(iii) The slag fluidity may be increased to aid diffusion.

(iv) A stable compound with lime may be formed which maintains a good activity gradient for diffusion.

The generally accepted and most widely used flux is fluorspar (CaF_2) which lowers the melting point of steelmaking slags and decreases slag viscosities. High grade metallurgical spar containing between 70 - 80% CaF_2 is becoming difficult to obtain and correspondingly more expensive. Stricter pollution controls have also made the use of fluorspar socially undesirable. Alternative fluxes to fluorspar have been widely studied [82, 83, 84] and have ranged in composition from ilmenite, bauxite, manganese ore and boric oxides. Obst [85] has described how crushed reactive lime and LD-fume or bauxite red mud has resulted in an earlier slag formation and a reduction in the blowing time. At Koverhar LD plant, Finland, LD-fume collected by electrostatic precipitators and contain-

ing primarily iron oxides, was added after the pig iron and scrap charge [86]. Lime additions were made at a rate of 15kg/ton steel with the start of the blow (average total lime quantity 40kg/TS), and lime solution proceeded rapidly without the need of a high lance position to provide "soft" blowing conditions associated with the generation of FeO on the bath surface. The limiting factor in the use of returned fume or LD dust was its fairly high sulphur content which delayed desulphurisation during the blow. An all-in-one flux material was successfully used at Republic Steel, which utilised a briquetting route involving mixtures of free-lime, dolomitic lime, fluorspar and iron oxide [87]. Good slag development always occurred but when rotary lime kilns were changed from gas to coal-fired, an unacceptably high sulphur content resulted in the briquette practice being abandoned.

The effect of temperature and slag FeO content has been studied by Schuman et al [88] in the basic open hearth process. High temperatures resulted in a lower slag FeO content necessary to avoid dicalcium silicate (C_2S) cortex formation. The transition range for C_2S shell/no shell formation crossed the 1400°C isotherm between FeO/SiO_2 ratios of 2.5 and 3. Iron oxide in both the 'FeO'-CaO and Fe_2O_3-CaO systems may be seen from published diagrams [50] to be an effective flux for lime, producing an initial liquidus temperature below 1300°C. However, the presence of FeO in LD slags is to primarily ensure that refining reactions readily occur through O^{2-} transfer. High slag FeO concentrations can lead to slop-

ping of the vessel contents during decarburisation. Baker [89] has proposed a series of slag paths that can occur in an LD blow, Fig. 15 (p. 271). Dry slag arose through excessive C_2S formation by entering part of the nose of the C_2S stability field. The slags were siliceous, low in iron oxide, low in volume and had poor refining properties. Slags entering region A of Fig. 15 (p. 271) were higher in iron oxide and led to increased lime dissolution but also increased the slopping tendency. This was partially alleviated by iron ore additions of up to 25% of the lime weight. Manganese ore additions tended to move the slag path towards the 'RO' corner of the diagram. Up to 5% of manganese ore addition was found to improve lime dissolution, but the dissolution effect was less noticeable than with iron ore addition. Split lime additions were also found to be beneficial.

White [90] has considered how far the effective range over which saturated slag coexisting with lime could be extended by use of a suitable oxide addition at steelmaking temperatures, for the system $CaO-Fe_2O_3-SiO_2$. It was found that MgO could be used to suppress the formation of dicalcium silicate at relatively high silica contents by effectively moving the slag composition away from the lime corner of the phase diagram. This would enable fluorspar flux additions to be reduced. However, MgO additions to iron silicate slags within the fayalite composition field reduced the rate of lime solution compared to other oxide additions [82]. This was explained as being due to the ability of MgO to form stable silicates thereby

reducing the activity gradient in (iv), p.53 . After reaction of lime in the magnesia doped slags, incomplete shells of dicalcium silicate were formed.

The Literature has indicated that flux practices and possible methods of accelerating lime dissolution can vary widely from plant to plant. The decision to use alternative fluxes to fluorspar may rest with the relative costs of raw materials and furnace operation. However, the direct costs involved in slagmaking materials purchases are not a particularly good method of selecting suitable fluxing agents. Indirect benefits through increased furnace availability brought about by increased refractory life may outweigh slagmaking materials costs, as indicated in the cost exercise presented in the Case Study (p.359).

2.8. LD refractory linings.

A slag is not only required to be highly basic and fluid at the operating temperature of the furnace but it must also be compatible with the refractory lining. The performance of the initial lining in an LD vessel is limited by four properties [91];

(i) Resistance to impact in the charge pad area.

(ii) Thermal stress resistance.

(iii) Resistance to early silicate slags.

(iv) Resistance to ferruginous slags.

The vast majority of LD linings are constructed from high temperature sintered natural dolomite (doloma), synthetic magnesia - doloma - coclinker (magnesia enriched

doloma), natural magnesia and seawater magnesia [92]. Tar or pitch may be used as a binding agent at amounts varying between 4 to 6 mass%C in pressed bricks [93]. It has been found that carbon is not "wetted" by metals and slags and so minimises penetration of slag into the refractory [94,95].

Herron and co-workers in America [94, 96] have carried out intensive studies on tar-impregnated magnesia refractories and established that the presence of 3 mass% or more of carbon prevented slag penetration into the brick pores. The fact that carbon prevented slag migration was attributed to the lack of wetting between the carbon and slag. The bulk of the MgO was removed by solution in the slag, with erosion playing a minor role. In addition, it was found that carbon and the refractory oxide constituents reacted via the vapour phase. The mechanism of reaction was believed to involve the production of a metal or suboxide vapour in a region of low oxygen partial pressure due to the formation of CO. Reoxidation and condensation of the metal (Mg) then occurred in a region of high oxygen partial pressure. A dense layer of MgO formed at this reaction interface which slowed down the rate of the internal brick reactions. Subsequent slag reaction appeared to be limited by diffusion across the dense MgO layer. The dense MgO layer tended to dissolve quickly in slags of low basicity but remained quite impervious to highly basic slags readily saturated with MgO. Howe et al [97] observed that the dense MgO layer was about 200μm wide with a porous region existing behind the interface on the carbon side of the magnesia zone. Metallic iron globules were

discovered within the dense magnesia layer. The presence of metallic iron suggested that FeO in the inward diffusing slag provided the oxygen necessary to react with the outward diffusing Mg vapour to precipitate MgO and iron. The composition of the slag found entering the brick was also very different to that of the bulk exterior slag with a Ca to Si ratio much lower than the 2:1 expected. Kim et al [98] discovered that although the dense MgO layer was impermeable to slags it did absorb some FeO and MnO. They concluded that there was a self-healing and impermeable MgO layer which could not form without the presence of carbon within the brick under steelmaking conditions, and this was the major factor in extending lining life.

Examination of the slag chemistry results in Tables 3 and 4 (p. 233) has indicated that siliceous slags are formed early in the course of the blow and are undersaturated with respect to lime and magnesia. The rate of lime solution in siliceous slags is retarded by the development of dicalcium silicate which has a melting point of 2130°C [50]. This reaction is of advantage in preventing slag penetration into lime containing refractories such as those based on doloma, which are widely used in the United Kingdom. An account of the refractory practices used currently and those projected for the 1980's in U.K. steelmaking are discussed in the Case Study (p.359). Reactions between doloma bricks and steelworks slags have been studied by Oeters [99] and Abratis [100]. Laboratory

tests were carried out using rotating discs of doloma brick. Wear of the brick cylinder occurred through dissolution from the surface or as infiltration followed by mechanical spalling. Dissolution from the surface took place when dicalcium silicate formed between slag and lime and when the MgO crystallites picked up 'FeO' from the slag to form magnesiowüstite. The magnesiowüstite formations expanded to provide a continuous protective layer on the surface of the brick. The growth of magnesiowüstite was diffusion controlled and only formed when the dissolution rate was slower than growth. Infiltration and mechanical spalling occurred when the slag path no longer intersected the heterogeneous zone of dicalcium silicate (C_2S) precipitation such that solid C_2S could not form. The dissolution rate was found to be proportional to the square root of the revolving speed. Tarred specimens showed retarded slag attack similar to that observed with tar or pitch containing magnesia bricks.

Where the slag turndown temperature and iron oxide content are both high, it has been demonstrated in the Case Study, Figs. 12 and 13 (p. 402) that magnesia linings are less prone to attack than doloma ones. However, earlier studies by Fetters and Chipman [101] on open hearth steelmaking slags indicated that magnesia may be progressively dissolved at increasing slag acidities. In Fig. 16 (p. 271), saturation levels of 5 to 7 mass% MgO can occur up to the orthosilicate composition with the potential for magnesia dissolution increasing to twice this value with silica-rich slags. With reference

to magnesia and to some extent doloma refractories, solution at the slag-refractory interface and diffusion from the interface through a boundary layer into the slag is the major rate controlling process in slag corrosion [102]. Recent work by Park and Barrett [103] has indicated that corrosion was transport controlled when a magnesia crystal was rotated in melts of metavanadate and sodium disilicate compositions. The rate of dissolution was found to be dependent on the square root of the stirring speed. Logically, one may predict that the dissolution rate at magnesia refractory-slag interfaces will be reduced if the slag is already saturated to some degree with magnesia. Over the past decade, dolomitic lime has been used as an economical means of adding magnesia to early formed slags in LD vessels. Slag practices have been modified so that dolomitic lime replaces part of the normal lime charge. This practice has brought about a marked extension in the life of magnesia and doloma LD refractory linings and subsequent increases in vessel availability.

2.9 Dolomitic lime and LD steelmaking slags.

Dolomitic lime practice was pioneered in 1963 at the Alquippa Works in the U.S.A. Initially, 680kg of dolomitic lime was charged in the bottom of a 60 tonne vessel before the normal flux charge and scrap additions. The quantity of dolomitic lime was raised to 1363kg and resulted in severe bottom build-up. This build-up was found to be beneficial in protecting the refractories of the charge pad as well as increasing the life of the

vessel refractories during a campaign. The proportion of dolomitic lime used in American LD vessels has ranged from 10 to 35% of the flux charge until 1970 [104]. From 1970 the amounts of dolomitic lime have been reduced to approximately 25kg/tonne of steel, to give 7.5 mass% MgO in the finishing slag.

In the United Kingdom, dolomitic lime practices began in 1967 and consumption rates of 12kg/tonne of steel were maintained until 1975. Depending upon steel specification, current practice has been to use up to 30kg of dolomitic lime per tonne of steel to achieve around 8 mass% MgO in the finishing slag [12]. LD-tapping slag analyses taken from Ravenscraig, Scotland (A.W.D. Hills, private communication), illustrate the desired end point MgO values required from a typical dolomitic lime slag practice. Averaged slag compositions on a mass% basis were as follows; 18.0 SiO_2, 2.0 Al_2O_3, 1.0 TiO_2, 47.0 CaO, 7.5 MgO, 0.9 P_2O_5, 4.5 MnO and 13.0 Fe (oxides converted to total iron). The CaO/SiO_2 ratio gave a value of 2.6; this basicity value becomes 3.0 when calculated upon the $CaO+MgO/SiO_2$ ratio. If it is assumed that all the SiO_2 comes from the oxidation of hot metal silicon and that blast furnace slag carry-over contains enough MgO to compensate for the additional SiO_2, then an approach described by Leonard and Herron [105] and Balla and Beechan [106] may be used to calculate the mass of dolomitic lime charge required to give 6 to 7 mass% MgO (saturation) in the turndown slag. An example of this type of charge calculation is discussed in the Case Study and illustrated through

Tables 1 to 3 (p. 391).

2.9.1 The system $CaO-MgO-FeO-Fe_2O_3-SiO_2$.

The addition of dolomitic lime to steelmaking slags yields a slag-making system with more than four components. Muan and Osborn [50] have shown that it is possible to show phase relationships in five component systems such as the $CaO-MgO-FeO-Fe_2O_3-SiO_2$ one, by using geometrical methods similar to those applied to four component systems. This is done by holding one of the independent variables constant. Investigations [50] of equilibria in contact with metallic iron have indicated that iron present in the oxide phases is almost exclusively in the ferrous state. The slagmaking and refractory relationships can largely be studied in the tetrahedra representing the system CaO-MgO-iron oxide-SiO_2 illustrated in Fig. 17 (p. 272). Data on the faces CaO-'FeO'-SiO_2, MgO-'FeO'-SiO_2 and CaO-MgO-SiO_2 are well documented, Figs. 12 [50] (p. 269); 18 [107] (p. 272) and 19 [50,108] (p. 273). Phase relationships on the front face of the composition tetrahedron in Fig. 17 (p. 272) represented by the system CaO-'FeO'-MgO are known only at 1500°C [50,100,109]. Clearly, this diagram is not only of importance to the behaviour of doloma refractories with ferruginous slags, but also to dolomitic lime reactions with such slags.

2.9.2 Dolomitic lime quality.

Material selection for dolomitic lime production is as important as the specifications required for burnt lime

(sect. 2.7.1. p. 47). In the United Kingdom, the Steetley Mineral Co. Ltd., produce a dolomitic lime product called "Dolomet". A typical Dolomet specification is shown on Table 6 (p. 235). Raw dolomite (dolomitic limestone) is calcined in rotating kilns at a temperature of 1400°C. A small percentage of ferric oxide is added to aid sintering and to stabilise the Dolomet during handling and storage. Bulk densities in the region of 1500 to 1700kgm^{-3} are obtained.

The consequences of adding magnesia to LD slags through dolomitic lime additions may be reviewed under three major headings;

1. Factors that lead to increased lining life.
2. Factors that affect the refining character of LD slags.
3. Factors that lead to savings on lime fluxes.

2.9.2.1 Factors that lead to increased lining life.

(a) The addition of dolomitic lime reduces the chemical gradient between the refractory lining and the slag.

Iyengar et al [76] measured the relative aggressiveness of early formed siliceous slags and found they were dependent upon the initial hot metal silicon and titanium contents. The oxides MgO and MnO reduced the degree of aggression, MnO enhancing the beneficial effect of MgO. It was concluded by van Hoorn et al [74] that the specific aggressiveness of the slag towards the lining was very high in the first 12% of the blow Fig. 20 (p. 273). During the main decarburisation period the specific aggres-

siveness is almost zero but increases towards the end of the blow due to increasing MgO solubility of the slag. A number of possibilities were suggested to reduce the slag aggressiveness towards the lining; (i) control of scrap and charging technique; (ii) timing the end of the blow; (iii) replacement of part of the lime by dolomitic lime.

(b) The magnesia content of the slag alters the iron-oxygen equilibrium such that the iron oxide content is reduced [104].

Limes [95] and Yarashenko [110] considered that iron oxide acts in a corrosive way during slag attack on refractories. The main contribution of iron oxide being the oxidation potential it imparted to slag and how this could effect the carbon within the refractory through oxidation of the carbon to CO. Reducing the oxidation potential of the slag would result in a decrease in carbon oxidation and refractory wear.

(c) The addition of dolomitic lime increases slag viscosity, giving rise to less "washing" of the refractory lining by slag thereby reducing slag penetration into the refractories.

This was believed by Iyengar et al [111] to occur at low basicities. Zarvin and co-workers [112] have investigated the properties of converter slags taken during the beginning, middle and end of the blow during the conversion of low manganese iron. When the MgO content was increased to 14.5 mass%, the viscosity of the slags from the beginning of the blow (3 to 6 mins) increased at any

temperature level within the range 1350 - 1600°C. When the MgO content of intermediate and finishing slags was increased to 4.5 mass%, there was reduction, followed by a sharp increase in the melting point and viscosity. When the MgO content did not exceed 7 to 8 mass% (but above 4.5%), the viscosity of intermediate slags remained below 80mPas at 1400 - 1450°C, Fig. 21 (p. 274). At the Wakayama Works, Japan [113], dolomite is used with returned LD slag to prevent slopping and reduce the fluidity of the slag. Endothermic decomposition of raw dolomite caused the slag to cool whilst magnesia reached supersaturated levels and decreased the slag fluidity. Kaufman and Aguire [114] found that dolomitic lime significantly increased AOD lining life when MgO saturation was achieved at a V-ratio of 1.3 (reducing stage). The formation of highly viscous slags helped reduce refractory wear rate due to the formation of calcium and magnesium silicates and oxides. The system $CaO-MgO-SiO_2$, shown in Fig. 19 (p. 273) was used to discuss the behaviour of AOD slags during decarburisation and reduction at 2900°F (1370°C).

(d) Dolomitic lime acts as a lime flux, increasing the rate of lime solution and reducing the acid slag/refractory contact time [12].

In trial heats reported by Yarashenko [110], slag formation was more rapid with dolomitic lime additions and slopping tended to occur. This latter problem was overcome by reducing the amount of fluorspar charge and lowering the lance 100mm below the level used for normal lime. When dolomitic lime was dissolved, the formation of a

dense dicalcium silicate shell was not observed around lime particles, enabling FeO to flux the lime more readily. Overall MgO dissolution in the liquid phase of the slag has been related to the apparent density of the dolomitic lime [115]. In slags containing 20 mass% P_2O_5, the slag-dolomitic lime interface showed a zone depleted in lime crystals whilst containing coarse MgO crystallites reflecting the lower dissolution rate of the magnesia component of dolomitic lime additions.

(e) Dolomitic lime or magnesia retards dicalcium silicate (C_2S) formation on lime particles [90]. The solid or impermeable structure of the C_2S layer on lime particles may be altered to a more open structure when 5 mass% MgO is added to acid slags [82].

(f) The presence of MgO in the LD slag system within the 5 to 7 mass% range will lower the fusion temperature of the slag and probably decrease its viscosity, accelerating slag development rate [104]

Using a flow-length technique and synthetic slags in air, Green and Quin [12] found that slags with CaO/SiO_2 ratios of 1:1 were very fluid at 1460°C, and MgO additions did not greatly reduce slag fluidity until the magnesia content exceeded 10 mass% MgO. An increase of basicity to 1.8 showed a decreased fluidity which became reduced further by the addition of up to 4.0 mass% MgO. Fluidity increased again with a magnesia content up to 9.2 mass% MgO. Complex variations in fluidity were observed in industrial slags with a V-ratio of 3. The

effects of magnesia upon the viscosities of slags within the system $CaO-Al_2O_3-SiO_2$ has been reviewed and the results are shown in Table 5 (p.234). Comparison has been made with viscosities determined by Bockris et al[45,46] and Bills [47] in simpler systems. The blast furnace slag system $CaO-Al_2O_3-SiO_2$ has much higher viscosity values than those slags containing FeO (sect. 2.5.2. p.38). The high silica values are largely responsible for this effect. Yakushev et al [116] has explained the reduced viscosities of slags with increased MgO contents of 4 to 12 mass% as being due to an increase of relatively small Mg^{2+} cations producing small units of viscous flow. As the MgO content rose, the liquidus temperature correspondingly decreased. For magnesia contents of 10 mass% MgO, there is good agreement between Machin [117], Majercak [118] and Hofmann [119] in slags of similar compositions at 1500°C (Table 5, p.234). Below 1500°C, the results vary quite markedly in the few cases where values have been recorded.

(g) Improved foaming of the slag favours steelmaking reactions as well as filling a larger volume of the vessel leading to more even refractory wear (Dr. J. Quin, private communication).

(h) Due to quicker slag formation with dolomitic lime additions, the final FeO contents of the slag tend to be lower so that metal yield is increased and lining wear reduced.

This effect has been observed by Yaroshenko [110], and Snyder [104] has commented on the fact that high MgO

slags are not as oxidising as lower MgO slags with the same FeO levels. Magnesia is, therefore, presumed to act as a neutraliser of some portion (excess) of the FeO in the slag.

2.9.2.2 Factors that affect the refining character of LD slags.

(a) Difficulties in meeting sulphur specifications have been reported when dolomitic lime was added to LD slags [120].

With the dolomitic lime practice, averaged MgO contents were 8.5 mass% as opposed to 2.8 mass% MgO for slags using a straight calcitic lime practice. A regression analysis of 19 variables was compared with the sulphur removal ratio for both types of slag practice. The results indicated that dolomitic lime charges used in place of lime showed a lower frequency of good desulphurisation performance. High magnesia slags were apparently detrimental to sulphur removal because of high slag viscosity and the lower desulphurising potential of MgO relative to CaO. However, several plants [111, 112, 113, 121] have reported that despite an increase in slag MgO, analysis of data revealed no evidence that desulphurisation was adversely affected within the particular slag practices. Replacement of part of the lime charge by dolomitic lime and subsequent decrease in CaO content of slags improved desulphurisation between 5 and 12% [112].

(b) LD-AC shops with high phosphorus hot metal (1.8 to 2.0 mass%) have reported loss of efficiency in phos-

phorus removal [104].

Plant trials at Nippon Steels Kimitsu Works in Japan [122] involved three steps according to dolomitic lime consumption.

(i)	1st step	5 to 7kg/tonne steel	3 mass% MgO in slag.
(ii)	2nd step	13 to 15kg/ " "	5 to 6 mass% MgO in slag.
(iii)	3rd step	20 to 40kg/ " "	7 - 8 mass% (MgO saturation).

With steps (i) and (ii) no change was recorded with dephosphorisation levels but with step (iii), end point phosphorus had a tendency to rise. This effect again confirms the thermodynamic relationship that MgO is less basic than CaO. At South Works, Chicago, Illinois, dolomitic lime schedules ranging from 14 to 36kg/tonne steel produced no change in end point dephosphorisation [122]. However, slag handling became more critical with increased amounts of dolomitic lime. Slag within slag pots set if they were not dumped promptly into the receiving slag yard. Slags supersaturated in MgO [113] were found to have a decreased dephosphorising effect partly due to the decrease in fluidity of the slag. High carbon heats have also reported problems with phosphorus targets when using high dolomitic lime charges [104]. Reducing or modifying the amount of dolomitic lime charged overcame many of the dephosphorisation problems, whilst still achieving high refractory life and good slag control. The dolomitic lime trials carried out by Obinata [121] at the Kimitsu plant in conjunction with a sub-lance system and programmed gun-

ning maintainance produced a lining life of 5035 heats in an LD vessel lined with magnesia refractories. The refractory consumption was calculated to be 1.25kg/tonne steel.

2.9.2.3 Factors that lead to savings in lime fluxes.

The apparent ability of magnesia to flux lime, modify, or even depress the formation of dicalcium silicates around lime particles, has meant that the amounts of fluorspar and other fluxes can be substantially reduced. Under identical metallurgical conditions it has been established that the addition of dolomitic lime or "Dolomet" to slags reduced the consumption of fluorspar by 30 to 60% (12, 110). In Japan, fluorspar additions have been totally replaced by dolomite or dolomitic lime additions

2.10 Conclusion.

The major benefit of dolomitic lime additions to LD steelmaking slags has been to radically improve the lining performance of magnesia or doloma vessel refractories by reducing the chemical gradient of MgO between the refractory and early formed slags in particular. Lining performances have been improved by at least 30% using the modified slag practice. In the United Kingdom, current levels of dolomitic lime usage are between 18 and 20kg/tonne of steel. The aim of the dolomitic lime practice is to attain a saturation level of between 6.5 and 8.0 mass% MgO in the turndown slag, and additions are made at the beginning of the blow. A large number of factors

are reported to be responsible for extending lining lives and in some cases the reasons given are contradictory. As a consequence of the hot metal chemistry and lining practice, there is no universally applied dolomitic lime charge practice throughout Europe, North America and Japan.

The inhibiting effect of dicalcium silicate formation on lime dissolution in the LD has been widely studied and the mechanism and dissolution kinetics well documented. In contrast, dolomitic lime studies are based upon works practice experience and no fundamental studies of the mechanism and kinetics of dissolution are reported. There is a lack of understanding of how dolomitic lime behaves as a lime flux and how magnesia in early-formed LD slags affects the viscosity and fusion temperature of the slag. It is within this fundamental context that the dissolution of dolomitic lime in iron silicate melts should be studied, and then related to the industrial situation.

3. Experimental Work.

3.1 Starting Materials.

A major part of the study involved in this work was to simulate the effect of dolomitic lime additions on melts of compositions similar to those formed during the early part of an LD blow. To allow comparison to be made with commercially available slag additives, samples were taken directly from the raw materials sources described below and prepared in the laboratory.

3.1.1 Dolomitic Limestone.

Raw material samples were taken from an occurrence of high purity, massively bedded dolomite currently mined by opencast methods at Whitwell near Worksop, Nottinghamshire, by the Steetley Group of Companies. Outcrops of Lower Magnesian Limestone were represented by Thuringian Series lithologies of Permian age [123]. The succession has been regarded as a secondary diagenetic deposit after calcite, permeated by magnesian solutions [123]. From the nomenclature proposed by Pettijohn [124], the dolomite formation may be classified as a dolomitic limestone comprised of 10 to 50% magnesium carbonate ($MgCO_3$) and 50 to 90% calcium carbonate ($CaCO_3$). The crushed and screened material may be calcined in rotary kilns at temperatures ranging from 1400 to 1700°C. One particular end product is currently sold to the steel industry as a slag additive or conditioner under the brand name "Dolomet".

3.1.2 Limestone.

Limestone samples were taken from a deposit of very pure Carboniferous Limestone mined at Dowlow near Buxton, Derbyshire, by the Steetley Company. Calcitic lime is produced for the steelmaking industry on this site by calcination of the crushed limestone in oil-fired rotary hearth kilns, at temperatures of 1200 - 1220^{o}C.

3.1.3 Sample collection.

Approximately 100kg of dolomitic limestone was taken from the primary crusher dump at the Whitwell mine and 50kg of limestone from the secondary crushing conveyor at Dowlow. Pieces within the size range 100mm by 80mm by 80mm were selected. Fragments which had obvious joint planes or solution cavities were disregarded; apart from this element of selectivity, the samples collected were representative of normal production.

3.1.4 Sample preparation.

Chip samples were taken from each rock piece and combined to give approximately 10kg of dolomitic limestone sample and 5kg of limestone sample. The pieces were washed to remove mud, and air dried for two days. A clean, dry, iron mortar and pestle were used to crush the rock samples to produce a minus 20mm fraction. A series of passes were made through a sample riffler to yield sufficient material for 600g of powdered dolomitic limestone and limestone. The retained fractions were care-

fully impacted and ground to produce two -300μm fractions. A hand magnet failed to detect any iron contamination. From each of the two fractions, approximately 150g of material was retained for chemical analysis by coning and quartering. The remaining fractions were retained for powder density tests. The smaller 150g samples of dolomitic limestone and limestone were recrushed to pass a 106μm sieve, and the portions analysed. Results of dolomitic limestone and limestone analyses are indicated in Tables 6 and 7 (pages 235 and 236). A typical "Dolomet" specification has been included in Table 6 for comparison.

In the present work, cylindrical samples were cut from natural dolomitic limestone and limestone, prior to calcination, using a diamond crown, single tube core barrel manufactured by Diagrit Tools, Stapleford, Kent. Water was used as the lubricant/coolant and recycled by a reservoir-pump system located at the base of the drilling unit. A water swivel and the attached core barrel were located into and driven by a "Pacera" drill head. The dimensions of the drilling table restricted the sample size to approximately 100mm by 100mm. The cored cylinders were checked visually for solution cavities or joint planes then cut to length on a "Mottacutta" horizontal diamond saw (Cutrock Ltd). The final length dimension was achieved by facing the ends on 240 grade silicon carbide paper. The finished cylinder size was 32mm in length and 15mm in diameter. The cylinders were washed in distilled water and stored in a drying oven at 110°C until required. Pill-test samples were cored with a 30mm diameter core barrel and were 40mm

high.

3.2 Synthetic slag preparation.

To model the slags formed during the early part of an LD blow, slag compositions corresponding to those intersected by the fayalite ($2FeO.SiO_2$) - dicalcium silicate ($2CaO.SiO_2$) tie line of the CaO-'FeO'-SiO_2 system were prepared, Fig. 22 (p. 275). Compositions ranged from an iron silicate base melt (fayalite) to a 32 mass% lime - fayalite. Advantage was taken of the low liquidus temperatures existing up to the composition of 38 mass% lime in fayalite (1205-1300°C).

Iron silicate base melts (fayalite) were prepared from BDH - grade calcined ferric oxide (>97 mass % Fe_2O_3), electrolytic iron powder (-320μm) and precipitated silica (SiO_2) according to the reactions;

$$Fe_2O_3 + Fe \rightleftharpoons 3FeO \qquad (3.1)$$

$$2FeO + SiO_2 \longrightarrow 2FeO.SiO_2 \qquad (3.2)$$

For synthetic slags containing lime (CaO), Analar-grade calcium carbonate (>99 mass % $CaCO_3$) was used on a gram equivalent basis and the gram molecular weights of reactants in (3.1) and (3.2) were adjusted to yield the required lime content. Analar grade "heavy" magnesia (MgO) was added directly to the base iron silicate and lime-iron silicate melts and the mixed powders re-melted.

Bulk synthetic slags were initially melted in an Electroheating, 15kW high frequency induction furnace and contained within a carbon crucible which acted as the

susceptor. Since iron oxide may also be considered as a part of the Fe - O system [50], the furnace atmosphere was controlled by 99.99% pure argon at a flow rate of 0.5ℓ/min to maintain a low oxygen partial pressure. The argon-rich atmosphere was maintained throughout the heating and cooling period.

The cooled melt was removed from the carbon crucible and allowed to fall onto a 10 mesh B.S. sieve. This prevented possible carbon contamination which could be brought about by the abrasive action of the chilled broken melt on the crucible wall. Only 100g of fused melt could be produced at any one time. The 100g batches were later combined to produce a bulk sample. The magnetic fractions of the melt were removed with a hand magnet at various stages of crushing. The final fraction was crushed to pass a 106μm sieve, any oversize material being ground in a "Morrice" mechanical mortar with agate components. Any remaining magnetic material within the -106μm fraction was removed with a hand magnet. The processed sample batch was thoroughly mixed on a W.B.A. (Glen Creston) Turbola mixer. A representative sample was derived by the cone and quarter technique and sent for analysis. The analyses of all melts used in the experimental work are given in Table 8 (p. 237) and also plotted on Fig. 22 (p. 275).

3.3 Experimental equipment.

The requirements of a high temperature experimental furnace were regarded as follows:

(i) The furnace should have an extensive stable hot zone with minimal temperature variation within the hot zone.

(ii) It should be capable of being driven to high temperatures rapidly (1600^{o}C) for extensive periods of time.

(iii) The vertical working tube should be of sufficient length to facilitate sample access from either above or below.

(iv) The furnace atmosphere should be readily controllable.

The furnace used by Green [80] and Edwards [125] was selected for viscosity and rotary dissolution experiments because it fulfilled the above criteria. The furnace used by Ojeda [126] was chosen for static immersion experiments because it possessed the above characteristics and also a 1.5m long working tube that enabled melts to be quenched rapidly under an inert atmosphere. A Carbolite muffle furnace, capable of reaching temperatures of 1600^{o}C was used for calcining cylinders of dolomitic limestone and limestone. A purpose built furnace (Carbolite, Sheffield) was also used to determine the dissociation characteristics of dolomitic limestone and limestone by differential thermal analysis.

3.3.1 The furnace used in viscosity and rotary dissolution experiments.

The working tube was made from a 1.0m long and 47mm internal diameter aluminous porcelain cylinder supplied

by Morgan Refractories. The working tube was heated by a helical Crusilite element sheath. Temperature control was operated by a thyristor drive Amalgams Eurotherm controller and temperature recorded by a Pt - Pt/13%Rh thermocouple. Water cooled aluminium sheaths supported the upper and lower ends of the working tube and each end was sealed by compressing an inset rubber "O" ring between an aluminium disc or gas seal bolted to the support sleeve.

3.3.2 The furnace used in the static immersion experiments.

The working tube was 1.5m in length with an internal diameter of 44mm and was made in recrystallised alumina (Morgan Refractories). The furnace, (Carbolite Limited) had provision for vacuum conditions. The heating elements consisted of four equi-spaced vertical "Super-Glo" bars and the temperature was controlled by a Carbolite controller and a Pt - Pt/13%Rh thermocouple. The lower gas seal could be swung rapidly out of the way to facilitate external quenching operations.

3.3.3 The cone fusion furnace.

A furnace was constructed in a similar manner to the viscometer furnace described in section 3.3.1, except that the furnace was arranged with a horizontal axis. A 900mm long aluminous porcelain tube (Morgan Refractories Ltd) of 54mm outer and 46mm inner diameter, was used as the working tube which was supported at either end by stacked insulation bricks. A helical "Crusilite" silicon carbide

element (Morgan Electroheat Ltd) was used as the heating source. Water-cooled aluminium end sleeves were fitted to either end of the working tube and arranged to allow entry and exit of an argon atmosphere (99.999% purity). One of the two end gas seal plates was modified to take a tinted green glass observation window. The window used was a lens obtained from a pair of foundry goggles. The other end plate was drilled to provide access for a Pt - Pt/13%Rh thermocouple which was fixed into position internally at the centre of the hot zone of the working tube.

3.3.4 The Viscometer.

3.3.4.1 Outline of viscometer theory.

Langhammer and co-workers [127] have reviewed a selection of methods for measuring slag viscosities. The majority of measuring devices described, operated on a rotation principle and enabled shear stress and shear rate measurements to be compared at some fixed position such as the boundary formed by a container wall. The following assumptions have to be made in order to arrive at the fundamental equations used in the theory of rotational viscometry [128]:

a) The liquid is incompressible.

b) The motion of the liquid is laminar.

c) The streamlines of flow are circles on the horizontal plane, perpendicular to the axis of rotation.

d) There is no slippage between the contents and the cylinder.

e) The system is isothermal (within experimental limits).

f) The motion is two dimensional.

For a coaxial configuration [128]

$$\mu_N = \frac{M}{4\pi h \Omega \ell}\left(\frac{1}{R_b^2} - \frac{1}{R_c^2}\right) \qquad (3.3)$$

where;

μ_N is the viscosity for Newtonian flow

M is the torque

Ω is the angular velocity

R_b is the radius of the measuring bob

R_c is the internal radius of the crucible

h is the height of the bob

ℓ is the distance between the base of the crucible and the base of the bob.

True or Newtonian fluids obey the relationship that shear stress is directly proportional to the rate of shear. Newtonian viscosity is independent of shear rate and only one viscosity value is required to fully characterise a Newtonian fluid. If a fluid is chosen of known Newtonian behaviour and viscosity at defined temperatures, then for a given viscometer dimension;

$$4\pi h\ell\left(\frac{1}{R_b^2} - \frac{1}{R_c^2}\right) = K \qquad (3.4)$$

can be applied, where K is an instrument constant such that

$$\mu_N = \frac{KM}{\Omega} \qquad (3.5)$$

This calibration technique has the advantage of including

all the end and edge effects, slippage and turbulent interferences etc, and allows calculation of apparent viscosity directly from the raw data.

3.3.4.2 Units of Viscosity.

A fluid, theoretically divided into endless thin layers will tend to move against adjacent layers under the influence of an external force [39]. The proportion of the force and size of the contact surfaces of the two adjacent layers, would give rise to a shear stress, expressed in Newtons per metre squared (Nm^{-2}) units or pascals (Pa). The difference in velocity of both layers, divided by their distance will represent the shear rate. The shear rate may be expressed as a velocity (Ls^{-1}) divided by a distance (L) to yield units of the reciprocal second (s^{-1}).

The ratio: $\frac{\text{shear stress } (Nm^{-2})}{\text{shear rate } (s^{-1})}$ = viscosity (Nsm^{-2} or Pa.s)

The centipoise (cP) is the most common unit tabulated for viscosity values in the general literature, and is taken to represent the viscosity of water at 17.7°C [129]. The viscosity quoted in cP for any particular substance is, therefore, an indication of that substance's viscosity relative to that of water. The cP is equivalent to a milli-Newton second per metre square unit ($mNsm^{-2}$) which can be represented as a milli pascal second (mPa.s) unit in the current S.I. system of units.

3.3.4.3 The commercial Viscometer.

There are two variations of rotating viscometers currently available commercially. In one type, the inner cylinder is stationary and the outer cylinder or crucible is rotated. In the second type, the outer cylinder (crucible) remains stationary and the inner cylinder is caused to rotate. The Haake Rotovisko RV1 was used in conjunction with the second component configuration to determine the melt viscosities described in this work. The Rotovisko is manufactured by Gebrüder Haake K.G., West Germany, and franchised by Baird and Tatlock, Chadwell Heath, Essex. The apparatus comprised of a motorised drive unit and recorder cabinet, an attached drive cable and a detachable measuring head.

The system was driven by a synchronous motor with integral gear box and stabilised power supply. The speed of rotation could be instantly varied by means of a 10-speed gear box, making possible checks on the consistency of shear and hence Newtonian or non-Newtonian behaviour (section 3.3.4.1, p. 79). Red-coloured numerals on the gear positions indicated the reciprocal of the true speed at 50 cycles A.C. e.g.

Speed (r p m)	Reciprocal Speed factor (U)
27	18
54	9
81	6
162	3
243	2
486	1

Measurement of viscosity was taken from the resistance to rotation caused by the sample material. The measuring head converted the torque into an electrical value which was proportional to the angle of displacement. Conversion was accomplished through torsion dynamometers which consisted of two coaxial shafts, coupled mechanically by a creep resistant torsion spring. The angle of displacement of the spring yielded a measure of the transmitted torque. Conversion of the torque angle into an electrical resistance was accomplished by a potentiometer mounted on the upper shaft of the dynamometer. A wide range of torque forces could be measured using the dual measuring head. A simple toggle switch on the measuring head altered the torsion system from 50gcm to 500gcm. Scale readings derived from the latter switch position required a multiplication factor of 10.

The flexible Bowden cable facilitated mechanical and electrical connections between the measuring head and the control cabinet. The electrical signals produced through torque measurement were indicated by the deflection of a knife edge needle across the face of a mirror scale on the control cabinet, graduated from 1 to 100 units. Scale readings were recorded as S-values. Viscosity measurements were interpolated by recording the rotational speed (U-value) and the scale (S-value). A constant, K (equ.3.4 p. 80) was determined for the crucible and measuring bob assembly such that

$$\text{viscosity } (\mu) = U \times S \times K \qquad (3.6)$$

The viscometer furnace was incorporated within a dexion framework and bolted to the viscometer support housing, to form a large, stable, unit. Provision was also made for an external measuring head support stand to allow calibration determinations to be made without dismantling the furnace head assembly. The assembled viscometer and furnace are shown in Plate 1 (p.307).

3.3.5. Crucibles.

3.3.5.1 Crucibles used in immersion tests.

The melts used in the static and rotary immersion tests were contained in iron crucibles (0.06% Carbon by mass), 40mm in diameter and 40mm high; supplied by Alfred A. Brown, Sheffield.

3.3.5.2 Crucibles used in viscosity determinations.

Ingots of "Swedish Iron" were purchased from BSC Swinden Laboratories and rolled into 40 and 28mm diameter bar stock by BISRA. A full analysis of the stock iron is given in Table 9 (p. 237). The bar stock was machined to produce 100mm high crucibles with an internal depth of 65mm and internal diameter of 32mm. The narrower stock was used to make measuring bobs.

Zirconia crucibles were purchased from Zirconal Ltd., Cosmos House, Bromley Common, Bromley, Kent and were manufactured from fine grain, slip cast, calcia-stabilised zirconia. The crucibles were 78mm high and had an interior depth of 74mm and internal diameter of 32.5mm.

3.4 Experimental Procedures.

3.4.1 Temperature Profiles.

Experimental conditions were established for temperature profile measurements on both vertical tube furnaces. The viscometer furnace was allowed to stabilise for 3 hours at 1400°C under an argon flow rate of 1.5ℓ/min. A sheathed Pt - Pt/13%Rh thermocouple was marked off in 20mm divisions to correlate the temperature profile with the working tube length. Working tube temperatures were recorded by a Cambridge Instruments potentiometer and the ambient temperature noted. The thermocouple was lowered through the hot zone and the temperature recorded at each 20mm division. A reverse profile was obtained to confirm the previous measurements and the temperature found to vary by approximately 2.5°C. A similar procedure was adopted for the Carbolite furnace. The recorded values differed by approximately 40°C from those recorded by the furnace controller thermocouple.

The viscosity-rotary immersion furnace was found to have a short linear hot zone 45mm long with a 5°C variation. A 10 and 20°C variation existed over 60 and 100mm respectively. The hot zone profile for the viscometer furnace is illustrated in Fig. 23 (p. 276), where the distances below the top gas seal are given in millimetres. The results of the temperature profile influenced the choice of dimensions for the crucible and measuring bob assembly, which are shown figuratively in relation to the

profile. The Carbolite furnace, shown diagrammatically in Fig. 24 (p. 277) had a linear hot zone 60mm long with 2.5°C variation and 105mm long with a 10°C variation. The temperature profile of the cone fusion furnace was measured under an argon flow rate of 0.8ℓ/min in a manner similar to that described for the Carbolite and viscometer furnaces. The centre of the hot zone was 455mm from the viewing window and with the gas seal plate in position, and 420mm with it removed. The temperature variation of the hot zone was 5°C over 40mm and 10°C over 55mm. A photograph of the cone fusion furnace is illustrated in Plate 2 (p. 308) and the hot zone profile in Fig. 25 (p.278).

3.4.2 Viscometer component materials.

The primary limitation for the measurement of viscosity was found to be the unavailability of suitable materials for parts of the viscometer in contact with the molten slag or melt. Any component had to be chosen on the following criteria (130);

(a) It must be machinable or reproducible to exact dimensions.

(b) It must remain inert to chemical attack from the slag.

(c) It should be a readily available material.

(d) The cost of the components should not be prohibitive to their use.

The highly reactive nature of FeO-rich melts prevented the use of alumina which even when present in low concentrations can form a low melting point compound of

wüstite plus spinel at 1330°C [50]. In the presence of FeO, platinum may form platinum-iron alloys and this relationship has been successfully utilised on a small scale to prohibit the interchange of Fe^{2+} and Fe^{3+} ions between the melt and the alloyed container [131]. However, the high cost of platinum and possible use of molybdenum components could not be reconciled with the relatively low temperatures under consideration (1100 - 1450°C).

Iron had been successfully used by Kozakevitch [51] and Clixby [132] and was selected as the component material since it not only fulfilled the manufacturing and resistance to slag attack prerequisites, but was readily available and economic to use. The temperature ranges measured during the viscosity experiments were well below the melting point of iron (1553°C).

Zirconia crucibles were used on a trial basis since they could overcome the temperature limitations imposed by the iron crucibles.

3.4.3 Choice of crucible dimensions.

The initial crucible and measuring bob dimensions were based upon those arrived at by Pratt [133]. The original iron crucible and bob sizes are illustrated, with the modified forms in Fig. 26 (p. 279) and Plate 3 (p.309). The long shank of the earlier measuring bob version was found to distort at high temperatures and was consequently made as short as possible. The crucible height was reduced to ensure that all of the liquid melt, the crucible

base and the measuring area of the immersed bob remained within the demarcated 10°C variation in Fig. 23 (p.276). Zirconia crucibles were selected with internal dimensions similar to those of the iron crucible (32mm). A 22mm and 25mm diameter measuring bob was manufactured for experimental trials. The length of the bob measuring surface was set at 35mm and the bob was recessed to remove end effects during viscosity measurements. The hollow end also allowed rapid temperature equilibration to be achieved between the bob and 'melt'. Both crucible types were loaded with 65g of powdered fused synthetic slag which provided a 10mm clearance between the bob end and crucible base when the bob was immersed to the full 35mm depth. The annular clearance between the 25mm and 22mm bob was 3.5 and 5mm respectively.

3.4.4 The viscometer shaft and air bearing.

Edwards [125] and Pratt [133] had attempted to use an 8mm stainless steel rod as a support shaft for the earlier types of measuring bob. A universal coupling was placed towards one end of the rod, effectively breaking it into two unequal lengths. The rotating assembly coupled to the rod was complicated by an oil filled-gas seal cup system, which produced high inherent friction and drag, and gave rise to large scale readings during rotation. These problems were overcome by using a solid 11mm diameter, centre ground stainless steel shaft attached to an air driven bearing which was located 100mm from one end

of the shaft and attached by grub screws. The air bearing was fabricated from aluminium and was based upon a modified design which was used by Baker [134] and Clixby [132], Plate 4 (p.309). A universal coupling was attached to a machined stub at the upper end of the shaft and to the measuring head stub. This helped to overcome any mis-alignment along a vertical axis between the gas seal entry port and the measuring head. The outer case of the bearing was clamped by four adjustable screws tapped into a cast aluminium block and supported from the rack down measuring head carrier, by 5mm thick angle iron supports and a stable coaxial configuration resulted, Plate 5 (p.310). Lateral adjustment of the bearing within the clamp allowed the vertical attitude of the shaft to be altered when required. The upper gas seal entry port was reamed to a diameter slightly larger than that of the shaft, to facilitate access and prevent rubbing. A periscope attachment enabled alignment and correct immersion depth of the bob to be made visually during operation. Detail of the viscometer shaft and method of attachment to the measuring bob are illustrated in Figs. 23 and 26 (pages 276 and 279). Argon was introduced through the base of the furnace to provide a positive pressure inside the working tube and prevent oxidation of the slag and iron components. An argon flow rate of 1.5l/min was found to be more than adequate in preventing the possibility of oxidation without affecting the thermal profile.

3.4.5 Crucible support stand.

Two lengths of aluminous porcelain tubing were used to support the iron and zirconia crucibles. At high temperatures, the iron crucible reacted with the aluminous porcelain tubing causing incipient melting of the crucible base. Graphite holders were fabricated from electrode carbon (Acheson Electrodes) to support the stub-like base of the iron crucible and to contain the flat base of the zirconia crucible. Details of the two types of holders, their dimensions and assemblies are shown in Fig. 27 (p.280) and Plate 6 (p. 311). The datum line for the crucible base was set at 495mm from the top of the gas seal (Fig. 23 p. 276). The aluminous porcelain support was 450mm long and 30mm diameter, for the iron crucible, and 490mm long for the zirconia crucible support assembly. Prior to the introduction of either crucible support assembly through the base of the furnace, the lower end of the support tube was slot-cut on a diamond saw and located onto a protruding boss which formed a part of the lower gas seal. Two locating pins set into the boss prevented the slotted support tube from rotating. Air dried C60 cement was used as a fixative. The crucible base datum line was consistently within a $\pm$ 2mm limit when the crucible support stands were fully assembled. A suspension of zirconia (Analar grade) in alcohol, was liberally smeared over all contact points to prevent the diffusion of carbon into the base of the iron crucible, at high temperature. Air dried C60 cement was used to cement the crucibles into position.

3.4.6 'Melt' temperature measurement.

A hole was drilled to within 5mm of the interior of the base of the iron crucible and a Pt - Pt/13%Rh thermocouple positioned to permit measurement of 'melt' temperatures. Access to the crucible base was made via a hole in the gas seal base and through the support tube and carbon holder, Fig. 23 (p. 276). The support tube was isolated from the atmosphere at the lower gas seal by Apiezon sealing compound, which also served to hold the thermocouple in place. A zirconia film prevented direct contact between the thermocouple and iron crucible. When using the zirconia crucible, the thermocouple was allowed to touch the base and was only 3mm from the molten melt-crucible base interface. The thermocouple, support tube and crucible, plus sample were assembled together before positioning them within the furnace.

3.4.7 Compressed air supply.

The air bearing was operated from a mains compressed air supply of 0.5MPa (75lb/in^2). The normal air bearing operating pressure was 0.15MPa (22lb/in^2) which was dependent upon the clearance between the main body of the bearing and the two fixed "pads" which enabled the mass of the viscometer shaft and bob to be supported in frictionless conditions. The air was exhausted through three radial arrays of holes drilled into the main body of the bearing from above and below, Plate 5 (p. 310). Two Norgren filters placed in series between the air on/off valve and

pressure gauge prevented particles of solid material and moisture from affecting the running efficiency of the bearing, Plate 7 (p. 311). A flexible high pressure hose attached to the air bearing enabled a large degree of manouverability to be achieved whilst positioning the viscometer shaft assembly.

3.5 Determination of the Calibration constant (K).

The calibration constant (K), for any crucible and measuring bob geometry, may be calculated utilising expression 3.6 (p. 83), and an oil of known viscosity from the relationship;

$$K = \frac{\mu}{S \times U} \qquad (3.7)$$

Where K is the calibration constant, μ the viscosity at a particular temperature and S and U, scale and speed values respectively.

Glycerol was initially used as the calibration oil and Newtonian behaviour was assumed. A sample of glycerol was sent for analysis to determine the weight percent water content and was found to have 0.912% water (99.08% glycerol). Using data for glycerol viscosities [129], a series of temperature-viscosity curves were constructed over the temperature range 20 to 30°C, Fig. 28 (p. 281). These enabled an estimate of glycerol viscosity to be made at temperatures which deviated from those point temperatures specified in the data [129]. The viscometer shaft and measuring head were assembled in the external head support and the crucible partially immersed within

a constant temperature bath. A 10mm clearance was maintained between the bottom of the measuring bob and the base of the crucible, and glycerol carefully added until the meniscus stabilised at the top of the bob. Results were recorded at average temperatures of 20, 25 and 30°C using a mercury thermometer. The water bath temperature was controlled by a Gallenkamp Thermo Stirrer TM860. A second series of runs was carried out with the crucible and bob assembled within the furnace, under simulated operating conditions. The values of measurements taken under both experimental conditions are tabulated in Tables 10 and 11 (pages 238 and 239). Strict temperature control of the glycerol contained within the furnace was problematic, but essential. Temperatures were, therefore, recorded immediately before and after measurement and the averaged temperature value used to obtain the viscosity of glycerol, Fig. 28 (p. 281). It was found that when immersing the bob to within 2mm of its overall length of 35mm, or submerging the total length of the bob by an extra 2mm, a variation in viscosity of 3.5% was recorded over that determined for the correctly immersed depth.

Rotational speed, multiplied by the scale value gave very similar totals at each specific temperature and confirmed the Newtonian behaviour, Tables 10 and 11 (pages 238 and 239). The crucible constant (K) would only be valid for Newtonian behaviour in other fluids. The results of viscosity values recorded on other fluids, such as liquid melts, would therefore be apparent viscosity measurements only.

An averaged arithmetical mean calibration constant was calculated from the results in Tables 10 and 11 (pages 238 and 239). The results were 8.692 for the 22mm diameter bob and 4.808 for the 25mm diameter bob. Initial high temperature work indicated that the 22mm bob was too insensitive with regards to the viscosity measurement on the melts studied. Consequently, the 25mm diameter bob was used in all subsequent viscosity experiments. The calibration constant, K = 4.808 was used for the iron crucibles until the value was checked against a known Newtonian fluid. The standard deviation of the constant was calculated to be $\pm$ 0.454 or 9%.

3.5.1 Re-determination of the calibration constant.

The viscosity of glycerol was found to be approximately ten times as great as viscosity values recorded for some of the melts. A Newtonian oil (purchased from Haake) was used to confirm the calibration constant. The Haake E200 oil had a viscosity of 156.3 mPa.s at 20.00^{o}C and was equivalent to some of the melt viscosity ranges recorded during the studies.

During melt viscosity determinations, the scale reading was initially zeroed using a rotation speed of U = 3 just prior to immersion of the measuring bob. Adjustment was facilitated by an electrical zero control screw on the motor console. In general, scale readings were ignored during actual measurement if their values fell below 10 units on the mirror scale, because there

was little equivalence of U x S values with varying rotational speed. Equivalence values were restored at low scale readings using the E200 oil and by adjustment of the electrical zero control screw. Scale sensitivity was found to have increased slightly overall. Re-determined values of the calibration constant for iron crucibles are illustrated in Table 12 (p. 240). All viscosity determinations were recorded with the head switch in the 50gcm position. Equivalence of values taken at both head switch positions are illustrated below Table 12.

Compared to the original constant, the new constant of 4.589 differed by only 4.8%. Since most of the viscosity readings at high temperature were achieved when U = 1 in iron crucibles, the old constant of 4.808 was retained for the previously determined melt viscosities. The original, lower sensitivity scale values were compensated for by the slightly higher constant.

3.5.2 Determination of the zirconia crucible constant.

The zirconia crucible constant was determined with the Haake E200 oil under the same conditions used for the iron crucibles in the external head assembly. The values of the constant at a particular rotational speed are shown in Table 13 (p. 240). The discrete constant value for a particular rotational speed was used in the plotting of melt viscosity-temperature curves rather than an averaged value. The variation between the constant (K) recorded at U = 1 and U = 3 was 3.8%.

3.6 Viscosity measurement procedure.

The crucible support stand assembly was introduced through the base of the furnace and centred within the working tube by viewing from the top, with the upper gas seal removed. A pliable "O"-ring allowed a small degree of centering adjustment to be made through differential tightening of the lower gas seal retaining bolts. The thermocouple leads were attached to the potentiometer and the instrument checked for correct operation.

3.6.1 Introduction of the viscometer shaft.

The rack-down head support clamp and air bearing carrier were screwed back into the upper position. The air bearing shaft was passed through the air bearing support block and negotiated into the upper furnace gas seal which remained unfastened. The measuring bob was located onto the shaft and secured by pushing the iron pin through the alignment holes. The assembly was lowered back into the furnace and the main body of the air bearing clamped by the four retaining screws. The universal coupling was attached to the stub on the air bearing shaft with a small bolt. The detachable measuring head was seated into the head support bracket and into a female section of the universal joint. A small bolt was used to secure the joint to the stub.

3.6.2 Furnace heating sequence.

Argon was allowed to flow through the furnace over-

night, after the upper gas seal had been bolted into position. The flow rate used was in the order of 300ml/min. The inert gas was passed through magnesium perchlorate crystals, contained within a U-tube, before entering the furnace at the lower gas seal support sleeve, Plate 7 (p.311). The drive or Bowden cable was not attached to the viscometer measuring head at this stage. The cooling coil water was switched on and all connections checked. The Eurotherms controller was adjusted at a rate of 5°C/minute for the first 500°C, to allow the working tube to warm up steadily. The rate was increased to 15°C/minute until the required temperature was obtained. This normally took between 2.5 and 3 hours, as opposed to 6 to 8 hours at the lower heating rate.

3.6.3 Alignment of the viscometer measuring bob.

Compressed air was fed to the air bearing at a pressure of 0.15MPa and the shaft centred with respect to the crucible by viewing through the periscope set into the upper gas seal. The shaft assembly was lowered using the rack-down mechanism until the bob was judged to be just above the liquid melt surface. Approximate liquidus temperatures were obtained from phase diagram data (50, 108) and temperatures of 50 to 100°C above these were used, to allow the bob to be immersed. Melts which contained magnesia were re-melted at 1300°C in an argon atmosphere, cooled and re-crushed to -350μm before being used. Melts containing 7.5^{w}/o MgO were liquid at 1300°C and no evidence of undissolved melt or magnesia was found in polished

samples. The bob was left above the melt surface for 1 hour, to equilibrate with the crucible and melt temperature. The drive cable was attached to the measuring head and the bob rotated at low rotation speed. Experience showed that at such low speeds, drag effects on the gas seal resulted in the scale needle oscillating. The whole working tube was carefully manoeuvred until the scale reading became zero. The bob was then immersed to the full 35mm depth. The 10mm clearance between the completely immersed bob and the crucible was worked out in a cold furnace under simulated operating conditions. A scale marked on the rack-down mechanism could be constructed for every run and the bob wound down to the particular level indicated. The bob was allowed to equilibrate with the melt for a further 30 minutes. The Bowden cable was disconnected and the air bearing shaft turned by hand to check that the bob was not hitting the side of the crucible. The drive cable was re-attached and the first reading taken and the time recorded. Temperatures were checked with the potentiometer at regular timed intervals prior to and after a viscosity reading. Viscosity measurements were taken every twenty to thirty minutes, depending upon the selected temperature increment from the previous level. Results were recorded on sheets in a manner similar to the temperature-viscosity values reported in Section 4.1, (p.116). Decreasing and increasing temperature runs were made to check the consistency of viscosity values with time. The measurement operations took between seven and eight hours to complete.

3•6.4 Alignment problems.

It was difficult to achieve the alignment of the viscometer bob, to produce a concentric configuration within the crucible, with every run. At high temperatures, the iron components tended to weld on impact and the run had to be aborted. The use of a zirconia crucible and an iron bob did not lead to these problems and a result was obtained every time.

3.7 Immersion, experiments.

All immersion experiments were carried out at I300°C as this represented the average hot metal and early formed slag temperatures at the initial stages of an LD blow [27]. The compositional range of melts in Table 8 (p. 237) melting points below 1300°C. The partial pressure of oxygen has been reported to range from 10^{-9} to 1 atmosphere in an LD vessel, whilst ferrous oxide is only stable below 1CT6 atmospheres (^0)^ ^o retain ferrous oxide as a phase, crucible and immersion tests were carried out under a *99o999%* pure argon atmosphere. Quenching trials indicated that melts, cooled in an argon atmosphere, differed .very little in structure from those quenched outside the furnace. The major difference between the two methods was that externally chilled melts had a pronounced iron oxide skin on the surface of the melt. To minimise the variation in doiomitic lime or calcitic lime properties, all cylinders were subjected to individual measurements of physical

parameters such as size, bulk density and apparent porosity.

3.7.1 Calcination of dolomitic limestone and limestone cylinders.

Dolomitic limestone and limestone cylinders were stored in a drying oven at 110°C. The cool, weighed cylinders were placed into a cold muffle furnace in silica dishes and calcined at a temperature of 1350°C for approximately 3 hours. However, the cylinders cracked badly and bulk densities were too low to allow comparison with "Dolomet" or calcitic lime. A technique suggested by Green (80) was adopted to overcome the problem of cylinder cracking. A section of insulating brick was hollowed out, lined with platinum foil and covered with a lid to produce a cocoon. Four cylinders were calcined simultaneously at temperatures varying between 1380 and 1400°C for two and a quarter hours. A Pt - Pt/13%Rh thermocouple was used to monitor the interior cocoon temperature. The cocoon interior temperature was achieved by holding the open furnace temperature at 1490°C. Dolomitic lime cylinders were allowed to cool within the furnace overnight. Lime cylinders were produced by heating the cocoon to 1200°C and then removing the cocoon and contents from the furnace to cool in air.

3.7.2 Cylinder properties.

Dolomitic lime cylinders were produced with an average length of 29.6mm and average diameter of 13.8mm. An

average bulk density of 1768kg.m^{-3} was achieved in the dolomitic lime cylinders. Lime cylinders were prepared in two forms to compare and contrast the dissolution mechanism with dolomitic lime in melts of the same composition. A "hard" burnt form of lime was prepared by holding the cylinders at 1200^{o}C for three hours. These cylinders had an average length of 27.7mm and diameter of 11.8mm whilst bulk density reached 2390kg.m^{-3}. "Soft" burnt lime cylinders were removed from the furnace when the cocoon temperature reached 1200^{o}C. The "softer" burnt cylinders were 30.2mm long and 14.22mm in diameter, and had a bulk density of 1870kg.m^{-3}. Comparison between the various types of cylinder properties may be made with reference to Tables 6 and 7 (pages 235 and 236) and to the green and calcined cylinder forms in Plate 8 (p. 312). The cylinders used for pill tests were 37mm in diameter, 35 to 40mm long with an internal 15mm diameter hole drilled to a depth of 20mm. Porosity and bulk density values were similar to those of dolomitic lime.

3.7.3 Density and porosity determinations.

The retained samples of minus 300μm (52 mesh) dolomitic limestone and limestone were used to determine powder densities by the Rees-Hugill flask method, described in B.S. 1902: Part 1A: 1966 [135]. Three determinations were carried out for each rock type and a 120g sample was required at each measurement.

Cylinder bulk densities were calculated using a

mercury balance method and an evacuation technique [135]. The density of mercury was corrected for a specific temperature [129]. Water was used as the immersion medium in the evacuation method for determining green cylinder bulk densities. Calcined cylinders were evacuated in a paraffin medium to prevent hydration. The density of paraffin was taken to be 800kgm^{-3} at the prevailing experimental conditions, as it represented the density of paraffin at 20^{o}C [129]. The evacuation method allowed the apparent porosity (Rapp%) to be calculated from

$$Rapp = 100 \left(1 - \frac{Db}{Das} \right) \% \times \rho \qquad (3.8)$$

Db = bulk density, Das = apparent solid density

ρ = density of water or paraffin (kgm^{-3}).

Repeated apparent porosity determinations on a single dolomitic limestone cylinder yielded a mean value of 20.32% with a standard deviation of $\pm$0.47%. The true mean for the porosity values within 95% confidence limits was 20.32 $\pm$ 0.65%. The powder density was assumed to be equivalent to the true density for calculation purposes. The chemical and physical properties of both raw and calcined materials have been given in Tables 6 and 7, (pages 235 and 236). In some cases a standard deviation has been given from the arithmetical mean value.

3.7.4 Differential thermal analysis.

Differential thermal analysis of dolomitic limestone and limestone was carried out to determine the dissociation characteristics of the various carbonates. The sample mat-

erial temperature was compared with that of calcined alumina by means of a differential thermocouple, constructed of chromel-alumel. The true temperature of the sample was taken from the inert material which was packed with the sample into a dual cell, and placed inside a small Carbolite D.T.A. furnace. Twin Kent chart recorders were used to record the linear increase in furnace temperature and the differential temperature of the sample during heating. The maximum recordable temperature was 1000°C.

3.7.5 Immersion tests.

Static immersion experiments at 1300°C were carried out in the Carbolite furnace, maintained continuously at this temperature during an experimental campaign i.e. isothermal conditions. The hot zone temperature was checked with a Pt - Pt/13%Rh thermocouple attached to a portable potentiometer, prior to undertaking an experimental run. An argon flow rate of 1.5 ℓ/min was maintained throughout the temperature checks and experiments.

Two small diametrically opposed holes were drilled in the top of the iron crucible, before weighing, to take two 0.5mm diameter Kanthal A1 wires (Hall-Pickles, Sheffield), which were cut to a length that enabled the crucible to be positioned within the working tube hot zone. The upper ends of the wire emerged through the top gas seal and were gripped by two bulldog clips. Cylinders were held within a 1.0mm diameter Kanthal wire holder, rigidly supported within a hollow recrystallised alumina

sheath, 820mm long and 8mm in diameter. Access for the sheath was made by a close fitting hole drilled into the central part of the gas seal. The protruding sheath was clamped by a retaining ring and screw, which then rested on the upper surface of the gas seal.

The crucible and cylinder holders were assembled outside the furnace. Cylinders were held firmly in place through compression of the wire holder by 0.5mm diameter stainless steel binding wire, fastened around it. A consistent cylinder immersion depth was maintained by seating the attached cylinder onto a 3mm thick perspex block in the bottom of the empty crucible. The cylinder support sheath ring clamp was adjusted to rest on top of the gas seal plate. The support sheath and attached cylinder were held in a pre-heat position by a bulldog clip. The perspex block was removed and the 3mm cylinder tip clearance checked. The support sheath and cylinder were relocated in the pre-heat position, 45g of powdered melt added and the assembly placed into position, through the top of the furnace. The furnace assembly and gas seal clamping arrangements are shown diagrammatically in Fig. 29 (p. 282). The crucible-cylinder assembly was allowed to equilibrate with the furnace temperature for thirty minutes. Direct observation of the cylinder and crucible contents could be made through the periscope attachment, illustrated in Fig. 29 (p. 282). The powdered melts were fully liquid within ten minutes. None of the cylinders spalled in the pre-heat position, which lay approximately

within the upper limit of the 10°C variation zone shown in Fig. 24 (p. 277). By removing the retaining bulldog clip, the cylinder was immersed to the correct depth within the melt. After the required immersion period, the crucible was dropped away from the cylinder by releasing the support wire clamps. The cylinders were withdrawn through the top of the furnace.

Dynamic isothermal experiments (1300°C) were performed by rotating cylinders at 50r.p.m. within melts. The experimental assembly and procedures were the same as those described for static experiments. A more rigid cylinder support tube and clamp were constructed. The support tube was made from aluminous porcelain (Morgan 361), with an outer diameter of 12mm and an inner diameter of 7mm. A short length of recrystallised alumina tubing, 7mm in outside diameter and 4mm internal, was cemented with C60 within the large diameter support tube. The cylinder wire holder was fixed to the smaller tube, Plate 9 (p. 313). An M80 reversible motor (Loughborough Glass Co.) was fixed above and to one side of the furnace head frame, to facilitate access of the assembly and withdrawal of the reacted cylinder. The drive coupling from the motor to the machined shaft located onto the end of the porcelain tubing was made from a length of polyethylene tubing, and could be removed quickly [80], Plate 10 (p. 313). The rotational speed was recorded by a Smiths tachometer with a 2r.p.m. scale division.

3.7.6 Quenching of reacted cylinders.

Problems were encountered in attempting to chill the reacted cylinders effectively, and still retain the phases present within the reaction zones, under isothermal conditions. Cylinders of dolomitic lime remained relatively intact after short immersion periods, when they were cooled in air. Both dolomitic lime and lime cylinders in particular, shattered at room temperature due to the inversion of dicalcium silicate from the β to γ form [50]. Oil was used as a quenching medium but it tended to be absorbed in the pores. This absorption was later demonstrated when the oil exuded from pores during vacuum impregnation treatment. Compressed argon was directed onto the hot cylinder at close range to increase the cooling rate and prevent the γ inversion tendency of β or α' dicalcium silicate at room temperature [50]. Under this treatment, none of the dolomitic lime cylinders collapsed, and they were retained completely intact. Lime cylinders still broke up due to the inversion process but larger pieces of cylinder were retained than previously. All cooled cylinders were weighed after the immersion experiments.

3.7.7 Pill tests.

A limited number of pill or melt penetration tests were carried out using 37mm diameter and 40mm long dolomitic lime cylinders. A 15mm diameter hole was drilled to a depth of 20mm in the top of the cylinder and packed

with approximately 5g of powdered synthetic slag. The melt was allowed to react for 25 minutes after the first signs of liquid formation. The hot cylinder and reacted contents were cooled in the same manner as the small cylinders.

3.7.8 Cylinder examination procedure.

Each cylinder was sectioned at a fixed point to allow comparison between all immersed cylinder experiments. To facilitate the sectioning process, each reacted cylinder was encased in cold setting Trylon SP701 PA resin and vacuum impregnated immediately after weighing. Reacted cylinders produced a well defined erosion line at a position coinciding with the melt surface/furnace atmosphere interface. Dissolution was enhanced at this position and a longitudinally cut section of a cylinder revealed a zone of reaction above the level of submergence. This effect was produced by the capillary suction of melt into the core of the cylinder. To offset capillarity and enhanced dissolution affects, all cylinders were cut approximately 2mm up from the entrant tip within the immersed section of the cylinder. The mounted sample was sectioned transversely by using a Mottacutta Mk II horizontal diamond saw and paraffin as the cooling and lubricating medium. Iron crucibles containing chilled melts were also sectioned by this method, using water as the coolant. This method of sectioning largely prevented the occurrence of surface damage on the face of the specimen. The 2mm thick offcuts of cylinder tips were remounted in

resin, ready for grinding and polishing of the cut surface.

3.7.9 Polished section preparation.

Mounted sections were ground sequentially on 240, 320, 400 and 600 grade silicon carbide papers, using paraffin as the coolant. Final polishing was achieved with 6, 1 and $^{1}/_{4}$ micron diamond paste. The harder polishing cloths such as Hyprocel Pellon (P.S.U.) or Beuhler 40-7616-types, were found to be superior to softer cloths which removed the mounting resin to produce an uneven polished surface.

Polished specimens were examined on a Zeiss polarising microscope with built in automatic light metering for photography. Kodachrome Pan. X film was used to record photomicrograph images.

A weak etchant had to be used to differentiate between various phases present within the reaction zones. Nital solution was used as the etchant, and a concentration of 0.1% Nital, for an immersion time of 10 seconds, gave excellent results.

3.8 Scanning Electron Microscope Studies.

3.8.1 Qualitative Studies.

Polished transverse sections of reacted cylinder tips were coated with volatalised gold, under vacuum and examined by a Phillips Scanning Electron Microscope (SEM), coupled to an EDAX 711 analyser system (Met. Dept., Sheffield Polytechnic). Specimens were inclined at 25^{o} to

the incident beam, operating at an acceleration voltage of 25kV, and a spot size of 0.125 μm. The gold coated surface allowed any induced charge from the beam to run to earth. Micrograph images were generally recorded in the emissive mode (secondary electrons) to highlight topographic effects, by allowing collection of back scattered primary electrons. Consistent 8mm thick samples ensured that the magnified images recorded by the SEM were comparable from sample to sample.

Line scans or x-ray maps were obtained for each elemental species by using the EDAX unit for the energy dispersive analysis of x-rays. Fixed traverse line scans gave an indication of a particular element concentration gradient. X-ray maps were used to distinguish possible phase relationships within the whole viewed image. Magnesium, Calcium, Iron and Silicon were the only elements analysed for. Images were recorded on 35mm Ilford Pan F or Polaroid film.

3.8.2 Quantitative Studies.

A semi-quantitative study of reaction interfaces has been used in the field of refractories by utilising electron probe micro analyser (EPMA) systems [98,136,137]. Stereoscan (SEM) imagery has also been used in studies of lime for the steel industry [69,85] and for simple profiling techniques [97]. An attempt was made to derive mass fractions of elements within the reaction interface

by use of the Sheffield Frame 3, ZAF correction program[138] which had been converted for use with the Polytechnic's SEM by Cawley (private communication). Counts on the sample were compared with those on pure standards of magnesium, iron, silicon and a series of mineral standards obtained from the British Museum (Natural History). A brass holder was fabricated to hold up to six standards and the sample. A constant geometry and specimen height was maintained between the samples, standards and incident beam. Carbon was used as the coating medium as it cannot be identified by the energy dispersive analysis of x-rays. Samples and standards were positioned horizontally with respect to the incident beam, which was operated at 12kV. This acceleration voltage was chosen as a compromise because of the large differences in critical excitation energy potential between magnesium and iron (1.253keV and 6.398keV respectively). Ideally, the acceleration voltage should have exceeded the critical excitation energy potential by a factor of approximately three [139]. As a result, mass fraction values of iron could be expected to be slightly low. Problems were encountered with counts from the Mg Kβ peak interfering with Mg Kα counts. Silicon was less of a problem and for calcium and iron, the Kβ peak was well separated from the main Kα peak. Plates 11a and 11b (p. 314) illustrate how the half peak method of counting was used to exclude Mg Kβ counts. Plate 11c (p. 314) shows the characteristic Kα and Kβ peak for silicon. A sample of mineral olivine (St. Johns Island) of known composition was used in conjunction with

pure metal standards to test the program. Mass fractions of Mg, Fe and Si were determined and oxygen calculated by difference. The results from whole and half peak methods are included in Table 14 (p. 241). The unsatisfactory values for magnesium suggested that a more sophisticated method of analysis correction was required. Use of the SEM and computerised Edax facilities at the Steetley Brick Plant near Worksop was made to establish the correction.

Detailed interface analyses were carried out, using a Phillips SEM and Edax 711 unit. ZAF corrections were calculated by a Nova 3/4 computer using an Edax twin floppy disc program, which derived oxide percentages by comparison with a fixed internal standard x-ray spectrum. Table 15 (p. 241) indicates the reasonable agreement between the wet chemical analysis and x-ray analysis of the St. John's Island olivine. Samples were inclined at 10^{o} to the incident beam and a 12kV acceleration voltage was used. The admixture of phases prevented the use of area scan analyses. A spot or point source of 0.25μm dia. was used to determine individual phase analysis. The presence of diffusion pump oil within the vacuum system resulted in the formation of an enhanced carbon spot at the location of the point source. Accurate sampling points were produced on SEM photomicrographs by utilising a micrometre scale which enabled detailed interface profiles to be constructed.

3.9 The melting behaviour of synthetic slags.

With the addition of dolomitic lime to early formed

slags in the CaO-'FeO'-SiO_2 system, magnesia can be dissolved into the slag to quite high saturation levels [101]. The influence of magnesia on the melting temperatures and melting ranges of early formed slags, was studied. A technique described in British Standards 1966, Part II, Section 6, for the determination of the melting behaviour of refractory clay materials using Seger cones has been modified for use with cones moulded from synthetic slags by Green [80], Saadat [140] and Dodds [141]. The technique has been used in this study to determine and compare the melting behaviour of synthetic slags in the system CaO-'FeO'-SiO_2-MgO.

3.9.1 Cone preparation.

A brass mould was used to shape the main body of the cone and a loose aluminium end plate formed the flat base. The triangular shaped cone base was 7.5mm long at each edge, and the cone was 25mm high. The height of the cone was restricted by the internal diameter of the working tube and thermocouple position, and was less than the standard Seger cone height of 30 or 65mm.

A binder of 6 mass % NH_4Cl was added to each sample batch of powdered synthetic slag. A 10g slag-binder mixture was sufficient to produce six cones. After thoroughly mixing the powdered slag and binder in a mortar and pestle, a small quantity of alcohol was added to produce a "dry" paste. The end plate was positioned at the base end of the cone mould, and the paste mixture pressed into the mould with a spatula. The cone was released onto a small

sheet of mild steel foil to partially air dry. The cones were centrally positioned onto fired C60 alumina cement bases and set into place with a slurry of C60 cement. The C60 cement bases were moulded in semi - circular sections of copper tubing, 40mm in length. After air drying overnight, the cast bases were fired at 1000°C in an electric muffle furnace. Cones were cemented onto the refractory bases so that a vertical face of the cone was parallel to the long axis of the working tube. A photograph of a mounted cone is shown in Plate 12 (p. 315). The mounted cones were dried overnight in an oven, maintained at 110°C. Some cones invariably collapsed whilst manoeuvering them into the hot zone position of the working tube, so that four cones were prepared for each sample. The cones were charged into a cold furnace. The furnace was heated at 3°C/min up to a temperature of 500°C, to allow the binder to volatise without disrupting the cone. The heating rate was then increased to between 8 and 10°C using a Variac controller.

The rate of collapse of the cone at the melting temperature was largely dependent on the physical properties of the first formed liquid. To ensure complete synthetic slag homogeneity, oxide additions were fused with the appropriate base slag and recrushed to -106μm before moulding into the cone form. Cone deformation was recorded as a temperature value at three different points. The first sign of deformation coincided with the cone tip bending slightly under the influence of liquid drainage

through the cone, by gravitational force. The intermediate temperature value was taken when the cone was half way to collapsing and the final temperature point coincided with complete melting of the cone. All three stages are illustrated through a series of photographs in Plates 13a, b and c (p.315). A telescopic cross-wire cathetometer was used to identify visually the cone behaviour during melting. The eyepiece of the cathetometer may be seen in position on the right hand side of Plate 2 (p.308). The cones were allowed to cool under an inert argon atmosphere after collapsing. Deformation temperatures were recorded on a Cambridge Instruments portable potentiometer, connected to the internally positioned Pt - Pt/13% Rh thermocouple.

4. Experimental Results and their interpretation.

Preface.

The experimental results section has been divided into three parts which comprise of viscosity, immersion, and cone fusion study results respectively. The results of the viscosity experiments are tabulated through Tables 16 to 27 (pages 242 to 251) and figuratively illustrated through Figures 30 to 34 (pages 283 to 286). The immersion study results have necessitated the inclusion of extensive photomicrograph interpretations, to maintain the coherency of this portion of the results section. To aid the reader, the photomicrographs, referred through Plates 17 to 86 (pages 318 to 357) have been correlated with the full sequence of experimental immersion studies which are listed in Table 30 (p. 253). A brief remark concerning the photomicrograph has been included within the Table. All cone fusion results are listed in Table 35 (p. 258). To provide a more meaningful interpretation of these results, a contour method has been utilised which relates melting isotherms against two composition axes of magnesia and lime. Composition sections based upon a fixed proportion of lime have been constructed to identify the effect of magnesia on the melting behaviour of synthetic slags. The results are shown figuratively through Figures 58 to 65 (pages 303 to 306).

4.1 Viscosity measurement of synthetic slags.

Viscosity measurements were made over the compositional range of synthetic slags listed in Tables 16 and 17 (page 242), and compositions in part of the CaO - 'FeO' - SiO_2 diagram, illustrated in Fig. 22 (p.275). The temperature range covered by the experiments was limited to 1100 to 1470°C because iron components were used. Three results were obtained using zirconia crucibles and iron measuring bobs, the remainder were determined with crucibles and bobs both of iron. Slag or melt compositions shown on tables or figures are referred to as melts 1 through to 7, with the experiment number enclosed within brackets. Tables listing experimental temperature and viscosity values represented a time interval of six to eight hours from the initial to the final measurement.

4.1.1 The viscosity of an iron silicate melt.

Iron silicate slags of fayalite (2 FeO.SiO_2) composition may be related to either the CaO - 'FeO' - SiO_2 or Fe_2O_3 - 'FeO' - SiO_2 phase systems [50,108]; Figures 22 (p.275) and 7 (p. 266). The liquidus in the diagrams is a locus of temperature - composition points representing the maximum solubility or saturation of solid phase in liquid phase [108]. In a ternary or pseudo-ternary system, the liquidus is represented as a curved surface. A fayalite slag of molar composition 2 FeO.SiO_2 has a theoretical liquidus temperature of 1205°C [50]. The

synthetic fayalite slag was heated to 1300°C to enable the viscometer measuring bob to be immersed. No chilling effect was observed during the immersion of the bob into the melt, the melt temperature being well above the theoretical liquidus temperature and the melting temperature of 1167°C determined for slag BF2 (FeO 63.04, Fe_2O_3 1.42, SiO_2 34.9 - mass %) in cone fusion studies (Table 35, p. 258). The viscosity of the iron silicate melt was measured through decreasing and then increasing temperature increments and the values recorded as illustrated in Table 18 (p.243).

A plot of viscosity versus temperature is illustrated in Figures 30 and 31 (pages 283 and 284) by the curve and melt composition 1 on both figures. Viscosity values measured at U = 1 (Table 18, p. 243) were used to plot the viscosity - temperature curve for the iron silicate melt. The very steep gradient and much flatter section of the viscosity curve for melt 1, Figs. 30 and 31 represented a change from solid + liquid to the liquid state. At 1192°C, the lowest temperature of measurement in Table 18 (p. 243), variation in rotational speed produced different viscosity values and suggested non-Newtonian behaviour. At the solidus/liquidus interface, scale values became difficult to read because of needle oscillation and an averaged reading was taken. Other melt compositions produced the same effect close to the solid + liquid and liquid interface. At temperatures greater than 1300°C, the slope of the viscosity curve appeared to become temperature independent and a value of

95mPa.s was recorded.

4.1.2 Viscosity relationships of lime - iron silicate melts.

4.1.2.1 The addition of 10 mass % CaO.

The addition of lime (CaO) as a third component produced a marked decrease in the melting temperature of the slag, indicated by a displacement of the viscosity - temperature curve 2 to the left of the iron silicate curve 1 on Fig. 30 (p. 283). An estimate of the liquidus temperature of 1100°C was taken from Fig. 22 (p. 275) and viscosity measurements made at decreasing then increasing temperatures as shown in Table 19 (p. 244). The majority of scale readings were taken when the rotation speed was 1 (486 r.p.m.) and these values were used to construct curve 2 in Fig. 30 (p. 283). The gradient of the lime - iron silicate melt appeared to be temperature dependent even above 1140°C, and reached only an equivalent viscosity with the iron silicate melt of 95mPa.s at 1400°C.

4.1.2.2 The addition of 32 mass % CaO.

The results of the 32 mass % CaO - iron silicate melts are illustrated in Table 20 (p. 245) and Fig. 30 (p. 283) as melt composition 3. The reason for the viscosity - temperature curve being drawn as a dashed line was because temperature values had to be extrapolated from a calibration chart due to the failure of the Pt-Pt/13% Rh thermocouple, sited in the base of the iron crucible. A

series of viscosity experiments were used to relate the Eurotherms controller temperatures to those recorded by a potentiometer connected to the crucible thermocouple. The resulting temperature plots are illustrated in Fig. 32 (p.285) and the linear relationship enabled the controller temperature to be converted to a crucible temperature value. This calibration technique was quite satisfactory and the loss of temperature sensing at the base of the iron crucible for these few experiments did not introduce any additional error into the accuracy of the results. The viscosity of the 32 mass % CaO melt was found to be approximately 50mPa.s higher than those of melt compositions designated 1 and 2 in Fig. 30 (p.283) at 1400°C.

A plot of viscosity versus mass % CaO in Fig. 33 (p.286) indicated that at temperatures exceeding 1250°C, the viscosity of an iron silicate melt increased with the addition of lime along the composition path shown on the CaO - 'FeO' - SiO_2 diagram illustrated in Fig. 22 (p.275). At a temperature of 1200°C, the addition of approximately 10 mass % CaO lowered the viscosity of the melt but this effect was considered due to the lower liquidus temperature produced at that composition. However, a comparison between curves 1 and 2 on Fig. 30 (p.283) suggested that a lower melting point slag does not necessarily have the lower viscosity values.

4.1.3 Viscosity relationships of some magnesia - iron silicate melts.

4.1.3.1 The addition of 2 mass % MgO.

Viscosity measurements were made over a series of increasing and decreasing temperature traverses as shown in Table 21 (p. 246). The majority of measurements were made with a rotational speed of U = 1 (486 r.p.m.). Variation of the rotational speed produced differing viscosity values at the lower end of the temperature scale shown in Table 21, and indicated the solidus - liquidus threshold. The viscosity - temperature plot of melt composition 4 in Fig. 31 (p. 284) produced a sharp change in gradient as the viscosity curve passed out of a solid + liquid regime into a fully liquid one. This occurred at approximately 1240°C, above which the gradient of the curve became independent of temperature. The relatively slight displacement of the steep gradient of viscosity curve 4, to the right of curve 1 in Fig. 31 (p. 284) could conceivably represent variation in experimental reproducibility, since the melt compositions varied only with respect to the minor amount of magnesia present, Table 16 (p. 242). However, the increase in liquidus temperature inferred from the position of curve 4 in Fig. 31 was confirmed by examination of the MgO - 'FeO' - SiO_2 phase diagram in Fig.18 (p. 272). The close relationship between viscosity curve 1 and 4 in Fig. 31 can be taken as a guide to the reproducibility of the rotational viscometer technique used in the absence of any individual experiments determined on

identical compositions.

4.1.3.2 The addition of 5 mass % MgO.

The viscosity measurement of a nominal 5 mass % MgO iron silicate was carried out in a zirconia crucible. The synthetic slag was heated to 1397°C to enable the measuring bob to be immersed. This temperature was approximately 160°C higher than that of the liquidus temperature inferred from cone fusion studies. A series of rotational speeds were used to determine the melt viscosity and the results were as indicated in Table 22 (p.247). Decreasing and then increasing temperature traverses were made and only at lower temperatures were there large deviations at a specific rotational speed. A plot of viscosity versus temperature for melt composition 5 is illustrated in Fig. 31 (p.284). The composition of melt 5 was contaminated by the dissolution of zirconia from the crucible wall. A recalculated slag composition has been used in Tables 16 and 17 (p.242), neglecting the effect of zirconia. The presence of zirconia in this and the other two melts is discussed in section 4.1.5.2. (p. 127). Curve number 5 in Fig. 31 (p. 284) was constructed from viscosity values determined at rotational speeds of 1 and 2 to reduce the number of points on the diagram. The increased addition of magnesia in melt number 5 moved the viscosity - temperature curve well to the right of the other melts in Fig. 31, which was the result of an increase in the liquidus temperature. Where previous curves approximately coincided with the 100mPa.s iso-viscosity line, the 5 mass %

MgO viscosity curve was at a level of 175 mPa.s. There was no apparent reason for this displacement to have occurred and measurement procedures were exactly the same as those previously carried out. There was also no indication of any drag exerted by the viscometer shaft on the upper gas seal entry port.

4.1.3.3 The addition of 7.5 mass % MgO.

Viscosity - temperature results of melt number 6, in Table 23 (p.248) and Fig. 31 (p.284) illustrated the effect of an increase in magnesia content on the liquidus temperature of an iron silicate slag. The gradient of the curve changed gradually until solid phases melted above 1350°C and the slope of the curve became less temperature dependent. The bob was immersed in the liquid melt at approximately 1400°C, and the temperature decreased for the first series of measurements. A rotational speed of U = 2 or 3 was used to make measurements and viscosity values obtained at U = 2 (243 r.p.m.) used to construct curve number 6 in Fig. 31 (p.284) There was a lack of scale sensitivity whilst operating at rotational speeds of U = 3 (162 r.p.m.) as indicated by low S values in Table 23 (p.248). The viscosity measurements were continued to a maximum temperature of 1472°C. Examination of the measuring bob after the experiment indicated that there had been no distortion along its length or diameter even though it had reached a temperature only 80°C below the theoretical melting point of iron. There was a marked separation of the temperature - viscosity curves

number 5 (5.8 mass % MgO) and 6 (7.4 mass % MgO) at 1400°C. Whilst at temperatures above 1400°C, the viscosity - temperature profile of melt number 6 (Fig. 31) coincided with the 100mPa.s iso-viscosity line reached by the other melt compositions.

A plot of viscosity versus magnesia addition, illustrated in Fig. 34 (p. 286), indicated that at low concentrations of magnesia there was no apparent change in the viscosity of iron silicate melts. However, above 2 to 3 mass % MgO, the viscosity of melts rose sharply, reflecting an increase in the liquidus temperatures. At 1300°C, magnesia additions up to 8 mass % increased the viscosity of an iron silicate melt by 250mPa.s. This trend was apparently reversed at temperatures of 1350 and 1400°C, with a viscosity maximum occurring at approximately 6 mass % MgO. At 1400°C, the 7.4 mass % MgO - iron silicate melt had a viscosity value similar to that of a magnesia - free iron silicate melt at the same temperature. The addition of a limited amount of magnesia to an iron silicate melt increased the viscosity of the melt threefold over that of an iron silicate melt containing up to 32 mass % lime at 1300°C.

4.1.4 The viscosity of a lime - magnesia - iron silicate melt.

The addition of magnesia as the fourth component in a 13 mass % CaO - iron silicate melt produced a displacement of the viscosity - temperature curve to a higher

temperature range than that recorded for the 13 mass % CaO - iron silicate melt (melt 2), illustrated in Fig. 30 (p. 283). Results of the viscosity measurement on the four phase melt were as tabulated in Table 24 (p.249) and are illustrated in Fig. 31 (p.284) by viscosity - temperature curve number 7. The viscosity of the lime - magnesia - iron silicate melt was 25 mPa.s lower than that of the lime - iron silicate melt at 1300°C. Scale sensitivity decreased with a rotational speed of U = 3 (162 r.p.m.) and values recorded at U = 2 (263 r.p.m.) in Table 24 (p.249) were used to plot the viscosity - temperature curve in Fig. 31 (p.284).

The addition of magnesia to an iron silicate melt normally produced an increase in the liquidus temperature and corresponding increase in melt viscosity at a specific temperature. In the case of the magnesia - lime - iron silicate melt, the liquidus temperature was again increased but the viscosity of the melt was reduced over that of a corresponding lime - iron silicate melt above a temperature of 1250°C.

4.1.5 The effect of crucible component materials.

Synthetic slag compositions were assumed to remain unchanged throughout the period of the viscosity experiments. To confirm this, crucibles containing furnace cooled slag were cut open and the contents analysed.

4.1.5.1 Iron components.

Iron components of the experimental apparatus were

found to have had no effect on melt compositions after completion of the viscosity experiment. The evidence for this may be illustrated with reference to Table 25 (p.250) which gives the composition of an iron silicate slag before and after the viscosity determination. The near constant ferrous oxide and decreased ferric oxide contents of the synthetic slag suggested that a low oxygen partial pressure was maintained throughout the experiment. In the initial experiments it had been noted that the graphite crucible holder showed significant signs of wear and surface softening due to oxidation. The cause of this was traced to a water bottle which was used to monitor the flow of argon into the furnace. The resultant CO - bearing argon atmosphere was swept out of the furnace without affecting the liquid melt composition contained within the crucible. Substitution of the water bottle for a U-tube containing magnesium perchlorate prevented the premature oxidation of the graphite crucible holders and allowed them to be utilised many times. The use of graphite as a material for the crucible holder proved to be a simple method of including an "oxygen getter" within the furnace, without the need for a specialised oxygen removing gas train.

The measuring bob was always retracted from the liquid melt after the conclusion of a successful experiment. Examination of the bob surface beneath chilled slag droplets, revealed that there had been no attack on the machined bob surface. In addition, it was observed

that none of the liquid melt ever penetrated the recessed volume at the base of the measuring bob. This indicated that shear measurements were restricted to the outer surface of the measuring bob.

One of the greatest difficulties encountered in the practical operation of the viscometer assembly, was to accurately align both measuring bob and crucible to produce a symmetrical annulus between the two components. Misalignment was associated with impact "welding" if severe, or the generation of a small electrical discharge, which was experienced by the operator of the equipment when the rotating iron bob touched the iron crucible wall. The induced electrical field, and resultant shock generated by the rotating bob and crucible within the large electrical field of the Crusilite heating element, served as a useful guide to the relative positions of both iron components. An earth strap connected to the viscometer head frame failed to prevent the passage of the induced current up the equipment. No electric effect was produced when the bob was rotating freely within the melt. Gimmel'farb [142], whilst working on the viscosity of the quaternary $CaO - SiO_2 - 'FeO' - Al_2O_3$ slag system, believed that a magnetic field of sufficient strength to attract the bob could be created by the furnace windings. The major cause of misalignment in the present work appeared to be due to geometrical factors, rather than to paramagnetic forces, which produced a decentralisation of the measuring bob. The problem of impact "welding" was

overcome when zirconia crucibles were used, although electrical effects were still registered whenever the iron bob hit the zirconia crucible wall.

4.1.5.2 Zirconia components.

At the end of each viscosity experiment, the furnace was allowed to cool under an inert atmosphere of argon and the crucible, attached to the support column, was withdrawn through the base of the furnace. All three zirconia crucibles produced the 'petaloid' form of crucible illustrated in Plate 14 (p. 316), which also includes an unused zirconia crucible for comparison. Expansion of the crucible wall occurred above the level of the cooled crucible contents, which served to hold the remainder of the crucible intact. In the presence of silica, Chesters [143] has described how the tetragonal form of zirconia can change reversibly at 1460°C to a monoclinic form that expands when cooled back to room temperature. However, if zirconia is heated with 5 to 7 mass % lime to 1700°C, a cubic form of zirconia is produced which remains stable on cooling. Although the zirconia crucibles used in the present work were calcia stabilised, reversal of zirconia from the cubic to the tetrahedral form must have occurred at experimental temperatures. This would have resulted in the formation of a monoclinic phase which expanded on cooling to produce the effect illustrated in Plate 14 (p.316).

The aggressive nature of ferruginous slags can be demonstrated with reference to the degree of zirconia

contamination produced in the melt compositions shown in Table 17 (p.242). A contamination level of 12 to 13 mass % ZrO_2 was attained by all of the synthetic melts. Dissolution of zirconia from the crucible wall was physically represented by the presence of two internal slag or erosion lines. The relative positions of the two slag lines are illustrated in the sketch through Figures 35a, b and c (p. 287). The largest and lowest slag line (Fig. 35b) occurred at the molten slag-furnace atmosphere interface, whilst the narrower, upper slag line was coincident with the upper position of the melt surface when it was displaced by immersion of the bob (Fig. 35c). Two samples taken from the core and crucible periphery of melt 7, Table 17 (p. 242) failed to detect the presence of any ZrO_2 concentration gradient across the crucible, after the measuring bob had been withdrawn and the melt allowed to furnace cool. This suggested that the melt was saturated with respect to zirconia. Published phase equilibrium diagrams can be used to estimate the solubility limits of zirconia in ferruginous and iron silicate - type melts.[144] If 1450°C is taken to represent the upper experimental range of temperature - viscosity measurement, a solubility of 10 mass % ZrO_2 could be predicted for a melt composed of 'FeO', as illustrated in Fig. 36 (p. 288). Similarly, from the 'FeO' - SiO_2 - ZrO_2 phase diagram illustrated in Fig. 37 (p. 288), an iron silicate melt would have a solubility limit of 13.7 mass % ZrO_2 at 1450 °C across the isoplethal section joining the fayalite ($2FeO.SiO_2$) - zirconia (ZrO_2) phase

fields. The similarity between the estimated figure of 13.7 mass % ZrO_2 and the analysed zirconia compositions of synthetic slags 5, 6 and 7 in Table 17 (p. 242) confirmed that the melts were saturated with respect to zirconia.

Polished sections of a 7.5 mass % MgO-iron silicate melt and a zirconia crucible plus lime - magnesia - iron silicate melt interface are illustrated in photomicrographs represented by Plate 15 and Plate 16 (p. 317), respectively. From Plate 15, it was inferred that the zirconia had been in solution and only precipitated during cooling, to produce the pale, grey coloured rectangular and bladed crystal forms visible in the fayalite primary phase. During cooling, exsolved zirconia also produced the exsolution lamellae present in the coarse fayalite crystals. The interface shown in Plate 16 illustrated melt penetration into the crucible wall and isolation of zirconia particles which have remained relatively undissolved within the melt. Some of the zirconia clearly was dissolved and on cooling produced a dendritic form associated with FeO. The zone of contraction present at the crucible - solid melt interface in Plate 16 facilitated removal of the cooled crucible contents from the crucible. The effects of zirconia on the viscosity and melting points of liquid melts are discussed below in section 4.1.5.3.

4.1.5.3 <u>The influence of zirconia on viscosity values and melting temperatures.</u>

The presence of solid particles in a liquid melt

would be expected to produce a type of non-Newtonian behaviour similar to that recorded by the viscometer at the solid + liquid - liquid interface, unless particles were small enough not to impede the flow of fluid. Within the annulus created by the crucible and measuring bob, it may be assumed that the concentration of zirconia in that region would be less than that of the bulk melt, because the larger volume of melt below the bob would provide the greater sink for dissolution. Examination of temperature-viscosity data in Tables 22,23,24 (p. 247, 248, 249), has indicated that solid zirconia does not alter the viscosity values of the respective melts over the duration of the experiment. For example, for the 5 mass % MgO - iron silicate melt (Table 22), the first viscosity reading taken at the start of the experiment was 175 mPa.s with U = 1 at 1397°C. Towards the end of the experiment, represented by a time interval of approximately six hours, a value of 180.2 mPa.s was recorded at U = 1 and a temperature of 1392°C. The similarity between the two viscosity values confirmed the observation that a solid zirconia phase does not influence the viscosity of a melt. Alternatively, if only negligible amounts of solid zirconia were present, the dissolved zirconia would have to achieve rapid saturation in the bulk melt prior to any viscosity measurement being taken, otherwise at any equivalent temperature, viscosity values recorded near the start and end of the experiment would differ. As indicated previously, there was some evidence from the sample examined in Plate 16 (p. 317) which suggested that zirconia may be

continuously "washed" out of the crucible wall by cavitation, produced through mechanical agitation of the melt by the rotating bob.

The effect of zirconia on the melting temperatures and ranges of iron silicate melts was studied using the cone fusion technique, described in sections 3.9 (p. 111) and 4.4 (p. 167). The results of the study are shown in Table 26 (p. 250). The addition of 15 mass % ZrO_2 to the synthetic iron silicate slag of composition FeO 63.04; Fe_2O_3 1.42; SiO_2 34.9 mass %, did not produce any significant alteration in the melting range of the slag, and the cone melting temperature (liquidus) was increased by 13°C. A cone comparison of melt number 7 and cone 5MCF13 (Table 26, p. 250), which had almost an identical composition but lacked zirconia, produced hardly any change in the melting range or melting temperature. Zirconia has been considered to have only a limited effect on the melting behaviour of synthetic slags over the zirconia levels of 13 to 15 mass %.

4.1.6 Liquidus temperature determinations extrapolated from viscosity - temperature curves.

Viscosity values encountered at a solid + liquid - liquid interface have been shown to coincide with the change from a steep gradient, highly temperature dependent region to a shallow gradient, weakly temperature dependent region in the temperature viscosity profile. The zone of inflection of the two gradients was well developed in all but the 32 mass % CaO - iron silicate (melt

Number 3, Fig. 30 p. 283). An estimation of the liquidus temperature of a melt should be provided by extrapolating the two gradients to a point of intersection, as illustrated in Fig. 30, below the temperature-viscosity profile of melt 1. Projection of this point of intersection down an ordinate to the temperature axis yielded the liquidus temperature. This construction was applied through melts 1 to 7 illustrated in Figs. 30 and 31 (pages 283 and 284). The estimated liquidus temperatures are tabulated with liquidus temperature values obtained from the cone fusion of samples of each melt (Table 27, p.251). The cone produced from a sample of melt 6 (Table 27) did not collapse in the normal manner. The cone contracted over a wide temperature range as a result of the drainage of liquid under the influence of gravity. The actual experiment was brought to a conclusion at 1430°C after the cone showed no further signs of shrinking. The collapse temperature of the cone was estimated to be between 1360 and 1380°C. Drainage of liquid from the cone of melt 6 was not affected by the presence of zirconia in any chemical sense, although the physical presence of solid zirconia particles may have impeded the movement of liquid through the cone. Liquidus temperatures determined from viscosity curves were in general only 20 to 50°C higher than those obtained from cone fusion tests.

4.2 Cylinder properties and reaction parameters.

4.2.1 Differential thermal analysis measurements (D.T.A.)

Dolomitic limestone may be regarded as a solid solution of calcium and magnesium carbonate phases which are iso-structural with one another and occur in alternating stacked layers. The differential thermal analysis (D.T.A.) curve of the Whitwell dolomitic limestone (Magnesian Limestone), illustrated in Fig. 38 (p.289),indicated that dissociation of the carbonates occurred in two stages. Magnesium carbonate liberated CO_2 to produce magnesia at 810°C and calcium carbonate dissociated to lime (CaO) and CO_2 at 940°C. Complete calcination was achieved at approximately 1000°C. A D.T.A. trace for the Dowlow limestone has been included on Fig. 38 (p.289) for comparison. Dissociation of the limestone to lime and CO_2 occurred at 980°C and was 40°C higher than the corresponding calcium carbonate dissociation peak in dolomitic lime. The small peak registered on the dolomitic limestone D.T.A. curve at almost 1000°C represented a possible recrystallisation stage of the two oxide components, suggesting that some degree of structural reorganisation of phases was occurring.

Although both lime and magnesia are cubic with NaCl - type lattices, the ionic radius of Mg^{2+} (0.66 Å) is significantly lower than that of Ca^{2+} (0.99 Å) so that solubilities between both phases will be limited [145]. Magnesia and lime will tend to crystallise away from one another. Ultimate separation should occur at high temp-

eratures ($\simeq$1700°C), after a sustained holding period, to lime and periclase (MgO) in a similar manner to that developed during the manufacture of doloma refractory bricks. During the calcination of dolomitic lime cylinders, a transient recrystallisation stage was developed with lime and magnesia rich crystallites or zones separating out. The recrystallisation reaction phenomena is well developed in the two SEM photomicrographs shown in Plates 17 and 18 (p. 318). The SEM image in Plate 17 represented a polished dolomitic lime cylinder surface and the photographic contrast of the image is partially due to the atomic number contrast of phases present. The atomic number contrast was consistent with the MgO and CaO crystallite distribution, with the higher atomic number phase (CaO) occurring in the flat, non porous, pale coloured areas of the image. A "hard" burnt polished section of dolomitic lime is shown in Plate 18 (p. 318) which represented an unreacted core of the cylinder after immersion for 420 s. in an iron silicate melt at 1300°C. The magnesia crystallites are visible as dark irregular patches with lime-rich areas represented by the paler grey coloured phase. Access for liquid melt to penetrate and react with either crystallite phase, adjacent to the pore network, would be facilitated by the increasing development of porosity.

4.2.2 Porosity relationships.

Dolomitic limestone and limestone cylinders used in

the calcined state for immersion studies would be expected to show some inconsistencies in the physical properties relating to porosity and bulk density, as a consequence of being a natural raw material. Careful selection of raw materials from the primary crusher dumps at Whitwell and Dowlow and subsequent cylinder inspection and controlled calcination within tight porosity tolerances, ensured that individual cylinders remained similar in every respect. The standard deviation recorded on average values of apparent porosity and bulk density in Tables 6 and 7 (pages 235 and 236), illustrates the consistency of the selection method. However, the apparent porosity measurements in particular do not give any indication of pore size and distribution. Plates 19a and 19b (p.319) represent a polished section SEM photomicrograph of a cylinder of dolomitic limestone. Plate 19a shows a fairly regular distribution of angular pores but in Plate 19b, representing another area of the sample, larger cavities or macropores existed containing rhombohedral crystals of secondary dolomite. The dolomite crystals were deposited by permeating solutions, and were observed in many of the dolomitic limestone cylinders, imparting a "sandy" aspect to the buff-coloured rock. Plates 20a and 20b (p.319) may be regarded as calcined equivalents of the material shown in Plates 19a and 19b (p.319) respectively. Plate 20a shows the development of a uniform sized pore system, the micrometre (μm) markers indicating that particles were approximately 5 μm

in size, with the pore dimensions ranging between 2 and 10 μm. In Plate 20b (p.319), a relic dolomite crystal has developed a pore structure similar to that of the matrix, although the cavity in which the crystal was sited was 10 times larger than the matrix porosity. During a number of static dissolution experiments, some parts of the immersed cylinder wall produced a greater degree of solution than other areas. This may have been caused by the presence of the relic crystal cavities on or below the surface of the cylinder. Enhanced dissolution would have occurred through the ingress of a greater volume of unsaturated melt and its occurrence could not have been predicted from apparent porosity values.

One of the objectives in the production of dolomitic lime cylinders was to reproduce similar physical properties to those developed in the commercially available slag conditioner, "Dolomet". Interpretations of dolomitic lime - iron silicate melt reactions could then be directly compared with those of "Dolomet" and similar melt compositions. This comparison would only be valid if the physical nature of the pore network was similar. Plate 21 (p. 319) represented the detailed structure of a dolomitic lime cylinder produced under laboratory conditions, whilst that in the SEM image in Plate 22 (p.319) represented an actual sample of "Dolomet". The bulk densities and apparent porosities of the two samples were very similar. Neglecting the slightly differing image magnification factor, there was no observable structural difference between the two types of calcined materials.

had been pre-heated in the furnace hot zone position and then allowed to air cool. The results indicated that once the initial calcination process had been carried out, no significant changes occurred to bulk density and apparent porosity values of cylinders held in the pre-heat position prior to immersion in the melt.

4.2.4 The hydration of calcined cylinders.

A 15 second immersion period was normally sufficient to allow the liquid melt to penetrate completely through the immersed section of cylinder. This reaction feature was particularly well developed in most of the dolomitic lime and "soft" burnt lime cylinders. However, several reacted dolomitic lime cylinders revealed no evidence of melt penetration in the core of sectioned cylinders. It was thought unlikely that the core resulted from the incomplete calcination of the cylinder because calcination times and temperatures were closely monitored.

The existence of unreacted core material in dolomitic lime cylinders submitted to static isothermal immersion experiments was believed to have occurred as a result of the hydration of the oxide phases, particularly lime. A potential source of water was traced to the "Esso Blue" paraffin used in the evacuation method for the determination of bulk density and apparent porosity. In addition, any hydration reactions resulting from the hydrous paraffin would have been accelerated during the removal of paraffin from the cylinder. Cylinders were maintained at a temperature of 110°C for a minimum of

five hours, to allow the paraffin to evaporate completely from the pore system. To minimise the hydration effects for future experiments, sodium wire was extruded into the Winchester of hydrous paraffin and the anhydrous paraffin decanted into a clean, dry Winchester 48 hours later. An alternative cause has been suggested for the occurrence of unreacted cylinder cores in specimens subjected to rotation in iron silicate melts, (Sect. 4.3.1.1., p. 149). Part of a hydrated core sample is detailed in the SEM photomicrograph in Plate 27 (p.321). The porosity network shown in Plate 27 was poorly developed and the cracks present on the polished surface represent expansion cracks, and were created as the hydration reaction proceeded. After a limited period of storage in a dessicator, the unused but partially hydrated core could produce sufficiently high expansion stresses to shatter the sample.

The susceptibility of calcined cylinders to hydration is indicated in Fig. 39 (p.290). The change in mass of dolomitic lime and lime cylinders was taken to represent the degree of hydration. Cylinders were either left exposed to the laboratory atmosphere or stored in a dessicator containing anhydrous silica gel. After 20 days storage there was a negligible mass increase in dolomitic lime cylinder A in Fig. 39 (p.290). Dolomitic lime cylinder B had a mass increase of 7.2% and had developed extensive surface cracks after 8 days exposure to the laboratory atmosphere. After a further

3 days, cylinder B had doubled its volume and had become soft and powdery. Lime cylinder C recorded a progressive mass increase culminating in 2.3% at the end of a 17 day period whilst stored in the dessicator. However, lime cylinder D which was in contact with the laboratory atmosphere, produced surface cracks after only 2 days exposure, and collapsed completely after 6 days after a mass increase of 6.6% was recorded. Dolomitic lime cylinders had a slightly higher resistance to hydration than lime cylinders during storage.

To counteract the degree of cylinder hydration during storage, cylinder storage times were kept to a minimum by calcining only 3 cylinders at a time and using them within a two or three day cycle. After the instigation of the above procedures, cylinder sections, irrespective of immersion time, were permeated fully by melt. Patches of isolated white coloured unreacted dolomitic lime were observed in some cylinder and "Dolomet" sections but these were small enough not to influence the overall dissolution process.

4.3 Immersion experiments.†

4.3.1 Static isothermal immersion studies on dolomitic lime.

Reflected light and scanning electron microscope (SEM) studies on the isothermal dissolution of dolomitic lime cylinders in iron silicate melts at 1300°C, revealed four distinct zones which remained constant after initial reaction.

iron silicate melt (ℓ) + wüstite dendrites (s)	wüstite globules (s) + calcic olivines (ℓ) + magnesium–iron–olivine (s)	dicalcium silicate (s) + magnesiowüstite (s)	dolomitic lime (s)

(s) = solid phase (ℓ) = liquid phase

Cylinder sections examined after a 15 s immersion period produced a melt cylinder interface characterised by an irregular boundary of dicalcium silicate (C_2S) and magnesiowüstite (MF'), Plate 28 (p. 321). Silica (SiO_2) and wüstite (FeO) derived from the iron silicate melt, penetrated the pore network of the cylinder very rapidly. The overall reaction can be represented by the phase

---

† Details of the immersion experiments undertaken in this work are listed in Table 30 (p. 253) and photomicrographs have been cross referenced with respect to the relevant immersion period. A brief comment has been included in Table 30 concerning each sample illustrated by a photomicrograph.

notation listed in the Glossary of terms (p.11).

$$F_2S_{(\ell)} + 2CM_{(s)} \longrightarrow C_2S_{(s)} + 2MF'_{(s)} \qquad (4\cdot1)$$

iron silicate — dolomitic lime — dicalcium silicate — magnesiowüstite

A consequence of reaction (4.1) was the development of a globular wüstite zone at the reaction interface. The continued presence of this phase is illustrated through Plates 29, 30 and 31 (p.322), which represented reaction times of 15, 180 and 360 s respectively. Plate 29 represented a dolomitic lime cylinder that became detached from the holder on immersion. The cylinder was totally immersed by the liquid melt and the convolution of the melt - cylinder interface occurred at regular intervals around the periphery of the reacted cylinder.

Due to the rapid infiltration of melt into the immersed portion of cylinders, the initial reaction front was never preserved in samples relating to sections on the 2mm datum line (Sect. 3.7.8., p.107). A series of reaction zones were intersected by cutting a cylinder perpendicular to its long axis and above the level of chilled melt adhering to the cylinder wall. These reaction zones originated through the capillary reaction of melt drawn into upper parts of the cylinder. The reaction interface between melt and cylinder was differ-

ent to that revealed in entrant tip sections and was considered to be representative of the "initial" reaction front, Plate 32 (p. 323). A series of x-ray maps were used to indicate where a particular phase was concentrated (Plates 32b, c, d, e and f, p.323). The "initial" reaction interface may be represented as follows;

iron silicate melt (ℓ)	wüstite (s) melt (ℓ)	Ca-Fe silicate (ℓ)	zone of MgO-FeO enrichment (s+ℓ)	dicalcium silicate (s) magnesiowüstite (s)	unreacted dolomitic-lime (s)

(s) = solid phase (ℓ) = liquid at reaction temperature (1300°C)

The dolomitic lime cylinder used for the experiment had a bulk density of 1420kgm^{-3}, and was atypical of the normal bulk density used (1740kgm^{-3}). A "shadow" zone was revealed by Plate 32a (p. 323) and was coincident with the topographic depression exhibited by the all-element x-ray map (Plate 32f, p. 323) and represented the possible formation of a contractile phase. Dolomitic lime was rarely encountered in entrant tip sections and SEM images and x-ray maps revealed a less complex series of reaction zones than those considered for the "initial" reaction (Plates 33a, b, c, d and e, p. 324). A schematic representation of the dolomitic lime reaction with iron silicate melts at varying reaction times is illustrated in Fig. 40 (p.291).

At the melt - cylinder reaction interface during

short immersion periods (15 s) an open, porous dicalcium silicate crystalline meshwork developed. The crystallinity of the dicalcium silicate phase reached a maximum at a 90 s immersion period and rapidly disappeared with increased immersion time. The structures were observed with the scanning electron microscope. Plate 34 (p. 325) indicated the nature of the interface porosity whilst Plate 35 (p.325) showed the maximum development of the "meshwork" texture. Plates 36 and 37 (p.325) demonstrated the absence of the open interface network at increased immersion times of 120 and 360 s respectively.

The rapid penetration of liquid melt into the submerged cylinder formed two reaction products by way of reaction (4.1, p. 142) and effectively produced a solid cylinder because both dicalcium silicate (C_2S) and magnesiowüstite (MF') were solid at the experimental temperature, Figs. 41 and 42 (p.292). The unusual microstructure developed by the two phases occurred as a result of lime and magnesia crystallite distribution during calcination (Sect. 4.2.1., p.133). The detailed relationship between the two phases are illustrated on the SEM image, representing a 15 s immersion, in Plate 38 (p.326). SEM spot analyses revealed that the magnesiowüstite phases averaged 52 mass % FeO and 47 mass % MgO whilst the dicalcium silicate phases contained 64 mass % CaO and 32 mass % SiO_2. The similarity of ionic radius between Mg^{2+} (0.66 Å) and Fe^{2+} (0.74 Å) ions [145] and the thermodynamic impetus of silicate formation between

CaO and SiO_2, inferred from Fig. 43 (p.293), ensured that reactions occurred at specific sites within the cylinder to produce the C_2S - MF' two phase region. An iron oxide (FeO) - rich liquid was identified in some of the reacted cylinder sections examined, Plate 39 (p.326).

There are three possible mechanisms which could account for the occurrence of the globular wüstite zone at the melt cylinder interface.

(a) The action of immersing the cylinder into the melt could have chilled the melt sufficiently to precipitate wüstite athermally. This would suggest that a large temperature differential existed between the cylinder in the pre-heat position and the melt. The temperature of a "hard" burnt dolomitic lime cylinder (P app 36%) was measured prior to immersion in melt by a Pt - Pt/13% Rh thermocouple, located centrally and to a depth of 15mm into the top of the cylinder. The temperature was recorded as a millivolt value on a flat bed chart recorder operated at a chart speed of 2cm/min. The cylinder equilibrated with the furnace temperature within 5 minutes of being placed into the preheat position. The furnace hot zone temperature was pre-determined as 1304°C by a suspended Pt - Pt 13% Rh thermocouple. During a 420 s immersion period, the variation in recorded temperature between cylinder and melt was only 7°C and indicated that cylinder temperature was of no consequence in the formation of the globular wüstite zone.

(b) Wüstite may have been produced as a byproduct from the formation of dicalcium silicate. From polymer

theory of slags [62,65], Sect. 2.6 (p. 42), iron silicate melts contain a high proportion of $Si_2O_7^{6-}$ ions, and FeO may form as a result of the notional reaction.

$$:Si\text{-}O\underset{F_2S_{(\ell)}}{FeO}\text{-}Si: + \underset{C_{(s)}}{CaO} \longrightarrow :Si\text{-}O\underset{C_2S_{(s)}}{CaO}\text{-}Si: + \underset{F'_{(s)}}{FeO} \qquad (4.2)$$

The negative free energy of formation of dicalcium silicate (C_2S - 1060kJ), extrapolated from Fig. 43 (p. 293) indicated that this phase would form in preference to magnesium silicate (-880kJ) at 1300°C.

(c) During the initial penetration of melt into the cylinder, FeO derived from reaction (4.2) combined with magnesia rich crystallites to produce magnesiowüstite.

$$\underset{F'}{FeO} + \underset{M}{MgO} \longrightarrow \underset{MF'}{MgO.FeO}_{(ss)} \qquad (4.3)$$

(ss) = solid solution.

As the dissolution of the C_2S - MF' interface progressed, globules of MF' remained relatively insitu until the interface receded. Once across the interface and in partial or total contact with the melt, magnesia was immediately taken up from the MF' phase and dispersed by the melt. Plate 40a (p. 327) illustrates the interface phenomenon with magnesiowüstite, and Plate 40b the dispersion of magnesium. The remainder of the x-ray maps in Plate 40 showed a similar distribution of interface phases as Plate 33 (p. 324).

A dendritic wüstite morphology was observed in many

melt - cylinder sections. Plate 41 (p.328) represented an immersion time of 120 s and provided evidence that parts of the solid wüstite globules had acted as nucleation sites for a dendritic form precipitated from a liquid phase. This and other observations, suggested that the globular wüstite zone was undergoing melt resorption at the margins, and athermal or isothermal precipitation allowed a dendritic form of wüstite to form. The reaction may be explained by a solubility relationship which at 1300°C can be estimated from Fig. 44 (p.294).

With increased immersion time, a zone of dark grey crystals appeared close to and within the globular wüstite zone, adjacent to the melt - cylinder interface (Plate 42, p.328). A similar phase occurred at the melt-cylinder reaction interface of the "hard" burnt dolomitic lime sample and showed well cored or zoned crystals, Plate 43 (p.329). The composition of the cored phase was determined by SEM analysis (Sect. 4.3.3.1, p.159), and proved to be a magnesium - iron rich silicate which was largely solid at the experimental temperature, Fig. 45 (p. 294). In Plate 43 (p. 329), the magnesium - iron olivine phases existed well within the melt and away from the cylinder interface. The margins of the cored olivine phases were liquid and were capable of diffusing into the bulk melt.

A cylinder tip from a 15 s immersion period was removed from its resin mount and annealed within an iron crucible at a temperature of 1300°C for one hour. Observation of the tip in reflected light, revealed that the reaction products were consistent to those formed prior

to annealing. Within the area occupied by the cooled melt, rounded globules of metallic iron (white) had precipitated. Plate 44 (p. 329). Although no iron occurs in the CaO - 'FeO' - SiO_2 - MgO pseudo quaternary system, it can form at low oxygen partial pressures as indicated by Fig. 7 (p.266) representing the 'FeO' - Fe_2O_3 - SiO_2 system, or by the reaction; (52)

$$3FeO_{(\ell)} \longrightarrow Fe_{(s)} + Fe_2O_3 \qquad (4.4)$$

or by the athermal precipitation from FeO (108)

$$4FeO_{(\ell)} \longrightarrow Fe_3O_4 + Fe_{(s)} \qquad (4.5)$$

At the margin of the melt - cylinder interface, a second interface was observed which was composed of dicalcium silicate and lobate areas of magnesiowüstite, Plate 45 (p. 330). The normally globular wüstite phases had produced a lobate morphology similar to that of the magnesiowüstite phases. The second or new interface was developed between the original melt - cylinder interface and represented a possible saturation limit between the limited volume of melt remaining in the cylinder and lime derived from the dissolution of the cylinder. The porous or open interface meshwork revealed by SEM imagery in Plate 34 (p. 325) had almost disappeared after the annealing process. In addition, an x-ray map for magnesium revealed that the magnesium was evenly dispersed through all phases at the melt - cylinder interface. X-ray maps for the other elements were similar to those exhibited by Plates 33, (p.324) and 40 (p. 327).

4.3.1.1 Rotational isothermal immersion studies on dolomitic lime.

Dolomitic lime cylinders rotated in an iron silicate melt at a peripheral velocity of 3.62 $cm.s^{-1}$ (50r.p.m.) produced no change in the composition of reaction products at the melt - cylinder interface. The most noticeable change occurred in the interface morphology with the formation of finger-like projections of melt penetrating into the reacted cylinder, Plate 46 (p.331). The globular wüstite zone followed the contour of the melt-cylinder interface and was reduced in thickness to the corresponding zone in static immersed samples. Relic wüstite clusters remained where fragments of dolomitic lime had been isolated by the transgression of melt (Plate 46, p. 331). With an increased immersion time, the cylinder melt interface became very irregular in shape and cored magnesium-iron olivine phases were correspondingly developed, Plate 47 (p. 331). Larger fragments of the reacted dolomitic lime cylinder became isolated and underwent solution by the melt. A section of a rotated cylinder immersed for 360 s, and observed under the SEM, revealed a well developed zone of magnesium - iron olivine phases, Plate 48 (p. 332). A negative bias was applied to the SEM grid to create a reflective backscatter mode which highlighted the atomic number effect of the phases present and prevented the collection of low energy secondary electrons. Phases of higher atomic number, such as those containing iron (At. No. 26) in Plate 48 (p.332) were revealed as

white or light coloured phases. Conversely, magnesium bearing phases (At. No. 12) were revealed in dark grey coloured cores within the chilled melt. The cored centres had a well developed orthorhombic symmetry.

Rotated cylinders of dolomitic lime produced a deep erosion line at the position of the melt - furnace atmosphere interface and indicated the level of cylinder submergence, Plate 49 (p. 332). Comparative sections of static and rotated cylinders revealed that the rotated cylinders contained unreacted, irregular shaped cores of dolomitic lime, Plates 50 and 51 (p. 333). After the instigation of the procedure outlined in Sect. 4.2.4. (p. 138), the cores did not represent hydrated material. With the increased rate of formation produced by rotating the dolomitic lime cylinders, the magnesium - iron olivine phases may have behaved as a viscous or semi solid barrier to the melt and reduced the amount of melt drawn through the cylinder by capillary attraction via the pore network. The reduced diameter of the rotated dolomitic lime cylinders can be contrasted with those of static immersions in Plates 50 and 51 (p. 333) and clearly indicate an increased rate of dissolution.

4.3.1.2 The addition of 5 mass % magnesia to the synthetic slag bulk.

When 5 mass % magnesia was added to the synthetic iron silicate melt , the dissolution rate of the dolomitic lime cylinder immersed into it was reduced, with only the peripheral areas of the cylinder producing any

reaction. After a static 15 s immersion period, patches of cylinder close to the reaction interface remained unreacted and the globular wüstite zone was reduced in thickness, Plate 52 (p. 334). In Plate 52, the unreacted areas of cylinder appeared as a black amorphous phase. A well developed area of cored magnesium - iron olivine phases were formed close to the melt - cylinder interface after an immersion period of 360 s, Plate 53 (p. 334). The magnesia rich phases extended into the melt beyond the globular wüstite zone. Unreacted patches of cylinder remained close to the melt - cylinder interface even after the 360 s immersion period.

4.3.1.3 The pill test.

The pill test represented the reaction between a small volume of synthetic slag and an infinitely large volume of cylinder. A large proportion of the melt was drawn by capillary suction into the sidewalls of the dolomitic lime cylinder recess but enough remained in the base of the recess to indicate that the reaction products were similar to those observed in the cylinder immersion experiments. The interface developed between the melt and dicalcium silicate - magnesiowüstite phases was difficult to identify except where the proportions of magnesiowüstite were low, Plate 54 (p. 335). The zone regarded as essentially wüstite at the melt - cylinder interface, was lobate in shape and a truly globular wüstite was absent. Rounded particles of metallic iron (white) occurred in the chilled melt and appear in Plate 54 (p. 335).

The unreacted regions of the dolomitic lime cylinder sidewall (dark grey) occurred as an amorphous area. The indistinct melt cylinder interface was very irregular in its distribution, and dicalcium silicate - rich areas occurred frequently. Detail of the interface region is illustrated in Plate 55 (p. 335).

4.3.1.4 The iron silicate - "Dolomet" reaction.

Samples of "Dolomet" were obtained from the Steetley Mineral Company Ltd., Worksop, and fabricated into a cylindrical form by shaping and grinding on dry 240 grade silicon carbide paper. The bulk density of the "Dolomet" was approximately 1700kgm^{-3}. After a static 15 s immersion period in an iron silicate melt at 1300^{o}C, the reaction interface revealed by sectioning was identical to the reaction interface produced by dolomitic lime cylinders prepared under laboratory conditions, Plate 56, (p. 336). The melt penetrated through most of the immersed cylinder and extensive globular wüstite zones were developed between the melt and reacted cylinder interface. Some areas of the "Dolomet" - melt reaction zone produced a granular metallic iron phase (white) as illustrated in Plate 57 (p. 336).

4.3.2 Static isothermal immersion studies on lime cylinders.

Lime (CaO) is the major constituent of LD steelmaking slags, the other slag components being silica (SiO_2) and iron oxide (FeO) derived from the oxidation

of metalloids in the bath. The dissolution of lump lime additions in contact with metallic iron and slag can be considered with respect to the phase equilibrium diagram in Fig. 12 (p. 269). At 1300°C, the isothermal section can be represented in two ways as shown by Figs. 46a and 46b (p. 295). A feature of both diagrams is the existence of a high temperature "nose" of dicalcium silicate plus liquid phases, which form a barrier and prevent the direct reaction between an iron silicate melt and lime. The influence of magnesia on the dissolution behaviour of lime can only be assessed by a consideration of the features of the lime - iron silicate reaction.

4.3.2.1 "Hard" burnt lime.

"Hard" burnt lime cylinders were examined optically by reflected light microscopy and revealed four distinct zones.

iron silicate (ℓ)	dicalcium-silicate(s)	An iron oxide-rich liquid.	Lime (s) + iron oxide-rich liquid in pores.

(ℓ) = liquid, (s) = solid.

After a 15 s immersion in an iron silicate melt, a granular dicalcium silicate (C_2S) layer began to precipitate out at the reaction interface between the melt and lime cylinder, Plate 58 (p. 337). An iron oxide (FeO) - rich phase occurred in front of and also behind the re-

action interface and penetrated the pore network of the lime cylinder. The FeO - rich phase was considered to represent calciowüstite (CF') which would have been liquid at the reaction temperature of 1300°C, Fig. 47 (p. 296). Calciowüstite and dicalcium silicate may be produced as a result of the heterogeneous reaction between lime and iron silicate, as follows;

$$\underset{\text{iron silicate}}{F_2S_{(s)}} + \underset{\text{lime}}{4C_{(s)}} \longrightarrow \underset{\text{calciowüstite}}{2CF_{(\ell)}} + \underset{\text{dicalcium silicate}}{C_2S_{(s)}} \qquad (4.6)$$

(ℓ) = liquid phase , (s)=solid phase

Plate 59 (p. 337) at high magnification, revealed that the dicalcium silicate particles were beginning to coalesce and that extensions of the pale grey coloured FeO rich liquid were becoming isolated in the melt. After an immersion time of 120 s, a dense C_2S layer had formed around the periphery of the lime cylinder, Plate 60 (p. 338). The etched, dark grey coloured C_2S layer was granular in parts and was separated from the lime cylinder by a thin layer of calciowüstite. An immersion period of 240 s produced a thickening of the C_2S layer which still exhibited a granular form, Plate 61 (p. 338). Calciowüstite was visible on the melt side of the C_2S interface in addition to the lime cylinder side. The dendritic wüstite phase within the "melt" represented in Plate 61 was produced athermally. A lime cylinder reacted for 360 s developed a continuous dicalcium silicate barrier

adjacent to the melt. A granular dicalcium phase occurred towards the cylinder side of the reaction interface, Plate 62 (p. 339). The proportion of calciowüstite had increased slightly and lime particles on the lime cylinder periphery became rounded and isolated by the liquid phase. Within the lime cylinder, the particles of lime remained sintered together. Where the melt had penetrated the pore network, rectangular crystals of tricalcium silicate were precipitated, Plate 63 (p. 339).

4.3.2.2 "Soft" burnt lime.

"Soft" burnt lime cylinders produced a reaction interface similar to that recorded by "hard" burnt lime cylinders when immersed in an iron silicate melt. One major feature of difference was the formation of an iron oxide (FeO) - rich, two-phase region between the dicalcium silicate layer and the lime cylinder. "Soft" burnt lime cylinders also developed a solid dicalcium silicate (C_2S) interface, adjacent to the melt after an immersion period of only 15 s, Plate 64 (p. 340). The C_2S layer has lost its granular appearance after 120 s and has produced a solid, irregular shaped boundary, Plate 65 (p. 340). The proportion of FeO - rich liquid increased and fragments of lime within the cylinder became isolated. Within the vicinity of the C_2S - lime cylinder interface, individual granules of C_2S were observed in association with small, rectangular shaped crystals of tricalcium silicate (C_3S), Plate 65 (p. 340).

A SEM image of the melt - cylinder reaction inter-

face revealed the granular nature of the dicalcium silicate layer adjacent to the melt and FeO - rich two phase region, Plate 66a(p.341). A series of x-ray maps provided an indication of the element distribution between the melt and the lime cylinder. Plate 66b (p. 341) indicated that silicon (Si) was absent from phases within the FeO - rich region and lime cylinder. Calcium(Ca) had a widespread distribution and produced a slight depletion in the FeO - rich region and concentration within the C_2S layer, Plate 66c (p.341). The distribution of Ca within the iron silicate did not reveal any areas of preferential concentration. Iron (Fe) was absent from the C_2S layer but showed enrichment in the calciowüstite - FeO rich liquid area, Plate 66d (p.341). The all element x-ray scan failed to detect any apparent zones produced by topographic depressions in the polished specimen.

An immersion period of 540 s produced a narrow and convoluted dicalcium silicate interface, Plate 67 (p.342). Within the iron oxide - rich liquid region, discrete particles of angular dicalcium silicate crystals became isolated and associated with partially dissolved lime particles and rectangular tricalcium silicate crystals. The two phase region of iron oxide rich material became more prominent with the increased immersion time, Plate 68 (p.342). The composition of the two phase iron oxide - rich region was determined by SEM spot analysis. The pale grey coloured phase in Plate 68 was composed of 95.7 mass% FeO and 4.25 mass % CaO and the darker grey coloured phase 55.3 mass % FeO, 43.37 mass % CaO and 1.2 mass % SiO_2.

The dark grey coloured, pear shaped phase in Plate 68 (p. 342) was dicalcium silicate. "Soft" burnt lime cylinders produced a greater proportion of FeO - rich liquid between the C_2S - lime cylinder interface than "hard" burnt lime cylinders. Sufficient liquid was available to penetrate into the immersed section of cylinder and isolate lime particles by dissolution, Plate 69 (p.343). Tricalcium silicate crystals were precipitated as a product of the dissolution reaction. Some of the lime particles produced a micro-corrugated surface at the interface with the adjacent iron oxide - rich liquid.

4.3.2.3. The addition of 5 mass % MgO to the synthetic slag bulk.

An initial preliminary experiment involving a "Soft" burnt lime cylinder immersed for 15 s in only 2 mass % MgO - iron silicate melt, produced an irregular and granular dicalcium silicate (C_2S) interface between the melt and reacted lime cylinder, Plate 70 (p.343). A zone of tricalcium silicate (C_3S) crystals was also observed within the iron oxide - rich region that separated the C_2S layer from the cylinder. With a melt containing 5 mass % MgO, the zone of tricalcium silicate crystals became more extensive after a 15 s immersion period, Plate 71 (p.344). The C_2S layer adjacent to the melt interface was irregular in shape and the granular form of C_2S extended into the C_3S zone. In the presence of magnesia, the melt - lime interface described in Sect. 4.3.2.1. (p. 153) may be modified as follows:-

iron silicate (ℓ) + wüstite dendrites	granular dicalcium silicate (s)	tricalcium silicate + FeO-rich liquid	lime (s) + FeO-rich liquid

(ℓ) = liquid (s)= solid

An immersion period of 360 s produced an extensive and dispersed granular dicalcium silicate zone containing a high proportion of FeO - rich liquid, Plate 72 (p.344). Rectangular crystals of tricalcium silicate showed signs of dissolution, indicated by the irregular shape and iron oxide - rich inclusions within some of the crystals. At each lobe of the C_2S extension within the melt, the proportion of iron oxide - rich phase increased, Plate 72 (p.344) and at one point had ruptured the tenuous C_2S envelope. An examination of the C_2S interface adjacent to the melt indicated a particle size distribution pattern to the C_2S granules, Plate 73 (p.345). The granular C_2S zone was approximately 60 μm wide with the smallest sized particles (1 to 5 μm) adjacent to the melt interface, and the larger sized particles (10 to 20 μm), 25 to 30 μm from it. A SEM image of the melt - C_2S interface in Plate 74 (p.345) revealed that the C_2S envelope around the reacted lime cylinder was discontinuous and no longer formed a solid barrier.

A series of x-ray maps across the SEM images illustrated through Plates 75a, b, c, d, e, and f (p.346), illustrated that magnesium was widely dispersed and occurred in slightly low concentrations only across the interface (Plate 75b). Silicon was distributed within the melt,

C_2S and C_3S zones and was almost absent from the lime cylinder area (Plate 75c, p.346). The distribution of calcium was widespread and irregular within the melt due to the development of a wüstite phase on cooling (Plate 75d). The x-ray map of iron indicated a zone of iron enrichment coincident with the FeO - rich phase which occurred between the C_2S - cylinder interfaces (Plate 75e). The all element scan (Plate 75f) did not reveal the cracks within the surface of the specimen. After an immersion period of 360 s, the distribution of the elements through Plates 76a, b, c, d, e and f (p.347) remained similar to the distribution patterns in the cylinder reacted for 15s. The magnesium x-ray map indicated a slight concentration of MgO, coincident with the melt - C_2S interface, Plate 76b.

4.3.3 Quantitative SEM studies.

4.3.3.1 Dolomitic lime.

The quantitative SEM studies yielded mass % of oxide data. This was used to calculate the mole proportions and mole fractions of phases present. Estimates were made of the compositions of phase assemblages even though the phases formed may not have been representative of equilibrium conditions. The composition of each phase assemblage has been annotated beneath the relevant Plate and oxide concentration profile.

Plate 77 (p. 348) represented a specimen of a dolomitic lime cylinder immersed in an iron silicate melt for 15 s. A globular wüstite zone developed adjacent to the

dicalcium silicate and magnesiowüstite association within the reacted cylinder but no clear phase relationships were observed within the area of melt. Lime and magnesia levels were low in the primary fayalite phase but lime values increased in the darker grey coloured eutectic region represented in Plate 77 (p. 348). The mole fraction values of oxide components within the eutectic, indicated that this phase was a calcic olivine (C-F-S). An indistinct zone (dark grey) coincided with the globular wüstite phases and magnesia showed progressive enrichment in this region.

Plate 78 (p. 349) represented a specimen which had been immersed for 120 s. The indistinct melt - cylinder interface developed a cored or zoned phase (dark grey) adjacent to, and within the globular wüstite zone. The mole proportions of oxides present on the dark grey coloured region were 2(MgO-FeO):1 SiO_2. A mineralogical notation described by Berry and Mason [143] has been used to define the olivine series $Mg_xFe_{1-x}.SiO_4$ to represent the Forsterite ($2MgO.SiO_2$) and Fayalite ($2FeO.SiO_2$) end members. This series is referred to as the Fo - Fa olivine series. The mole fraction of one end member automatically fixes the value of the other member (Fig. 45, p. 294). The terminology of forsterite (Fo) has been used throughout this section to describe the composition of the phase. The magnesia values obtained from the oxide distribution profile in Plate 78 (p. 349) showed a progressive forsterite enrichment towards the cylinder, ranging from Fo_{72} to Fo_{80}.

After a 360 s immersion period, a granular and dif-

fuse Fo - Fa olivine phase formed, Plate 79 (p. 350). Isolation of the granular olivine phase and progressive resorption occurred at the margin between melt and globular wüstite.

The reaction interface for the pill test was represented as illustrated in Plate 80 (p. 351). The mole proportions and mole fractions of phases derived from oxide concentrations suggested some 4 - component assemblages. The possibility that simultaneous measurement of two or more phases occurred at some of the analysis points cannot be overruled due to the spot size used. The proportions of Fo - Fa olivine phases were low in the sample and this may have been as a consequence of the low volume of melt available for reaction. The reacted parts of the "crucible" were composed of dicalcium silicate and magnesiowüstite, and produced a similar interface to that of a dolomitic lime cylinder immersed in a correspondingly large volume of melt.

The addition of 5 mass % MgO to the melt produced a well developed Fo - Fa olivine zone which followed closely the contours of the globular wüstite margin after a cylinder immersion time of 360 s, Plate 81 (p. 352). Penetration of melt into the cylinder was limited to the margin after a 15 and 360 s immersion period. The Fo - Fa olivines (Fo_{69}) represented by the dark grey coloured areas of the melt (Plate 81) showed signs of resorption within a calcic olivine phase.

Four zones were distinguishable in a composition profile represented by the hard burnt dolomitic lime cyl-

inder in Plate 82 (p. 353). Analysis point 1 indicated a lime rich fayalite phase (C - F - S) which persisted into the well developed cored Fo - Fa olivine region, adjacent to the globular wüstite and Fo - Fa assemblages. A crack separated the reacted cylinder from the melt interface after the cylinder had cooled. Analytical points 3, 4, 7 and 8 (Plate 82, p.353) indicated a gradual enrichment of the forsterite (Fo) component towards the cylinder interface, progressing from Fo_{64}, Fo_{60}, Fo_{71} and Fo_{74} respectively.

The melt cylinder interface concentrations of FeO and MgO have been compared at immersion times of 15, 120 and 360 s using the oxide concentration results, Figs. 48 and 49 (p.297). Composition profiles were related to the same melt - cylinder interface position and adjusted to an equivalent scale. Phases composed of wüstite globules or dicalcium silicate were ignored. Analytical points that may possibly have represented mixed phases were also ignored. The profiles in Figs. 48 and 49 may be envisaged as a mean free path from the melt through to the cylinder.

The concentration of FeO decreased rapidly towards the melt cylinder interface and rose sharply again due to the formation of magnesiowüstite. The widest zone of FeO depletion occurred within the 120 s immersed sample. Magnesia (MgO) produced a corresponding increase in concentration towards the cylinder interface for all three immersion periods. A compatible phase of MgO and FeO formed within the cylinder (magnesiowüstite) but a divergent relationship existed when both oxides diffused into the melt.

The relationships were equated with the formation of magnesium silicates containing quantities of FeO (Fo - Fa olivine) and CaO - FeO silicates which were liquid under the prevailing isothermal conditions.

4.3.3.2 Lime.

An immersion period of 15 s produced a well developed CaO concentration gradient between a "soft" burnt lime cylinder and an iron silicate melt, Plate 83 (p.354). Lime (CaO), silica (SiO_2) and iron oxide (FeO) contents of the melt remained relatively constant up to the interface with dicalcium silicate (C_2S) which formed a barrier approximately 10 μm thick. The silica concentration gradient indicated an absence of SiO_2 in the zone between the C_2S barrier and the lime cylinder. The silica - free zone coincided with a FeO - CaO association corresponding to the phase calciowüstite (CF').

An extended static immersion period of 540 s produced a 200 μm wide reaction interface containing C_2S and a 2-phase region of wüstite and calciowüstite, Plate 84 (p. 355). Silica showed the same distribution pattern to that in the 15 s immersed cylinder (Plate 83, p.354).

A lime cylinder reacted with an iron silicate melt containing 5 mass % MgO produced a granular dicalcium zone, with magnesia reaching a 10 mass % level at the melt - cylinder interface after a 15 s immersion period, Plate 85 (p. 356). The level of magnesia fell to around 2 mass % MgO between the C_2S and lime cylinder interface. Silica showed a progressive depletion from the melt, C_2S

and tricalcium silicate (C..S) phases, and only a trace occurred in the iron oxide - rich phase adjacent to the cylinder. The distribution of lime indicated a steep concentration gradient from the edg*e of the reacted cylinder into the melt, Plate 85 (p.356). A cylinder immersed for 360s in a 5 mass % MgO - iron silicate melt produced a mixed zone 150 ,um wide of CpS, C^S and OF' phases, Plate 86 (p.357). Magnesia remained at the 5 mass % MgO level close to the melt " CpS boundary but was reduced to between 1 and 2 mass % MgO within the CpS - lime cylinder interface.

The oxide concentrations derived from the analyses of phases produced by the melt - cylinder reactions have been plotted across the 1300°C isothermal section of the CaO - 'FeO1 - SiOp phase diagram (Figs. 50a and b, p.298). Lime cylinders immersed in magnesia free and 5 mass % MgO-iron silicate melts have been compared at varying times. The reaction of lime with an iron silicate melt produced a displacement of the melt composition towards the CaO - SiOp edge of the CaO - 'FeO' - SiOp isothermal diagram. The formation of solid calcium silicate phases produced a liquid enriched in FeO relative to the bulk melt, and the oxide composition plots moved across to the FeO corner of the diagram. At this position, the liquid phase was capable of reacting directly with the lime cylinder,(Figs. 50a and b, p. 298). Magnesia enriched iron silicate melts produced a similar type of reaction but the reaction profile was deflected into the tricalcium silicate phase field before the composition moved across to the FeO corner of the diagram.

4.3.4 Dissolution Experiments.

4.3.4.1 Dolomitic lime cylinders.

The results of the immersion experiments on static and rotated dolomitic lime cylinders are tabulated in Tables 31 and 32 (p. 256). The results are presented graphically in Figs. 51 and 52 (p.299) and represent plots relating the mass % of lime (CaO) and magnesia (MgO) recorded in the bulk synthetic slag after analysis against the cylinder immersion time. The mass % CaO and MgO contents of the reacted melts were corrected by subtracting the values of CaO and MgO present in the starter slag. This allowed the mass % - time plots to be extrapolated through to the zero point or origin. The graphs representing the static dissolution of dolomitic lime produced a marked inflexion of the CaO and MgO gradients after 60 s, Fig. 51 (p.299). The magnesia mass values produced a degree of scatter with increased immersion time, but after 60 s, the line drawn through the points maintained a horizontal trend. Both CaO and MgO plots had similar gradients up to that point in time. The inflexions recorded by both CaO and MgO gradients did not represent the chilling of the melt by the immersed cylinder. Rotated dolomitic lime cylinders produced an erratic spread of CaO mass values with increasing immersion time, Fig. 52 (p.299), but the slope of the magnesia gradient was steeper than that recorded in the static immersion studies. The slope of the lime gradient was apparently similar to that produced in the static experiments.

The width of the ubiquitous globular wüstite zone was measured directly from photomicrographs of the reaction interface and the values related to the period of cylinder immersion, Fig. 53 (p. 300). The zonal width was measured in relative units of thickness, with one unit equivalent to 10mm. All photomicrograph images were based on a magnification factor of x128 and all measurements taken perpendicular to the reaction interface. Only the first major interface that occurred between the edge of the mounted sample and the reacted dolomitic lime cylinder was measured and a minimum of 10 readings were taken to provide an average thickness value. Fig. 53 (p. 300) illustrated that the thickness of the globular wüstite zone averaged 1.2 relative thickness units. The equivalent zone produced by the rotated cylinders was remarkably linear and constant with immersion time and was reduced to 0.6 relative thickness units.

4.3.4.2 Lime cylinders.

The results of the static immersion of both "hard" and "soft" burnt lime are tabulated in Tables 33 and 34 (p. 257). The results are presented graphically in Figs. 54 and 55 (p. 301) and represent plots relating the mass % CaO recorded in the bulk synthetic slag after analysis, versus the period of cylinder immersion. Mass % CaO versus time plots for "hard" burnt lime cylinders produced a linear, gently sloping gradient that remained unchanged from the origin. "Soft" burnt lime cylinders produced a steep mass % CaO - time gradient which also remained apparently unchanged with increased immersion

time. There were a limited number of experimental points for the longer immersion periods.

4.4 Cone fusion studies.

Cone fusion studies were carried out on synthetic slags ranging in composition from iron silicate (fayalite) up to 38 mass % lime on the fayalite - dicalcium silicate tie - line of the CaO - 'FeO' - SiO_2 system, Fig. 56 (p.302). From the pseudo - binary diagram in Fig. 57, (p.303) which was projected from the fayalite ($2FeO.SiO_2$)- dicalcium silicate ($2CaO.SiO_2$) tie - line of Fig. 56, the liquidus temperatures across the section were found to range between 1150 and 1300°C. Using the synthetic slag compositions illustrated on Fig. 56, nominal magnesia additions were made at 5, 10 and 15 mass % MgO intervals. The close agreement between the aim and actual magnesia contents of the synthetic slags listed in Table 35 (p.258), suggested that melts which were not analysed through lack of sufficient sample mass would have magnesia contents similar to the aim values. The addition of zirconia to an iron silicate melt has been dealt with in section 4.1.5.2, (p.127). Repeat measurements on a number of cones listed in Table 35 indicated that a high degree of replicability could be achieved with the measurement technique. Cones containing in excess of 8 mass % MgO contracted before collapsing. The sequence of cone deformations illustrated through Plates 13a, b and c (p. 315) and described in section 3.9 (p. 111), was only observed in the high magnesia cones when liquid drainage had caused the erect cone

to contract to approximately three quarters of its original height.

To facilitate the description of cone melting behaviour, the initial melting and final collapse temperatures illustrated in Table 35 (p. 258) have been plotted on compositional axes of mass % MgO versus mass % CaO, to produce isothermal contour plans which are shown in Figs. 58 and 59 (p. 303). Below the surface of Fig. 58, the system would be entirely solid with liquid only just appearing on the actual surface. Although this first-formed liquid was based only on the observation of movement of the cone tip through the telescopic cathetometer, Fig. 58 can be approximated to a solidus plan. Similarly, the surface of Fig. 59 (p. 303) containing specific temperature points at which the cones were observed to collapse can be approximated to a liquidus plan. A point above the surface in Fig. 59 would be all liquid whilst a point lying immediately beneath the surface would contain liquid with a small proportion of solid phase. The interval between the solidus and liquidus surface would represent the melting range. The contour plans in Figs. 58 and 59 have been used to construct sections showing the effect of magnesia on the melting ranges of synthetic slags at fixed lime compositions. The results of the cone fusion studies are discussed with reference to the melting ranges exhibited by sections at 0, 10, 15, 20, 30 and 35 mass % CaO shown through Figs. 60 to 65 (pages 304 to 306).

4.4.1 The effect of magnesia on the melting range of an iron silicate melt.

The variation in the melting range of an iron silicate melt with magnesia additions, is shown in Fig. 60, (p. 304). The melting range remained relatively constant at 12°C from zero to 5 mass % MgO and gradually increased to 28°C up to 9 mass % MgO. Above the 9 mass % magnesia level the melting range increased rapidly and reached 75°C at 12 mass % MgO. The rate of increase of liquidus and solidus temperatures was linear for the most part, with the liquidus curve becoming steeper at 9 mass % MgO.

4.4.2 The effect of magnesia on the melting range of a 10 mass % CaO - iron silicate slag.

The melting ranges exhibited by the 10 mass % CaO melt with magnesia additions in Fig. 61 (p. 304) was substantially increased over that of the corresponding iron silicate melt in Fig. 60 (p. 304). The melting range remained at about 10°C up to 4 mass % MgO before diverging, whilst the liquidus temperature was reduced by 50°C at zero MgO content. The reduction in the liquidus temperature of the magnesia free - lime - fayalite melt was due entirely to the addition of lime. The liquidus surface increased in temperature in a linear manner with the addition of magnesia, whilst the slope of the solidus curve decreased to extend the melting range to approximately 130°C at 14 mass % MgO.

4.4.3 The effect of magnesia on the melting range of a 15 mass % CaO - iron silicate slag.

The section drawn through the 15 mass % CaO composition line in Fig. 62 (p.305) highlighted the existence of the minimum in the liquidus and solidus surfaces of Figs. 58 and 59 (p.303) which again reflected the effect of the lime addition rather than magnesia. This effect was also illustrated in the pseudo - binary section in Fig. 57 (p.302). The melting range varied from 8 to 24°C up to 5 mass % MgO and increased rapidly to 130°C at 14 mass % MgO, at which point the liquidus value had increased by 305°C from the magnesia - free liquidus temperature.

4.4.4 The effect of magnesia on the melting range of a 20 mass % CaO - iron silicate slag.

The most irregular variations in the melting ranges of magnesia - bearing lime slags were illustrated in the section in Fig. 63 (p.305). An apparent decrease in the melting range occurred at 8 mass % MgO, whilst at 14 mass% MgO the melting range had increased to 125°C. The initial liquidus temperature had increased to 1140°C in the absence of any magnesia and rose by 250°C with the addition of 14 mass % MgO.

4.4.5 The effect of magnesia on the melting range of a 30 mass % CaO - iron silicate slag.

The initial liquidus temperature in the magnesia - free melt, Fig. 64 (p.306) rose to 1170°C and the melt-

ing range increased from 6°C to 75°C at 14 mass % MgO. Compared to the melting ranges recorded by the 10, 15 and 20 mass % CaO sections, there was a marked reduction with respect to the 14 mass % MgO level.

4.4.6 The effect of magnesia on the melting range of a 35 mass % CaO - iron silicate slag.

Cones whose compositions were close to the 35 mass% CaO section line (Table 35 p. 258) showed an increase in the liquidus temperature (1242°C) compared to all the other lime - bearing cones in the absence of magnesia. This trend was confirmed in the section illustrated in Fig. 65 (p.306). There was a steady divergence of the liquidus and solidus temperatures which gave a melting range of 80°C at 14 mass % MgO. Both the 30 and 35 mass% CaO sections gave a decreased melting range compared with the other CaO - bearing slags at the 14 mass % MgO level. Cone 10MCF38 in Table 35 (p.258) powdered on cooling due to the inversion of α or β dicalcium silicate to the γ polymorph.

4.4.7 Polished section examination of melts used in cone fusion studies.

Synthetic slags used for cone fusion studies were fused at 1300°C with the exception of those containing high proportions of magnesia (10 to 15 mass % MgO) and slag CF38 (FeO 27.3, Fe_2O_3 1.2, SiO_2 32.04, CaO 38.5 mass % - Fig. 56 p. 302) which were fused at 1340°C. To verify the assumption that all the slags were fully

molten and homogeneous, polished specimens were prepared and examined with the Zeiss optical microscope. Slags fused at 1300°C and sample CF38 were found to have melted completely. Slag compositions at 15 mass % MgO - 13 mass % CaO iron silicate, 10 mass % MgO - 20 mass % CaO iron silicate and 15 mass % MgO - 32 mass % CaO iron silicate were prepared to provide additional information on the solubility of magnesia at a temperature similar to that encountered during the early part of an LD blow. These slags were subsequently studied as cones 15MCF13, 10MCF20 and 15MCF32, Table 35 (p.258). The melts were rapidly withdrawn through the top of the Carbolite furnace (sect. 3.3.2) and water quenched to retain isothermally the phases present at 1340°C. A 10 and 15 mass % MgO - lime iron silicate slag is represented by the photomicrographs in Plates 87 and 88 (p. 358) respectively. A high proportion of both slags was liquid at the fusion temperature but small areas of "crystal-mush" have acted as nucleation sites in the athermally cooling liquid to produce the dendritic form of wüstite (FeO). The radial development of dendritic wüstite away from a partially sintered wüstite globular phase is well illustrated in Plate 88. An essentially sub-liquidus surface is illustrated in Plate 89 (p. 358) where liquid has developed within a sintered agglomeration of phases. The clustering of the irregular-shaped globular phase in Plate 88 (p. 358) appeared to be magnesiowüstite, a solid solution of FeO and MgO. There was no visible evidence of a discrete magnesia phase in the sections studied in Plates 87, 88 and 89 or in high magnesia iron silicate melts.

5 Discussion.

The discussion of the results and their interpretation are described under the following headings;

5.1 Assessment of Experimental techniques.

5.2 Kinetics and phase relationships.

5.3 Relevance to the LD or basic oxygen steelmaking process.

5.1 Assessment of Experimental techniques.

5.1.1 Viscosity studies.

One of the aims of the investigation was to establish a viscometer technique to study the effect of magnesia on the fluidity of iron silicate melts at temperatures corresponding to those of early formed LD steelmaking slags (1300 to 1450°C). It was not the intention to determine precise, absolute viscosities of synthetic iron silicate (fayalite) slags or to describe the slags over the full range of rheological properties.

The condition of laminar flow has to be fulfilled to be able to utilise equation 3.6 (p. 83) to calculate a viscosity value and, by definition, assumes that the measured fluid behaves in a Newtonian manner. The instrument or crucible calibration constant (K) is itself determined from a Newtonian fluid, and the apparent viscosity is derived from an expression ($\mu = K \times S \times U$) that employs an apparent or Newtonian rate of shear. Hence the apparent viscosity of a fluid used in conjunction with an instrument constant (K), determined with a calibration oil, has been considered

to represent an apparent "apparent" viscosity [128]. For the purpose of presentation, the results described under section 4.1 (p. 116) represent apparent viscosity values only and the synthetic slag viscosity - temperature curves imply Newtonian behaviour. The errors on the viscosity measurements have thus been assessed.

5.1.1.1 The thermal expansion of components.

Instrument or calibration constants (K) were measured with a Newtonian fluid at 20°C, whilst viscosity measurements were undertaken at temperatures in excess of 1150°C (Section 4.1). Shiraishi and co-workers [53] have estimated that for iron components similar in size to those used in this work, a maximum error of 2.3% occurs due to the changes in linear dimensions, based on the linear expansivity of iron of 16.6×10^{-6} per °C. Zirconia crucibles would also produce a slight expansivity in their overall dimensions at an equivalent range of temperatures, and a linear value of 12.2×10^{-6} per °C has been reported for the cubic form of zirconia by Binns [146]. The comparative error equivalence due to the expansivity of iron and zirconia components would be of a similar order. Viscosity measurements on melts contained in iron and zirconia crucibles would have viscosity values that incorporated the expansile properties of the measuring components irrespective of melt composition, and therefore the expansile properties of the measuring components would not affect the recorded viscosity values.

5.1.1.2. The geometrical arrangement of the crucible and measuring bob.

The relative position between the measuring bob, melt and crucible was observed with the aid of the periscope attachment located into the top of the upper gas seal. It was possible to ensure that the bob was centred coaxially within the crucible and immersed to the correct depth. The electrical effect produced by the rotating measuring bob hitting the sidewall of the crucible indicated the extent of misalignment along a vertical axis. End effects were minimised with the hollow measuring bob and a constant quantity of 'melt' ensured that the immersed bob remained within 1 to 2mm of the 10mm clearance limit between the base of the crucible and bob. Over, or under immersion of the measuring bob by 2mm or less, produced no more than 3.5% variation in the recorded viscosity value.

5.1.1.3. Errors due to temperature measurement.

The crucible, measuring bob, crucible contents and thermocouple were all located within the 10°C variation limit of the hot zone. This accounted for an error of no more than 1.5% in the recorded temperature. Thermocouples (Pt - Pt/13% Rh) were used without any calibration against the melting temperature of a reference material. A measure of the replicability of the crucible/melt temperature, recorded by the crucible thermocouple, can be estimated from the temperature calibration chart in Fig. 32 (p.285). The variation of points at a specific temperature represented

a temperature difference of 12°C (1.5%) between each experiment, and in addition, revealed the high degree of consistency achieved in positioning the crucible assembly within the hot zone profile. The temperature of the stirred melt was identical to that of the static melt.

5.1.1.4. Composition changes within the melt.

Contamination from zirconia crucibles did not influence the viscosity values recorded on various synthetic slag systems studied during the duration of the experiment. Additional cone fusion studies have shown that the melting behaviour of the synthetic slag is only slightly influenced by the presence of zirconia at saturation levels of 13 to 15 mass % ZrO_2. Within the duration of the viscosity experiment, any compositional change within the melt, with respect to time, can be assessed by relating temperature - viscosity points between the ascending and descending temperature - viscosity traverses; or by comparing the synthetic slag compositions before and after the experiment. The viscosity variation of corresponding points at an equivalent temperature, derived from the descending and ascending temperature - viscosity traverse, is not greater than 7%. This value includes the variation recorded by melts contained in zirconia crucibles. The value may also be used as an indicator to the replicability of the technique in the absence of trials repeatedly conducted with melts of an identical composition.

5.1.1.5. Factors affecting the calibration constant.

The aggressive nature of 'FeO' - rich synthetic slags

was demonstrated by the formation of erosion or slag lines on the walls of the zirconia crucibles. The existence of the lower, deeper slag line in particular, alters the width of the annulus between the crucible and bob over that region, Fig. 35,(p. 287). This effectively leads to an underestimation of the calibration constant used to calculate viscosity values using zirconia crucibles. Careful examination of a section cut down the long axis of the crucible revealed that the reduced crucible wall thickness existed over approximately 25% of the measuring bob height, Fig. 35. As a consequence of this, recorded viscosity values would be slightly lower than those taken where the annular distance remained constant i.e. in the iron crucibles. Valid comparisons can still be made between the apparent viscosity values of different melts measured by the zirconia crucible - iron measuring bob configuration, because all zirconia crucibles produced the same effect. The calibration constant determined for iron crucibles and based on the viscosity of glycerol at three temperature levels, produced a standard deviation of $\pm$ 9% of the measured constant (4.808).

The cumulative total error of the viscosity measurement technique described in this work does not exceed 20%. Even though this value appears high, the errors due to temperature measurement, the thermal properties of the measuring components and the various crucible constants will remain consistent at a given temperature and melt composition. Consequently, the relative error inherent in the technique will not exceed a value of about 10%, which is

mainly accreditable to the replicability of the method.

The viscosity measurement is, therefore, adequate and sensitive enough to enable the comparative studies to be made between melts whose compositions are altered through oxide additions. The extrapolation of apparent viscosity results measured from iron and zirconia components is valid, since the components have thermal expansion properties of a similar order, and viscosity values obtained in zirconia crucibles tend to be slightly underestimated. The addition of magnesia to iron silicate melts produces a real increase in the apparent viscosity, in response to an increase in the liquidus or melting temperature. This effect decreases with increased temperatures when the fluidity of the melts increases with the change from a solid + liquid phase association to a totally liquid one. The results of apparent viscosities derived by this experimental method can be compared with those cited in the Literature (51, 52, 54, 79) if minor compositional or possible Po_2 variations are ignored. Published results of viscosity values on iron silicate (fayalite) melts have been taken from tables or temperature - viscosity curves, and compositions related on a mass% basis. The results of apparent viscosities obtained in this work are shown in Table 36 (p. 259) and compare favourably with published values for fayalite - type melts.

5.1.2 Cone fusion studies.

For comparative purposes, the cone fusion method is a satisfactory technique for the study of melting behaviour

in synthetic slags. Temperature variations between individual cone fusion measurements are within 1% and the replicability of the method is within a similar limit. The melting behaviour of the cone is predominantly dependent upon the physical properties of the fused material and the interaction between the solid and liquid phases. The melting range, which represents solid plus liquid phase associations, produces an apparent increase in the viscosity of the liquid phase in a "closed" system and the viscosity results confirm this behaviour. In an "open" system, such as that represented by a cone, the first formed liquids, usually represented by eutectic compositions, are free to leave the system under the influence of gravity. The withdrawal of liquid produces an increase in the proportion of higher melting point components within the cone and the physical and chemical characteristics of the associated solid plus liquid phases undergo changes.

Cones containing upwards of 8 mass % MgO and cones with zirconia (12 to 15 mass % ZrO_2) produced a marked contraction phenomenon before eventual collapse. Relic "pools", indicative of liquid withdrawal, formed around the bases of the collapsed cone forms after furnace cooling. The retention of the cone morphology after collapse suggested that the properties of the remaining liquid phases became less fluid, and that liquid drainage ceased under a type of physical or chemical disequilibrium. The cones eventually collapsed in the accepted manner as the liquidus temperature of the phase associations remaining was reached.

A cone fusion represents a miniature example of selec-

ted fusion and recrystallisation under chemical and physical disequilibrium and thus gives an indication of the melting behaviour of synthetic slags. Cones which produced no contraction event prior to collapse are more representative of melting behaviour. In the case of magnesia - free, lime-iron silicate melts, the liquidus temperature remains at a relatively constant value as the lime content varies from zero to 35 mass % CaO (Fig. 57, p. 302), and any small changes in physical or chemical properties of the phases are masked by the high proportion of liquid produced with a small increase in temperature; the large volume of liquid causing the cone to collapse rapidly under the influence of gravity.

5.1.3. Cylinder immersion studies.

5.1.3.1 Duration of immersion.

The immersion time was monitored with a stopwatch and any error in recorded time, for both static and rotational studies, represented the period taken to remove the reacted cylinder from the furnace and cool the liquid products to a sub-liquidus temperature. For static experiments, this represented a period of approximately 5 seconds, the cooling rate under the argon jet being approximately $13^{o}C\ s^{-1}$ (measured in the core of the cylinder). The flexidrive connector had to be removed and the upper gas seal unbolted in the rotational experiments. These actions took no longer than 10 seconds, during which time the reacted cylinder was suspended in the furnace hot zone, the crucible and its contents having been dropped previously to

the base of the furnace tube to cool. The narrow, outer, iron oxide - rich skin and lack of wüstite or dicalcium silicate dendrites, suggested that rapid quenching of the high temperature phases was achieved and primary crystallisation/precipitation prevented.

5.1.3.2 Cylinder submergence.

One factor which affected all dissolution experiments was the variations recorded in the lengths of cylinders immersed into the melt. This produced a variation in the submerged area of the cylinder available for reaction with the melt. Assuming that the variations in these depths was normally distributed, one standard deviation had a value of 0.40cm for cylinders of "hard" burnt lime, immersed to an average depth of 1.07cm. "Soft" burnt lime cylinders partially collapsed at room temperature due to the inversion of dicalcium silicate but the immersion depth was assumed to be similar to that of the static dolomitic lime cylinders. Static dolomitic lime cylinders had an immersed zone length of 1.13cm and a standard deviation of 0.16cm. Rotated dolomitic lime cylinders had an average reaction zone length of 1.18cm with a standard deviation of 0.26cm.

5.1.3.3 Quantitative results.

Quantitative immersion results were derived from the concentration of oxide phases within the bulk melt relative to a specified immersion time (Figs. 51, 52, 54 and 55, pages 299 and 301). Between 1.5 to 6g of melt was removed from the crucible via capillary suction due to the high

apparent porosities of dolomitic lime and "soft" burnt lime cylinders. With short periods of immersion, a high mass of melt was removed in this manner but with longer immersion times, the gradual dissolution of the cylinder counteracted the material losses from the crucible. An average of 43g of synthetic slag, containing the oxide components of the reaction, remained from an original starting mass of 45g.

Porosity effects and the formation of reaction products created a chilled melt cortex around the immersed section of cylinder after withdrawal from the melt. The concentration of oxide species adjacent to and within the adhered layer was high (viz. SEM concentration profiles). A deficiency resulted in terms of the oxide species transferring into bulk melt, but since the effect was reproduced for all immersion periods, the composition trends of the oxide concentrations with respect to time, remained consistent. The combined effect of immersion depth variation, which affects the surface area available for reaction, and the development of a chilled melt layer around the periphery of the reacted cylinder accounts for the major source of scatter recorded in the results shown in Figs. 51, 52, 54 and 55 (pages 299 and 301), and indicated that the experimental method is only semiquantitative. A measure of the replicability of the experimental method can be inferred from Fig. 55 (p.301), where an average value has been utilised for a repeat immersion at 120s.

Within the constraints of the immersion method, the experimental results show an increase in the concentration

of oxide species diffusing into the bulk melt with increased immersion time. A standard, linear, least squares regression analysis was applied to the results to obtain the best fit straight line to the data. This unique value for the slope obtained in this way obviated any degree of subjectivity from the gradients constructed by eye through the scatter points. Tabulated results of the least squares regression analysis are given in Appendix 1 (p. 215).

5.2 Kinetics and phase relationships.

5.2.1 The dissolution of dolomitic lime in iron silicate melts.

The dissolution of dolomitic lime in iron silicate (fayalite) melts produced a reaction interface totally different in morphology to that of lime in melts of a similar composition at 1300°C. The melt penetrated through both dolomitic lime and "soft" burnt lime samples very rapidly. With the samples of lime, the bulk of the unreacted lime remained isolated from the melt by a dicalcium silicate envelope, and relied on a FeO - rich liquid phase for dissolution. The CaO and MgO crystallites of the dolomitic lime however, reacted almost instantaneously with the melt to form two solid reaction products of dicalcium silicate and magnesiowüstite respectively. Pore networks and capillary mechanisms which feature in both dolomitic lime and lime reactions in the initial stages of melt penetration, ceased to exist or became severely limited in dolomitic lime after the initial reaction period. Evidence for the lack of residual porosity in dolomitic lime can be inferred from the annealed sample of cylinder reacted initially for 15secs., (Plate 45, p. 330). Although the amount of iron silicate was limited to fracture fillings and the adhered zone around the reacted cylinder (Plate 44, p. 329), no further melt penetration occurred during the annealing period (60 min. at 1300°C). The interface region became saturated with CaO from the dicalcium silicate component, to

produce an outer or secondary skin of dicalcium silicate with no apparent reduction in distribution of the dicalcium silicate - magnesiowüstite association of the reacted dolomitic lime sample. The globular wüstite phase combined with magnesia to produce magnesiowüstite with the typical lobate morphology normally associated with the magnesiowüstite component of the reacted dolomitic lime cylinder.

Three possible mechanisms were proposed in section 4.3.1 (p. 141) to account for the development of the globular wüstite zone around the periphery of the reacted dolomitic lime cylinders. The chilling effect produced by the immersion of dolomitic lime samples in the melt, after being in the pre-heat position, may be discounted since there was a negligible temperature differential between the cylinders and melt prior to the immersion. The globular wüstite zone resulted through a combination of reactions involving the formation of dicalcium silicate (eq. 4.2, p. 146) and the isolation of the magnesiowüstite component, as the reacted cylinder interface receded by dissolution (eq. 4.3, p.146). Magnesia from the magnesiowüstite phase reacted with the iron silicate melt to form a solid solution series of magnesium - rich iron olivines (forsterite - fayalite), leaving a residual globular wüstite region around the reaction interface. The simultaneous development of the forsterite - fayalite solid solution series with the globular wüstite zone produced an additional concentration gradient for the transferrence of magnesia into the melt around the periphery of the

reacted dolomitic lime cylinder. In some respects, a situation analogous to the lime reaction in the CaO - 'FeO' - SiO_2 system is established, but instead of a continuous dicalcium silicate zone separating the melt from the partially reacted lime sample, a magnesium - rich olivine zone developed around the reacted dolomitic lime phase assemblage of dicalcium silicate and magnesiowüstite.

If the slopes of the gradients derived from plots of mass % CaO and MgO versus time in Figs. 51 and 52 (p. 299) and 54 and 55 (page 301) are utilised, it is possible to assess the influence of either the forsterite-fayalite olivine series of dolomitic lime or the dicalcium silicate component of lime on the relative dissolution rates of these slag forming materials. In addition, the dolomitic lime - iron silicate (fayalite) reaction within the system CaO - 'FeO' - SiO_2 - MgO, produces a dicalcium silicate phase similar to that established by lime in the system CaO - 'FeO' - SiO_2, and consequently enables an estimation to be made of the rate of CaO diffusing from dolomitic lime and lime. If it is assumed that the mass of melt at all times during reaction is constant (45g), the slope values of the gradients in terms of CaO or MgO can be converted from mass % per unit time to grams per unit time of transferring species, Tables 37 and 38 (p.260). From the tabulated values, a rate factor can also be calculated by dividing through by the lowest value and making it equivalent to 1 with respect to lime (CaO) diffusing from both the lime and dolomitic lime samples. A similar approach can be applied to relate the rate of magnesia

(MgO) diffusing under static and stirred conditions.

Dolomitic lime produced a similar dissolution rate for CaO to that of the "soft" burnt lime in an iron silicate melt, but after approximately 60s, there was a marked reduction in CaO transfer from dolomitic lime under both static and stirred conditions (Figs. 51 and 52, p. 299, and Table 37, p. 260). Even though dicalcium silicate is an interface component of dolomitic lime and provides an equivalent concentration gradient for CaO dissolution to that of the lime samples, the presence of magnesia as as interface component in dolomitic lime has to be considered to explain the measured differences in the rate of lime (CaO) solution between lime and dolomitic lime. Initially, magnesia dissolution from dolomitic lime proceeds as rapidly as the lime component but then is reduced dramatically in the static experiments (Fig. 51 p. 299). The dissolution rate of magnesia in the dolomitic lime is retarded under the influence of a viscous melt of forsterite - fayalite which is confirmed by the viscosity measurement and photomicrographic evidence, and the diffusion of CaO is correspondingly reduced through the inability of the melt to react wholly with the dicalcium silicate component of the interface.

Under stirred conditions (rotation), the dissolution of magnesia from dolomitic lime increases by a factor of approximately 8 over that of the static immersed samples, yet the CaO dissolution value remains virtually constant to that obtained under static conditions (Tables 37 & 38, p. 260). This suggests that the forsterite - fayalite

olivine series form rapidly, and establish a physical and chemical barrier that restricts not only the movement of CaO out of the sample, but also the transport of melt into the sample. This mechanism led to the dolomitic lime cylinder cores remaining unreacted under stirred conditions, Plate 51,(p. 333). These relationships could be of importance under industrial slagmaking practice, since it is assumed that the CaO component of dolomitic lime supplements the slag CaO derived from calcitic lime, and creates a basic slag at an earlier stage in the blow. This assumption, now proved invalid, was based on the observation that because there was no continuous barrier of dicalcium silicate around reacted dolomitic lime fragments, the slag could combine directly with the lime and magnesia components and enhance the solution rate.

The increased rate of solution of "soft" burnt lime over "hard" burnt lime in the system CaO - 'FeO' - SiO_2, illustrates clearly the importance of porosity as an aid to increased solution (Figs. 54 and 55, p. 301 and Table 37, p. 260). Both slopes showed no apparent inflexion, and the development of the dicalcium silicate interface regime for both types of lime in iron silicate (fayalite) melts, does not alter the rate of solution. The dicalcium silicate barrier in "soft" burnt lime becomes continuous and relatively impermeable to the melt after a short immersion period (Plate 65, p. 340). The mechanism of lime solution has been discussed in detail by various workers (79, 80, 81). Matsushima and co-workers (79) proposed that the dissolution rate of lime is controlled by the

diffusion of calcium from the surface of the dicalcium silicate film. Under stirred conditions, the solution rate increased in a linear manner with increased rotation speed and temperature, the mass transfer step through the slag boundary layer being rate determining. Green [80] suggested that the rate controlling step was initially the transfer of lime to the liquid - dicalcium silicate interface, but later the transport of melt became rate controlling. Natalie and Evans [81] have reported that a discontinuous dicalcium silicate layer will provide significant impediment to the diffusion of CaO away from the lime surface, owing to the restriction of the area available for diffusion. The results recorded in static immersion experiments in this work agree with the results obtained by Green and Matsushima and suggest that the formation of dicalcium silicate is not the rate controlling step to the dissolution of calcitic lime.

5.2.2 The estimation of experimental mass transfer coefficients.

In stirred or turbulent systems, reactions involving the transfer of solutes across the phase boundary are usually of interest. Bulk and interface concentrations occur and it is normally assumed that the solute is removed from the surface in a manner that keeps the interface concentration constant [40] ; the interface being regarded as a sharp and well defined plane. Material will move down a concentration gradient from the inter-

face into the bulk and the mass flow rate of species from the interface into the bulk phase may be represented diagrammatically as follows:-

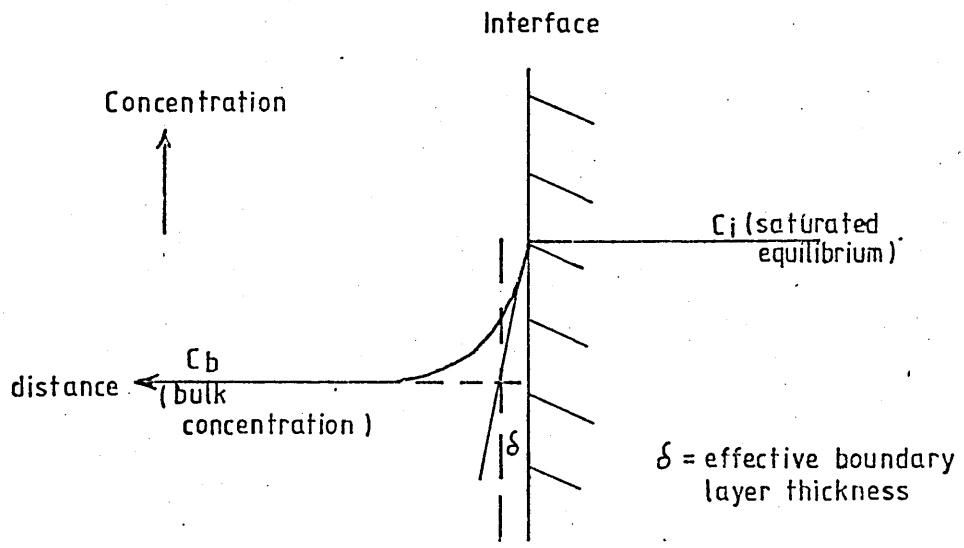

The mass flow of solute $\dot{n}$ from the saturated interface to the bulk phase is given by the equation

$$\dot{n} = k A (Ci - Cb) \qquad (5.1)$$

where

$\dot{n}$ has units of mass per unit time (g s^{-1}) and is equivalent to the slope values obtained from the immersion studies.

A is an area term which has values of cm^2

Ci is the saturated interface concentration, and

Cb is the bulk melt concentration, both values having units of g cm^{-3}.

At the interface between dolomitic lime and lime samples immersed in iron silicate melts, it can be assumed under dissolution controlled conditions that there will be

a zone of laminar flow through which the transfer of solute takes place by diffusion, the rate being described as follows [40,103]:-

$$\dot{n} = D A (Ci - Cb) / \delta \qquad (5.2)$$

where

D is the diffusion coefficient ($cm^2\ s^{-1}$)

A is the area (cm^2)

Ci, Cb are the saturated interface and bulk concentration respectively ($g\ cm^{-3}$)

δ is the effective boundary layer in cm, representing a stagnant layer in the fluid across which mass transport is by molecular diffusion only because the layer is not distributed by convection.

The distance (δ) may be obtained by extending the slope of the concentration distance curve from Ci to Cb as illustrated in the diagram above (p.190). An effective film thickness will exist in stirred systems and realistically in so-called static systems, where density and thermodynamic gradients and natural convection combine to stir the liquid. The effective film thickness (δ) will be much wider in static systems than in stirred systems but the film thickness will still be difficult to estimate. For static immersion experiments, the film thickness can only be as wide as the confines of the crucible wall. This will, however, allow an estimate of the maximum value to be used. Richardson [40] has stated that the use of effective film thicknesses coupled with diffusion coefficients (D) is not a very helpful approach to mass

transfer problems, because it has been found experimentally that k is rarely proportional to D, so that δ varies as the diffusivity varies for different solutes, even with the same flow conditions. Conversely, an estimate of mass transfer rather than diffusion coefficients can be approximated for both static and stirred immersion experiments using equation 5.1 (p. 190) which will also enable the rate of CaO dissolution from dolomitic lime and lime to be assessed. The dissolution rate of MgO from dolomitic lime can also be considered on the basis of experimental mass transfer coefficient values.

The surface area term (A), which represents the area available for reaction, can be reasonably estimated from the cylinder dimensions taken from section 5.1.3.2. (p. 181) and Tables 6 and 7 (pages 235 and 236). Subsequent calculations of the mass transfer coefficient will involve an error due to the range of standard deviations recorded on cylinder immersion depths and diameter dimensions. For "hard" burnt lime, the error in the area value could be as high as 27%, and for "soft" burnt lime and static and rotated dolomitic lime, it will be 12, 14 and 19% respectively. The area term (A), which has units of cm^2, can be incorporated by division into the slope value, represented by $\dot{n}$ ($g\ s^{-1}$), to yield a flux ($\dot{n}''$) which will have the units gCaO or MgO $cm^{-2}\ s^{-1}$. If it is assumed that the mass of lime or magnesia transporting does not change the mass of the melt (45g), an experimental mass transfer coefficient can be derived from

$$\dot{n}'' = k\ (Ci\ mass\ \%) \qquad (5.3)$$

The term Cb can be neglected in this case since it has a negligible concentration with respect to Ci. The mass% concentration term of Ci requires conversion from a mass% to g cm^{-3} value.

At 1300°C, the driving force for CaO dissolution will represent the saturation limit at the interface with lime or dolomitic lime. In both instances this coincides with the development of a dicalcium silicate phase, and a value for CaO concentration can be estimated from a line taken from $2FeO.SiO_2$ to the CaO corner of the CaO - 'FeO' - SiO_2 phase equilibrium diagram (Fig.12 , p. 269) to intersect the 1300°C isotherm, and is 27 mass % CaO.

During the dissolution of dolomitic lime, magnesia will diffuse from an additional source to that provided by magnesiowüstite due to the development of a forsterite-fayalite solid solution series. With an increased immersion time, the margin of the dolomitic lime phase association, comprised of dicalcium silicate and magnesiowüstite, becomes encased by the magnesium - rich olivines. The driving force for MgO dissolution into the bulk melt can now be assumed to come from the magnesium - rich olivine zone and will be related to the average composition of these phases at this saturated interface. The mass % MgO concentration of the saturated interface can be obtained from an average value based on that obtained from SEM analyses. This value is 34.5 mass % MgO and was taken to calculate Ci.

The conversion of Ci values for CaO and MgO require that the mass % terms be converted to g cm^{-3} by involving

a density term. The density of a melt corresponding to 27 mass % CaO at 1300°C can be approximated as 3.18 g cm^{-3} from the density measurements reported by Lee and Gaskell[58]. The density of the forsterite - fayalite series has a linear relationship so that the density of an olivine can be directly related to its composition. At a mole composition corresponding to Fo_{70} (34.5 mass % MgO), the solid density is 3.58 g cm^{-3} (14).

The experimental mass transfer coefficient for both CaO and MgO can be calculated from the expression:

$$k = \frac{\dot{n}''}{\frac{\text{mass\% sat}}{100} \times \rho \text{ melt}} \qquad (5.4)$$

where

$\dot{n}''$ has units of gCaO cm^{-2} s^{-1}

and ρ melt has units of g cm^{-3}

and k has units of cm s^{-1}

An example of the method of calculation is shown in Appendix 2 (p. 216) for "hard" burnt lime and the values of the other cylinder types are included in tabulated form. Experimental mass transfer values are shown in Tables 39 and 40 (p. 261). The lowest value of the experimental mass transfer coefficient for CaO in lime and dolomitic lime samples can be divided into all higher values to produce a series of rate factors which give an indication of their respective dissolution rates (Table 39 p. 261). The recorded rate factors in Table 39 have a similar range of numerical values to those rate factors

derived solely from slope data in Table 37 (p. 260). Rate factor values can be similarly assigned to MgO diffusing from static and rotated dolomitic lime samples (Table 40, p. 261).

The experimental mass transfer coefficient for CaO in "soft" burnt lime (9.8×10^{-4} cm s^{-1}) had a rate factor value 3.5 times higher than that of "hard" burnt lime (2.8×10^{-4} cm s^{-1}), Table 39 (p. 261). The increased rate factor is due to the higher porosity of the "soft" burnt lime, through the increased surface area available for reaction with the melt. These relationships support the contention that "soft" burnt lime will dissolve more rapidly than "hard" burnt lime under industrial conditions, even though the formation of dicalcium silicate may be accelerated around the particles of "soft" burnt lime.

The initial transfer of CaO from dolomitic lime under static and stirred conditions produced a similar experimental mass transfer coefficient value, both of which were higher than that recorded by the "soft" burnt lime. This may have some significance in producing a more basic slag during the initial reaction of early formed, siliceous, LD slags with the lime and dolomitic lime charge. However, the samples of dolomitic lime have an apparent porosity 7% higher than that of the "soft" burnt lime samples, and this may explain the apparent high dissolution rate for the CaO component of the dolomitic lime. Of greater significance, is the 3 times reduction recorded in the rate of CaO transferrence from dolomitic lime under

static or stirred conditions, after a reaction period of 60 to 70 seconds (Table 39 , p. 261). The reduced CaO mass transfer values derived from the dolomitic lime are only half those obtained from "soft" burnt lime and suggests that the lime component present in dolomitic lime does not play a significant role in achieving a basic slag early in an LD blow.

From the trend of mass % concentration versus time plots in Figs. 51 and 52 (p. 299), the dissolution of MgO from dolomitic lime is responsible for inhibiting the rate of CaO transfer from dolomitic lime into the melt. Consideration of experimental mass transfer values of MgO in Table 40 (p. 261) shows that the initial dissolution rate of MgO is reduced by a factor of 60 under static conditions. The experimental mass transfer rate for magnesia becomes very low relative to the CaO component of dolomitic lime under static conditions. The mechanism that maintains a near equivalent CaO transfer rate under stirred conditions is problematical since the rate of MgO dissolution from the forsterite - fayalite phase assemblage is increased 8-fold. It is not clear whether the maintainance of similar CaO transfer rates from static to rotated dolomitic lime samples represent an increased viscosity effect at the melt/forsterite - fayalite boundary, or an increased rate of formation of the forsterite-fayalite solid solution series around the reacted dolomitic lime sample. In stirred systems , the increased rate of MgO transport could preferentially react with the FeO component of the melt. This mechanism may also depend

upon the rate at which the globular wüstite zone can be resorbed at the interface with the melt.

Matsushima and co-workers [79] have utilised a self diffusion coefficient for CaO (D_{Ca}) of 2.7×10^{-5} cm^2 s^{-1} in a melt comprised of FeO and 35 mass % SiO_2 to estimate the thickness of the boundary layer or film. From film theory it has been established that [40]

$$k_M = \frac{D}{\delta} \qquad (5.5)$$

where k_M is the mass transfer coefficient, D the diffusion coefficient of the transporting species within the melt, and δ is the film thickness (cm). For the static experiments carried out in this work, the boundary layer can conceivably extend from the cylinder rim to the crucible wall, an average distance of 1.31cm. A value of k_M for CaO can be assessed by using the diffusivity value of D_{Ca} 2.7×10^{-5} cm^2 s^{-1}.

$$k_M = \frac{2.7 \times 10^{-5}}{1.31} \quad \frac{(cm^2\ s^{-1})}{(cm)} = 2.06 \times 10^{-5}\ cm\ s^{-1}$$

The calculated value of the mass transfer coefficient for CaO is lower by a factor of approximately 10 from the experimental values derived in this work using the worst case for an estimate of δ . In reality, it is generally accepted that δ values for these systems are in the order of mm or less [4, 79]. For simplicity the calculation can be repeated with δ at $\frac{1}{10}$ of the original, (quoted values are 0.003cm and 2.7×10^{-2}cm [4, 79]). The values of the experimental mass transfer coefficients of

CaO are very similar in magnitude to the value derived by calculation, 2.06×10^{-4} cm s^{-1}.

Other estimates of experimental mass transfer coefficients for CaO have been made by Green [80] and Matsushima [79] which compare favourably with the values obtained by this semiquantitative method, Table 41(p.262). Green used pressed cylinders of Analar grade $CaCO_3$, sintered at 1300°C, to produce a cylinder of dimensions similar to those used in this work. The apparent porosity of the cylinder was 25% and a volume change per unit area versus time plot was used to establish the experimental mass transfer value. Matsushima also used analytical grade $CaCO_3$, pressed into cylinders 19.4mm in diameter after sintering. However, graphite caps were placed on both ends of the cylinder to ensure that lime dissolution occurred from the sidewall only. The apparent porosity of the cylinders was 40%. A rotation speed of 200 and 400 r.p.m. was used in a slag composed of 20 mass % FeO, 40 mass % CaO and 40 mass % SiO_2 heated to 1400°C. Values of mass transfer coefficients produced in this work, using natural raw materials, are subject to a degree of variation due to the deviation recorded on cylinder diameter and immersed zone length dimensions. If this dimensional variation is included in the calculation of experimental mass transfer coefficients, as shown in Table 42 (p.262), the range of values exhibited are still comparable to those produced by other experimental methods.

A theoretical estimate of the mass transfer coefficient of CaO can be calculated from the dimensionless

relationships proposed for the dissolution of a solid cylinder rotating in a liquid [40].

$$\frac{k}{U} = 0.079\ (Re)^{-0.3}\ (Sc)^{-0.644} \qquad (5.6)$$

k is the mass transfer coefficient (cm s^{-1})

Re and Sc are the Reynolds and Schmidt numbers respectively, and are explained fully in Appendix 3 (p. 218).

U represents the peripheral velocity of the rotating cylinder (cm s^{-1}). The physical properties of the melt used and method of calculation are also explained in Appendix 3.

A theoretical mass transfer coefficient for CaO of 3.2×10^{-4} cm s^{-1} was obtained. This theoretical value is lower than that obtained experimentally for "soft" burnt lime (9.8×10^{-4} cm s^{-1}). This anomaly may be explained by the high apparent porosity values of "soft" burnt lime which would provide a greater surface area for dissolution. Experimental mass transfer values obtained for CaO transfering from dolomitic lime are, however, similar to the theoretical value, if the lower of the two mass transfer values is used (3.5×10^{-4} cm s^{-1} for static, and 4.3×10^{-4} cm s^{-1} for rotated). These values are not influenced by porosity. It may be assumed that in the absence of any published values, the experimental mass transfer values for MgO in dolomitic lime, are also within the correct range of magnitude.

The estimation of experimental mass transfer coefficients for CaO and MgO were calculated on the assump-

tion that an effective film or boundary layer exists at the reaction interface between iron silicate (fayalite) melts and dolomitic lime or lime cylinders. This approach assumes that diffusion across the boundary layer, and not chemical reaction, is rate limiting.

5.2.3 The effect of magnesia on lime dissolution.

The solution of lump lime is difficult to achieve due to the formation of a continuous dicalcium silicate barrier (melting point 2130°C [50]) at the melt - lime interface region. The heterogeneous reaction between lime and siliceous melts produces a liquid calciowüstite or calcium ferrite phase, which is itself an effective lime flux, in addition to the dicalcium silicate. However, this FeO - rich liquid phase which forms between the dicalcium silicate (C_2S) barrier and the lime fragment is not present in sufficient quantity to dissolve lime rapidly enough during the early stages of slag formation. This action can only be achieved by a mechanism or mechanisms which limit or suppress C_2S formation; modifies the structure of the C_2S cortex; lowers the fusion temperature of C_2S or increases slag fluidity to aid diffusion processes [82].

With the addition of 5 mass % MgO to synthetic iron silicate (fayalite) slags, a continuous dicalcium silicate (C_2S) barrier no longer forms at the melt - lime reaction interface. Instead, the C_2S barrier becomes porous and disseminated across the melt - lime interface region (Plates 72 and 74, pages 344 and 345). The

interface region contains, in addition, a well developed tricalcium silicate (C_3S) zone. The limited solubility of MgO in CaO, which is determined by the large differences in ionic radii, suggests that magnesia either suppresses C_2S formation and/or modifies the structure of the C_2S cortex. The viscosity measurement on a CaO-MgO iron silicate melt (Fig. 31, p. 284) has shown that magnesia can also increase the fluidity of the melt to a small degree above 1300°C. This would aid directly any diffusion process but the fluidity effect is considered to play only a minor role in the fluxing mechanism in this particular instance.

The existence of tricalcium silicate within the interface zone indicates that an excess of silica (SiO_2) was available for reaction even after C_2S had precipitated at the melt - lime interface. The interface region between the melt, which supplied FeO and SiO_2, and dicalcium silicate must have remained discontinuous to enable a C_3S phase to precipitate. This would imply that magnesia actually modifies the structure of the C_2S cortex and prevents the development of a continuous C_2S barrier. In the presence of a porous C_2S network, direct contact between the bulk melt and the FeO - rich liquid region of the interface would lead to a countercurrent action of FeO replenishment and CaO transfer and would increase the driving force for lime dissolution.

Iron silicate (fayalite) reactions with "soft" and "hard" burnt lime, within the system CaO - 'FeO' - SiO_2, produced pear-shaped granules of dicalcium silicate which

sintered together to form a continuous barrier between the melt and lime sample interface. With an increased immersion time, the pear-shaped texture of the C_2S envelope disappeared to form a uniform morphology (Plate 65,p.340). Within the system CaO - 'FeO' - SiO_2 - MgO, similar pear-shaped granules of dicalcium silicate were formed but these did not sinter together even with a relatively long immersion period (360s). If volume diffusion is accepted as a general flow mechanism for the sintering of solid particles in the presence of a liquid phase [147], the densification process, accompanying sintering, will involve shrinkage as the solids move towards an equilibrium state. The presence of a low concentration of magnesia within the iron silicate - lime system at 1300°C would appear to act in one or more of the following ways:-

a) Magnesia may prevent the attainment of the solid equilibrium state.

b) Magnesia may affect the mechanism of volume diffusion, by vacancy substitution.

c) Magnesia may reduce the dihedral angle between the liquid melt and solid C_2S granules, a dihedral angle of zero producing the complete isolation of partially sintered C_2S particles.

The culmination of one or all of the above steps will lead to the granular form of dicalcium silicate (Plate 73 , p. 345), which creates a much greater surface area for dissolution.

If the term "lime-flux" can be applied to any addition which produces one or more of the effects described

i.e. a C_2S modifier or suppressor etc., then magnesia must be considered to be an effective lime flux in small concentrations in the melt - slag phase.

5.2.4 The rate controlling mechanism.

The dissolution of dolomitic lime isothermally, within an iron silicate (fayalite) melt at 1300°C, involves the following processes. Iron oxide (FeO) and silica (SiO_2) from the bulk melt react, under capillary action, with porous dolomitic lime to produce two solid reaction products, magnesiowüstite (MF') and dicalcium silicate (C_2S). Simultaneously, magnesia and lime are transferred from the two solid reaction products of dolomitic lime into the bulk melt, from a saturated interface, and under the influence of steep concentration gradients. Within the interface region, wüstite (FeO) is precipitated isothermally through a combination of reactions involving the formation of C_2S and MF'. With the development of the globular wüstite zone, MgO combines with FeO and SiO_2 in the melt to produce a forsterite - fayalite olivine solid solution series which contributes an additional MgO concentration gradient.

From the kinetic studies on dolomitic lime, magnesia produced a significant increase in the dissolution rate under rotated conditions, with no inflexion in the gradient of the rate curve. A second indicator to the increased dissolution rate of dolomitic lime under stirred conditions was the reduction in width of the globular wüstite zone (Fig. 53 p. 300). These factors indicate

that the dissolution process is governed by the diffusion of reactants to, or the products away from the interface through the boundary layer i.e. a transport (or diffusion) control mechanism was operative.

The quantity of CaO transferred into the bulk melt produced similar values under both static and stirred conditions. The rate of lime (CaO) dissolution from the dolomitic lime cylinder was governed by the distribution of the forsterite - fayalite solid solution series which formed a chemical and physical barrier between the melt and the C_2S - MF' components of the interface. The rate controlling step for CaO diffusion from dolomitic lime is, therefore, related to the rate of formation of the forsterite - fayalite olivine series, which restricts the quantity of melt available to transfer CaO away from the CaO - saturated interface of dicalcium silicate.

5.3. Relevance to the LD or basic oxygen steelmaking process.

The work reported here suggests that when a siliceous slag is produced in the LD process by the rapid oxidation of silicon from the metallic bath during the early stages of the blow, dolomitic lime will react rapidly with it. The reacted dolomitic lime product is composed of dicalcium silicate and magnesiowüstite. From this stage onwards, the experimental results show that the reacted dolomitic lime behaves in a multi-role manner, changing not only the physical properties of the early formed slag, but producing chemical conditions that will be less aggres-

sive towards the basic (magnesia or doloma) lining.

During the dissolution of dolomitic lime, magnesia diffusing from the magnesiowüstite phase will react with some of the silica component of the slag to form a refractory solid solution series of magnesium - iron olivines. The magnesia - rich, forsterite - fayalite olivine series would produce an increase in the fusion temperature and extend the melting range of the early formed slag. These combined effects result in an increase in the kinematic viscosity ($\nu = \frac{\rho}{\mu}$ cm^2 s^{-1}) of the early formed slag, and agree with the industrial observation that slag penetration into the refractories is reduced at a low slag V - ratio, through the formation of relatively viscous magnesia - rich slag. In a calcitic lime slag practice with fluorspar addition, the progressive solution of calcitic lime and increasing slag temperature would combine to lower the kinematic viscosity of the slag components. With a dolomitic lime and calcitic lime slag practice, the presence of magnesia, derived from the dolomitic lime addition, increases the liquidus temperature and melting range of the slag [85], and enables the slag to maintain a relatively high kinematic viscosity. During the first 5 to 7 minutes of the blow, or possibly for longer periods, the dolomitic lime - bearing slag would be viscous due to the solid phase associations of magnesiowüstite (or magnesio-ferrite at higher oxygen partial pressures), magnesium - iron olivines and dicalcium silicate. A combination of these phases would form an effective refractory layer on the surface of the lining if any slag

adherence occurred during this period. The relatively viscous slag (> 40mPa.s [37]) may also control any tendency for the vessel contents to slop during the Stage I decarburisation period.

Phase relationships within the CaO - 'FeO' - SiO_2 slagmaking system (Fig. 12, p. 269), and experimental studies involving calcitic lime, have shown that the formation of a basic slag will be retarded by the rapid development of a continuous barrier of dicalcium silicate around the particles of lime. In a dolomitic lime - calcitic lime practice, slagmaking components relate to phases occurring in the system CaO - Iron oxide - SiO_2 - MgO in contact with metallic iron (Fig. 17, p. 272) or air. High temperature (1300°C) crucible tests between iron silicate (fayalite) melts, containing low concentrations of magnesia (5 mass %), and porous calcitic lime samples, show that a continuous dicalcium silicate morphology is not developed around the particles of lime. For an industrial practice operating a mixed calcitic lime and dolomitic lime addition, the progressive dissolution of dolomitic lime (in siliceous slags) via the forsterite-fayalite olivine series or magnesiowüstite, would enable low concentrations of magnesia to accumulate within the slag. As a result, the tendency for the continuous dicalcium silicate layer to form around calcitic lime pieces in a siliceous slag would be inhibited; a granular dicalcium silicate morphology will form instead. The rate of calcitic lime solution will be accelerated, especially within a dynamic system, where the granular

dicalcium silicate zone around the calcitic lime fragments may conceivably be swept into the melt by convection, leaving fresh reaction surfaces. The low values of experimental mass transfer coefficients for MgO indicates that solution of dolomitic lime will continue through a large proportion of the blow. Works practice observation that a basic slag is produced earlier in the blow with a dolomitic lime slag practice, can be explained as being due mainly to the fluxing properties of the magnesia - bearing slag on calcitic lime, rather than from any additional lime solution resulting from dolomitic lime and despite increases in viscosity.

The generation of siliceous slags within the first 5 to 7 minutes of an LD blow, and corresponding reactions involving dolomitic lime and calcitic lime additions, imply that dolomitic lime should be added at the commencement of the blow, and either simultaneously or slightly before the calcitic lime charge. The early stages of slag development are the most crucial in terms of refractory wear rate since magnesia rich linings have a high susceptibility to chemical solution in siliceous slags. With the generation of increasing amounts of FeO, derived from the oxidation of the metal bath, a solid solution series - type of diffusion would exist between the magnesia bearing slag components of forsterite - fayalite and magnesio-wüstite from the reacted dolomitic lime. This would limit the fluxing action of 'FeO' on the basic lining phase containing either lime (doloma) or calcium - magnesium silicates (magnesia).

6. Conclusions.

A rotating bob-fixed crucible viscometer technique has been established for the measurement of synthetic slag viscosities within the system CaO - 'FeO' - SiO_2 - MgO, at temperatures of 1150 to 1450°C, corresponding to those obtained during the early stages of an LD blow. Lime additions up to 32 mass % CaO increased the viscosity of an iron silicate melt by approximately 50mPa.s at 1400°C. Magnesia levels of 2 to 3 mass % MgO produced only a small increase in the viscosity of an iron silicate melt but with 7.5 mass % MgO, the viscosity was increased by 250mPa.s relative to that of the iron silicate at 1300°C. This viscosity interval was reduced dramatically at higher temperatures. The viscosity values recorded for a synthetic iron silicate (fayalite) slag containing 13 mass % CaO - 7.5 mass % MgO, were similar to those of the iron silicate melt at 1300°C. The viscosity measurements for MgO - iron silicate melts reflected the corresponding increase in liquidus temperatures due to magnesia addition.

The investigation of the melting behaviour of synthetic slags with compositions ranging between iron silicate (fayalite) and 38 mass % CaO - iron silicate, revealed that magnesia increased both the liquidus and solidus temperatures at all levels of addition. At magnesia levels of 10 mass % MgO, the liquidus temperatures of lime-bearing iron silicate melts were increased by between 140 to 200°C and the melting range increased by between 45 to

80°C. The initial magnesia - free melting range was only 10 to 15°C.

The investigation of the mechanism of dolomitic lime and lime dissolution in iron silicate (fayalite) melts at 1300°C leads to the following conclusions:-

1. The initial reaction between dolomitic lime and an iron silicate (fayalite) melt produced two solid reaction products, one of magnesiowüstite and the other of di-calcium silicate, the distribution of both phases being determined by the crystallite disposition and degree of porosity during the calcination process. The dicalcium silicate always formed as a discontinuous phase.

2. The diffusion of magnesia into the melt produced a magnesium - iron olivine solid solution series (forsterite - fayalite) around the periphery of the reacted dolomitic lime sample. This olivine - rich region was always directly associated with a globular wüstite (FeO) zone which became a characteristic of every immersion experiment, irrespective of immersion time.

3. The rate of dolomitic lime dissolution was increased under dynamic (stirred) conditions. In addition, the width of the globular wüstite zone became narrower than that recorded in the static experiments and remained constant with respect to time. These features suggested a transport (or diffusion) controlled dissolution mechanism. Even though the rate of magnesia dissolution increased due to stirring, the dissolution rate of the CaO component

from dolomitic lime remained similar under both static and stirred conditions.

4. The static dissolution of "soft" and "hard" burnt lime in an iron silicate melt at 1300°C produced two reaction products, one liquid and rich in iron oxide (FeO), the other solid dicalcium silicate which precipitated with a continuous morphology to form a barrier between the bulk melt and lime sample.

5. The dissolution rate of "soft" burnt lime was greater than that of the lime component present in dolomitic lime by a factor of approximately 3, under static isothermal conditions.

6. A 5 mass % MgO level within the iron silicate (fayalite) was found to be an effective lime flux. The reaction regime between the lime and magnesia bearing - iron silicate melt produced three reaction products; namely a granular morphology of dicalcium silicate, tricalcium silicate and an FeO - rich liquid phase. Photomicrographic evidence shows that the fluxing action of magnesia occurred through its ability to behave as a dicalcium silicate modifier.

7. The lime fluxing ability of magnesia and mechanism of dolomitic lime dissolution clearly indicates that under industrial LD steelmaking practice, dolomitic lime must be charged early in the blow to be of any direct benefit in the slagmaking practice. If possible, dolomitic lime additions should be added prior to, or simultaneously with

the calcitic lime charge and at the beginning of the blow, to enable early formed siliceous slags to react with dolomitic lime and form magnesiowustite and forsterite - fayalite solid solutions. The resultant early formed, relatively viscous and refractory slag, would become chemically enriched in magnesia and less aggressive towards the basic refractor}'-lining.

8. The formation of a solid FeO phase as a by-product of the fayalite - dolomitic lime reaction serves to reduce the activity of FeO in the early stages of the blow for slag temperatures below 1360 C. The reduced activity of FeO in a ferruginous or iron silicate (fayalite) slag would correspondingly extend the lining life of the vessel by diminishing the fluxing properties of the slag with respect to the lime and/or silicate components of the basic lining, until the melting point of wustite (1369°C) was exceeded.,

It has been established that dolomitic lime does not represent' a replacement for calcitic lime. However, it is essential for,reducing.refractory wear rates and enhancing the formation of a basic early formed slag when used in conjunction with calcitic lime, provided it is added at the commencement of the blow.

7. Suggestions for further work.

The combination of zirconia crucibles and iron measuring bobs has proved successful in the determination of synthetic slag viscosities between temperatures of 1100 and 1460°C, but higher temperature viscosity studies are restricted by the melting point of the iron measuring bob. If a zirconia measuring bob could be fabricated by inverting a smaller diameter crucible, and a method employed to attach it to a sleeve or shaft, then viscosity measurements can be made to temperatures limited only by the capabilities of the furnace and the excessive reaction of zirconia. Within the system CaO - 'FeO' - SiO_2 - MgO, the upper temperature limits available as a result of this development would allow viscosity measurements to be carried out on melt compositions corresponding to the mid and end points of an LD blow. Slagmaking systems may be varied considerably with respect to the number of components, and consequently viscosity determinations need not be restricted to LD steelmaking. Other slagmaking systems, natural or synthetic, could therefore be studied with the appropriate measuring components.

The length of the air bearing support shaft, which gave rise to alignment problems in the present work, could be reduced if a furnace could be aquired which produced a restricted, long, stable hot zone, without the need for an excessive working tube length. This action may also enable iron crucible and bob components to be used more successfully, as the vertical alignment problem would not be so critical.

Quantitative measurement techniques need to be developed to measure the rate of "soft" burnt calcitic lime solution in magnesia - bearing synthetic slags. The semi-quantitative method described in this work could be extended using static and stirred isothermal conditions, to quantify the fluxing action of low concentrations of slag magnesia on calcitic lime. The effect of stirring speed could also be quantified.

The influence of magnesia on slag - steelmaking reactions may be examined from droplet - slag studies involving iron - carbon, iron - carbon - sulphur or iron - carbon - phosphorus alloys. Synthetic slag compositions corresponding to those achieved up to the mid - point of an LD blow could be utilised. Magnesia may be added in the form of powdered dolomitic lime at an amount which gives a specific MgO level. The effect of magnesia on decarburisation, desulphurisation and dephosphorisation reactions may be quantified by relating the rates of removal (on a mass basis) with the droplet immersion time. The effect of viscosity can also be assessed for the slag-making systems used.

The melting behaviour of synthetic slags in the presence of magnesia or powdered dolomitic lime can be further extended to other slag compositions within the system CaO - 'FeO' - SiO_2 - MgO by use of the cone fusion furnace. The effect of both high and low oxygen partial pressures may produce interesting data.

A mechanistic and phase relationship study, involving iron silicate (fayalite) melts and cylinders of mag-

nesite ($MgCO_3$), cored and calcined to yield a porosity similar to that of dolomitic lime, would complement the dissolution studies undertaken in the system CaO - 'FeO' - SiO_2 - MgO. The interaction of dolomitic lime with synthetic slags more basic than iron silicate, may indicate the point at which the forsterite - fayalite series changes from the principal source of slag magnesia to a minor one. The magnesiowüstite phase possibly becoming the main source of slag MgO, which may yield information on the problem of slag control during the mid and end stages of an LD blow.

Appendix 1.

Calculation by the least squares regression method of the slope values relating plots of mass % CaO and MgO versus time (s). Figs. 51, 52, 54 and 55.

$$\text{Slope } m = \frac{\Sigma(y_i - \bar{y}_i)(x_j - \bar{x}_j)}{\Sigma(x_j - \bar{x}_j)^2}$$

"Hard" burnt lime.

x (s)	y (mass %)	$(y_i - \bar{y}_i)(x_j - \bar{x}_j)$	$(x_j - \bar{x}_j)^2$	m(mass % CaO s^{-1})
15	0.17	74.256	28224	
120	0.34	17.136	3969	
180	0.66	-0.144	9	
240	0.84	12.996	3249	
360	1.05	77.526	31329	
$\bar{x}$ 183	$\bar{y}$ 0.612	Σ 181.77	Σ 66780	$m = 2.72 \times 10^{-3}$

"Soft burnt lime.

$\bar{x}$ 195	$\bar{y}$ 2.698	Σ 2182.26	Σ177300	$m = 1.23 \times 10^{-2}$ mass% CaO.s^{-1}

Dolomitic lime (static).

CaO slope 1	$\bar{x}$ 37.5	$\bar{y}$ 0.69	Σ 15.3	Σ1012.5	$m = 1.51 \times 10^{-2}$ mass% CaO.s^{-1}
CaO slope 2	$\bar{x}$ 201.43	$\bar{y}$ 1.836	Σ614.75	Σ145295	$m = 4.2 \times 10^{-3}$ " "
MgO slope 1	$\bar{x}$ 37.5	$\bar{y}$ 20.025	Σ 20.025	Σ1012.5	$m = 1.97 \times 10^{-2}$ mass % MgO.s^{-1}
MgO slope 2	$\bar{x}$ 201.43	$\bar{y}$ 0.884	Σ 50.355	Σ145295	$m = 3.46 \times 10^{-4}$ " "

Dolomitic lime (rotated).

CaO slope 1	$\bar{x}$ 37.5	$\bar{y}$ 0.845	Σ 16.876	Σ1012.5	$m = 1.66 \times 10^{-2}$ mass % CaO.s^{-1}
CaO slope 2	$\bar{x}$ 242	$\bar{y}$ 2.538	Σ520.658	Σ96480	$m = 5.39 \times 10^{-3}$ mass % CaO s^{-1}
MgO slope	$\bar{x}$ 233.6	$\bar{y}$ 0.99	Σ593.55	Σ205135.7	$m = 2.89 \times 10^{-3}$ mass % MgO s^{-1}

Appendix 2.

Estimation of experimental mass transfer coefficients.

"Hard" burnt lime.

equation $k = \dfrac{\dot{n}''}{\frac{\text{mass\% sat}}{100} \times \rho_{sat}} \quad \dfrac{(g\ cm^{-2}\ s^{-1})}{(g\ cm^{-3})}$

Average length of immersed zone (ℓ) = 1.07cm

Average diameter of cylinder (d) = 1.18cm, r = 0.59cm

Area of submerged cylinder is $(\pi r^2) + \pi \times \ell \times d$.

Area of cylinder in contact with melt at 1300°C is

$$\pi \times (0.59)^2 + \pi \times 1.07 \times 1.18 = \underline{5.06cm^2}.$$

Slope is equivalent to $(\dot{n})$ in g CaO s^{-1}. (Table 37 p.260).

The mass flux is given by

$$\dot{n}'' = \frac{1.224 \times 10^{-3}}{5.06} = \underline{2.42 \times 10^{-4}\ g\ CaO\ s^{-1} cm^{-2}}$$

Converting mass % CaO to g cm^{-3} at (27 mass % @ 1300°C)

ρ melt at 1300°C = 3.18g cm^{-3}.

$$k = \frac{2.42 \times 10^{-4}}{\frac{27}{100} \times 3.18} \quad \frac{(g\ cm^{-2} s^{-1})}{(g\ cm^{-3})}$$

Experimental mass transfer coefficient for "hard" burnt lime = $\underline{2.82 \times 10^{-4}\ cm\ s^{-1}}$

The relevant data for "soft" burnt lime and dolomitic lime are tabulated as follows:-

Experimental Mass transfer coefficients for CaO.

Sample	Porosity (P app%)	Immersion depth(cm)	Cylinder diameter(cm)	area submerged cm^2	Slope value $g\ s^{-1}$	Flux ($\dot{n}''$) $g\ cm^{-2}s^{-1}$	Density at saturated interface $\times \frac{mass\%}{100}\ g cm^{-3}$	Experimental mass transfer coefficient(k) $cm\ s^{-1}$ CaO
"Soft" burnt lime	43	1.13	1.42	6.59	5.54×10^{-3}	8.4×10^{-3}	0.27x3.18	9.8×10^{-4} (CaO)
Dolomitic lime (static)	51	1.13	1.38	6.39	(1)6.8×10^{-3}	1.06×10^{-3}	"	12.3×10^{-4}
	"	1.13	1.38	6.39	(2)1.89×10^{-3}	3.0×10^{-4}	"	3.5×10^{-4}
Dolomitic lime (rotated)	"	1.18	"	6.61	(1)7.47×10^{-3}	1.13×10^{-3}	"	13.1×10^{-4}
					(2)2.43×10^{-3}	3.68×10^{-4}	"	4.3×10^{-4}
Experimental mass transfer coefficients for MgO								
Dolomitic lime (static)	51	1.13	1.38	6.39	(1)8.86×10^{-3}	1.4×10^{-3}	0.345x3.58	11.3×10^{-4}
					(2)1.56×10^{-4}	2.4×10^{-5}	"	1.9×10^{-5}
Dolomitic lime (rotated)	"	1.18	"	6.61	1.3×10^{-3}	2.0×10^{-4}	"	1.6×10^{-4}

Appendix 3.

Calculation of a theoretical mass transfer coefficient (k) for a lime or dolomitic lime cylinder rotating in an iron silicate melt.

It is assumed that the densities of the cylinder and melt are nearly equal.

For the mass transfer of a solid cylinder rotating in a liquid, the equation is [40];

$$\frac{k}{U} = 0.079\ (Re)^{-0.3}\ (Sc)^{-0.644}$$

Re is the Reynolds number $\left(\frac{\rho U d}{\mu}\right)$

Sc is the Schmidt number $\left(\frac{\mu}{\rho\ Di}\right)$

where U = peripheral velocity = 3.61 cm s^{-1}

d = diameter = 1.38 cm

μ = viscosity (mPa.s 0.01g cm^{-1} s^{-1} :- for an iron silicate melt at 1300°C, μ = 0.95g cm^{-1} s^{-1} (this work)

ρ = density :- for an iron silicate melt at 1300°C, ρ = 3.65g cm^{-3} [58].

Di = diffusivity :- for lime or Ca in an iron silicate, Di = 2.7×10^{-5} [79] cm^2 s^{-1}

k = mass transfer coefficient cm s^{-1}

$$k = U \times 0.079 \left(\frac{\rho U d}{\mu}\right)^{-0.3} \left(\frac{\mu}{\rho\ Di}\right)^{-0.644} \text{ cm } s^{-1}$$

$$k = 3.61 \times 0.079\ (0.4125)(0.00272) \text{ cm } s^{-1}$$

$$\underline{k = 3.2 \times 10^{-4} \text{ cm } s^{-1}}$$

REFERENCES

1. BSC Annual statistics, 1979.

2. Michaelis E.M. Basic Oxygen Steelmaking - a new technology emerges. Met. Soc. Conf. 1978, London, May.

3. Ward R.G. The physical chemistry of iron and steelmaking. Edward Arnold, 1962.

4. Bodsworth C. and Bell H.B. Physical chemistry of iron and steel manufacture. 2nd Edn., Longman, London.

5. Langmead E.C. Iron and Steel Engineer. 1971, Sept., p. 117.

6. Pearson T.F., et al. Critical comparison of slag metal reactions in the LD and Kaldo processes at Consett. J.I.S.I. 1966 Oct, p. 997.

7. Trentini B., et al. Comments on the OLP process. J.I.S.I. 1959, June, p.143.

8. Nilles P. and Boudin M. Oxygen steelmaking in bottom blown converters. Ironmaking and Steelmaking (Qtrly), 1974, No.1, p.22.

9. Freuhan R.J. Rates of several gas-metal reactions in the Q-BOP. Ibid. 1976, No.1, p.33.

10. Brotzmann K., et al. Recent advances in Q-BOP steelmaking. Ibid. 1966, No.5, p.259.

11. Nilles P., et al. The physical chemistry of top and bottom blowing. Met. Soc. Conf. 1978, London, May.

12. Green J. and Quin J. Influence of MgO on BOF slag fluidity and its correlation with BOF refractory wear rate. Open Hth. Proc. Conf. (Chicago), 1978, April.

13. Walker R.D. and Anderson D. Reaction mechanisms in Basic Oxygen Steelmaking.
    J.I.S.I. Part I, 1972, June, p.271
    " Part II, " Aug., p.403
    " Part III, " Oct., p.409.

14. Acheson, R. Oxygen steelmaking - advanced study module. Sheff. City Poly., May - June, 1978, Department of Metallurgy Lecture.

15. Lange K.W. Refining reactions in top blowing processes. Proc. Versailles Conf., 1978.

16. Turkdogan E.T. and Pearson J. Activities of constituents of steelmaking slags. - III Phosphorus pentoxide. J.I.S.I., 1953, Dec., p.393.

17. Winkler T.B. and Chipman J. An equilibrium study of the distribution of phosphorus between liquid iron and basic slag. Trans. AIME, 1946, 167, p.111

18. Bookey J.B. The free energy formation of magnesium phosphate. J.I.S.I., 1952, Sept., p.66.

19. Flood H. and Grjotheim K. Thermodynamic Calculation of slag equilibria. J.I.S.I., 1952, 171, May, p.64.

20. Healey G.W. A new look at phosphorus distribution. J.I.S.I., 1970, 208, p.664.

21. Mori K. and Doi S., et al. Rate of transfer of phosphorus between metal and slag. Trans. I.S.I.J., 1978, 18, p.261.

22. Ward R.G. and Salmon K.A. The kinetics of sulphur transfer from iron to slag. J.I.S.I., 1960, Dec.,393.

23. Ward M.D. Consistent iron: the steelmakers viewpoint. Ironmaking & Steelmaking (Qtrly), 1975, 2, p.89.

24. Potocic R.F., et al. Desulphurization - Sulphur control plus more production. Symposium on External Desulphurization of hot metal. McMaster University, May 1975, p.2 - 1.

25. Sandberg H. Desulphurization of hot metal. Ironmaking and Steelmaking, 1977, 5, p.280.

26. Meyer H.W. Oxygen Steelmaking : Its control and Future. J.I.S.I., 1969, June, p.781.

27. Kawakami K. Kinetics of blowing reaction in a basic oxygen furnace. J.Metals, 1966, July, p.836.

28. Bardenheur F., et al. Contribution to the Metallurgy of the "LD" process. Blast Furnace & Steel Plant, 1970, June, p.401.

29. Oeters F. Arch. Eisenh. 1966, 37, p.209. BISI No.5505.

30. Meyer H.W., et al. Slag - metal emulsions and their importance in BOF steelmaking. J. Met.,1968, p.35.

31. Trentini B. Comments on Oxygen steelmaking. Trans. Met. Soc. AIME, 1968, 242, p.2377.

32. Kozakevitch P. Foams and emulsions in steelmaking. J. Met. 1969, July, p.57.

33. Hazeldean E.W., et al. Visualisation of slag - metal reactions by x-ray fluoroscopy: Decarburization in basic oxygen steelmaking. J.I.S.I., 1973, p.632.

34. Price D.J. Chemistry and kinetics of LD Steelmaking. Symp. Proc. Chemical Metallurgy of Iron and Steel. Iron and Steel Inst. Pub. 1971, p.112.

35. Chatterjee A., et al. Process metallurgy of LD steelmaking. Ironmaking and Steelmaking, 1976, No. 1.,p.21.

36. Schoop J., et al. Reactions occurring during the oxygen top - blown process and calculation of metallurgical control parameters. Ibid. 1978, No. 2, p.72.

37. Nazyuta L. Yu. Problems of stabilisation of metal - slag emulsions. Steel U.S.S.R., 1977, July, p.378.

38. Okhotsku V.B. Content of metallic phase in slag-metal emulsion. Ibid. 1978, March, p.135.

39. Szekely J. and Themelis N.J. Rate phenomena in process metallurgy. Wiley Interscience, 1971.

40. Richardson F.D. Physical chemistry of melts in metallurgy. Vol. I and II. Academic Press, 1974.

41. Acheson R. and Hills A.W.D. Rate controlling mechanisms in basic oxygen steelmaking. Pub. Conf. Proc. : Physical Chemistry in Process Metallurgy : The Richardson Conference. Inst. Min. Met. 1974, p.153.

42. Kinsman G.J.M., et al. Physiochemical factors affecting the vacuum deoxidation of steels. J.I.S.I., 1969, 207, Nov. p.1463.

43. Aeron S.M., et al. Mass transfer from metal drops falling through a static liquid. Trans. Inst. Min. Met., 1974, [C] 83, 814, p.168.

44. Belton G.R. On the rate limiting step in the decarburization of iron droplets in an oxidising slag. Met. Trans. B. 1979, 10B, March, p.118.

45. Bockris J.O'M. and Lowe D.C. Viscosity and the structure of molten silicates. Proc. Roy. Soc. 1954, 226 p. 423.

46. Bockris J.O'M. and Mackenzie J.D., et al. Viscous flow in silica and binary liquid silicates. Trans. Farad. Soc. 1955, 51, p.1734.

47. Bills P.M. Viscosities in silicate slag systems. J.I.S.I., 1963, Feb., p.133.

48. Geiger G.H. and Poirier D.R. Transport Phenomena in Metallurgy. Addison-Wesley, 1973.

49. Uvarov E.B., et al. A Dictionary of Science. Penguin, 1964.

50. Muan A. and Osborn E.F. Phase equilibria among oxides in steelmaking. Addison-Wesley Comp. Inc. 1965.

51. Kozakevitch P. Tension superficielle et viscosité des scories synthetiques. Rév. Met. 1949, No.8, p.505.

52. Röntgen P., et al. The structure and properties of metallurgical slags. Erzmetal 1960. 13, Aug., BISI, No. 2475, 1961.

53. Shiraishi Y., et al. On the viscosity and density of the molten FeO - SiO_2 system. Trans. JIM, 1978 19, p.265.

54. Toguri J.M., et al. The viscosity of the molten FeO - Fe_2O_3 - SiO_2 system. "Extractive metallurgy of copper" Vol. I, 1976, p.259.

55. Kozakevitch P. Tension superficielle et viscosité des scories synthetiques. Rév. Met. 1949, 9, p.573.

56. Kilau H.W., et al. Viscosity of BOF slags fluidised with fluorspar, colemanite, and fused boric acid. Report 8292. United States Bureau of Mines.

57. Lee Y.E. and Gaskell D.R. The densities and surface tensions of calcium - iron othosilicate melts. Proc. ICSTIS. Supp. Trans. ISIJ. 1971.

58. Lee Y.E. and Gaskell D.R. The densities and structures of melts in the system CaO - 'FeO' - SiO_2. Met. Trans. 1974, 5, April, p.853.

59. Lopatin V.M., et al. Density of iron oxide based melts. Steel USSR. 1974, Dec, p.953.

60. Sharma S.K. and Philbrook W.O. The influence of atmosphere on the surface tension of calcium and manganese-silicate melts. Proc. ICSTIS Supp. Trans. ISIJ 1971, 11, p.569.

61. Cooper C.F. and Kitchener J.A. Foaming of molten silicates. JISI. 1959, Sept., p.48.

62. Toop G.W. and Samis C.S. Activities of ions in silicate melts. Trans. Met. Soc. AIME 1962, 224, Oct., p.878.

63. Richardson F.D. and Fincham C.J.B. Proc. Roy. Soc. 1954, A223, p.40.

64. Gaskell D.R. Thermodynamic properties of the Masson polymerisation model of liquid silicates. "Chem. Met. of Iron & Steel" 1971, p.12, ISI Pub.

65. Masson C.R. Thermodynamics and constitution of silicate slags. JISI 1972, Feb., p.89.

66. Mertin G., et al. Thermodynamic models of slags in "Physical Chemistry and Steelmaking". 1978, Conf. Versailles - France. Oct. 2 p.2-3.

67. Masson C.R., et al. Activities and ionic distributions in liquid silicates:application of polymer theory. Con. Journ. Met. 1970, 48, p.1456.

68. Distin P.A., et al. Thermodynamics and constitution of ferrous silicate melts. Can. Met. Qtrly. 1971, 10, 2, p.73.

69. Anderson L.C. and Vernon J. The quality and production of lime for basic oxygen steelmaking. JISI 1970, April, p.329.

70. Leonard L.A. Influence of lime quality on oxygen steelmaking. JISI 1970, April, p.324.

71. Slatter D. de L. Effect of lime reactivity variations upon rate of slag formation in basic oxygen steelmaking. (Technical Note). Ironmaking and Steelmaking Qtrly. 1975, 2, p.145.

72. Ibid. Exposure of reactive lime to atmosphere and influence this has on its aqueous reactivity and its rate of dissolution in steelmaking slag. Ironmaking and Steelmaking Qtrly. 1976, 3, p.159.

73. Limes R.W. and Russel R.O. The triangle : Lime, slags, refractories. McMaster Symp.,Hamilton, Canada. 1976, May, 9 - 1. Ed. W. K-Lu.

74. van Hoorn A.I., et al. Evolution of slag composition and weight during the blow. Ibid.

75. Oeters F. amd Scheel R. Studies of the dissolution of lime in CaO - 'FeO' - SiO_2 slags. Arch. Eisen. 1974 9, Sept., 575.

76. Iyengar I.K. and Petrilli F.C. Slagmaking reactions in in the BOF process. J. Met. 1973, July, p.21.

77. Biochenko B.M., et al. Kinetics of the solution of lime and its basicity. Steel in USSR. 1971, p.204.

78. Yershov G.S., et al. Lime assimilation by molten slag. Ibid.

79. Matsushima M., et al. A fundamental study on the dissolution of solid lime into liquid slag. Trans. ISIJ 1977, 17, p.442.

80. Green J. The dissolution of lime in iron silicate melts. Sheffield Polytechnic. PhD, 1975, Nov.

81. Natalie C.A. and Evans J.W. Influence of lime properties on rate of dissolution in CaO - SiO_2 - FeO slags. Ironmaking and Steelmaking 1979, 3, p.101.

82. Baker K. and Cavanagh N.J. The production and properties of lime for the steel industry. BSC Rpt. PC5632/4/69/A, 1969 (Unpub.).

83. Quin J. Fluxes for basic oxygen steelmaking. Steetley Co. Ltd., Rpt. CR3/1973, (Unpub.).

84. Hutnik A.W. and Buzdor J. Substitutes for fluorspar at the National - Duquesne works BOP shop. National Open Hearth and Basic conference, Cleveland, Ohio., 1973.

85. Obst K.H., et al. Reducing the blowing time in LD processes by the use of special lime products. JISI 1970, May, p.450.

86. Holappa L.E.K. amd Kostamc P.A. Development of blowing practice in the Koverhar LD plant. Scan. J. Met., 1974, 3, p.56.

87. Limes R.W., et al. The triangle : Lime, Slags, Refractories. McMaster Symp., Hamilton, Canada. 1976, May, p. 9 - 1. Ed. W. K-Lu.

88. Schuman E., et al. Importance of the temperature and ferrous oxide content of the slag during the dissolution of lime in the basic open hearth process. Arch. Eisen. 1969, 39, 11 Nov., p.815.

89. Baker R. Desirable slag composition paths and method of control in the LD process. BSC Report CAPL/SM/A/31/74. 1974.

90. White J. Slag control in basic steelmaking processes: an examination of the possibility of eliminating fluorspar. Iron and Steelmaking (Qtrly) 1974, 2, p.115.

91. Hardy C.W. and Owen A.J. Development of refractory linings to meet operational requirements in oxygen vessels. Met. Soc. Conf, London 1978, May - "Basic oxygen steelmaking - a new technology emerges".

92. Peatfield M. and Spencer D.R.F. Developments in refractory materials for LD linings. Ibid.

93. Betts W.D. The use of tar and pitches in refractories for oxygen steelmaking. J. Brit. Ceram. Soc. 1974.

94. Herron R.H., et al. Slag attack on Carbon-bearing basic refractories. Ceram. Bull. 1967, 46, 12, p.1163.

95. Limes R.W. BOF refractory experience at Republic Steel in the U.S.A. J. Brit. Ceram. Soc. 1974.

96. Leonard R.J. and Herron R.H. Significance of oxidation - reduction reactions within BOF refractories. J. Am. Ceram. Soc. 1972, Jan., 55, 1, p.1.

97. Howe R.A., et al. Attack of tar bonded periclase refractory by a dolomitic BOF slag. Am. Ceram. Bull. 1976, 55, 2, p.205.

98. Kim S.M., et al. On the mechanisms of attack of carbon - bearing BOF bricks for steelmaking slags. Mc Master Symposium, Hamilton, Canada. 1976, May. Ed. W. K-Lu.

99. Oeters F., et al. Reactions between dolomite bricks and steelworks slags. Arch. Eisen. 1973, 44, 6, June, p.443. BISI 12756.

100. Abratis H. Reaction of refractories with slag melts. Ibid. 1973, 9, Sept., p.691. BISI 11906.

101. Fetters K.L. and Chipman J. Equilibria of liquid iron and slags of the system CaO - MgO - 'FeO' - SiO_2. Trans. AIME 1941, 145, p.95.

102. Tae - Il OH, et al. Slag penetration into oxide refractories. Am. Ceram. Bull. (Technical Note), 1977 56, 7, p.649.

103. Park H.K. and Barrett L.R. Transport-controlled dissolution of magnesia in melts. Trans. and Journ. Brit. Ceram. Soc. 1979, 78, 2, p.33.

104. Snyder E.B. High calcium lime, dolomitic lime and other fluxes for steelmaking furnaces. Iron and Steelmaker 1, 1976, p.11.

105. Leonard R.J. and Herron R.H. Dolomite additions required to saturate BOF slags with MgO. Proc. Nat. O.H. Conf. AIME 1977, April 17th.

106. Balla D.M. and Beechan C.R. Development of a guide-line for the efficient use of dolomitic lime in BOF operations. I. and S.M. 1977, July.

107. Bowen N.L. and Schairer J.F. The system MgO - FeO - SiO_2. Amer. J. Sci. 1935, 29, p.151.

108. Levin E.M., et al. Phase diagrams for ceramicists. Pub. Am. Ceram. Soc. Inc. 1964.

109. Johnson R.E. and Muan A. Amer. Ceram. Bull. 1964 43, 4, p.301.

110. Yarashenko N.I., et al. Operation of basic oxygen furnaces using magnesia slags. Steel in the USSR 1971, Sept.

111. Iyengar R.K. and Petrilli F.C. Statistical analysis of BOF lining life. J. Met. 1972, March, p.46.

112. Zarvin E.Ya., et al. Effect of MnO and MgO on some physical properties of converter slags and the reaction between these slags and fluxes. Steel USSR. 1973, 2 Feb., p.118.

113. Nishawa H., et al. Effective use of returned LD slag and dolomite, and operation with a sublance system. Ironmaking and Steelmaking 1978, 3, p.95.

114. Kaufman J.W. and Aguirre C.E. Characterisation of refractory wear provides basis for new practice for AOD process. Ind. Heating. 1978, April - p.12. May - p.32.

115. Gaye H., et al. Influence of dolomitic lime reactivity on BOF refractory consumption. McMaster Symposium, Hamilton, Canada. 1976, May, p. 13 - 1. Ed. W. K-Lu.

116. Yakushev A.M., et al. Viscosity of CaO - base slags with varying contents of Al_2O_3, SiO_2 and MgO. Steel in the USSR. 1977, Nov., p.177.

117. Machin J.S. and Hanna D.L. Viscosity studies of the system CaO - MgO - Al_2O_3 - SiO_2 (40% SiO_2). J. Am. Ceram. Soc. 1945, 28, 11, p.310.

118. Majercak S. The influence of magnesia on the viscosity and phase composition of synthetic slags. Sharnik V.S.B. Ostrave. Rada Hutnicka, 1967, 13 paper 395, p.103. BISI 7713, 1969, Dec.

119. Hofmann E.E. Viscosity behaviour of synthetic slags in relation to composition and temperature. Stahl und Eisen 1959, 79, 12, p.846.

120. Harhai J.G. and Dukelow D.A. Factors affecting sulphur removal in the basic oxygen process. J. Met. 1966, July, p.833.

121. Obinata T. High magnesia - slag operation in BOF McMaster Symp., Hamilton, Canada, 1976 - Role of slag in basic oxygen steelmaking processes. Ed. W.K-Lu.

122. Bosley J.J., et al. The effect of dolomitic lime on BOP operations at South Works. Ibid.

123. Wells A.K. and Kirkaldy J.F. Outline of Historical Geology. 1966, Allen and Unwin.

124. Hatch F.H. and Rastall R.H. Petrology of the Sedimentary Rocks. Thomas Murby & Co., London, 1965, 4th Edn.

125. Edwards J.S. The calibration and development of the Haake 'Rotovisko' RV1 viscometer, for use with basic oxygen steelmaking slags. BSc Thesis, Sheff. City Poly. 1976.

126. Ojeda M. Decarburization of iron - carbon alloys with oxidising slags. PhD Thesis. Sheff. City Poly. 1977.

127. Langhammer Von H.J. and Geck H.G. Viskositätsmessungen an Schlacken. Arch. Eisen. 1967, Sept, p.6991.

128. van Wazer J.R. Viscosity and Flow Measurement. 1963 Interscience.

129. Kaye G.W.C., Laby T.H. Tables of physical and chemical constants and some mathematical functions. Longmans 1966, 13th Edn.

130. Michel J.R. and Mitchell A. A study of the rheological behaviour of some slags in the system CaO - SiO_2 - Al_2O_3 - CaF_2. Can. Met. Qtrly. 1975, 14, 2.

131. Ford C.E. Platinum - iron alloy containers for melting experiments on iron - bearing rocks, minerals and related systems. Min. Mag. 1978, June, 42, p.271.

132. Clixby G. An experimental study of blast furnace bosh slags and its application to blast furnace practice. Unpub. Manuscript, 1978.

133. Pratt R. The development of viscometric techniques and their application to steelmaking slags. BSc Thesis. Sheff. City Poly. 1977.

134. Baker K. and Engeldow D. Development of the Haake 'Rotovisko' viscometer for use with steelmaking slags. BSC report No. SM/6659/-/73/A. 1973.

135. British Standards. B.S. 1902: Part 1A: 1966.

136. Jones D.G. and Melford D.A. Comparison of high-temperature constitution of sea water magnesites with that of natural creek magnesite. Trans. Brit. Ceram. Soc. 1969, 68.

137. Robijn P., et al. Changes in Basic Checker bricks of glass furnaces due to the heavy elements of fuel. Trans. Brit. Ceram. Soc. 1970, 69.

138. Horsefield J.W. and Haworth C.W. Sheffield Frame 3 - A correction program for Electron Probe Micro Analyser University of Sheffield, 1978.

139. Grundy P.J. and Jones G.A. Electron Microscopy and the study of materials. Edward Arnold, 1976.

140. Saadat A. El. The role of volatile species in the softening of blast furnace burden. PhD Thesis, 1979, Sheffield City Polytechnic.

141. Dodds B. BSc Thesis, 1979, Sheff. City Poly.

142. Gimmelfarb A.A. Viscosity of CaO - SiO_2 - FeO - Al_2O_3 slags. Russ. Met. 1968, 8, Aug., p.43.

143. Chesters J.H. Refractories : Production and properties. Pub. Iron and Steel Inst. 1973.

144. Levin E.M., et al. Phase diagrams for Ceramicists. 1969 Supplement. Pub. Am. Ceram. Soc.

145. Berry I.G., et al. Mineralogy : Concepts : Descriptions : Determinations. W.H. Freeman & Co. 1959.

146. Binns D.B. The use of special ceramics in handling molten iron and steel. Trans. & Journ. Brit. Ceram. Soc. 1978.

147. Ford W.T. The effect of heat on Ceramics. Inst. Ceram. Textbook series No. 4. Maclaren & Sons, 1967.

Table 1 Basic Oxygen Steelmaking in the United Kingdom

Plant	Steelmaking Practice	Start Up Date	Shut Down Date	No. of Vessels And Capacity (Tonnes)	Rated Annual Output (Tonnes)
Ebbw Vale	LD	1960	1975	3 x 45	
Llanwern	"	1962		3 x 180	3.5×10^6
Consett	"	1964		2 x 130	1.5×10^6
Normanby Park*	"	1964		2 x 85	1.4×10^6
Ravenscraig *	"	1964		3 x 125	3.2×10^6
Port Talbot	"	1969		2 x 305	3.2×10^6
S. Teesside	"	1971		3 x 250	4.5×10^6
Anchor	"	1973		3 x 300	4.6×10^6
Corby	LDAC	1962		3 x 130	1.5×10^6
Consett	Kaldo	1964	1969	2 x 120	
Parkgate	"	1964	1974	2 x 120	
Shelton	"	1964		2 x 70	0.75×10^6
Redbourn	Rotor	1961	1974	1 x 100	
Port Talbot	VLN	1959	1969	1 x 60	

(after Green and Quin [12])

* Started operating with LDAC practice.

Table 2 Structural relationships in basic oxide–silicate melts

Total oxygen atoms / Silicon atoms	Corresponding binary molecular formula	Structure	Equivalent silicate ion
2:1	SiO_2	All corners of tetrahedra shared	Infinite network
5:2	$MO \cdot 2SiO_2$	One broken link per tetrahedron	$(Si_6O_{15})^{6-}$ or $(Si_8O_{20})^{8-}$
3:1	$MO \cdot SiO_2$	Two broken links per tetrahedron (ring)	$(Si_3O_9)^{6-}$ or $(Si_4O_{12})^{8-}$
7:2	$3MO \cdot 2SiO_2$	Three broken links per tetrahedron (chain)	$(Si_2O_7)^{6-}$
4:1	$2MO \cdot SiO_2$ (orthosilicate)	All links broken	Discrete $(SiO_4)^{4-}$ tetrahedra

(after Geiger et al[48])

O_2 blown comp.	2,000 %(m/m)	4,000 %(m/m)	6,000 %(m/m)	8,000 %(m/m)	10,000 %(m/m)	12,000 %(m/m)
CaO_{diss}	36.2	40.5	44.3	47.4	48.9	48.8
CaO_{free}	15.6	7.6	14.0	7.0	7.3	6.2
Fe	16.9	12.7	12.0	12.1	12.4	13.0
SiO_2	28.5	27.4	26.2	25.8	23.4	21.3
MnO	7.6	9.1	8.8	7.8	6.5	5.3
MgO	3.0	2.3	1.9	1.9	2.2	2.6
S	0.02	0.03	0.03	0.03	0.04	0.04
P_2O_5	0.50	0.57	1.58	1.60	1.68	1.78

Table 3. The average slag composition during the blow.

(after van Hoorn. et.al.[74])

Table 4. In-blow metal and slag analyses from a 90ton converter

(reproduced from Bodsworth[4])

Table 4

MINUTES AFTER CLEAR MELT	METAL TEMPERATURE °C	METAL COMPOSITION WEIGHT-PER CENT C	Mn	Si	S	P	O	SLAG COMPOSITION WEIGHT-PER CENT SiO_2	CaO	P_2O_5	MnO	MgO	FeO(total)
Cast 2737													
9·5	1463*	1·80	0·30	0·01	0·052	0·116	0·059	21·70	32·7	6·2	12·1	3·0	18·2
12·0	1507*	1·31	0·32	0·01	0·054	0·113	0·059	23·65	35·0	5·5	10·75	3·5	17·48
14·5	1550*	0·55	0·23	0·01	0·051	0·08	0·075	17·90	32·5	5·0	8·2	3·0	24·3
end blow 20·0	1660	0·09	0·17	0·01	0·037	0·022	0·150	10·6	41·0	4·5	7·6	2·4	31·2
Cast 2864													
10·0	1455*	1·21	0·44	0·01	0·039	0·09	0·015	23·0	35·0	5·6	8·55	4·15	13·4
11·5	1475*	1·06	0·20	0·01	0·041	0·10	0·024	23·0	34·8	5·5	8·0	4·2	14·9
13·5	1510*	0·77	0·20	0·01	0·039	0·11	0·048	21·0	35·2	5·4	7·7	4·15	18·1
15·0	1530*	0·55	0·22	0·01	0·043	0·091	0·069	19·1	37·0	5·0	6·8	3·9	19·4
19·0	1600	0·21	0·21	0·01	0·030	0·022	0·09	14·9	47·2	4·9	7·9	1·3	22·6

* Estimated temperatures based on initial hot metal temperature, ore, limestone additions for cooling and turn-down temperature.

FeO(total) is (FeO + Fe_2O_3) converted to FeO.

Table 5 Viscosity studies of slag systems by various workers.

Author	Slag System	Measurement Method	Component	Temp. Range °C	Composition (wt.%) CaO	SiO_2	Al_2O_3	FeO	MgO	Viscosity Poise (0.1 Pa.s) Temp. °C 1300	1400	1500	1600	1700
(46) Bockris. et al	$CaO-SiO_2$	Rotating crucible viscometer (R.C.V)	Molybdenum	1450–1800	37·2 56	62·8 44						14·4	7·3 1·13	3·92 0·74
(47) Bills.	$CaO-SiO_2-Al_2O_3$	Vertical movement of bob suspended in slag	Iridium bob Platinum or Ir. crucible.	1250–1500	50 40	40 40	10 20				8·3 21·4	3·85 8·3		
(117) Machin. et al	$CaO-40\%SiO_2$ Al_2O_3-MgO	Oscillating cylinder viscometer	Platinum.	1250–1500	45 45 50	40 40 40	5 15 10		10	40·27	13·23 5·23	2·24 5·16 4·0		
(118) Majerčak.	$CaO-SiO_2-Al_2O_3-MgO$	Electrovibration viscometer		1300–1500	43·5 42·5 40	43·5 42·5 40	10·5 10 10		2·5 5·0 10·0	34·0 18·55	8·0 7·8 3·3	3·88 3·26 2·22		
(132) Clixby.	$CaO-SiO_2-Al_2O_3$ $FeO-MgO$	R.C.V	Graphite. Mild steel-iron	≤ 1550 ≤ 1430	46·4 37·6	32·9 35·3	13 10·8	2·6	5·4 9·5	4·9	5·8 2·5	2·3		
(116) Yakushev. et al	$CaO-SiO_2-Al_2O_3-MgO$	Electrovibration viscometer	Molybdenum	1450–1720	52 45·5	20 30	20 17·5		8·0 8·0			8·4	2·4 4·1	1·5 0·8
(119) Hofmann.	$CaO-SiO_2-Al_2O_3-MgO$	R.C.V	Graphite	1400 1550	40 45	40 40	10 10		10·0 5·0		5·6 5·8	2·6 2·9		

TABLE 6 Dolomitic limestone and dolomitic lime cylinder properties

Analysis %	Raw basis	Calcined basis	"Dolomet" specification
CaO	29.8	56.32	57.0
MgO	22.0	41.58	39.0
SiO_2	0.2	0.38	0.75
Fe_2O_3	0.7	1.32	1.35
Al_2O_3	0.09	0.18	0.40
S	< 0.02	< 0.04	max 0.05
Mn_2O_3	0.09	0.18	0.22
CO_2	47.10	-	0.50
Size grading			-45 + 15mm
Bulk density (kgm^{-3})			1500 - 1700

Dolomitic limestone properties.

Green bulk density (kgm^{-3})	2480	± 120
Green apparent porosity (%)	18.5	to 20.0
True porosity (%)	12.4	
Powder density (kgm^{-3})	2832	± 15

Dolomitic lime cylinder properties.

Bulk density (kgm^{-3})	1768	± 60
Apparent porosity (%)	50.86	± 0.97
Cylinder length (mm)	29.62	± 0.92
Cylinder diameter (mm)	13.80	± 0.6
Cylinder mass (g)	7.9200	± 0.62

TABLE 7 Limestone and lime cylinder properties.

Analysis %	Raw basis	Calcined basis
CaO	54.2	97.50
MgO	0.33	0.58
SiO_2	0.11	0.19
Fe_2O_3	0.11	0.19
Al_2O_3	< 0.1	< 0.18
S	0.14	0.25
Mn_2O_3	< 0.01	< 0.02
CO_2	42.90	-
Moisture	0.31	-
Na_2O	0.32	0.56
K_2O	0.27	0.48

Limestone properties.

Green bulk density (kgm^{-3})	2610 ± 10
Green apparent porosity (%)	2.0
True porosity (%)	2.7
Powder density (kgm^{-3})	2682 ± 8

Lime cylinder properties.

	"Hard Burnt"	"Soft Burnt"
Bulk density (kgm^{-3})	2390 ± 70	1870 ± 80
Apparent porosity (%)	24.47 ± 2.52	43.23 ± 1.0
Cylinder length (mm)	27.7 ± 1.0	30.2 ± 0.5
Cylinder diameter (mm)	11.8 ± 0.6	14.22 ± 0.22
Cylinder mass (g)	9.5295 ± 0.17	9.5098 ± 0.19

TABLE 8

Analyses of base melts used in immersion and viscosity experiments

Sample	w/o FeO	Fe_2O_3	SiO_2	CaO	MgO
BF1	64.33	1.95	32.30	-	-
BF2	63.04	1.42	34.90	-	-
BF3	62.73	1.77	34.30	0.18	0.06
BF4	60.16	2.69	36.34	0.74	0.07
CF10	56.70	3.16	29.30	10.50	-
CF13	54.93	2.86	29.00	13.10	0.07
CF32	30.50	1.00	35.90	32.60	-

TABLE 9

Analysis of stock iron used for the viscometer crucible and bob components

Material "Swedish Iron"

Price £750 tonne (Sept. '78)

Supplier Swinden Laboratories (BSC)

C	0.04	Mo	0.01
Mn	0.20	Cu	0.04
Si	0.01	V	0.01
S	0.014	Sn	0.005
P	0.006	Al	0.005
Ni	0.05		
Cr	0.03		

TABLE 10 Determination of calibration constant (K) using aqueous glycerol solution and measuring bob diameter of 25mm.

Temp °C	Speed (U)	Scale (S)			UxS(av)	Viscosity mPa.s	Calib. Const. (K)
		1	2	3			
Calibration constant measured in constant temperature bath assembly.							
	9	25.5	26.6	26.6	240	1194	4.975
20.00	6	40.0	40.0	40.2	240.6	"	4.963
	3	81.5	81.5	81.3	244.0	"	4.893
	9	17.0	17.0	17.2	153.9		5.016
25.00	6	27.0	27.0	27.0	162.0	772	4.765
	3	54.5	54.6	54.4	163.5	"	4.736
	2	81.0	80.5	80.5	161.0	"	4.795
	6	17.0	17.0	17.0	102	525	5.140
29.60	3	35.2	35.2	35.2	105.6	"	4.972
	2	53.2	53.2	53.0	106.4	"	4.934
Calibration constant determined within the furnace.							
	9	32.5	22.2	22.0	200.1	1150	5.75
20.30	6	35.5	35.4	35.7	213.2	"	5.394
	3	74.0	73.5	74.0	22.15	"	5.192
23.8	18	11.2	11.3	-	202.5	860	4.246
	9	26.0	25.6	25.6	231.6	"	*3.713
	6	37.8	37.8	38.0	227.2	"	*3.785
	3	71.0	71.0	70.8	212.0	"	4.056
	9	22.5	23.5	22.7	206.1	885	4.294
	6	34.5	35.0	36.3	209.6	"	4.222
	3	70.0	70.5	70.2	210.7	"	4.200

*values reflect some drag of viscometer shaft on the gas seal.

TABLE 11 Determination of calibration constant (K) using aqueous glycerol solution and measuring bob diameter of 22mm.

Calibration constant measured in constant temperature bath assembly.							
Temp °C	Speed (U)	Scale (S)			UxS(av)	Viscosity mPa.s	Calib. Const. (K)
		1	2	3			
	6	22.0	22.0	21.5	131.0	1194	9.114
20.02	3	46.2	46.2	46.0	138.9	"	8.596
	2	70.0	70.1	71.0	140.6	"	8.490
	1	-	-	-			
	6	14.6	14.6	14.5	87.3	772	8.843
25.02	3	29.6	29.2	29.5	88.3	"	8.743
	2	44.0	43.0	-	87.0	"	8.874
	1	85.0	86.0		85.5	"	9.029
	9	7.0	6.7	6.7	61.2	530	8.660
29.75	6	10.5	10.5	10.0	62.0	"	8.548
	3	21.5	21.2	21.5	64.2	"	8.255
	2	32.8	32.7	-	65.6	"	8.0916
Calibration constant determined within the furnace.							
	6	23.2	23.0	23.0	138	1194	8.627
(19.95)	3	50.0	50.0	-	150	"	7.960
	2	78.0	78.0		146	"	7.654
	1	13.5	13.5	(x10)	136	"	8.779

TABLE 12 Re-determination of the iron crucible constant using Haake E200 oil.

E200 oil viscosity 156.3 mPa.s at 20.00°C

Temp °C	Speed U	Scale (S)			UxS(av)	Viscosity mPa.s	$K=\frac{\mu}{UxS}$
		1	2	3			
20.02	3	12.0	11.8	11.9	35.7	156.30	4.378
	2	17.5	17.5	17.5	35.0	"	4.466
	1	34.0	34.2	34.0	34.06	"	4.589

50gcm head U = 1, S = 34

500gcm head U = 1, S = 3.3 x 10 = 33

TABLE 13 Determination of the zirconia crucible constant using Haake E200 oil.

Temp °C	Speed U	Scale (S)			UxS(av)	Viscosity mPa.s	$K=\frac{\mu}{UxS}$
		1	2	3			
20.00	3	9.8	10.0	9.8	29.6	156.3	5.280
	2	15.0	15.0	15.0	30.0	"	5.210
	1	30.8	30.8	30.8	30.8	"	5.075

Table 14 Mass fraction of elements using full and half peak count method (Polytechnic S E M).

Conditions			
Sample OLIVINE	Accel. Volt. 12 kV		Specimen height 24 mm
Count time 40 sec.	Spot size 0·25 μm		
Elements 4	Standard Fe, Mg, Si.		Retract. distance 12 mm

Element	Mg	Si	Fe	O	Mg	Si	Fe	O	Mg	Si	Fe	O
*K value	·3314	·1226	·0482	-	·2920	·1320	·0529	-	·3171	·1361	·0509	-
Mass. Fract.	·4000	·1559	·0572	·3868	·3568	·1660	·0604	·4168	·3834	·1721	·0603	·3842
Oxide %	66·3	33·35	7·36	-	59·2	35·5	7·77	-	63·56	36·8	7·75	-
Whole peak	×	×	×				×				×	
Half peak					×	×			×	×		

Wet analysis	MgO	SiO_2	FeO
%	49·08	40·54	9·50

$$* K = \frac{\text{(Peak - Background) sample counts}}{\text{(Peak - Background) standard counts}}$$

$$\text{Mass. Fract} = K(ZAF)$$ (138)

Table 15 Comparison between the wet chemical analysis of the St. John's Island olivine and the results obtained from the Steetley S E M

Oxide W%	Wet chemical	S E M
MgO	49·08	51·34
SiO_2	40·54	40·73
FeO	9·50	7·92
total	99·12	99·99

TABLE 16 Compositions of synthetic slags used in the measurement of melt viscosities.

Melt Number	Experiment Number	Synthetic slag composition mass %				
		FeO	Fe_2O_3	SiO_2	CaO	MgO
1	3	64.33	1.96	32.2	-	-
2	8	56.7	3.16	29.3	10.5	-
3	16	30.5	1.00	35.9	32.6	-
4	15	63.5	0.64	31.9	-	1.9
* 5	21	57.22	2.68	32.14	2.06	5.88
* 6	23	54.45	2.61	32.89	2.13	7.45
** 7	24	49.68	3.8	25.75	15.0	6.13

* Recalculated analyses neglecting zirconia (see Table 17).

** Average of two analyses which were recalculated after neglecting Zirconia contamination (see Table 17).

TABLE 17 Compositions of synthetic slags after viscosity measurement in zirconia crucibles.

Melt Number	Experiment Number	Synthetic slag composition mass %					
		FeO	Fe_2O_3	SiO_2	CaO	MgO	ZrO_2
5	21	50.92	2.39	28.6	1.83	5.24	11.0
Recalculated value		57.22	2.68	32.14	2.06	5.88	-
6	23	47.45	2.27	28.6	1.85	6.48	13.0
Recalculated value		54.45	2.61	32.89	2.13	7.45	-
7	24A	42.7	3.69	22.6	13.6	5.8	12.9
Recalculated value		48.79	4.20	25.8	15.5	6.6	-
7	24B	44.69	3.28	22.6	12.8	5.0	12.2
Recalculated value		50.57	3.70	25.57	14.5	5.66	-

Sample 24A taken from centre of crucible.

Sample 24B taken from periphery of crucible.

TABLE 18 Viscosity values determined for iron silicate melt.

Viscosity (μ) = U x S x K (K = 4.808)

Crucible temp. °C	Speed (U)	Scale (S)			UxS(av)	Viscosity mPas (cP)
		1	2	3		
1222	2	8.5	9.0	-	17.5	84.0
	1	27.0	26.0	-	26.5	127
1206	3	11.0	12.0	-	34.5	166
	2	18.0	17.0	-	36.0	173
	1	68	55	-	61.5	296
1192	6	10.0	9.0	-	57	274
	3	16.0	15.0	-	46.5	224
	2	20.0	20.0	-	40.0	192
1244	1	23.0	23.0	-	22.9	110
1256	1	22.0	22.0	21.6	21.9	105
1290	1	21.0	21.0	21.0	21.0	101
1300	1	20.0	19.8	20.0	19.9	96.7
1325	1	20.0	19.7	19.8	19.8	95.2
1327	1	19.5	19.5	19.5	19.5	93.7

Melt composition 1 (3)	FeO	Fe_2O_3	SiO_2
after viscosity determination	64.33	1.96	32.30

TABLE 19 Viscosity values determined for lime-iron silicate melt.

Viscosity (μ) = U x S x K (K = 4.808)

Crucible temp. °C	Speed (U)	Scale (S) 1	2	3	UxS(av)	Viscosity mPas (cP)
1235	1	29.0	28.3	27.8	28.36	136
1234	1	27.2	27.1	-	27.15	130
1183	1	30.5	30.0	-	30.25	145
1155	1	33.0	32.8	-	32.9	158
1153	1	33.7	33.0	-	33.35	160
1128	1	36.0	36.0	-	36.0	173
1126.5	1	37.0	37.2	-	37.1	178
1108	3	14.0	17.0	19.0	50	240
	2	33.0	37.0	-	70	336
	1	88.0	78.0	-	83	398
1216	1	28.2	28.0	-	28.1	135
1233	1	27.0	26.2	-	26.6	128
1234	1	27.0	26.5	-	26.75	128
1278	1	26.5	26.5	-	26.5	127
1279	1	26.0	25.0	-	25.5	122
1324	1	24.0	22.5	23.0	23.16	111
1325	1	24.0	24.0	24.0	24.0	115
1376	1	20.0	20.0	19.8	19.93	95.8
1375	1	21.0	21.0	-	21.0	101

Melt composition 2 (8) before viscosity measurement.	CaO	FeO	Fe_2O_3	SiO_2
	10.50	56.70	3.16	29.30

TABLE 20 Viscosity values determined for a high lime-iron silicate melt.

Viscosity (μ) = U x S x K K = 4.808

Crucible temp. °C	Speed (U)	Scale (S)			UxS(av)	Viscosity mPa.s (cP)
		1	2	3		
1318	2	14.1	14.0	-	28.0	135
	1	36.0	37.0	-	36.5	176
1374	1	30.0	30.5	31.0	30.5	147
1327	1	33.0	32.5	32.5	30.6	157
1280	1	37.0	36.5	36.2	36.6	176
1255	1	38.0	38.5	38.0	38.3	184
1232	3	13.5	13.5	13.0	40.0	192
	2	21.5	21.5	-	43.0	206
	1	52.0	50.0	50.0	50.66	244
1224	3	13.5	13.0	-	39.75	191
	2	21.2	21.2	-	42.4	204
	1	51.5	51.5	51.5	51.33	247

Comments. Crucible thermocouple broke during early part of experiment. Crucible temperature values are based upon the calibration curve illustrated in Fig. 32 .

Melt composition 3 (16)	CaO	FeO	Fe_2O_3	SiO_2
before viscosity experiment.	32.60	30.50	1.00	35.90

TABLE 21 Viscosity values determined for a 2 mass % MgO - iron silicate melt.

Viscosity (μ) = U x S x K

(K = 4.808)

Crucible temp. °C	Speed (U)	Scale (S)			UxS(av)	Viscosity mPa.s (cP)
		1	2	3		
1330	1	20.0	20.5	19.8	20.1	96.5
1325	1	19.0	19.3	19.0	19.1	92.0
1391	1	17.8	18.0	18.2	18.0	86.0
1394	1	17.0	17.0	16.8	16.9	81.0
1324	1	19.5	19.0	18.7	19.1	92.0
1290	1	19.6	19.0	18.8	19.1	92.0
1255	1	21.8	20.5	21.0	21.1	101
1253	1	22.0	22.0	21.0	21.7	104
1231	1	22.0	21.5	22.0	21.8	105
1219	1	24.0	25.0	25.2	24.7	119
1215	3	15.0	15.5	16.0	46.5	224
	2	22.5	22.5	-	45.0	216
	1	44.0	46.0	-	45.0	216
1210	3	15.0	15.5	16.0	46.5	226
	2	26.0	28.0	-	54.0	259
	1	55.0	57.0	56.5	56.2	270
1226	3	13.0	13.0	-	39.0	187
	2	19.0	18.5	-	37.5	180
	1	39.0	40.0	-	39.5	190
1247	1	19.5	19.5	19.5	19.5	94
1286	1	18.0	18.0	18.2	18.06	87
1318	1	18.2	18.0	18.0	18.06	87
1369	1	17.5	17.5	17.6	17.53	84.2
1420	1	17.5	17.0	17.0	17.16	82.0
1444	1	17.0	17.5	17.3	17.26	83.0

Melt composition 4 (15) after viscosity determination.

MgO	FeO	Fe_2O_3	SiO_2
1.9	63.50	0.64	31.90

TABLE 22 Viscosity values determined for a 5 mass % MgO - iron silicate melt.

Viscosity (μ) = U x S x K

K=5.280 when U=3 : K=5.210 when U=2 : K=5.075 when U=1

Crucible temp. °C	Speed (U)	Scale (S)			UxS(av)	Viscosity mPa.s (cP)
		1	2	3		
1397	3	11.5	11.5	12.0	35.0	185
	2	17.0	17.5	18.0	35.0	182
	1	35.0	34.0	-	34.5	175
1346	3	13.0	12.5	12.5	38.0	200
	2	19.5	19.5	-	39.0	203
	1	39.0	38.5	-	38.75	197
1321	3	15.0	14.5	14.5	44.0	232
	2	21.5	22.0	21.5	43.4	226
	1	43.5	43.5	-	43.5	221
1306	3	18.0	17.5	17.5	53.0	280
	2	27.0	26.5	-	53.5	279
	1	47.0	47.5	-	47.25	240
1296	2	33.0	31.0	32.0	64.0	333
	1	56.0	57.0	-	56.5	287
1286	3	27.0	26.0	26.5	79.5	420
	2	36.0	37.5	-	73.5	383
1318	2	22.5	23.0	22.5	45.3	239
	1	43.0	44.0	-	43.5	221
1368	2	17.0	17.0	16.5	33.67	175
	1	34.0	34.5	-	34.25	174
1427	2	17.0	17.0	17.0	34.0	177
	1	33.0	34.0	34.5	33.8	172
1392	2	18.0	18.0	-	36.0	188
	1	35.5	35.6	35.5	35.5	180
1291	2	37.5	39.0	-	76.5	398
	1	63.0	65.0	-	64	325
1279	6	33.0	34.0	-	201	>1000
	3	45.0	44.5	43.5	134	706
	2	54.5	55.5	-	110	573

Composition melt 5 (21) after viscosity determination

MgO	CaO	FeO	Fe_2O_3	SiO_2	ZrO_2
5.24	1.83	50.92	2.39	28.6	11.0

TABLE 23 Viscosity values determined for a 7.5 mass % MgO - iron silicate melt.

Viscosity (μ) = U x S x K K=5.280 when U=3
K=5.210 when U=2

Crucible temp. °C	Speed (U)	Scale (S)			UxS(av)	Viscosity mPas (cP)
		1	2	3		
1361	3	8.5	7.5	8.0	24	127
	2	12.5	12.5	13.0	25	130
1341	3	10.5	10.5	10.8	31.8	167
	2	15.5	15.0	15.5	30.7	160
1327	3	12.0	12.5	12.0	36.5	193
	2	18.0	17.5	-	35.5	185
1302	3	27.0	22.0	21.0	70.0	370
	2	28.0	30.0	28.0	57.3	300
1410	3	7.5	7.5	7.5	22.5	119
	2	12.0	11.5	12.0	23.7	123
1433	3	5	4.5	5.5	15.0	79.2
	2	9.0	9.0	9.0	18.0	93.8
1454	3	4.5	4.5	4.5	13.5	71.3
	2	8.5	8.8	9.0	17.5	91.0
1472	2	7.0	7.0	7.0	14.0	73.0
1414	3	5.5	5.5	5.5	16.5	87.0
	2	9.5	9.0	9.5	19.0	97.3
1382	3	6.5	7.0	7.0	20.5	108
	2	11.5	11.0	11.5	22.7	118

Melt composition 6(23) after viscosity determination.	MgO	FeO	Fe_2O_3	SiO_2	CaO	ZrO_2
	6.48	47.34	2.27	28.60	1.85	13.0

TABLE 24 Viscosity values determined for a 7.5 mass % MgO - lime - iron silicate melt.

Viscosity (μ) = U x S x K K=5.280 when U=3

K=5.210 when U=2

Crucible temp. °C	Speed (U)	Scale (S)			UxS(av)	Viscosity mPas (cP)
		1	2	3		
1362	3	4.0	4.5	4.5	13.0	68.6
	2	7.5	8.0	7.5	15.3	79.6
1397	3	4.0	3.8	4.0	11.8	62.0
	2	7.0	7.0	7.0	14.0	73.0
1321	3	5.0	5.2	5.2	15.4	81.0
	2	8.5	8.5	8.5	17.0	88.6
1293	3	6.0	5.5	6.0	17.0	88.6
	2	10.0	9.5	9.5	19.3	101
1264	3	6.5	6.5	6.5	19.5	103
	2	10.0	10.	11.0	21.0	109
1249	3	8.5	8.5	8.5	25.5	135
	2	13.5	13.5	13.5	27.0	141
1230	3	10.0	10.0	10.0	30.0	158
	2	15.0	15.0	-	30.0	156
1209	3	12.5	12.5	12.5	37.0	195
	2	17.0	17.5	17.0	34.3	179
1195	3	22.0	19.0	20.0	61.0	322
	2	26.0	27.0	26.0	52.7	274
1350	3	4.0	4.0	4.0	12.0	63.4
	2	6.5	6.5	6.5	13.0	67.8
1442	2	6.0	6.0	6.2	12.1	63.0

Melt composition 7(24) after viscosity run.

MgO	FeO	Fe_2O_3	SiO_2	CaO	ZrO_2
5.2	43.7	3.49	22.6	13.6	12.55

Average of 2 analyses (Table 17 p. 242).

TABLE 25 The compositions of a synthetic iron silicate slag before and after a viscosity measurement in an iron crucible.

Composition (mass%)	FeO	Fe_2O_3	SiO_2	magnetics
Before experiment	64.33	1.95	32.3	-
After experiment	65.00	0.87	32.7	0.57

TABLE 26 The effect of zirconia on the melting temperatures of some synthetic iron silicate slags.

Sample	Melt Number	Composition mass %						Cone melting range °C	
		FeO	Fe_2O_3	SiO_2	CaO	MgO	ZrO_2	start	end
BF 2	1	63·04	1·42	34·9				1143	1167
BF 2 Z		55·12	2·67	26·9	0·1	0·11	15·0	1155	1180
5MCF 13		50·55	2·66	27·3	14·2	4·55		1178	1186
*24 B	7	50·57	3·70	25·57	14·48	5·66	[12·0]	1171	1192

* Melt composition recalculated back to 100% after neglecting amount of zirconia present [12.0]

TABLE 27 The liquidus temperatures of synthetic slags determined by both viscosity and cone fusion studies.

Experiment Number	Melt Number	Composition mass %						Liquidus temperature from viscosity curve °C	cone fusion melting range °C
		FeO	Fe_2O_3	SiO_2	CaO	MgO	ZrO_2		
3	1	64.33	1.96	32.2	-	-	-	1212	1149 to 1166
8	2	56.7	3.16	29.3	10.5	-	-	1127	* 1098 to 1109
16	3	30.5	1.0	35.9	32.6	-	-	1238	1176 to 1188
15	4	63.5	0.64	31.9	-	1.9	-	1229	not determined
21	5	57.22	2.68	32.14	2.06	5.88	[11.0]	1310	1227 to 1250
23	6	54.45	2.61	32.89	2.13	7.45	[13.0]	1348	** 1290 to (1360 - 1380)
24B	7	50.57	3.70	25.57	14.5	5.66	[12.2]	1233	1171 to 1192

* cone contained 13.5 mass % CaO

** cone contracted rather than collapsed

[ ] Zirconia content of melt not included in the recalculated analysis

TABLE 28 The effect of pre-heat holding temperature on dolomitic lime cylinder properties.

Sample	Bulk density before, kgm^{-3}	Bulk density after, kgm^{-3}	P app % before	P app % after
1	1740	1800	51.40	49.61
2	1620	1620	54.70	54.87
3	1980	1980	44.12	47.85
4	1780	1780	51.10	50.10
5	1560	1560	56.55	56.47

TABLE 29 The effect of pre-heat holding temperature on lime cylinder properties.

Sample	Bulk density before, kgm^{-3}	Bulk density after, kgm^{-3}	P app % before	P app % after
1	2290	2300	32.25	32.15
2	2440	2450	27.81	27.73
3	1770	1780	48.32	47.48
4	1790	1800	47.83	47.22
5	1860	1900	45.56	43.52

Table 30 Cylinder immersion studies and related photomicrographs.

Melt composition (mass%)	FeO	Fe_2O_3	SiO_2	CaO	MgO
BF3	62.73	1.77	34.30	0.18	0.06
BF4	60.16	2.69	36.34	0.74	0.07

Cylinder type	Immersion time (s)	Static - rotated	Plate Number	Remarks
"soft" burnt dolomitic lime Papp%58 + BF3	15	static	32	Initial reaction, upper section of cylinder.
	45	"		
	60	"		
	75	"		
	90	"		oil quenched
	120	"		" "
	120	"		" "
	180	"		" "
	180	"		" "
Dolomitic lime Papp 50% + BF3	15 Annealed (1 hour)	static	28,33,34	melt-C_2S,MF'interface
			44, 45	secondary C_2S interface.
	15	static	29,38,77	melt-cylinder reaction.
	60	"		
	90	"	35,39,41	C_2S meshwork, wüstite dendrites, FeO-rich liquid.
	120	"	27	hydrated core.
	120	"	36,78	melt-cylinder interface.
	180	"		
	180	"		
	240	"		hydrated core.
+ BF4	240	static		

Cylinder type	Immersion time (s)	Static - rotated	Plate Number	Remarks
Dolomitic lime + BF3	300	Static		
	360	"	37,40,79	globular wüstite, Fo-Fa series.
	540	"	42	
+ BF4	420	static	43,82	"hard" burnt cylinder globular wüstite, Fo-Fa.
+ BF4	15	rotated		
	60	"	46	finger-like melt projections.
	120	"		
	240	"		
	300	"	47	granular olivine.
	360	"	48,49	SEM reflective mode, cylinder.
	540	"		
+ BF4	15	static	52	5mass % MgO addition.
	360	"	53,81	5 mass % MgO addition.
Pill test + BF3	1500		54,55,80	lobate wüstite, unreacted dolomitic lime.
"Dolomet" + BF4	15	static	56	melt-"Dolomet" interface.
	360	"	57	metallic iron.
"Hard" burnt lime	15	static	58,59	granular C_2S formation.
	120	"	60	continuous C_2S barrier.
	180	"		
	240	"	61	thickened C_2S interface.
	360	"	62,63	continuous C_2S barrier, Lime + C_3S + CF'.

Cylinder type	Immersion time (s)	Static - rotated	Plate Number	Remarks
"Soft" burnt lime	15	static	64,66,83	granular C_2S + CF' phases x-ray maps, SEM analyses.
	60	"		
	60	"		
	120	"		hydrated cylinder.
	120	"	65	convoluted C_2S layer.
	180	"		
	240	"		
	300	"		
	360	"		
	540	"	67,68,69	convoluted C_2S layer.
			84	profile analyses.
"Soft" burnt lime + BF4	15	static	70	2 mass % MgO in melt.
	15	"	71,75,85	5 mass % MgO in melt.
	360	"	72,73,74	5 mass % MgO in melt.
			76,86	disseminated C_2S, C_3S phases.

TABLE 31 The static dissolution of dolomitic lime cylinders in iron silicate melts.

Immersion time (s.)	Melt composition after experiment (mass%)				
	FeO	Fe_2O_3	SiO_2	CaO	MgO
15	62.33	1.59	34.99	0.29	0.16
60	61.98	1.50	33.95	0.97	1.05
90	61.26	1.97	33.90	1.53	0.84
120	61.65	1.34	33.10	1.22	0.69
180	61.37	1.50	32.60	1.26	0.87
240	59.93	1.79	32.16	1.66	0.58
300	60.56	1.59	34.22	1.78	1.27
360	60.49	1.82	33.92	2.14	1.19
540	59.36	1.82	33.54	3.26	0.75

TABLE 32 The dissolution of dolomitic lime cylinders rotated in an iron silicate melt.

Immersion time (s.)	Melt composition after experiment (mass%)				
	FeO	Fe_2O_3	SiO_2	CaO	MgO
15	62.4	1.25	34.30	0.47	0.16
60	61.72	1.23	33.96	1.22	0.49
120	61.84	1.73	34.10	0.52	0.53
240	59.80	1.80	32.60	3.31	1.48
300	60.00	2.37	32.40	2.76	1.42
360	60.60	1.80	32.60	2.78	1.13
540	59.60	1.90	32.40	3.32	1.72

TABLE 33 The static dissolution of "hard" burnt lime cylinders at 1300°C.

Immersion time (s.)	Melt composition after experiment (mass%)			
	FeO	Fe_2O_3	SiO_2	CaO
15	62.4	1.62	34.85	0.17
120	62.15	1.94	34.74	0.34
180	61.60	2.10	34.30	0.66
240	60.20	4.00	33.75	0.84
360	61.44	1.93	34.00	1.05

TABLE 34 The static dissolution of "soft" burnt lime cylinders at 1300°C.

Immersion time (s.)	Melt composition after experiment (mass%)			
	FeO	Fe_2O_3	SiO_2	CaO
15	62.69	1.19	35.7	0.03
60	62.65	1.03	34.97	0.74
120	61.51	1.19	33.70	2.25
120	61.03	1.63	31.0	3.02
300	58.87	1.50	32.7	3.21
540	57.79	2.06	28.4	6.8

TABLE 35 The melting range of synthetic slags in the system CaO - 'FeO' - SiO_2 - MgO.

Sample	Nominal MgO content	Analysed melt composition (mass %)					Cone description at temperature °C		
		FeO	Fe_2O_3	SiO_2	CaO	MgO	Initial bend	Intermediate	Collapse
BF4	-	60.6	2.69	36.3	0.74	0.07	1169	1177	1179
BF2	-	63.04	1.42	34.9	-	-	1149	1160	1166
BF2	-	63.04	1.42	34.9	-	-	1143	1159	1167
MF4	4.0	55.45	2.66	36.9	0.21	4.77	1211	1217	1221
MF8	8.0	57.60	1.93	30.6	1.00	7.83	1242	1247	1262
CF13	-	54.93	2.86	29.0	13.10	-	1098	1106	1109
5MCF13	5.0	50.55	2.66	27.3	14.20	4.55	1178	1180	1186
10MCF13	10.0	48.78	3.60	26.4	12.0	9.94	1209	1222	1308
15MCF13	15.0						1269	cone contraction.	>1400
CF20	-	53.51	3.06	24.0	19.03	0.07	1126	1132	1136
5MCF20	5.0						1199	rapid cone collapse.	1232
10MCF20	10.0						1269	1286	1293
CF32	-	30.50	1.00	35.90	32.60	-	1176	1185	1189
CF32	-	30.50	1.00	35.9	32.6	-		1181	1188
5MCF32	5.0	27.53	1.73	33.65	32.0	4.90	1232	1242	1247
10MCF32	10.0	26.72	1.56	31.88	29.8	9.95	1260	1286	1306
15MCF32	15.0						1308	1372	1379
CF38	-	27.3	1.20	32.04	38.5	-	1217	1230	1242
10MCF38	10.0						1301	1347	1354

Table 36 Experimental Viscosity values of some iron silicate (fayalite) melts.

Author	Melt composition (mass %)			Viscosity mPa.s				
	FeO	Fe_2O_3	SiO_2	1200	1250	°C 1300	1350	1400
Kozakevitch (51)	66.98	–	33 02	80	70	60	60	50
Toguri et al (54)	Fe/Si 3.88/1			120	92	70	53	–
Röntgen et al (52)	70.6		29.40	480	75	55	50	–
Shiraishi et al (53)	67.0	–	33.0	-	98	84	74	60
This work	64.33	1.95	32.3	320	110	95	82	

TABLE 37 Slope values from immersion experiments converted from mass % $CaOs^{-1}$ to $gCaOs^{-1}$.

Cylinder	Static slope $gCaOs^{-1}$	Rotated slope $gCaOs^{-1}$	Rate Factor	App.Porosity %
Lime "hard"	1.224×10^{-3}		1	24.47 ± 2.52
"soft"	5.54×10^{-3}		4.5	43.32 ± 1.0
Dolomitic lime	1) 6.8×10^{-3}		5.5	50.86 ± 0.97
	2) 1.89×10^{-3}		1.5	"
		1) 7.47×10^{-3}	6.1	"
		2) 2.43×10^{-3}	2.0	"

1) represents the first slope value before the inflexion.

2) represents the second slope value after the inflexion.

(see Figs. 51, 52, 54 and 55).

TABLE 38 Slope values from immersion experiments converted from mass % MgO to $gMgOs^{-1}$.

Cylinder	Static slope $gMgOs^{-1}$	Rotated slope $gMgOs^{-1}$	Rate Factor	App.Porosity %
Dolomitic lime	1) 8.86×10^{-3}		57	50.86 ± 0.97
	2) 1.56×10^{-4}		1	"
		1.30×10^{-3}	8.3	"

TABLE 39 Experimental mass transfer coefficients for CaO based on 1300°C isothermal dissolution studies in iron silicate (fayalite) melts.

Cylinder	Static k_{CaO} cms^{-1}	Rotated k_{CaO} cms^{-1}	Rate Factor	Apparent porosity%
Lime "hard"	2.8×10^{-4}		1	24.47 ± 2.52
"soft"	9.8×10^{-4}		3.5	43.32 ± 1.0
Dolomitic lime.	1) 12.3×10^{-4}		4.4	50.86 ± 0.97
	2) 3.5×10^{-4}		1.2	"
		1) 13.1×10^{-4}	4.6	"
		2) 4.3×10^{-4}	1.5	"

1) represents the first slope value before inflexion.

2) represents the second slope value after inflexion.

(see Figs. 51, 52, 54 and 55).

TABLE 40 Experimental mass transfer coefficients for MgO based on 1300°C isothermal dissolution studies in iron silicate (fayalite) melts.

Cylinder	Static k_{MgO} cms^{-1}	Rotated k_{MgO} cms^{-1}	Rate Factor	Apparent Porosity%
Dolomitic lime.	1) 11.5×10^{-4}		60	50.86 ± 0.97
	2) 1.9×10^{-5}		1	
		1.69×10^{-4}	8.5	

TABLE 41 Experimental and theoretical values of mass transfer coefficients of CaO taken from the Literature.

Author	Static k_{CaO} cms^{-1}	Rotated k_{CaO} cms^{-1}	r.p.m.	Temp ^{o}C	App. Porosity
Green (80)	1.74×10^{-4}	3.5×10^{-4}	32	1300	25
Matsushima (79)	-	9.7×10^{-4}	200	1400	40
		17.1×10^{-4}	400	1400	40
*Theoretical (40)		3.2×10^{-4}	50	1300	-

*Calculation illustrated in Appendix 3 (p. 218).

TABLE 42 The influence of the immersed cylinder surface area term on the experimental mass transfer coefficient values of k_{CaO}

Cylinder	Static k_{CaO} cms^{-1}	Rotated k_{CaO} cms^{-1}	Range due to surface area variation
Lime "hard"	2.8×10^{-4}		$\pm 0.76 \times 10^{-4}$
"soft"	9.8×10^{-4}		$\pm 1.12 \times 10^{-4}$
Dolomitic lime	2)3.5×10^{-4}	2)4.3×10^{-4}	$\pm 0.55 \times 10^{-4}$
			$\pm 0.85 \times 10^{-4}$

2) slope value above the inflexion.

Fig 1 Free Energy Diagram – OXIDES

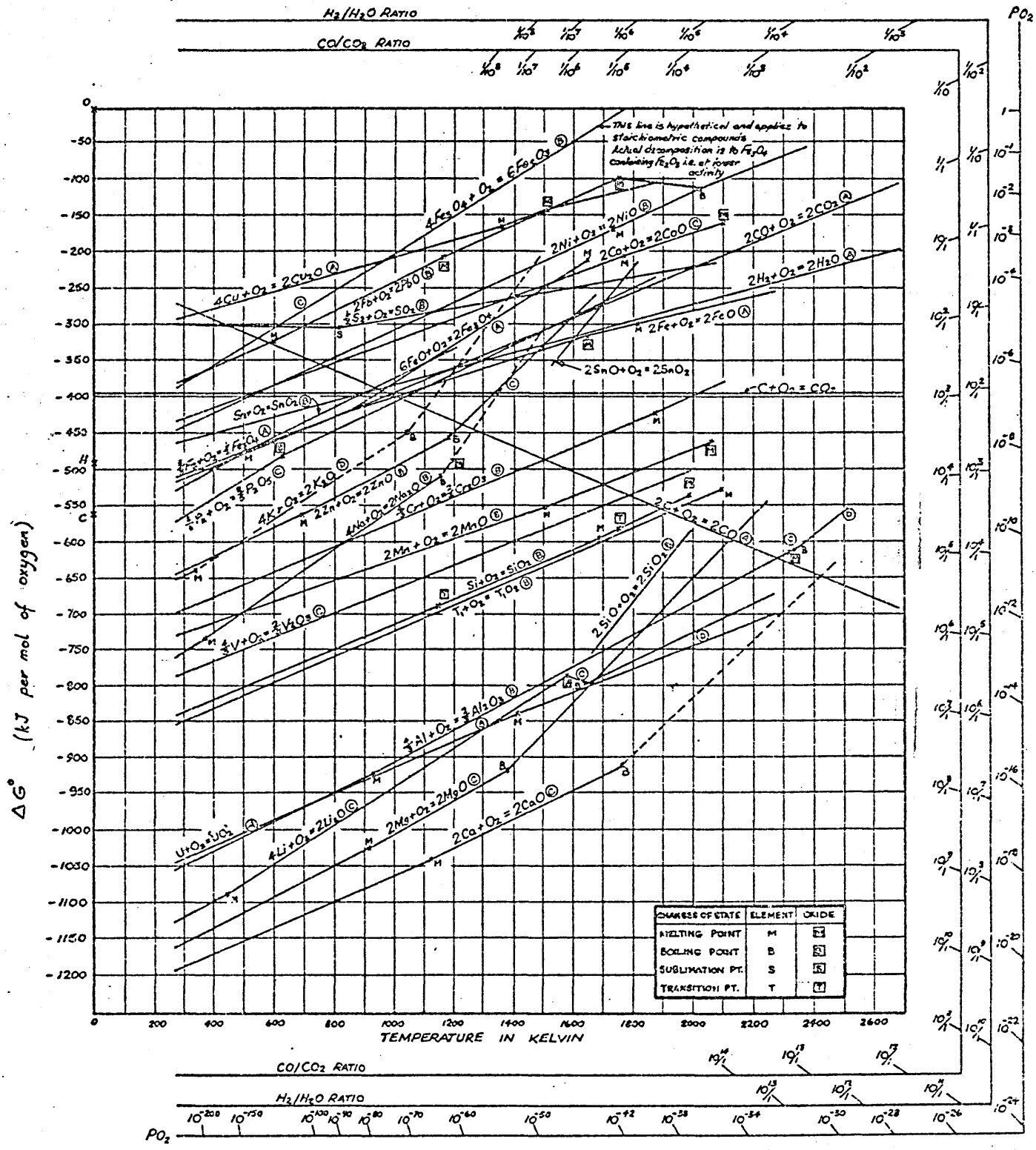

Oxygen potentials in oxide systems

SHEFFIELD POLYTECHNIC
(After Richardson)

Fig 2 The changes in bath compositions during the blow

[after Walker & Anderson [13]]

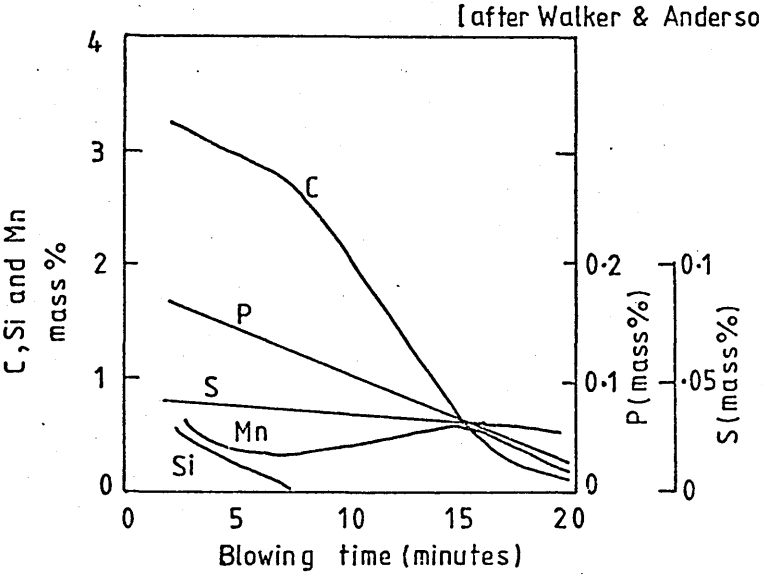

Fig 3 Decarburisation rate curves

[after Meyer et al [30]]

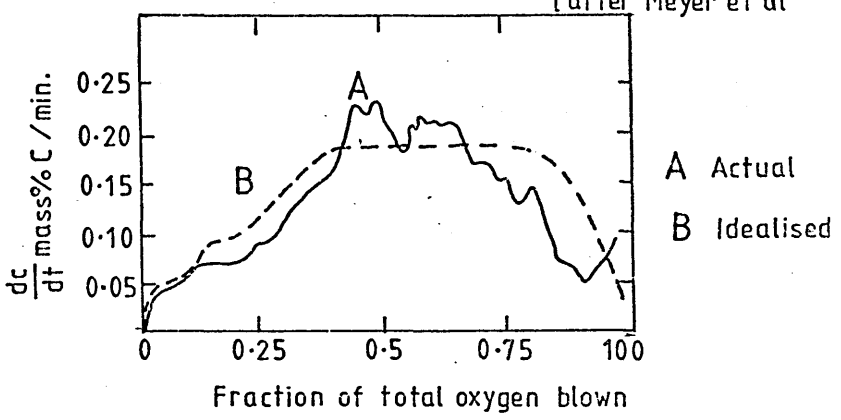

Fig 4 The idealised decarburisation rate curve [4]

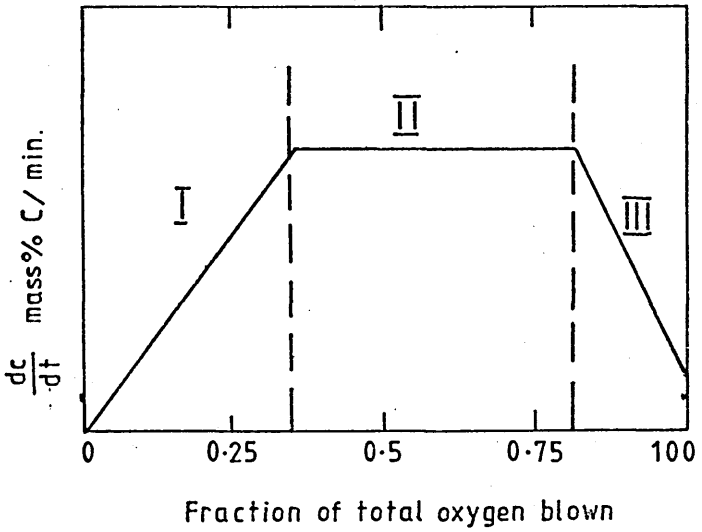

Fig 5 Decrease of the activation energy of viscosity for silica as basic oxides are added

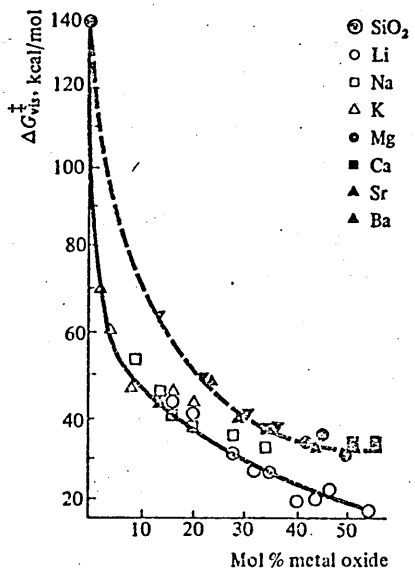

(after Geiger et al.[48])

Fig 6

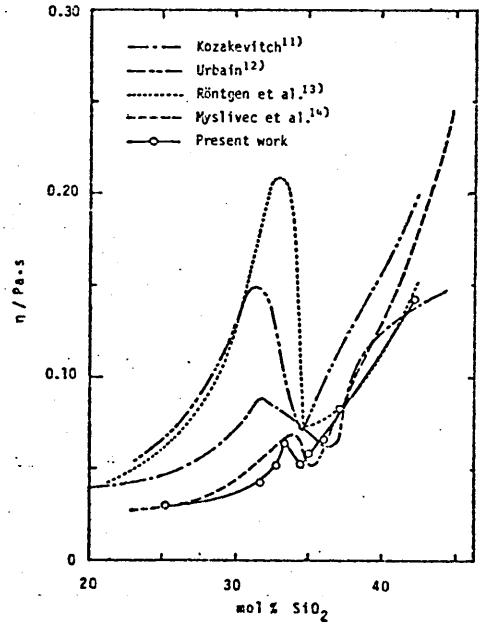

Viscosity coefficient of the molten FeO–SiO_2 system at 1300°C.

(after Shiraishi et al[53])

Fig 7 Section of the $FeO - Fe_2O_3 - SiO_2$ system at 1350°C

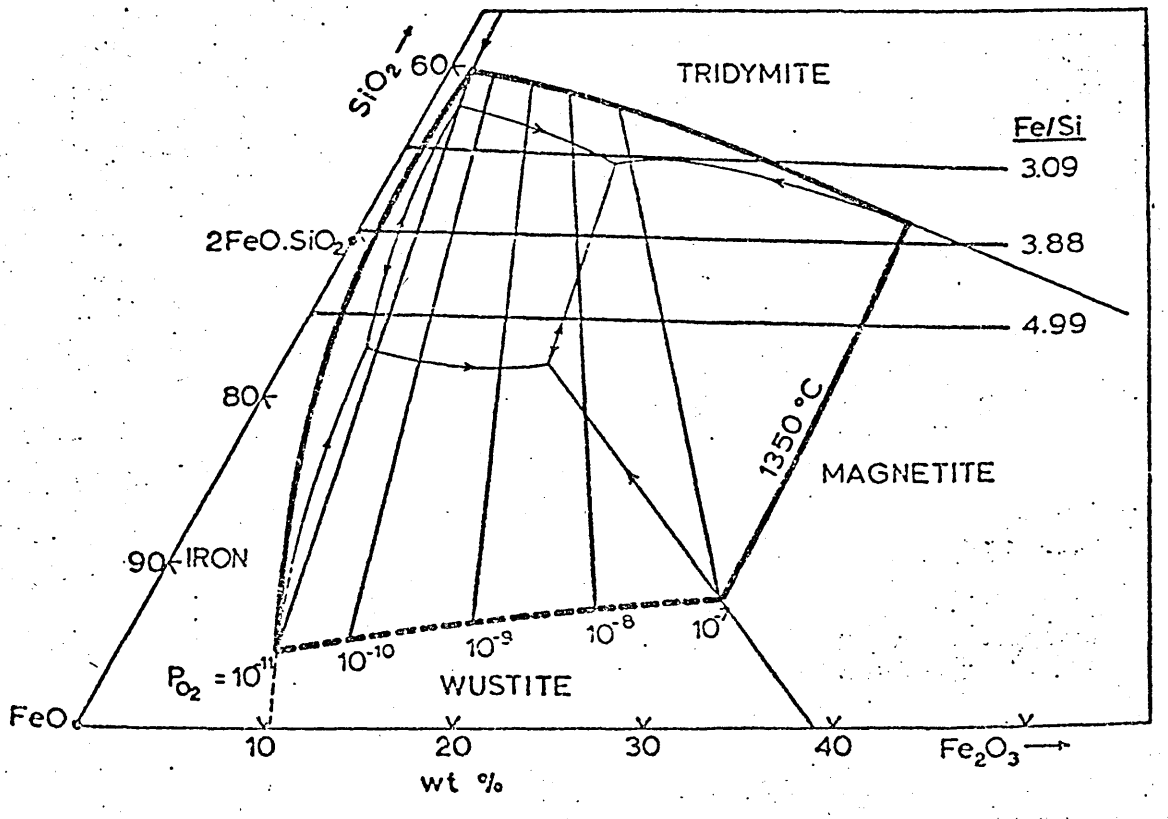

(after Toguri et al [54])

Fig 8 Iso-viscosity contours of the system $CaO - FeO - SiO_2$

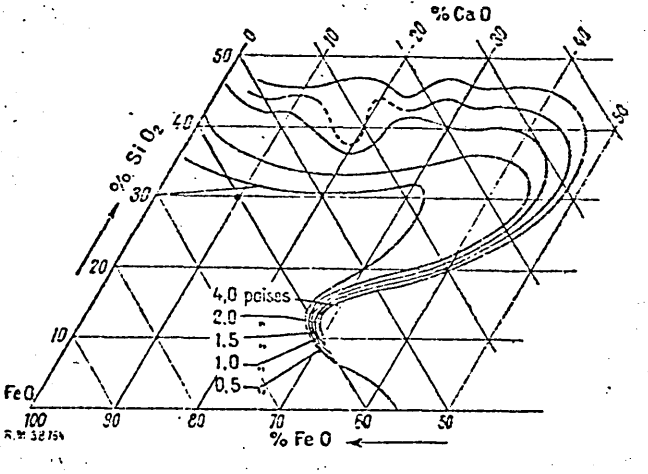

(after Kozakevitch [55])

Fig 9a

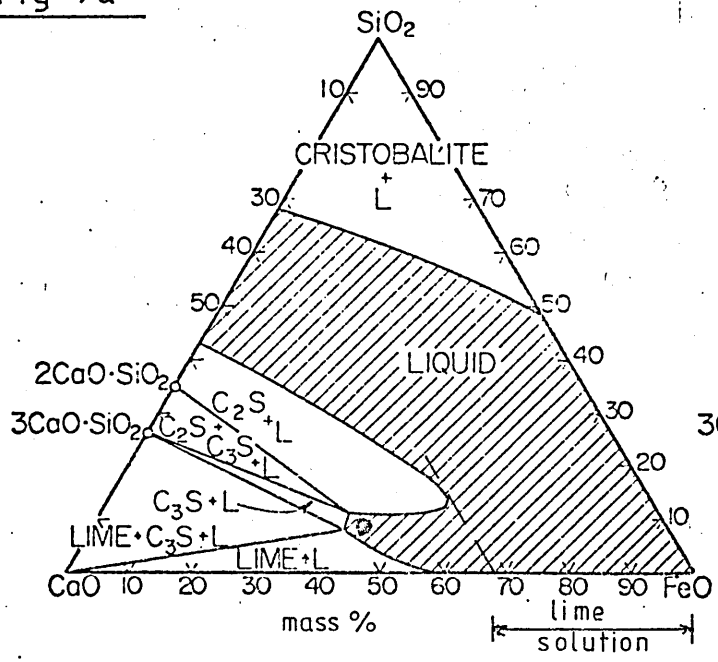

Fig 9b

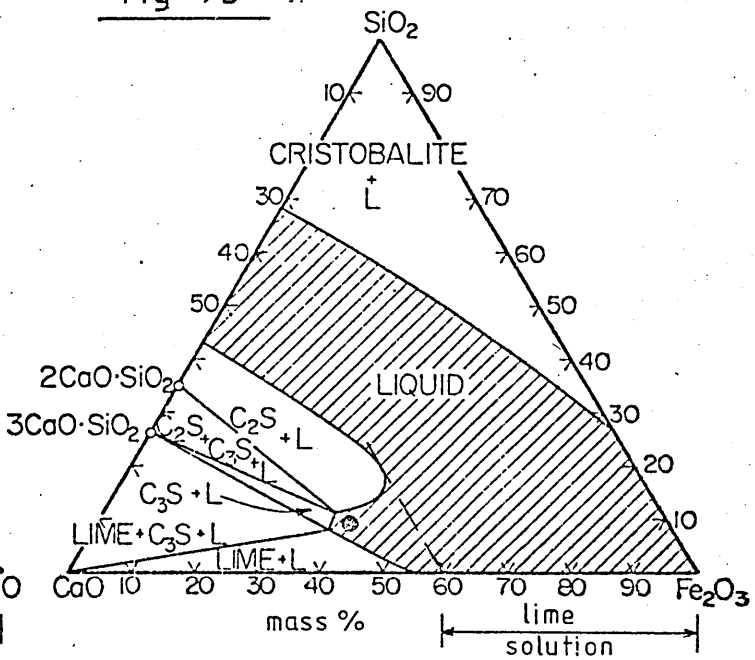

The 1600°C isothermal sections through the system CaO-iron oxide-SiO_2 at two different levels of oxygen pressures, those prevailing in contact with metallic iron in (a) and that of air in (b). Up to 10 mass% more lime may be dissolved at 1 atmosphere pressure before the C_2S+L phase field is intersected (b).

Abbreviations used have the following meanings:

$C_3S = 3CaO{\cdot}SiO_2$, $C_2S = 2CaO{\cdot}SiO_2$, L = liquid.

(modified after Muan and Osborn [50])

Fig 10. Evolution of slag composition

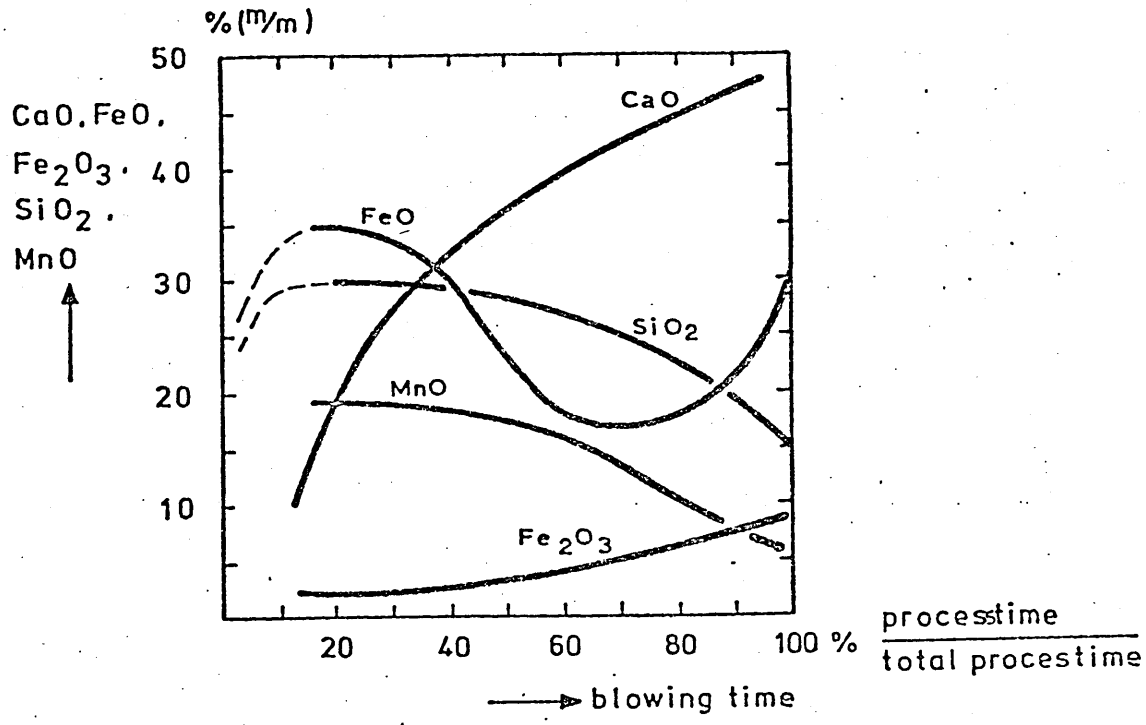

Fig 11. Evolution of the slag composition during the blow: curves of CaO, SiO_2, Fe dissolved into the slag.

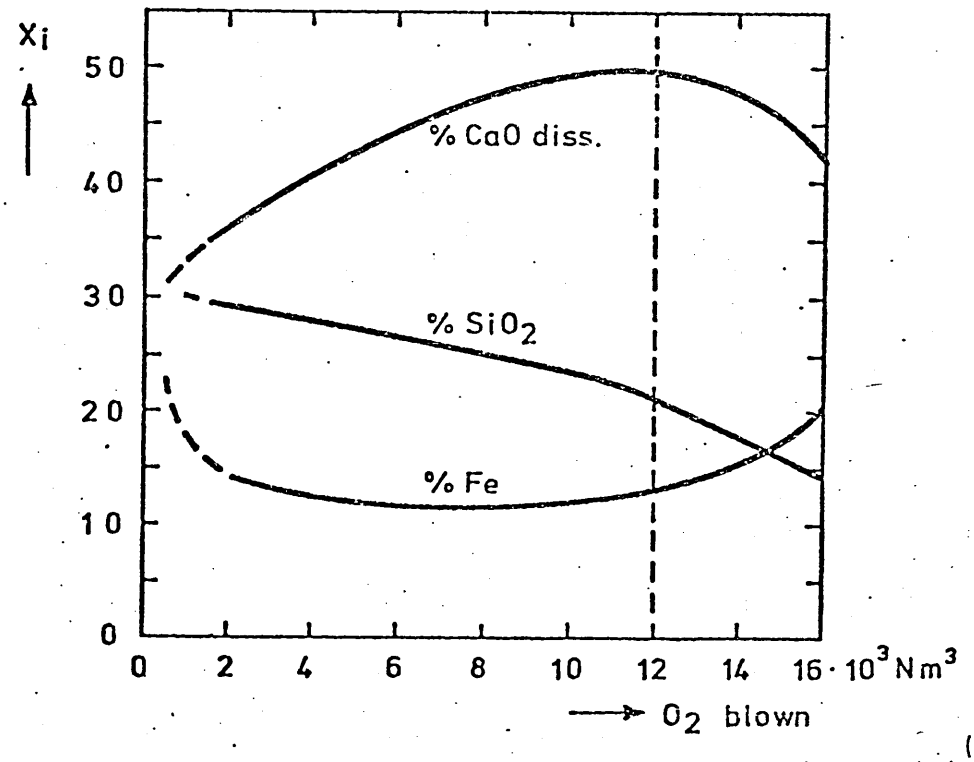

(both Figs. after van Hoorn et.al. (74))

Fig 12 The system CaO-FeO-SiC^ in contact with metallic iron

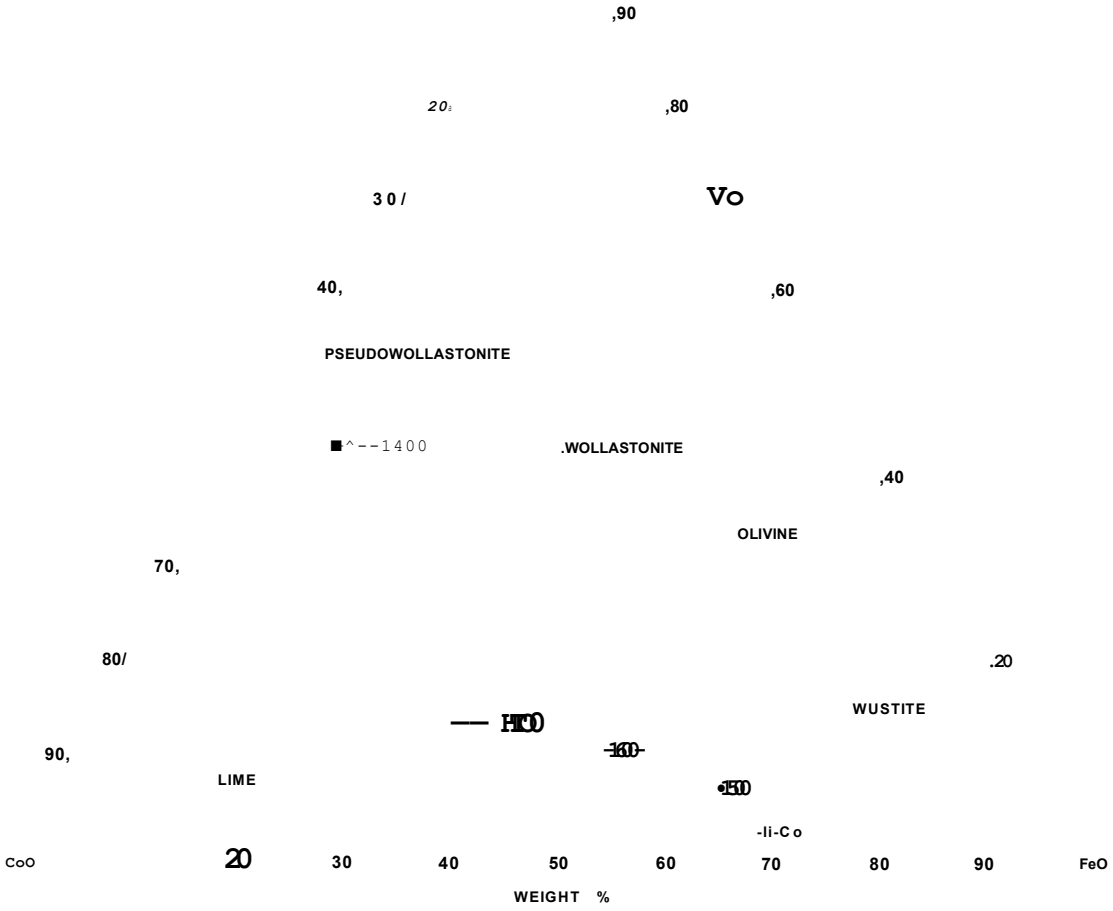

(after Muan and Osborn

Fig 13.

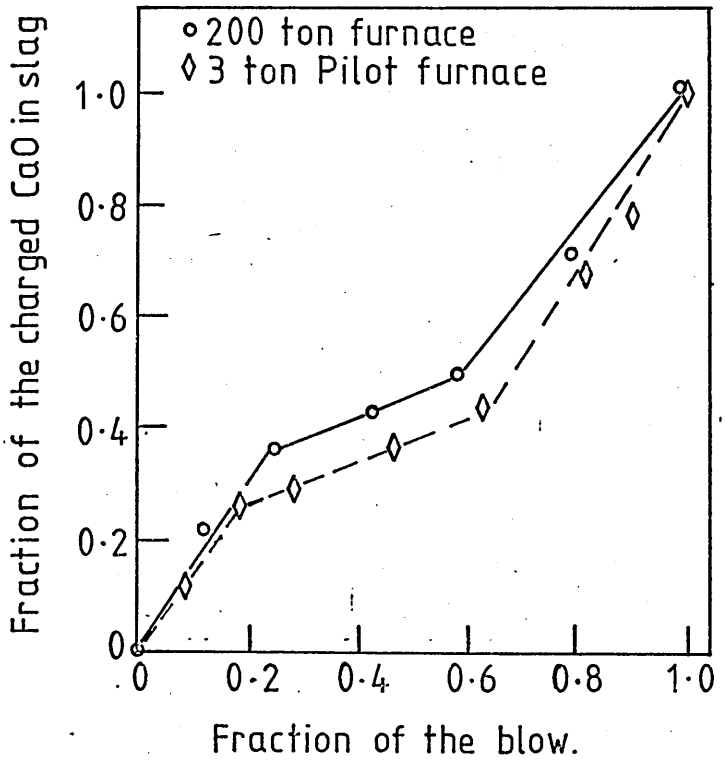

Relationship between fraction of lime dissolved and fraction of time from start of lime charge to finish of blow.

(after Iyengar et al[76])

Fig 14.

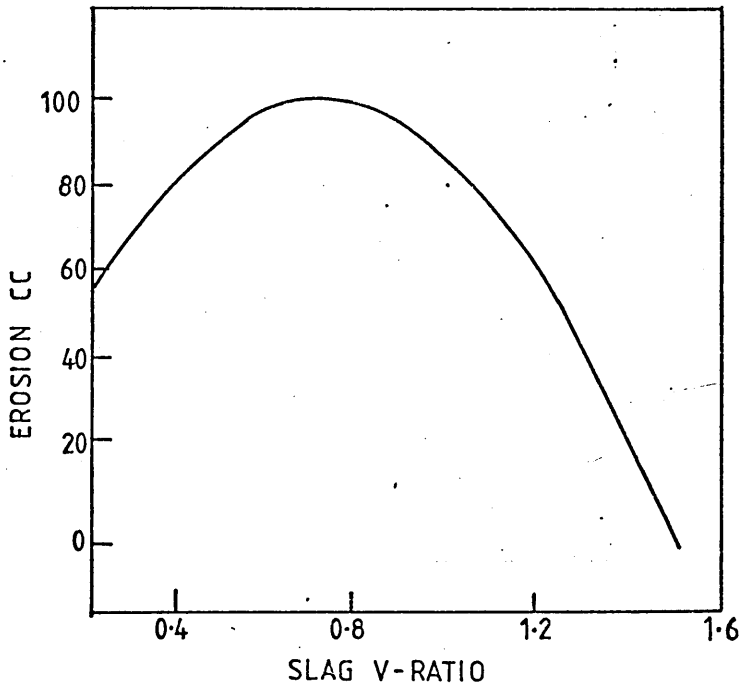

Effect of slag basicity on the erosion of B O F refractory bricks.[76]

Fig 15. Typical slag formation paths

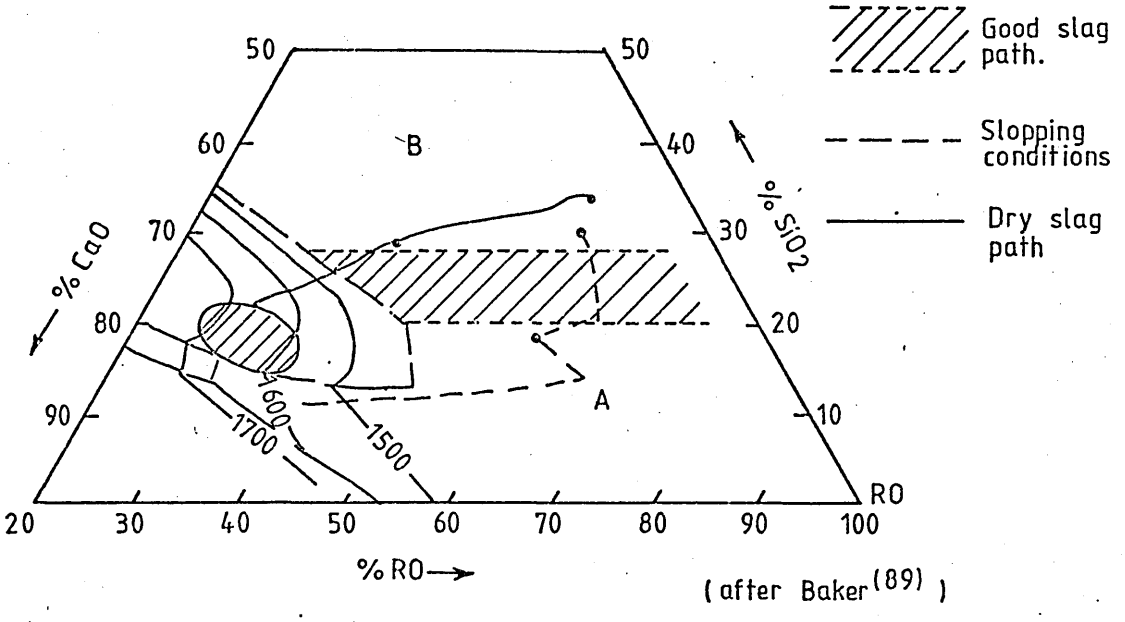

(after Baker[89])

Fig 16 Solubility of magnesia in $CaO-FeO-SiO_2$ slags at 1600 °C

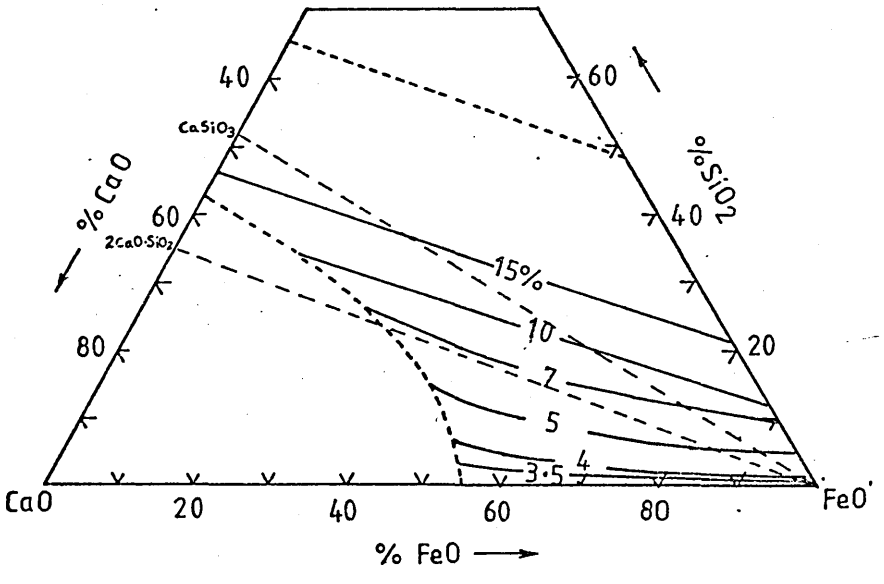

(after Fetters and Chipman[101])

Fig 17 Tetrahedron representing the system CaO-MgO-iron oxide —Si02 in contact with metallic iron.

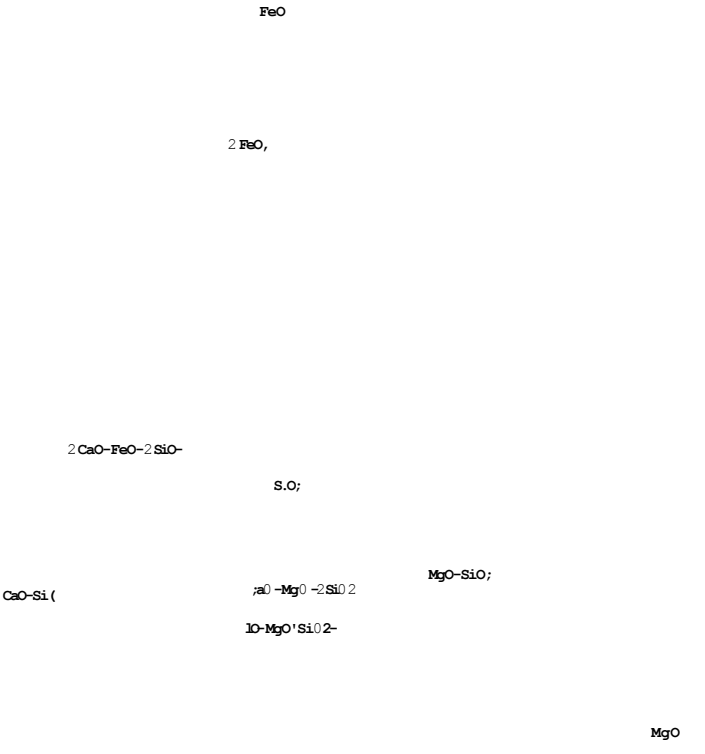

(after Muan and Osborn^®^ y

Fig 18 Phase relations in the system MgO-iron oxlde-Si02 in contact with metallic iron.

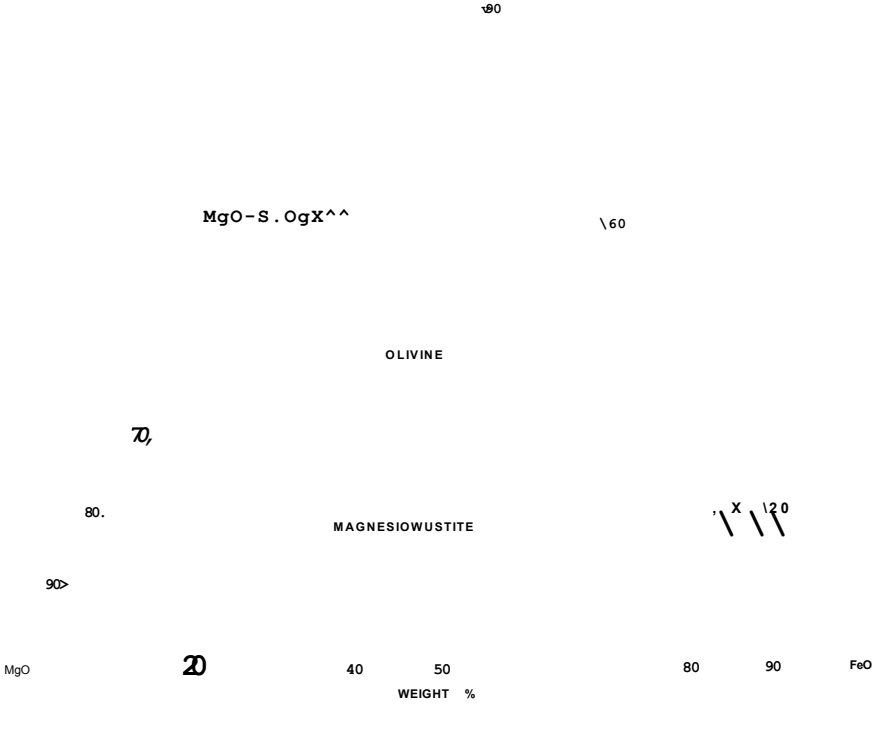

(after Bowen and Schairer^®^)

Fig 19 **Phase diagram for the system CaO—MgO—Si0 2**

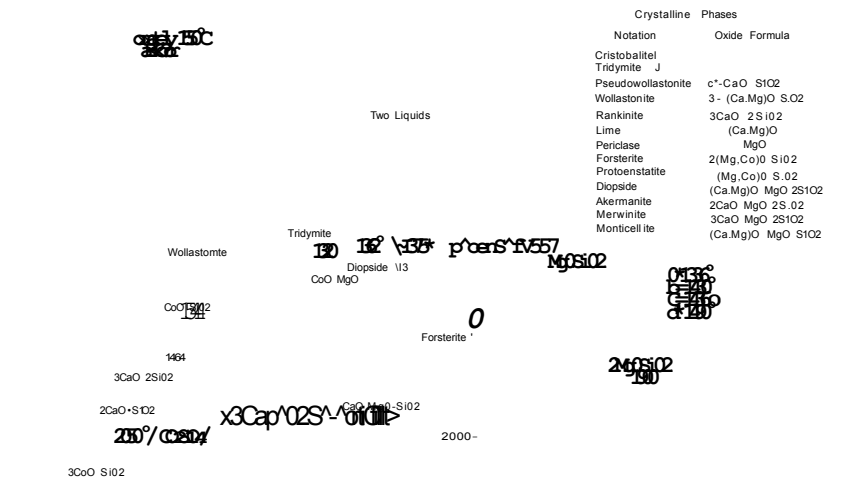

{ reproduced from Levin et.al.[108] after Muan and Osborn)

Fig 20 The specific aggressiveness of the slag towards the lining with time.

Curve I is the determined aggressiveness.

Curve H is the equilibrium aggressiveness.

0*04

d

0-03

0.03

0*01

msl^massof slag o2 blown x10**3** Nm**3**

(after van Hoorn e t a l^ ^)

Fig 21 Effect of MgO on some physical properties of converter slags

Content m.%

Slag number	Time of sampling min.	CaO	SiO_2	FeO	Fe_2O_3	MnO	MgO	$\frac{CaO}{SiO_2}$	Melting point, °C (beginning - end)
3	14	43·6	25·0	5·7	7·0	9·1	1·5	1·75	1315-1360
4	24	57·3	15·1	8·4	7·0	4·2	2·3	3·80	1475-1492

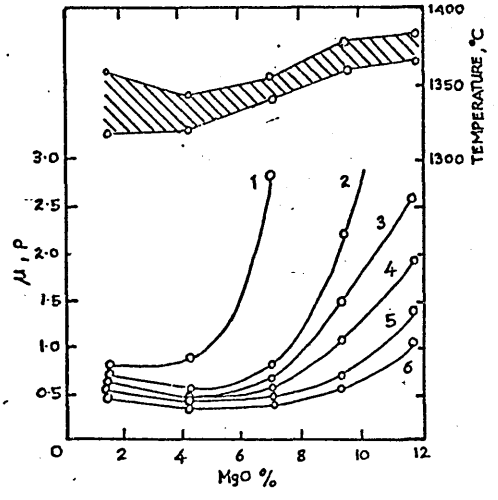

Effect of MgO on melting point of a slag of basicity 1·75 (no 3) and its viscosity at

1. 1350 °C
2. 1400
3. 1450
4. 1500
5. 1550
6. 1600

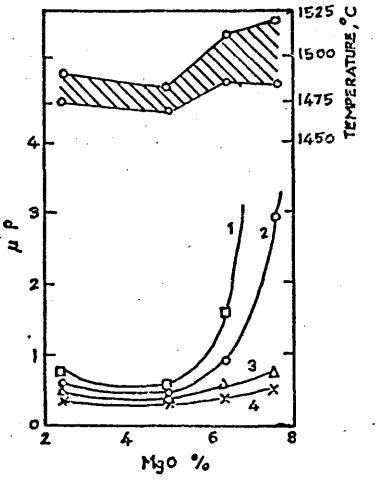

Effect of MgO on melting point of a slag of basicity 3·8 (no 4) and on its viscosity at

1. 1500 °C
2. 1525
3. 1550
4. 1600

(after Zarvin et al [112])

Fig 22 The composition of synthetic slags used in viscosity and immersion experiments, and shown in relation to the system $CaO-FeO-SiO_2$ in contact with metallic iron.

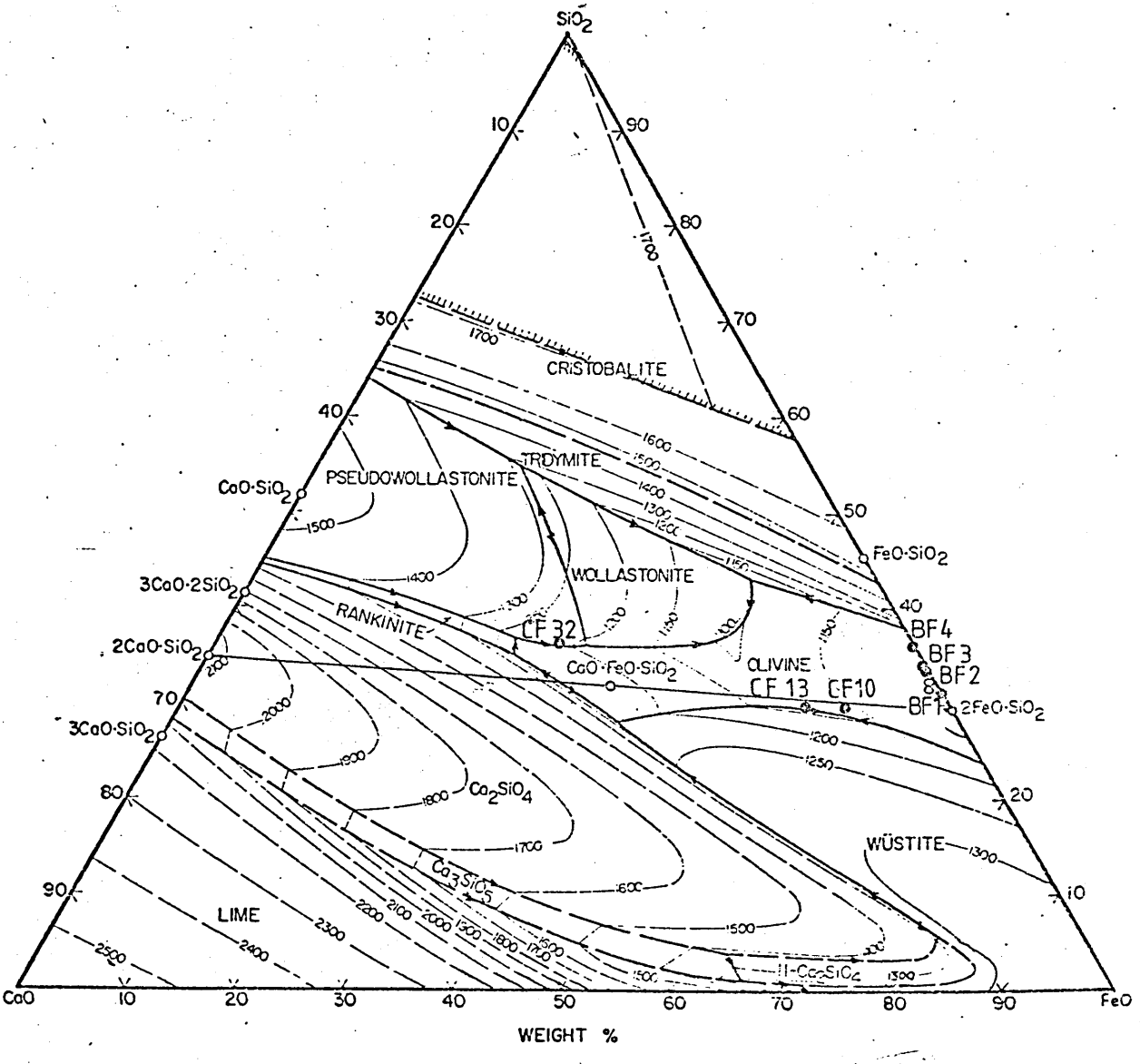

(after Muan and Osborn [50])

Fig 23 Furnace Temperature Profile With Respect To The Viscosity Measuring Assemblage

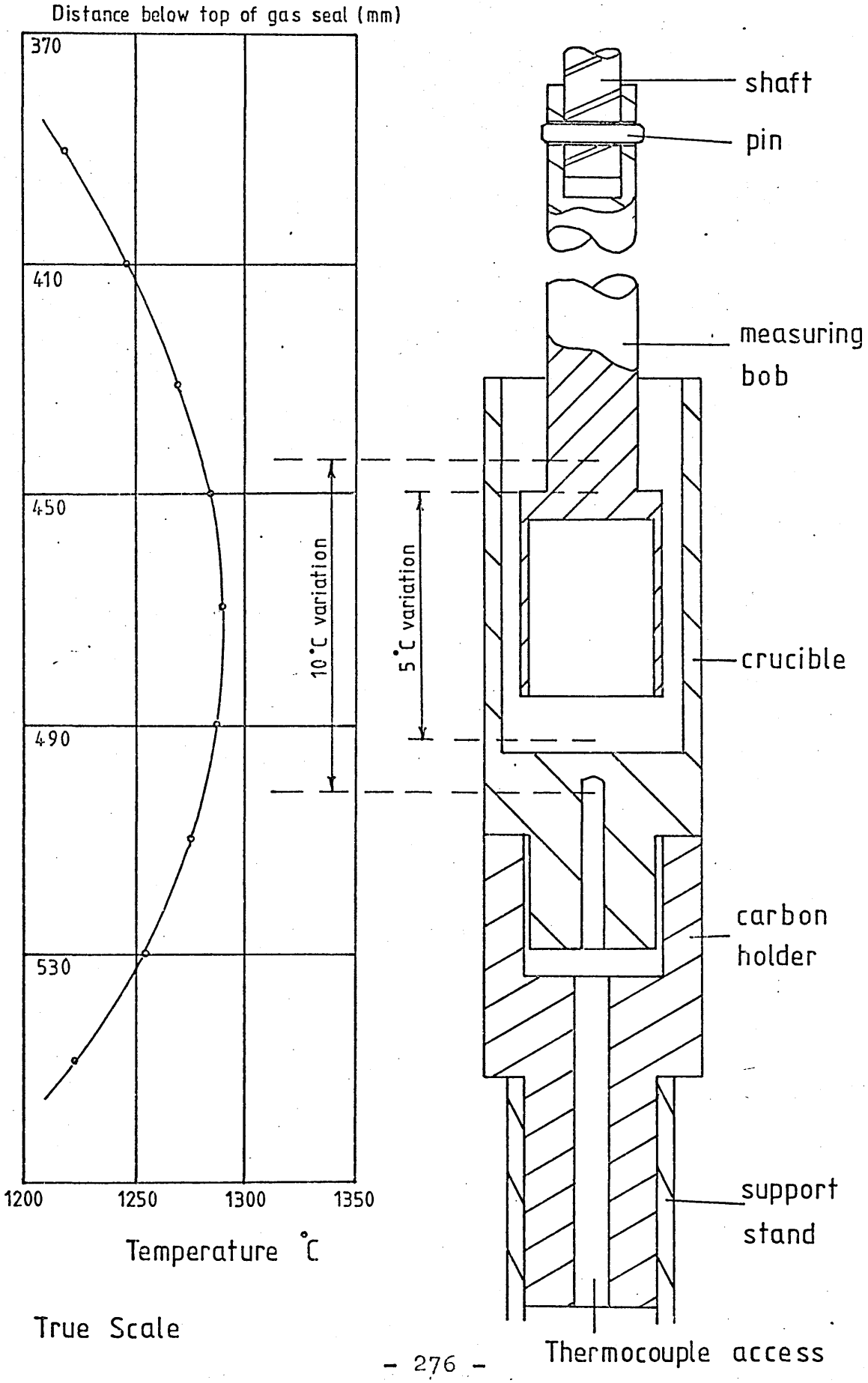

Fig 24

Furnace used for crucible tests and static immersion studies.

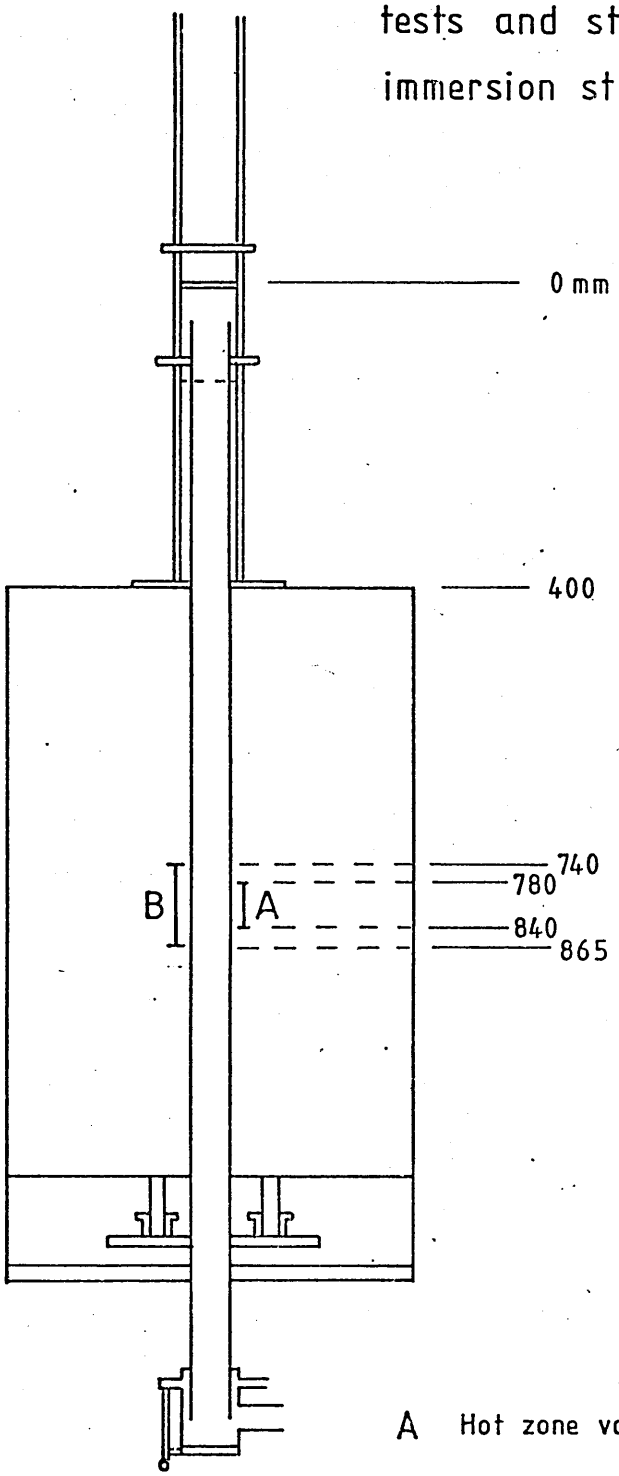

A Hot zone variation 2·5 °C

B Hot zone variation 10 °C

Scale 1:10

Fig 25 The temperature profile of the cone fusion furnace

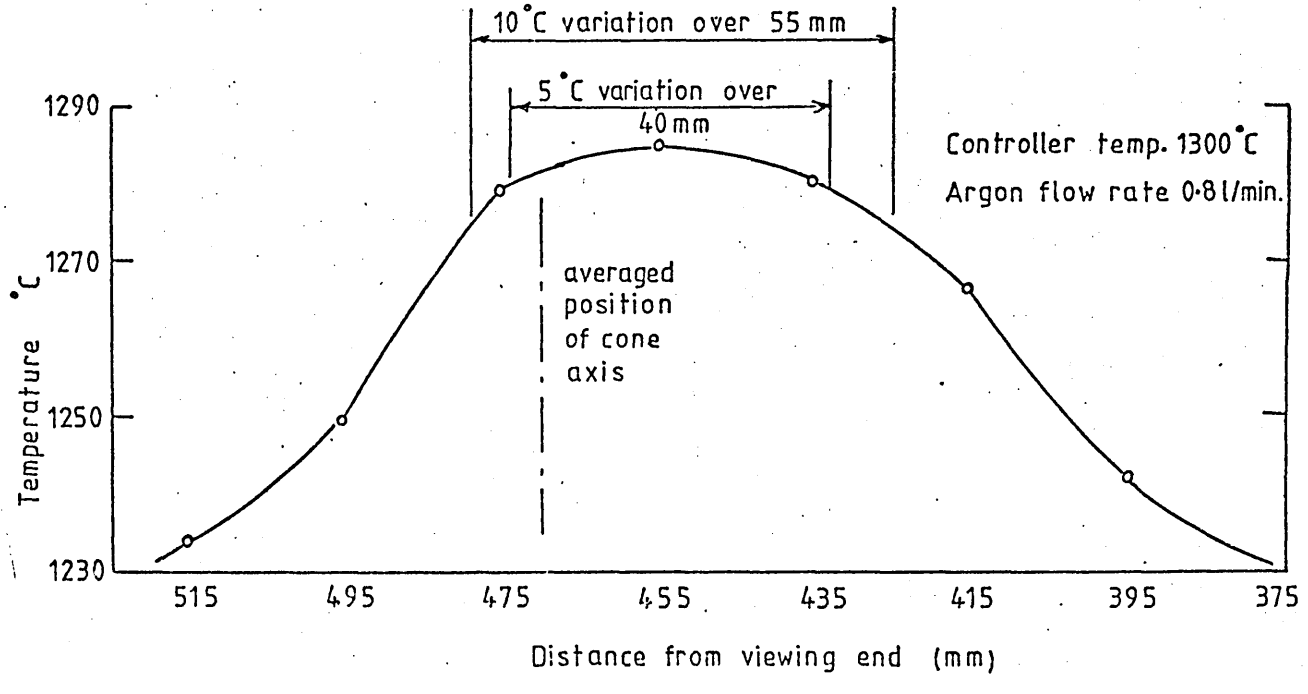

Fig 26 Viscometer measuring bob and crucible dimensions

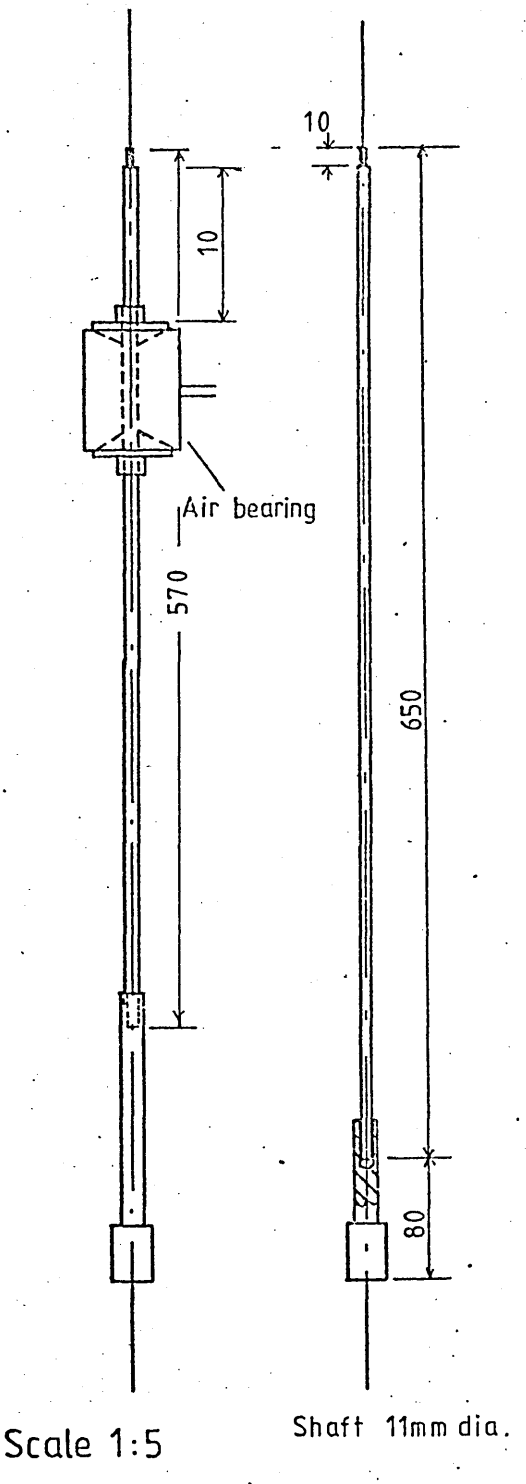

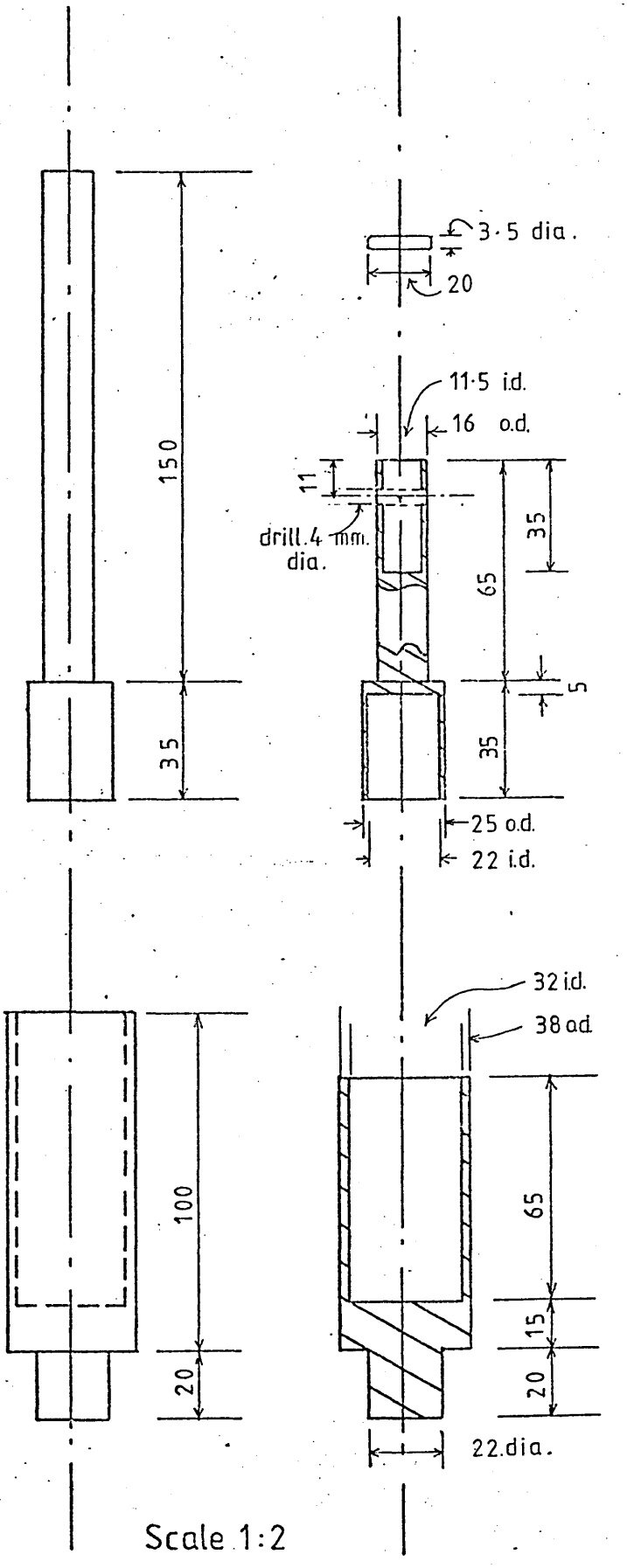

All dimensions in mm

Fig 27 Graphite crucible holders

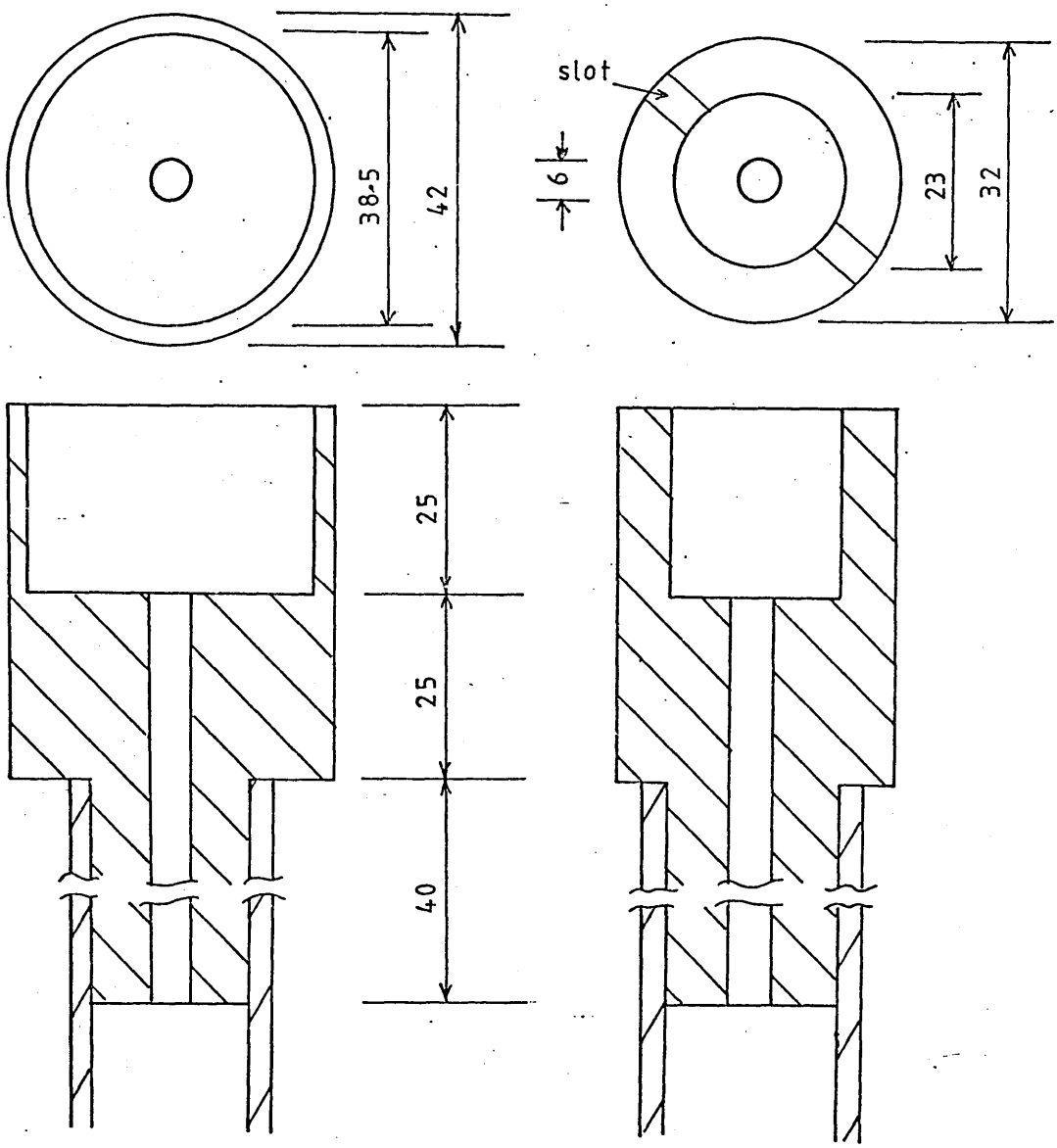

dimensions in mm.

Fig 28 Viscosities of Aqueous Glycerol Solutions

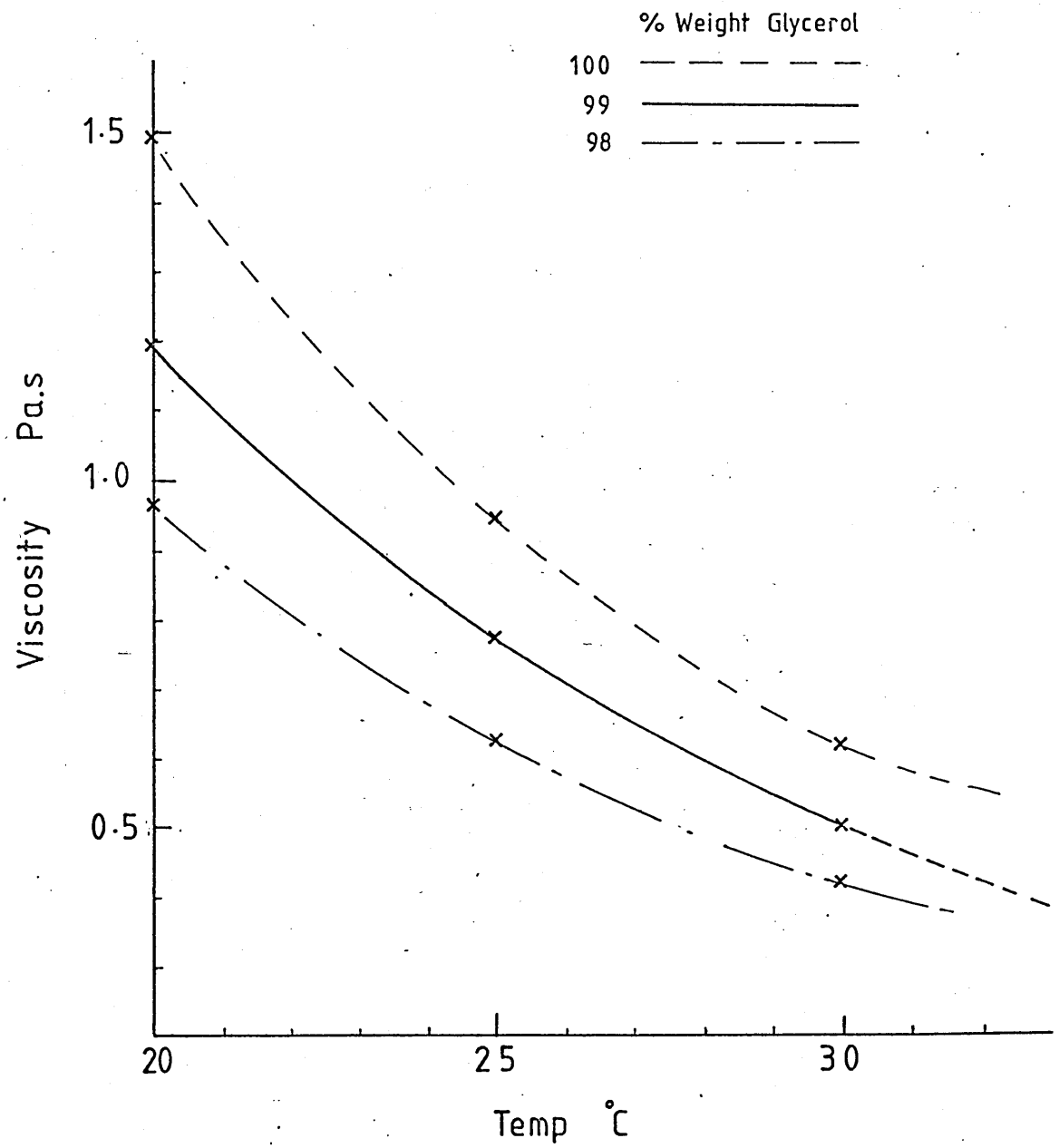

1 cP = m Pa.s

Glycerol analysis 99·08% glycerol

Fig 29 Cylinder immersion assembly

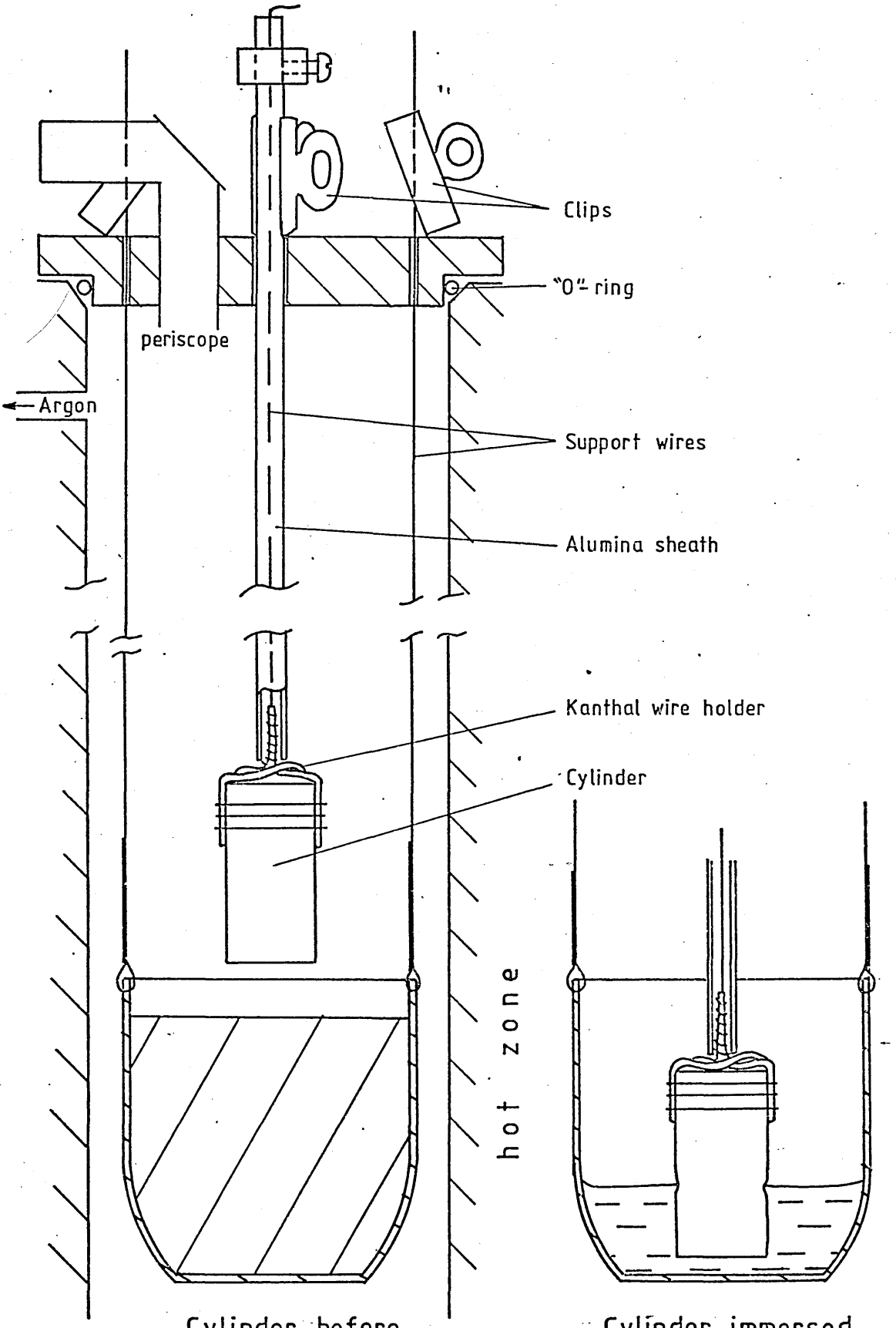

Fig 30. Viscosities of Lime–iron silicate melts

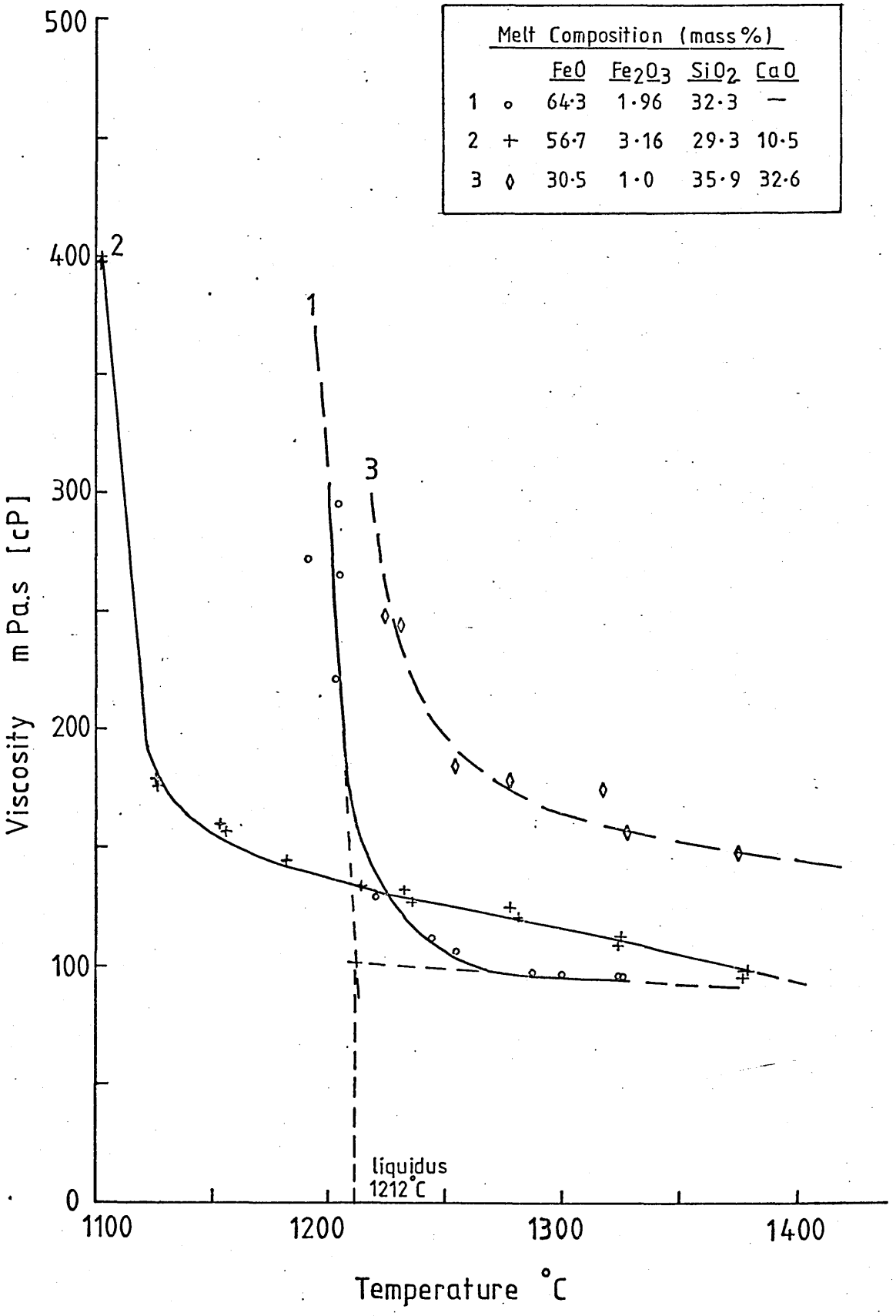

Fig 31. The viscosity of iron silicate and lime-iron silicate melts with varying concentrations of magnesia

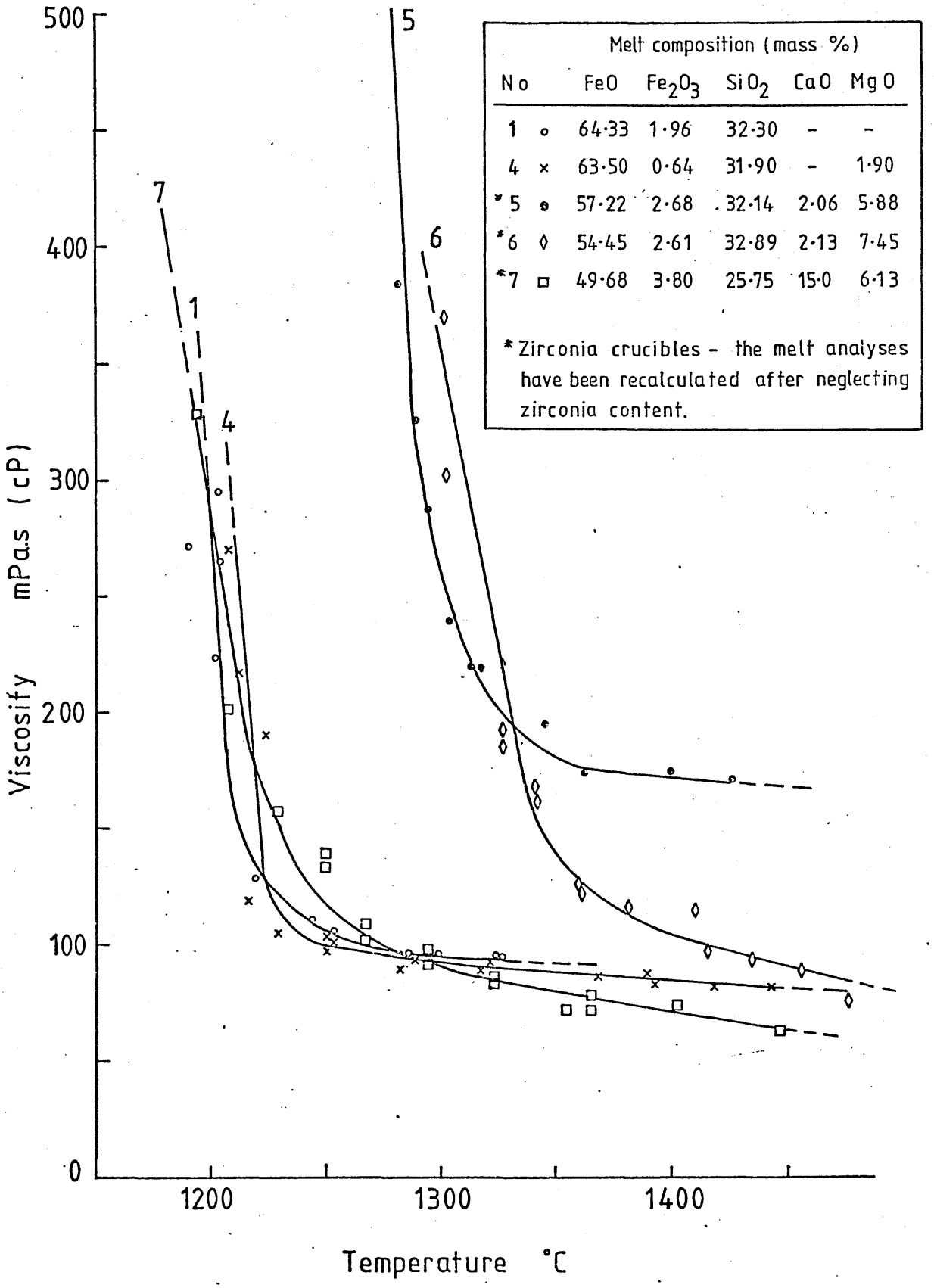

No		FeO	Fe_2O_3	SiO_2	CaO	MgO
		Melt composition (mass %)				
1	○	64·33	1·96	32·30	-	-
4	×	63·50	0·64	31·90	-	1·90
*5	●	57·22	2·68	32·14	2·06	5·88
*6	◊	54·45	2·61	32·89	2·13	7·45
*7	□	49·68	3·80	25·75	15·0	6·13

*Zirconia crucibles - the melt analyses have been recalculated after neglecting zirconia content.

Fig 32 Eurotherms Controller — Crucible thermocouple calibration curve

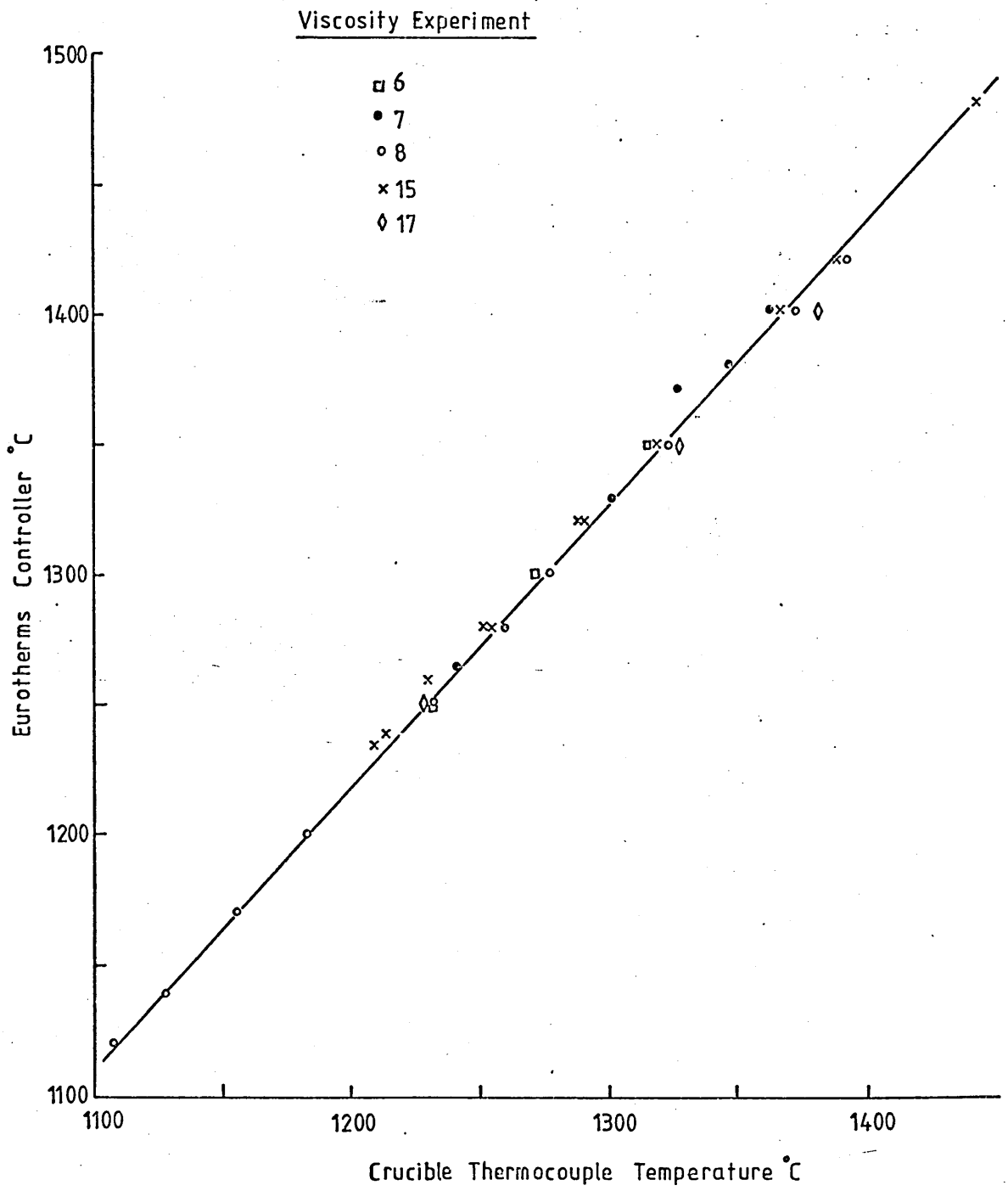

Fig 33 The effect of lime(CaO) addition on the viscosity of an iron silicate melt

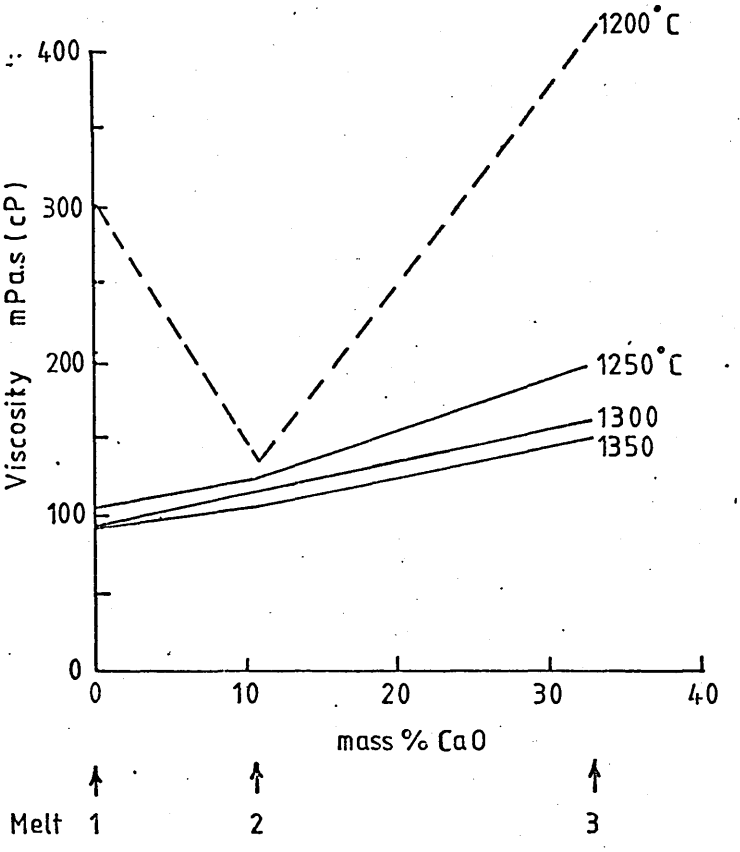

Fig 34 The effect of magnesia(MgO) addition on the viscosity of an iron silicate melt

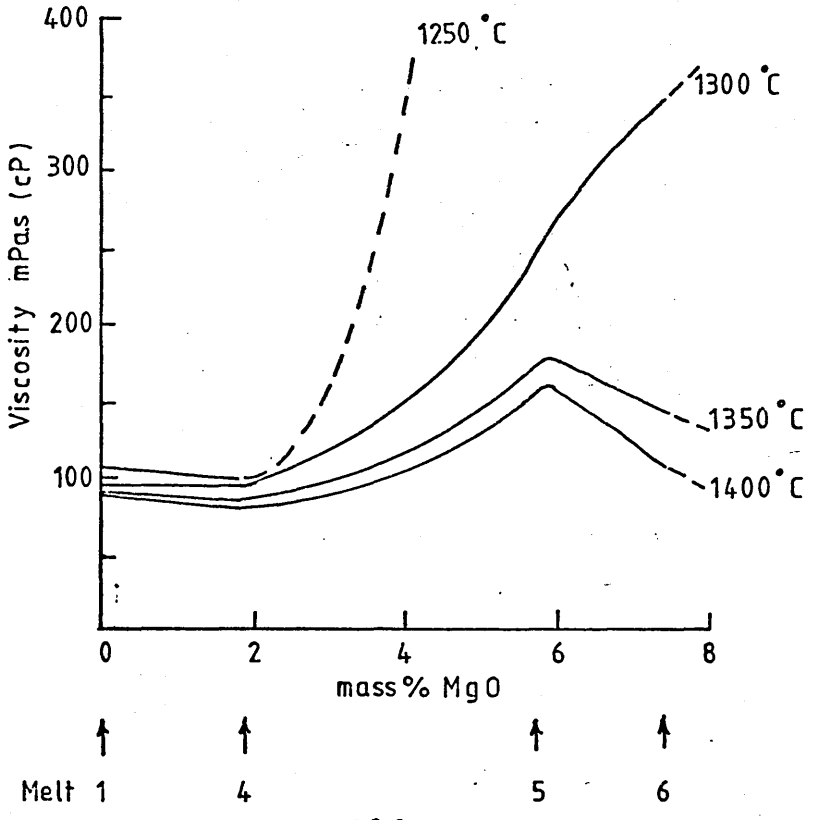

Fig 35 The development of eroded slag lines on the wall of a zirconia crucible after a viscosity determination.

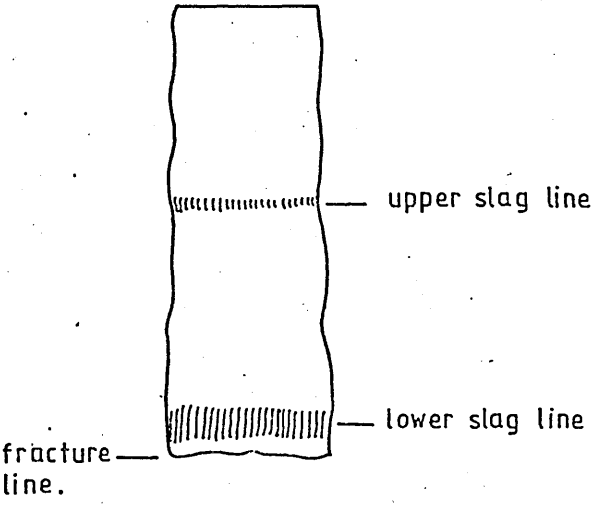

(a) sketch of a zirconia crucible wall showing slag erosion line positions after a viscosity determination.

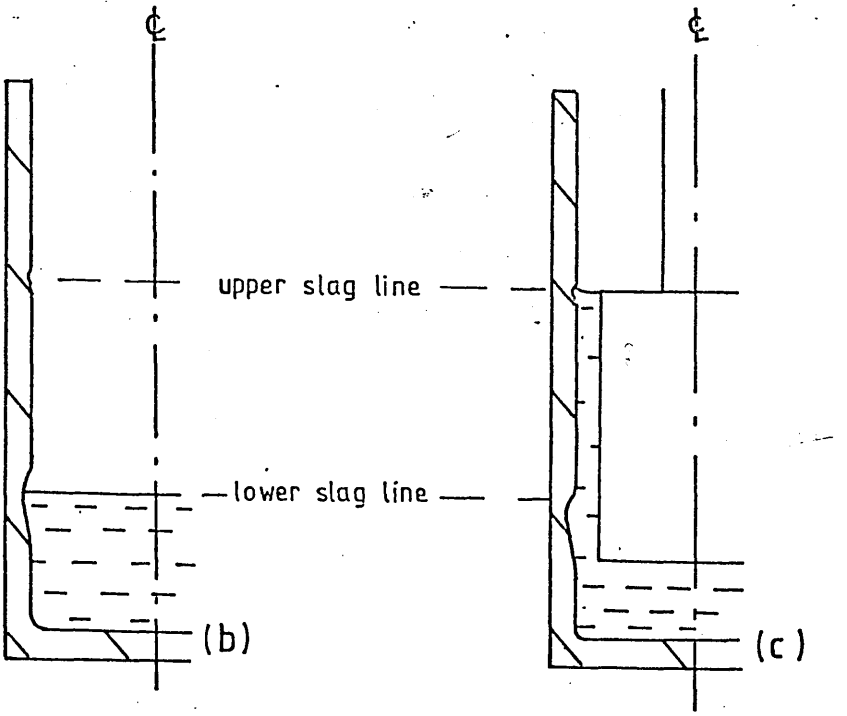

Sections of a zirconia crucible with molten synthetic slag,(b) and with the measuring bob immersed,(c).

Fig 36 The System $FeO-ZrO_2$

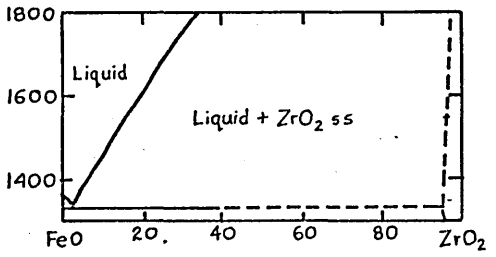

(after Levin and McMurdie[108])

Fig 37 The System $FeO-SiO_2-ZrO_2$

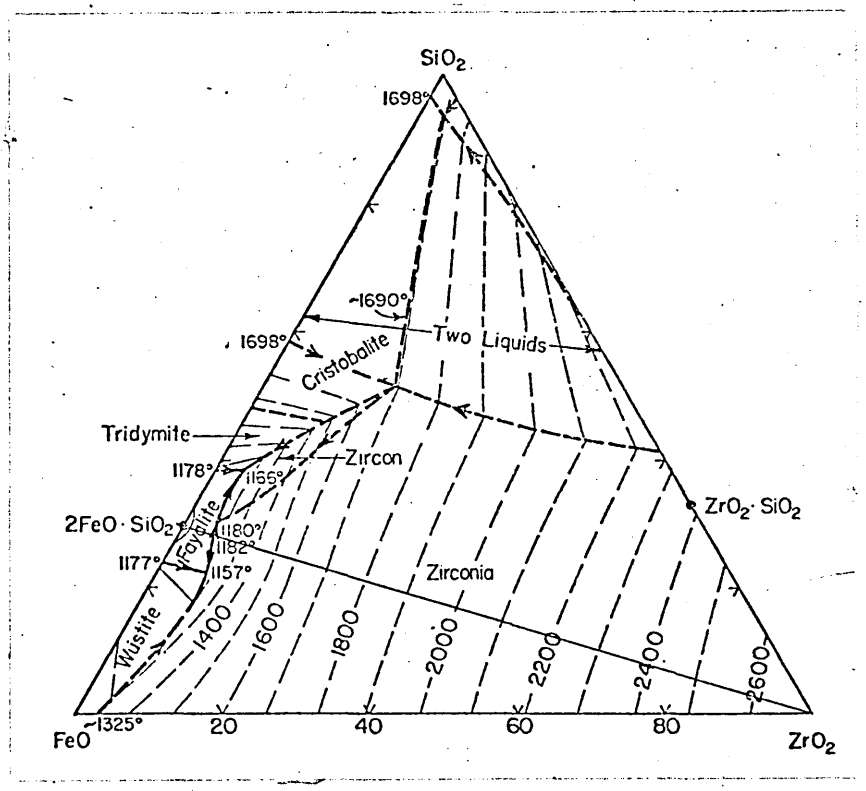

(after Levin and McMurdie[108])

Fig 38 D.T.A CURVES FOR DOLOMITIC LIMESTONE AND LIMESTONE

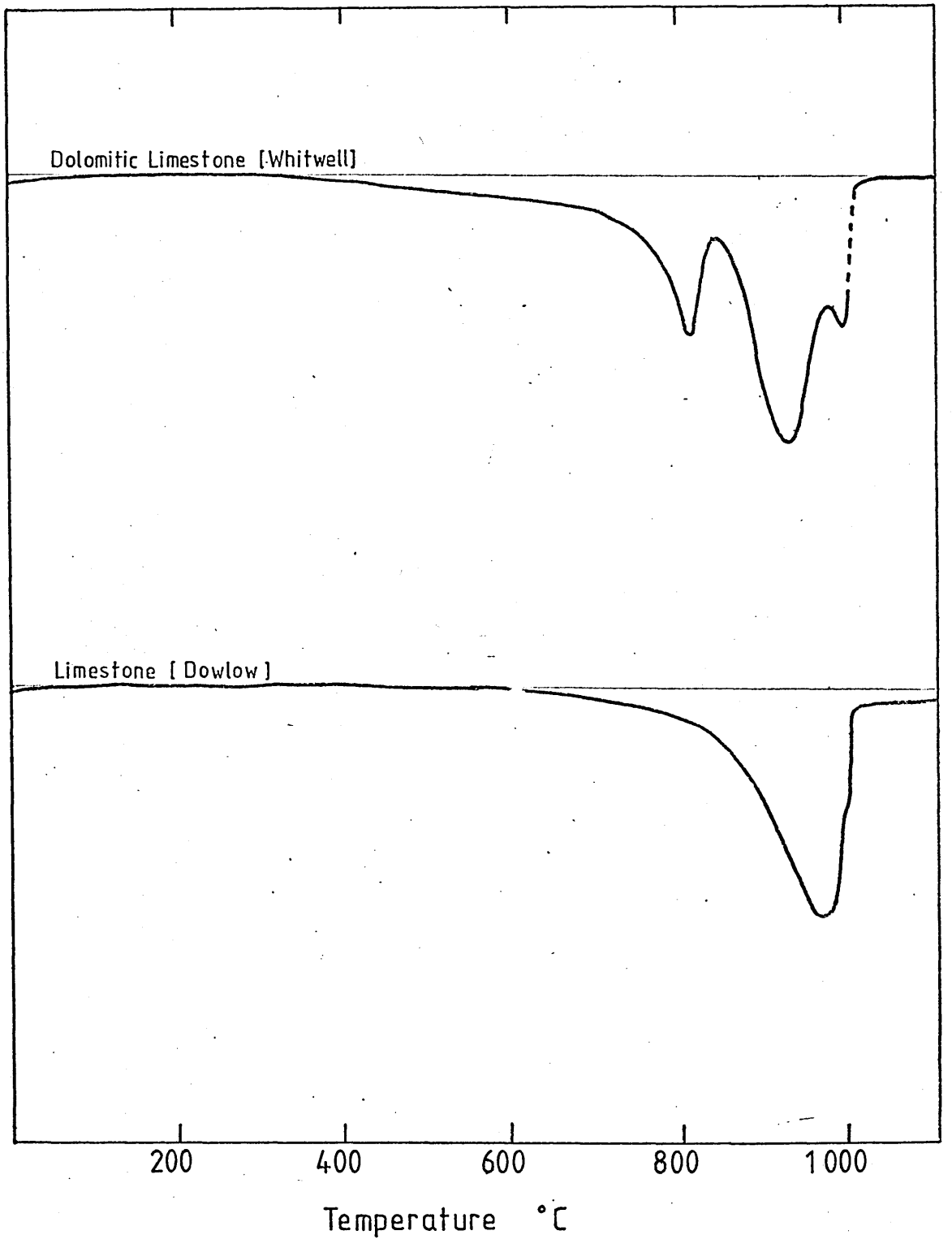

Fig 39 The effect of hydration on dolomitic lime and lime cylinders stored in a dessicator and exposed to the atmosphere

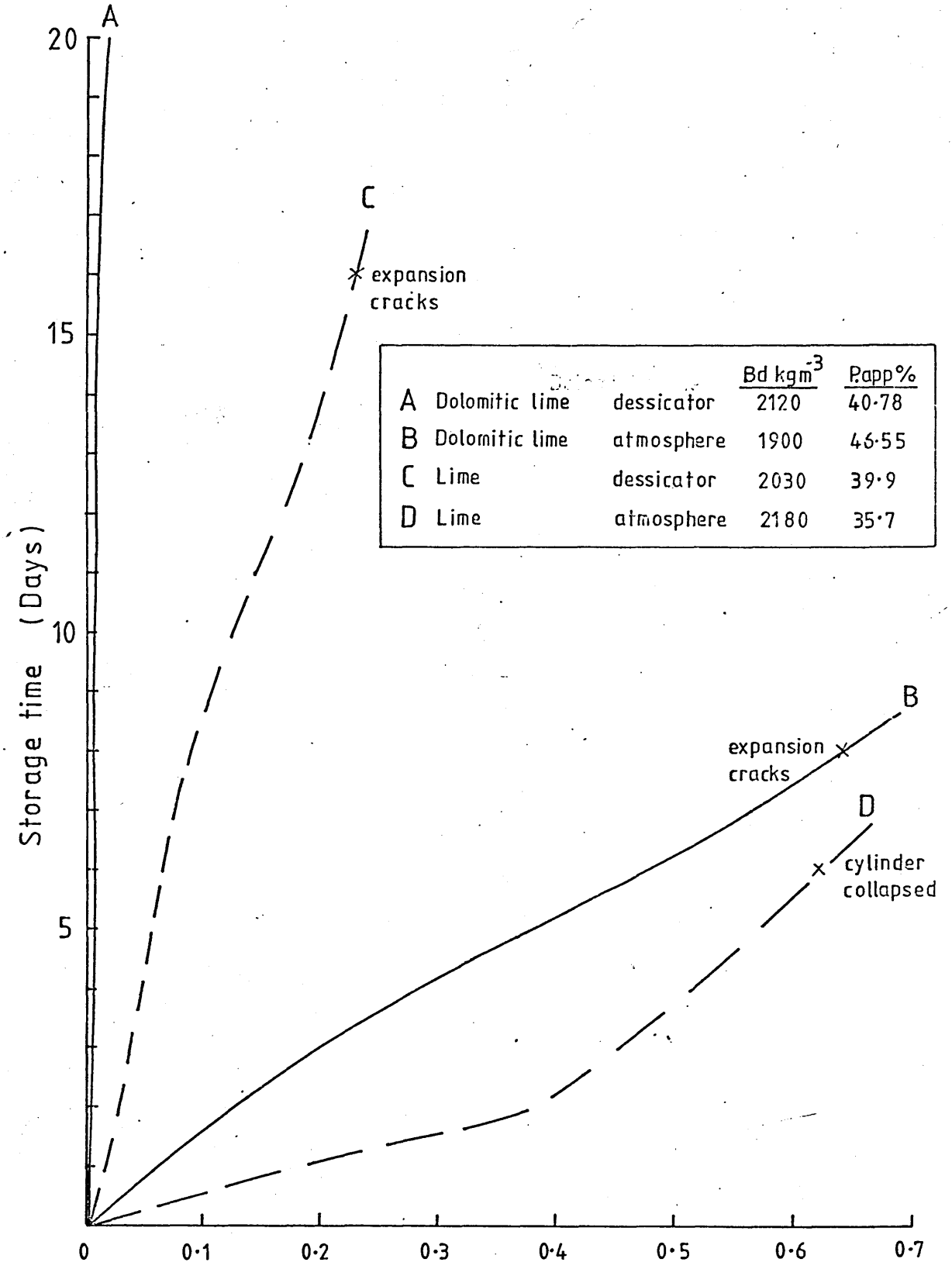

			Bd kgm^{-3}	Papp%
A	Dolomitic lime	dessicator	2120	40·78
B	Dolomitic lime	atmosphere	1900	46·55
C	Lime	dessicator	2030	39·9
D	Lime	atmosphere	2180	35·7

Mass increase (in grams) of calcined cylinders through hydration reactions.

Fig.40 The schematic dissolution of dolomitic lime in an iron silicate melt at 1300°C.

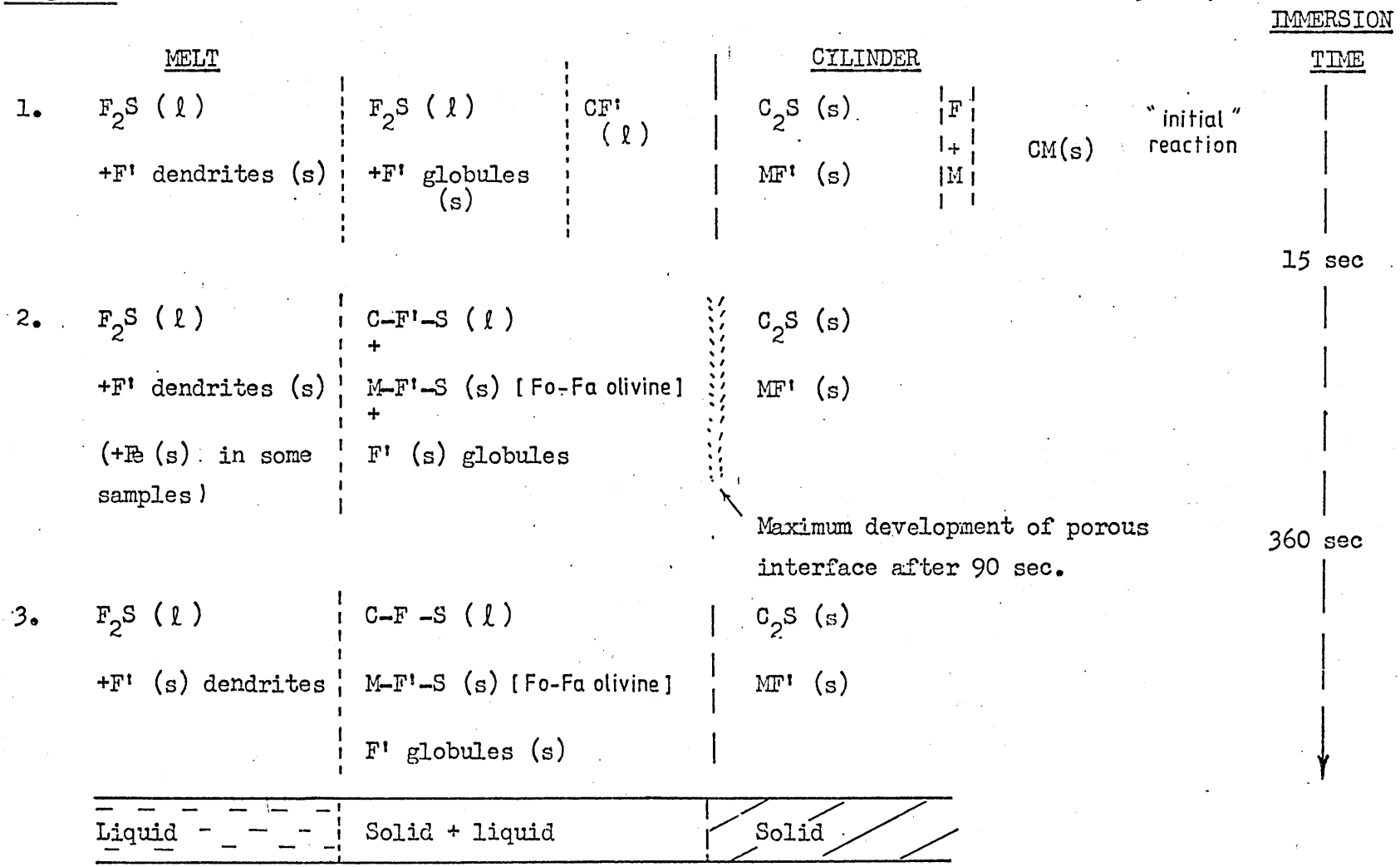

Fig 41 The system SiO_2–CaO

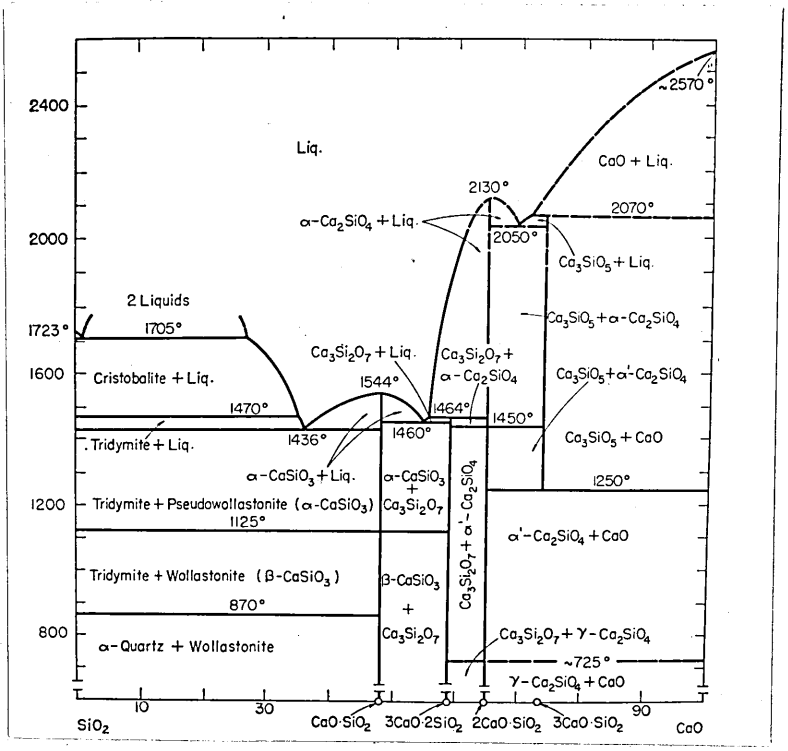

(after Muan and Osborn [50])

Fig 42 The system Fe – Mg – O

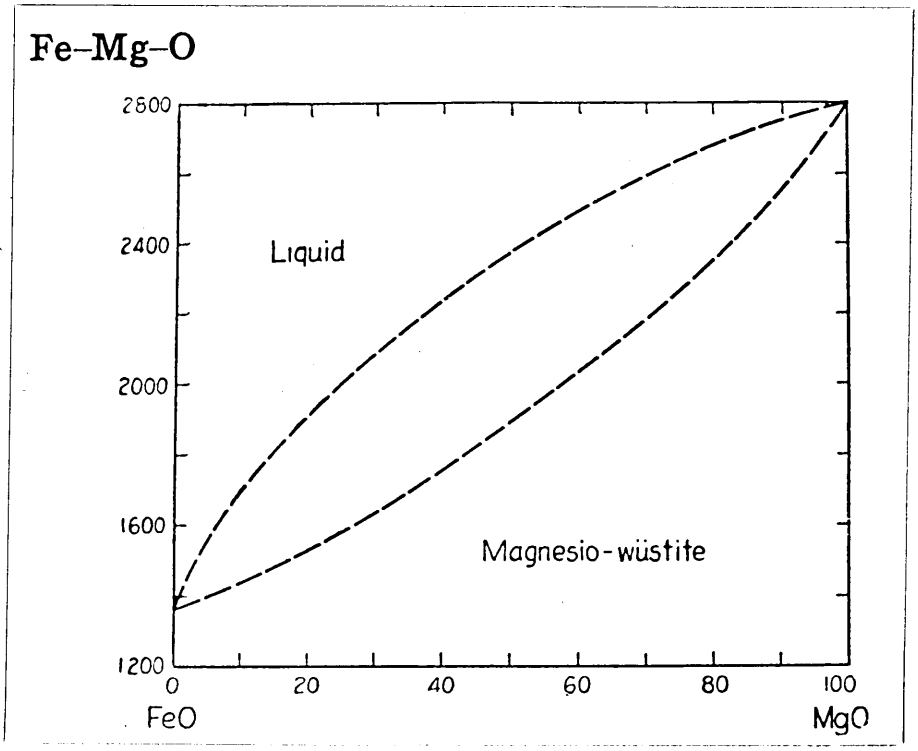

(after Muan and Osborn [50])

Fig 43 Standard free energies of formation of metal silicates.

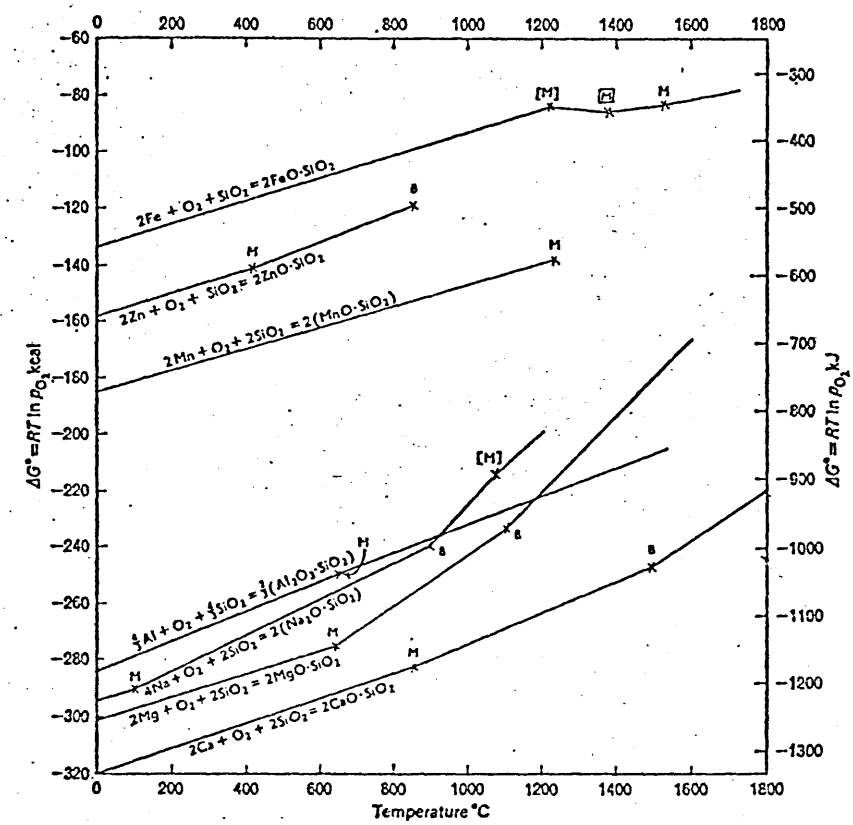

M = Melting point

B = Boiling point

(from Bodsworth et al. 4.)

Fig 44 The system $2FeO \cdot SiO_2 - FeO$

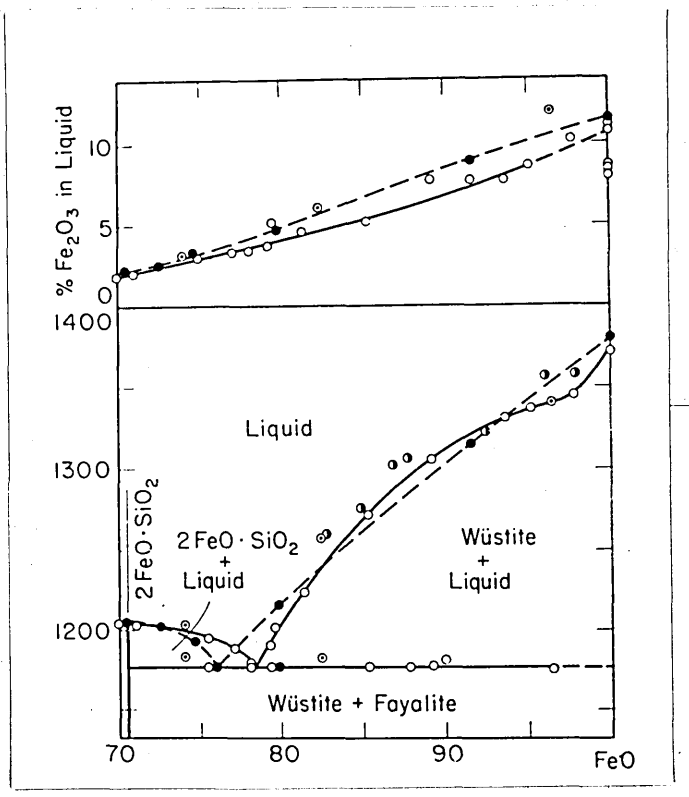

(after Levin and McMurdie [108])

Fig 45 The solid solution series $2MgO \cdot SiO_2$ — $2FeO \cdot SiO_2$

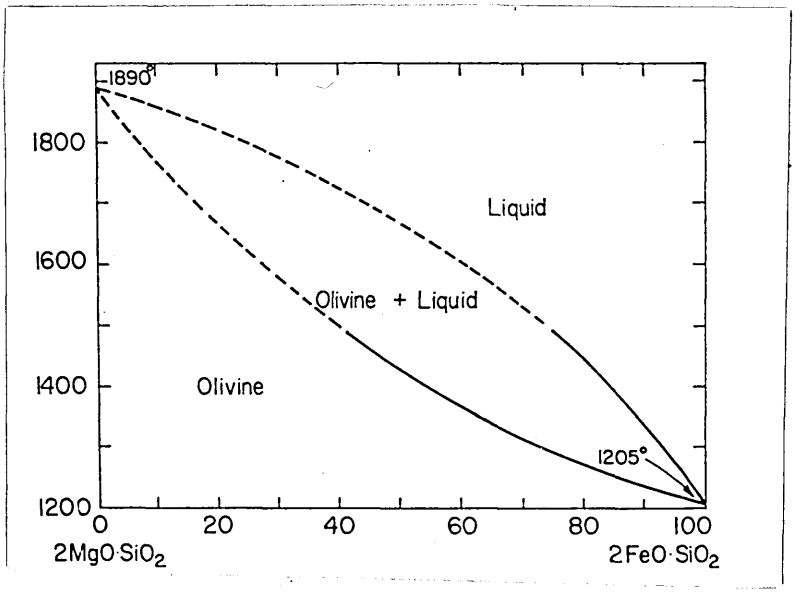

 (after Bowen and Schairer [107])

Fig 46a The 1300 °C isothermal section in the system $CaO-FeO'-SiO_2$

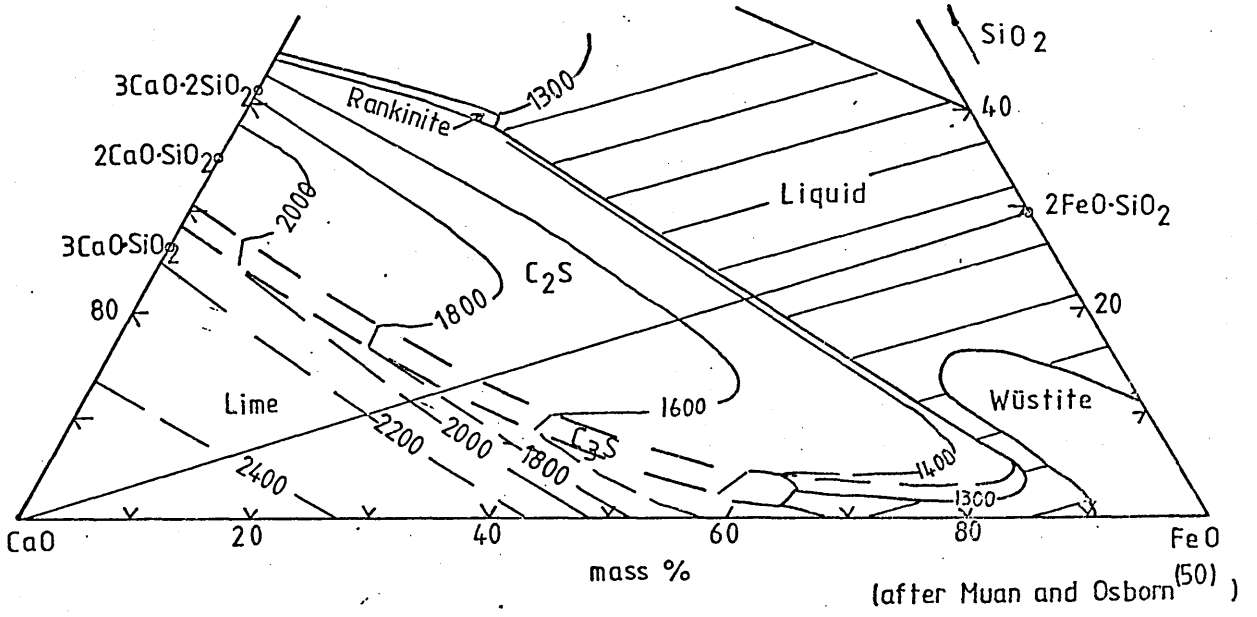

(after Muan and Osborn[50])

Fig 46b The 1300 °C isothermal section in the system $CaO-FeO'-SiO_2$ showing phase relationships

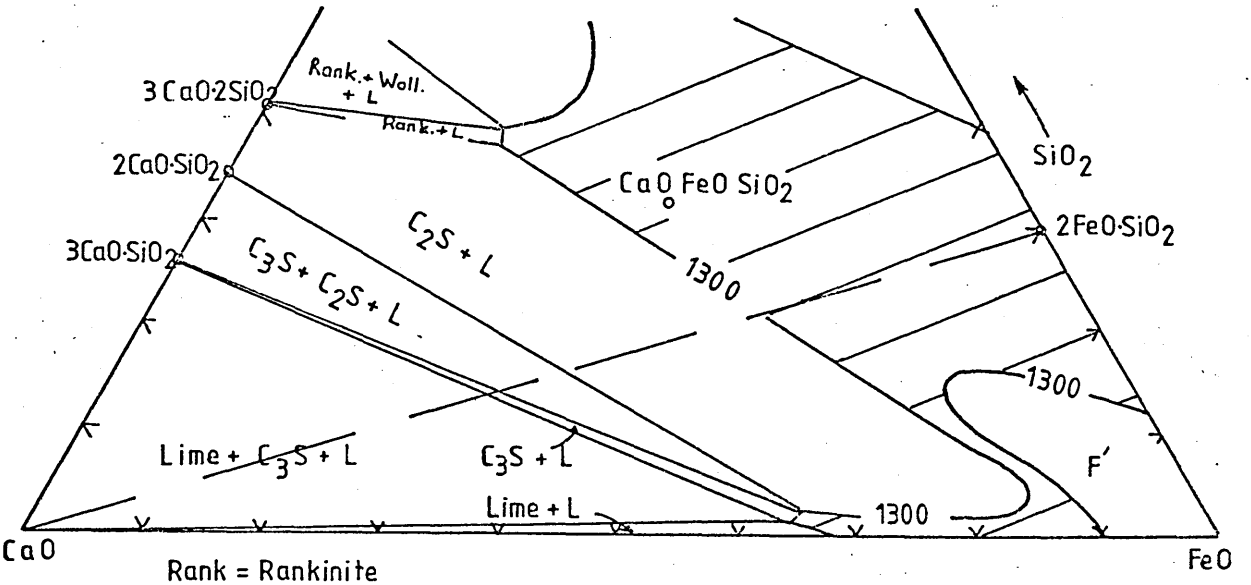

Rank = Rankinite

Woll = Wollastonite

Fig 47 The system CaO – FeO

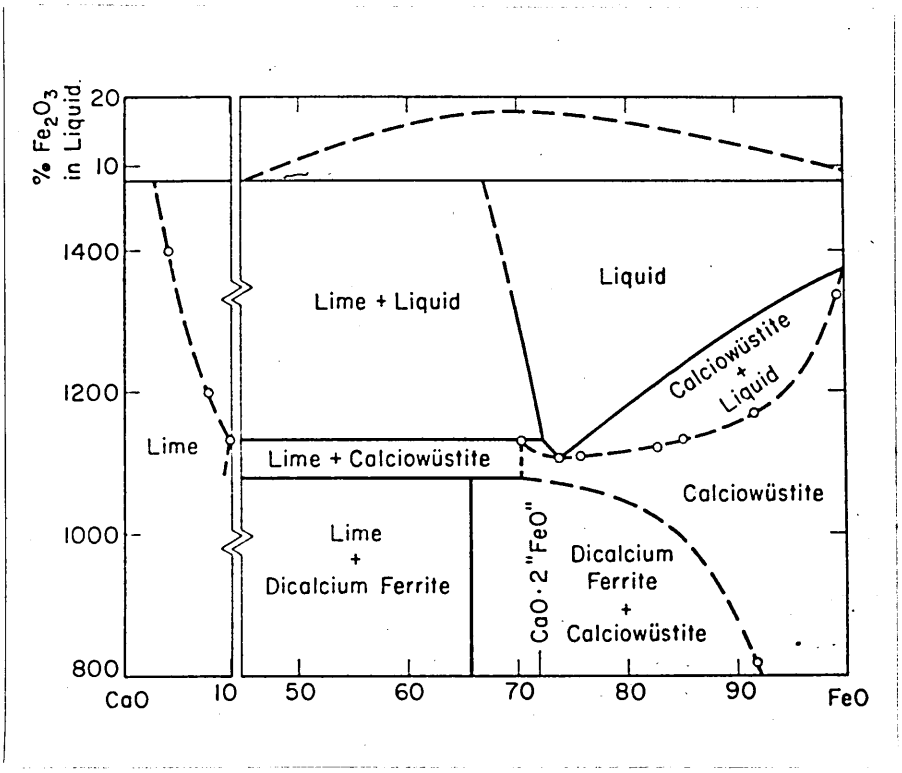

(after Levin and McMurdie [108])

Fig. 48

The melt - dolomitic lime cylinder interface concentration profile of iron oxide (FeO) representing static immersion times of 15, 120 and 360 s respectively. The profiles are based upon quantitative SEM results which have been selected to define a mean - free path from the melt to the cylinder. Globular wüstite (FeO) and dicalcium silicate phase assemblages have been ignored.

Fig. 49

The melt - dolomitic lime cylinder interface concentration profile of magnesium oxide (MgO) representing static immersion times of 15, 120 and 360 s respectively. The profiles are based upon qualitative SEM results which have been selected to define a mean - free path from the melt to the cylinder. Globular wüstite (FeO) and dicalcium silicate phase assemblages have been ignored.

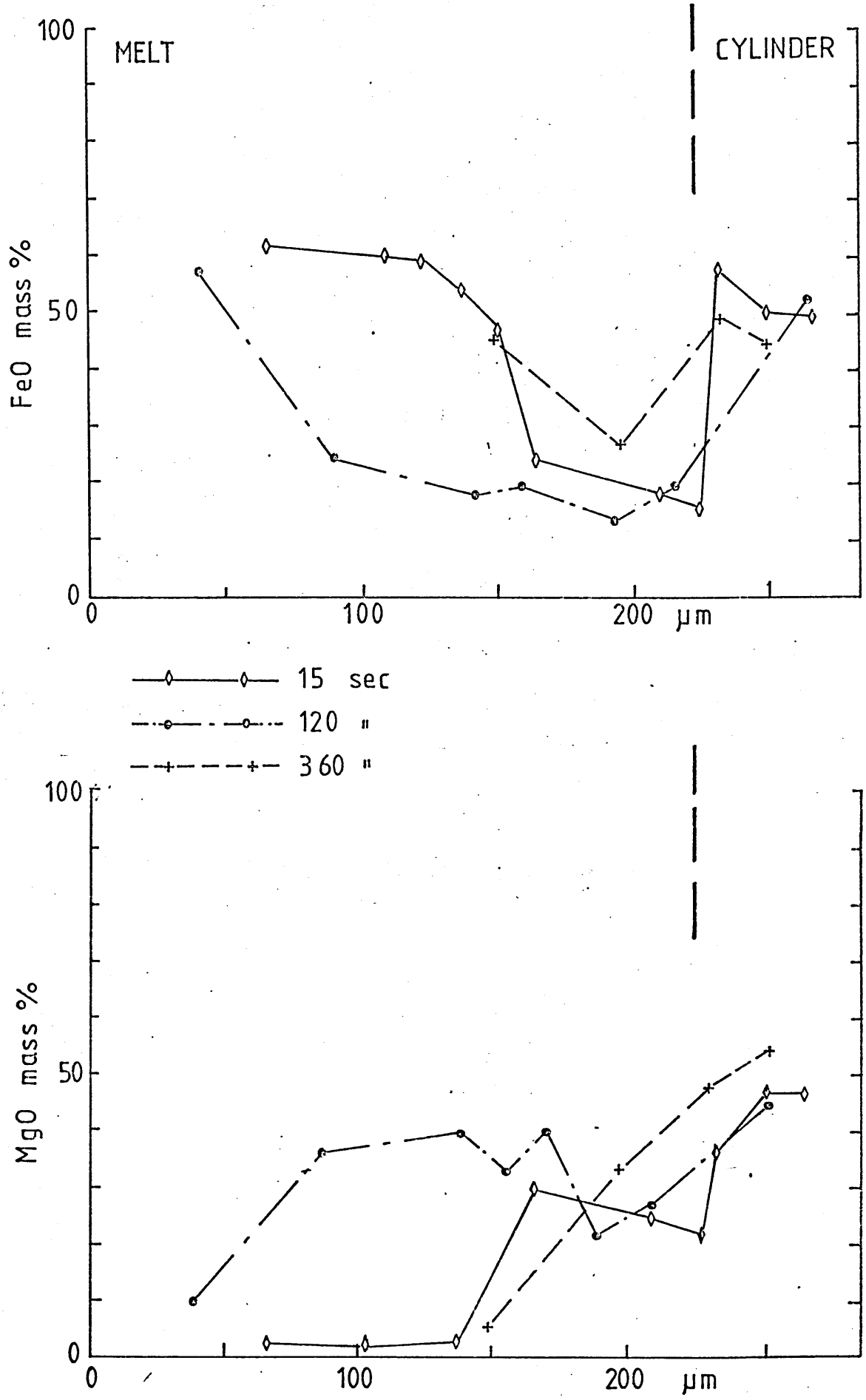
MELT
CYLINDER
FeO mass %
100
50
0
0
100
200 µm
15 sec
120 "
360 "
MgO mass %
100
50
0
0
100
200 µm

Fig 50 The distribution of oxides across the interface between a fayalite (iron silicate) melt and lime and a 5 mass % MgO fayalite melt and lime, plotted on the 1300 °C isothermal section of the CaO–'FeO'–SiO_2 diagram.

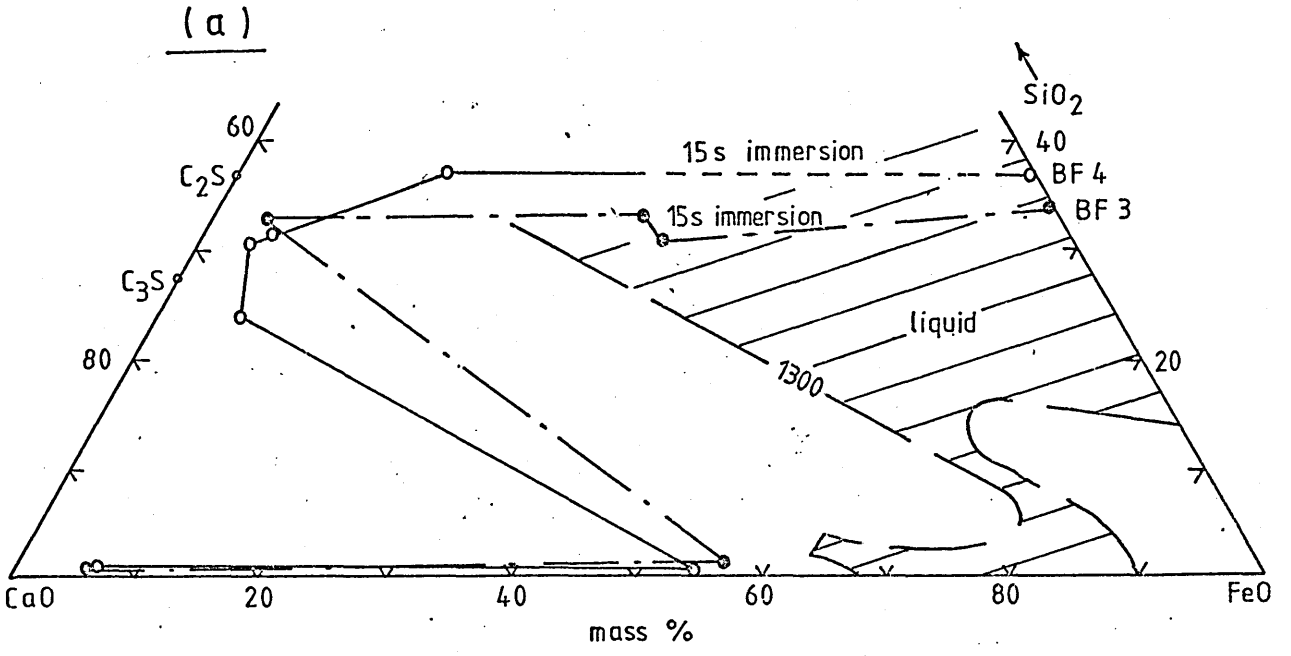

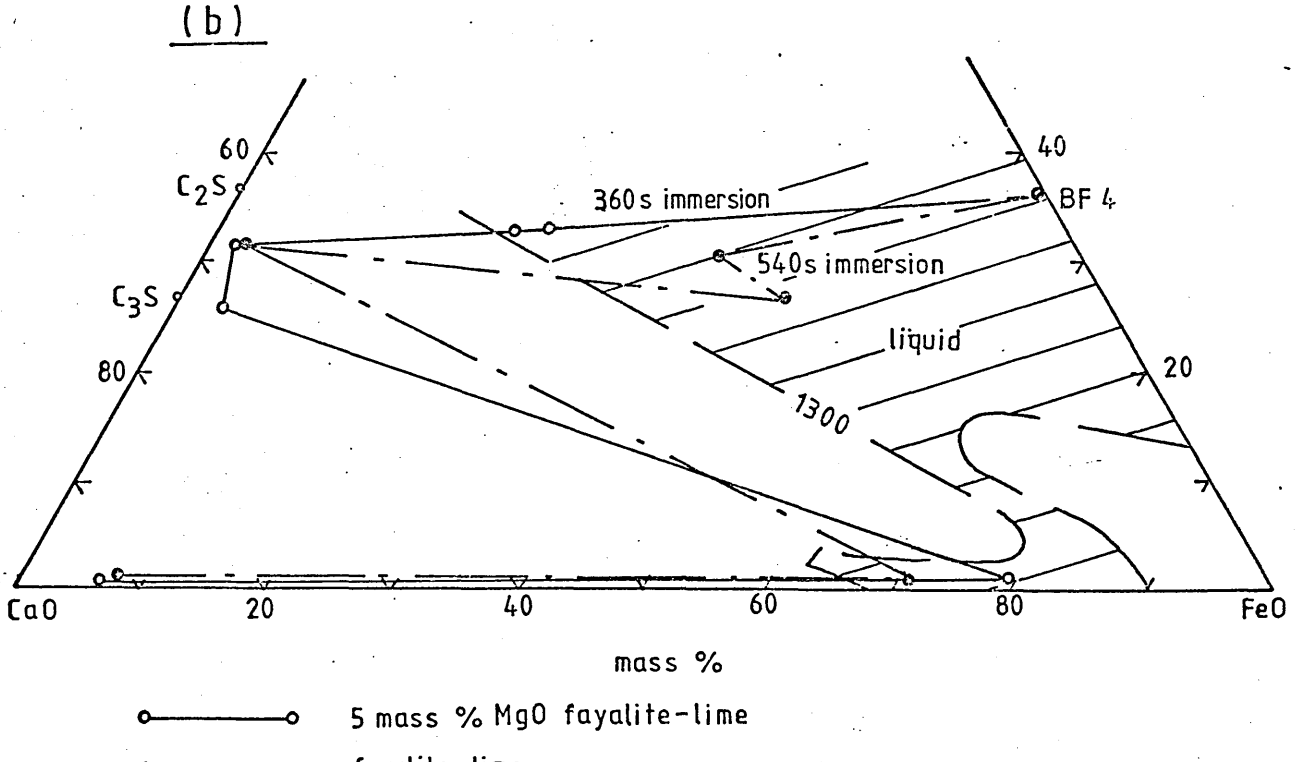

Fig 51 Static dissolution of dolomitic lime at 1300°C

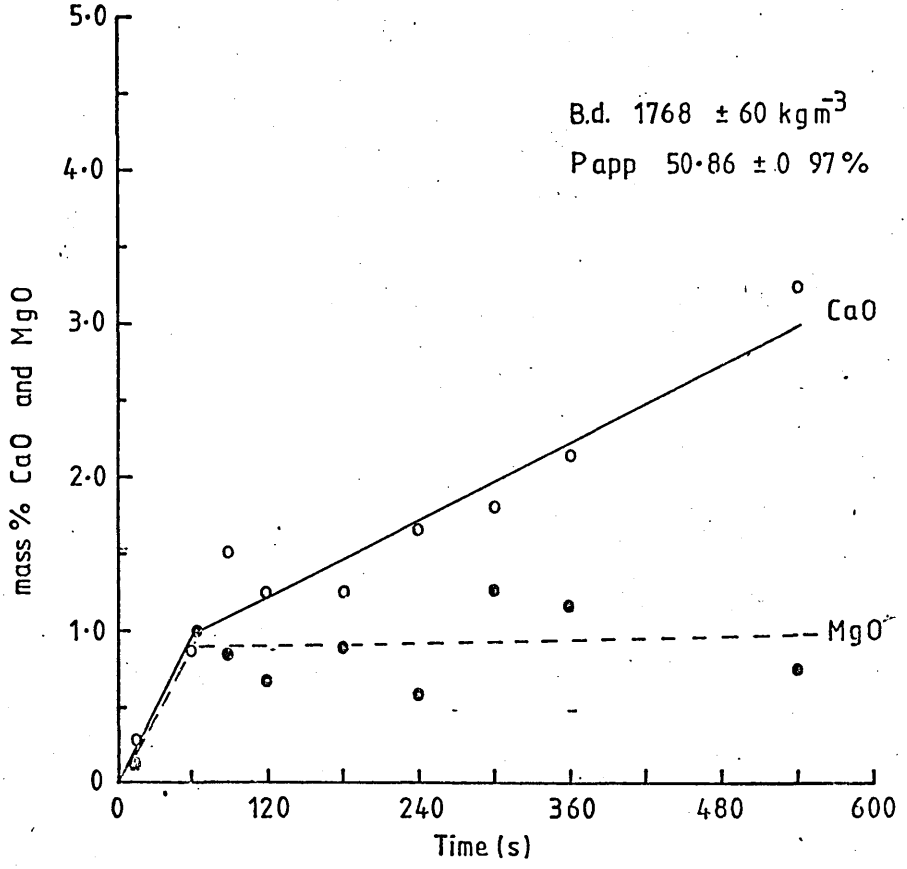

Fig 52 Rotary dissolution of dolomitic lime at 1300°C

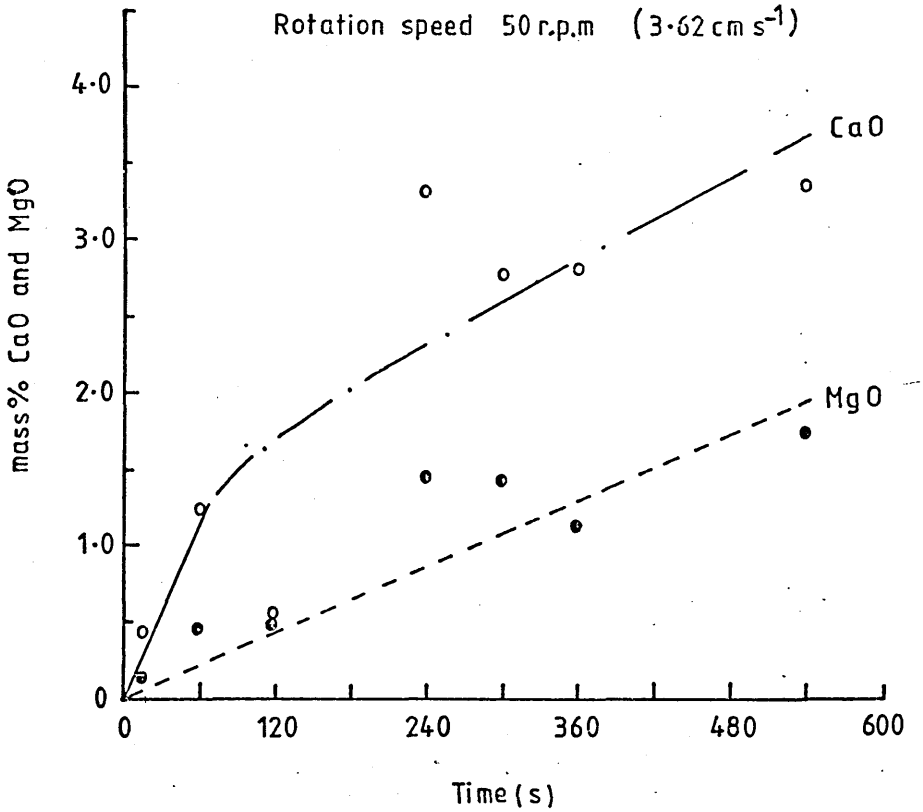

Fig 53 The width of the globular wüstite (FeO) zone with respect to immersion time, developed at the interface region between dolomitic lime and iron silicate (fayalite) melts at 1300°C.

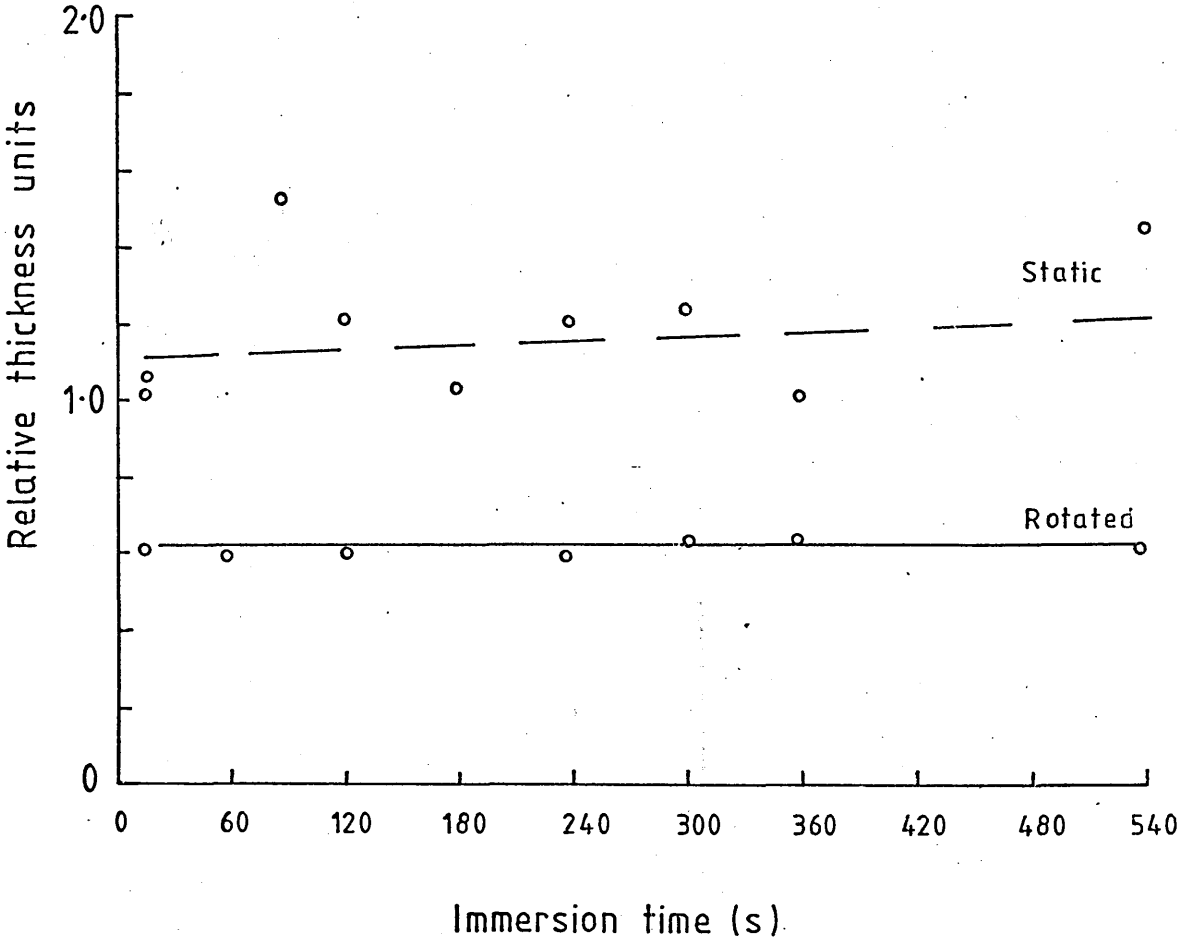

Fig 54 Static dissolution of "hard" burnt lime at 1300°C

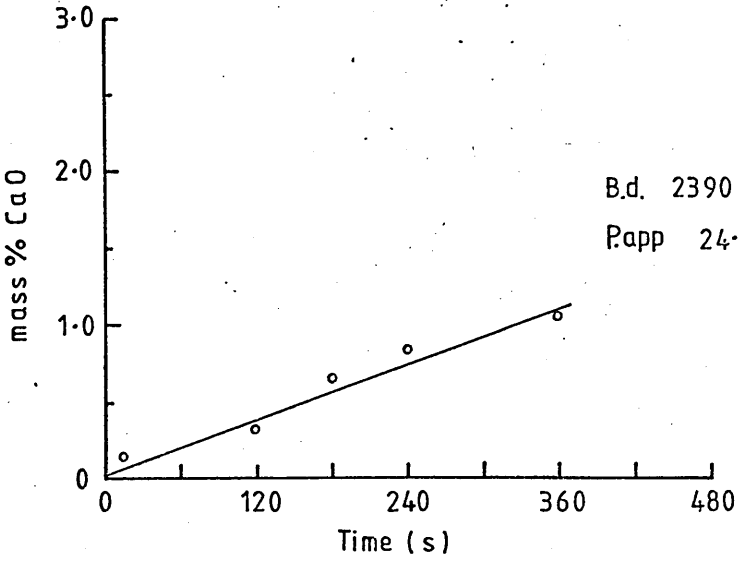

Fig 55 Static dissolution of "soft" burnt lime at 1300°C

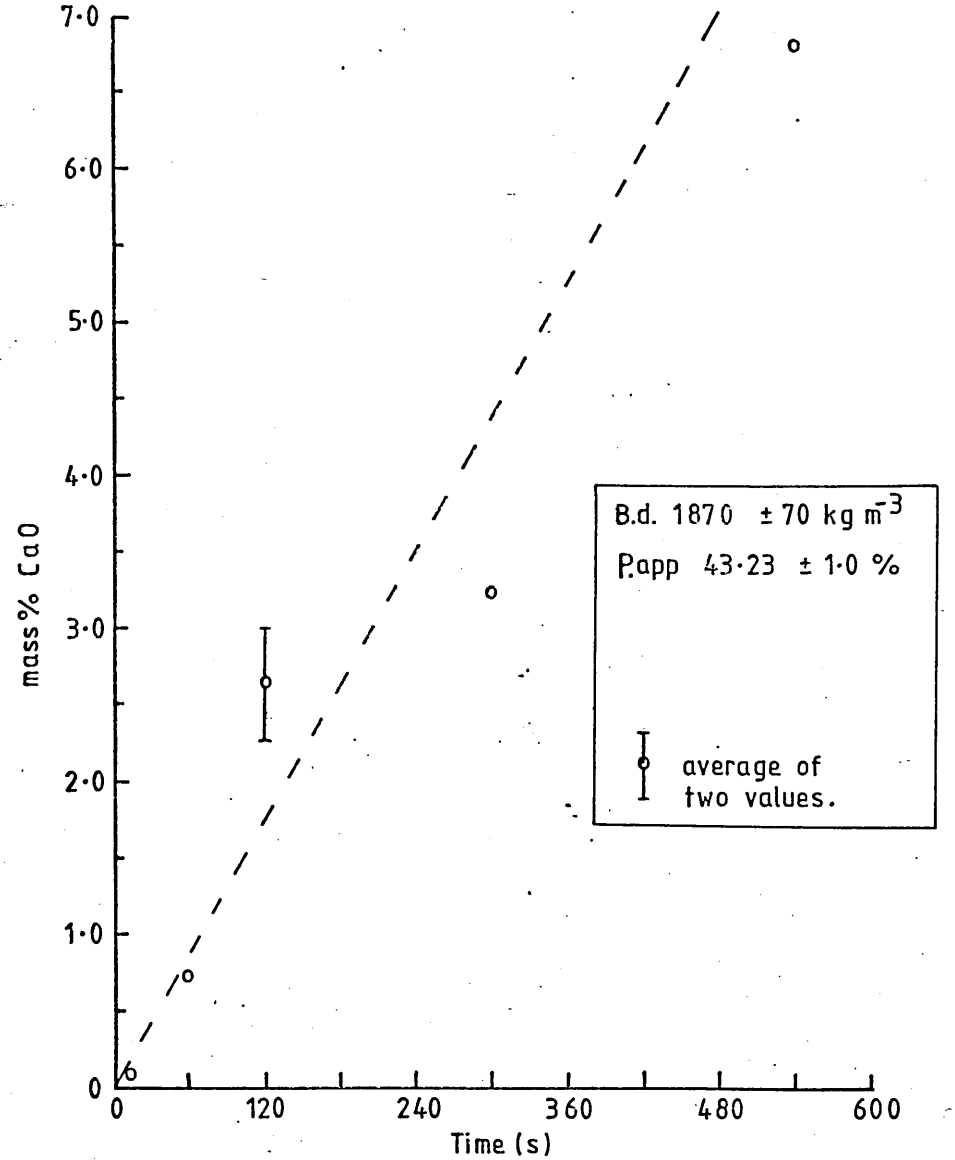

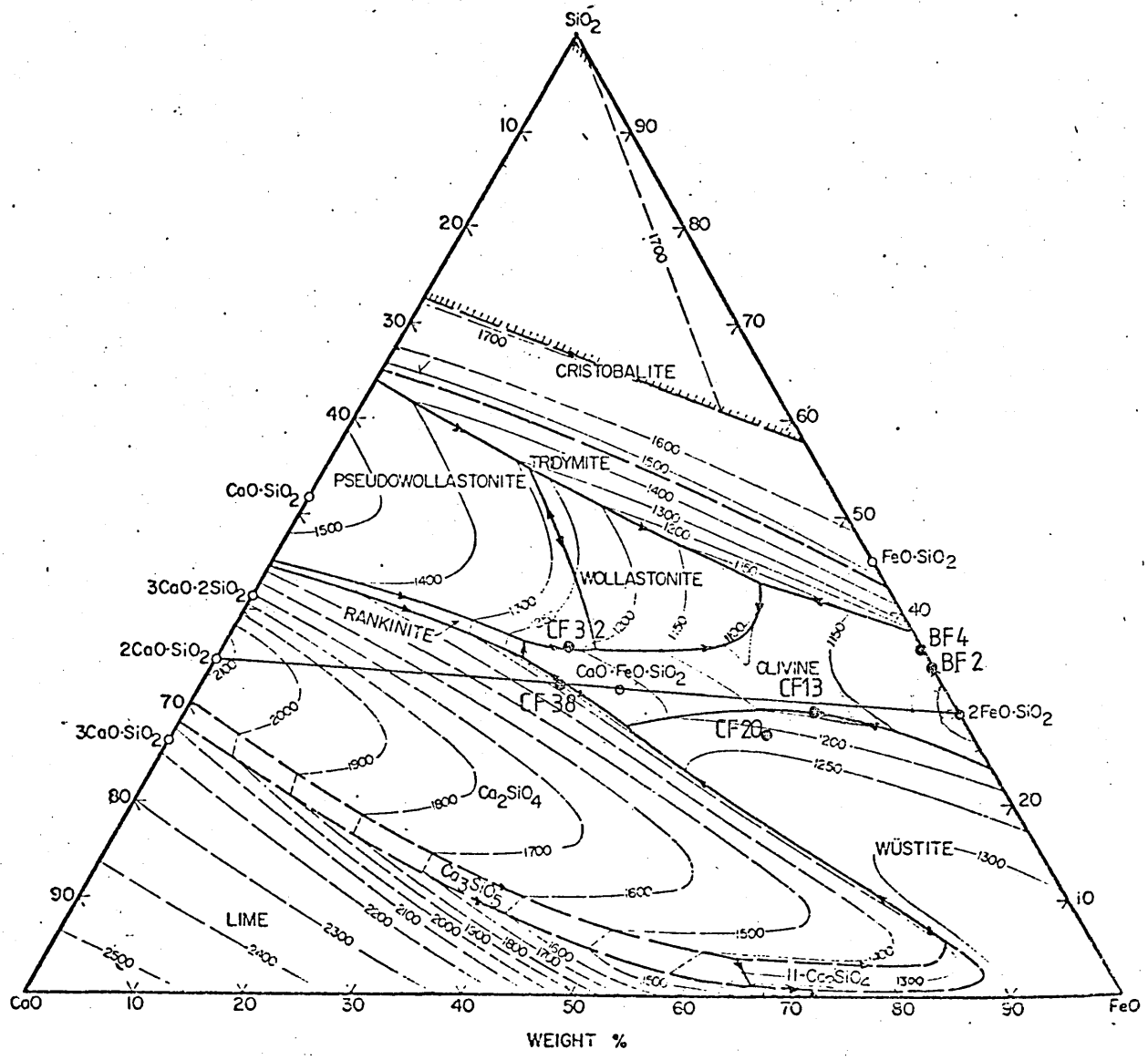

Fig. 56 Synthetic slag compositions used in the cone fusion studies
(diagram after Muan and Osborn[50])

Fig. 57 Part of the pseudo binary system across the tie-line $2FeO \cdot SiO_2 - 2CaO \cdot SiO_2$ showing sub-liquidus phase relationships

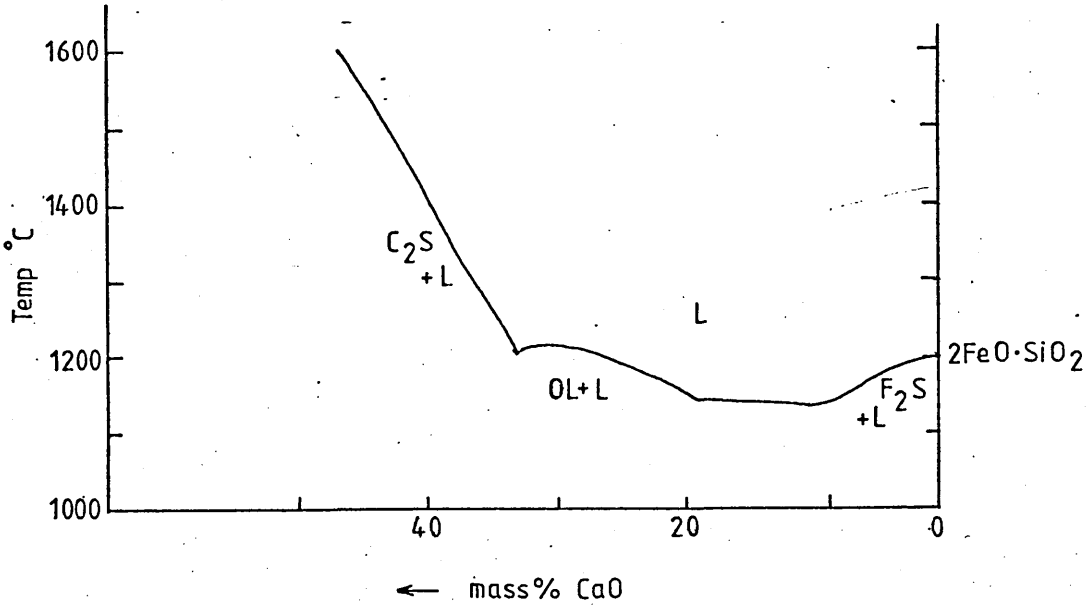

Fig 58 A solidus surface plan constructed from cone fusion data for synthetic slags in the system $CaO-FeO-SiO_2-MgO$

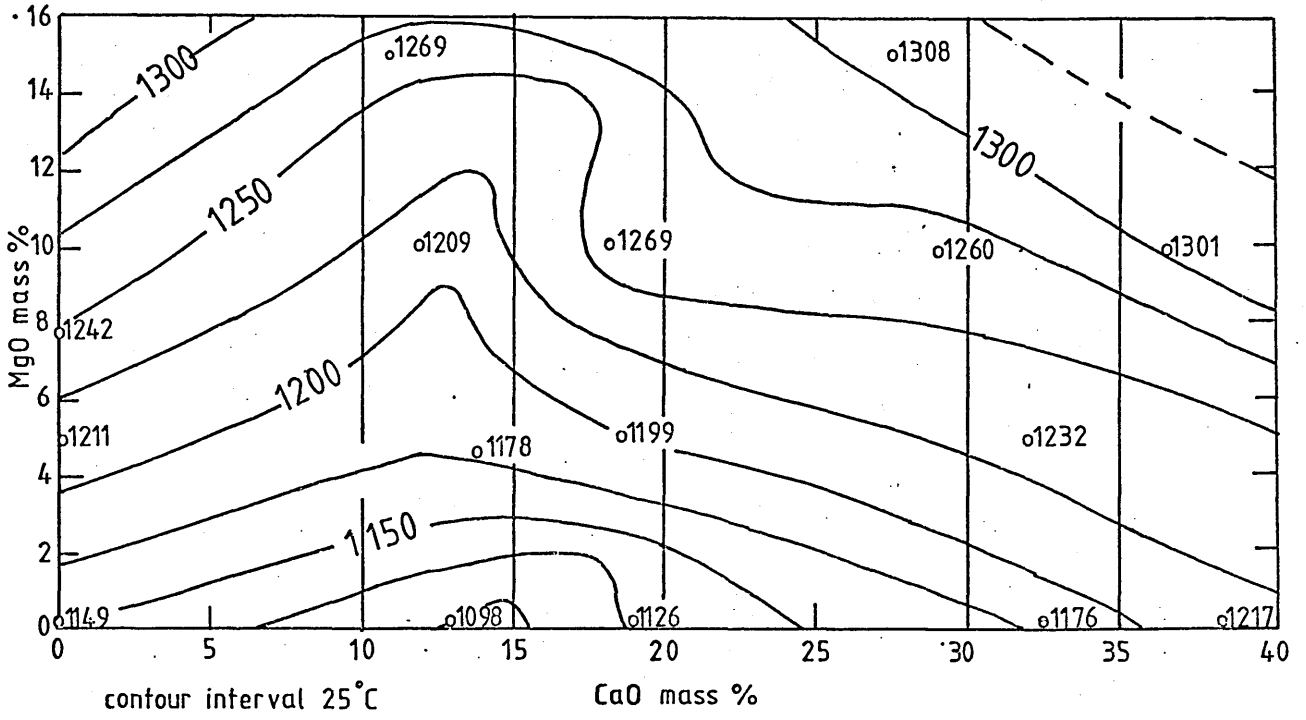

Fig 59 A liquidus surface plan constructed from cone fusion data for synthetic slags in the system $CaO-FeO-SiO_2-MgO$

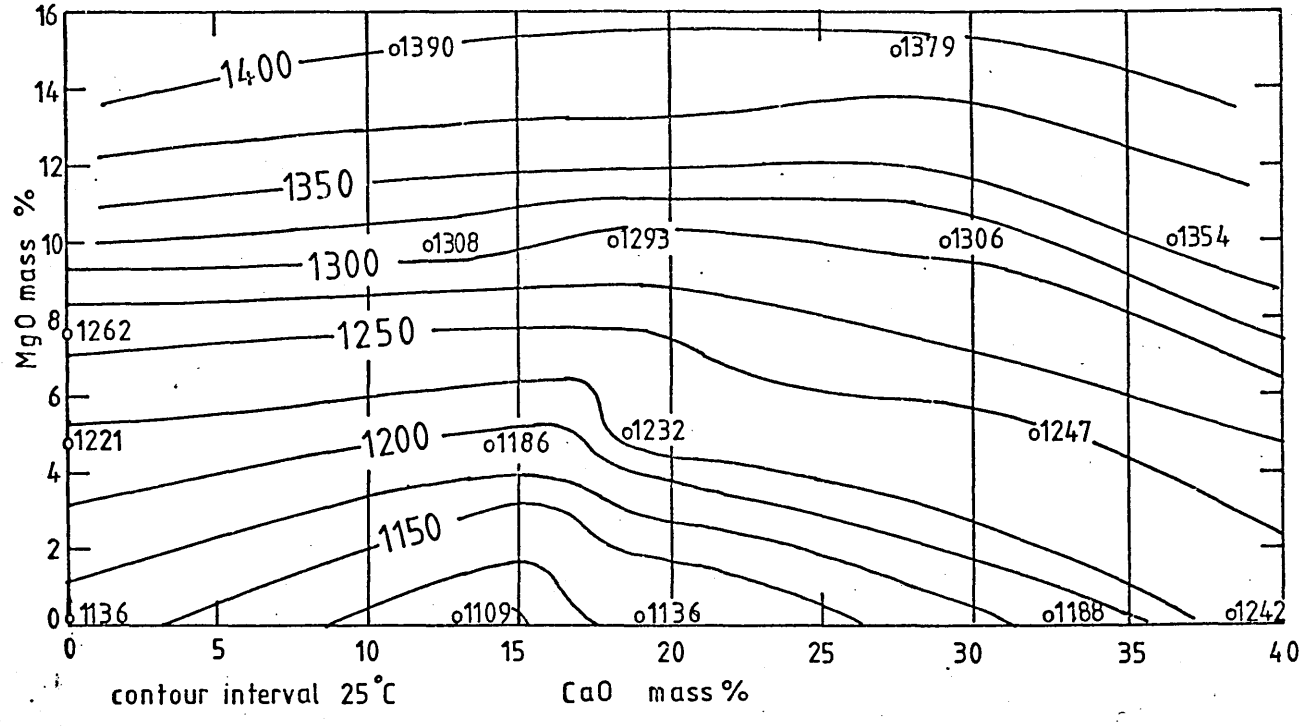

The influence of magnesia on the melting ranges of synthetic slags in the system $CaO-FeO-SiO_2$

Fig 60 Iron silicate (fayalite)

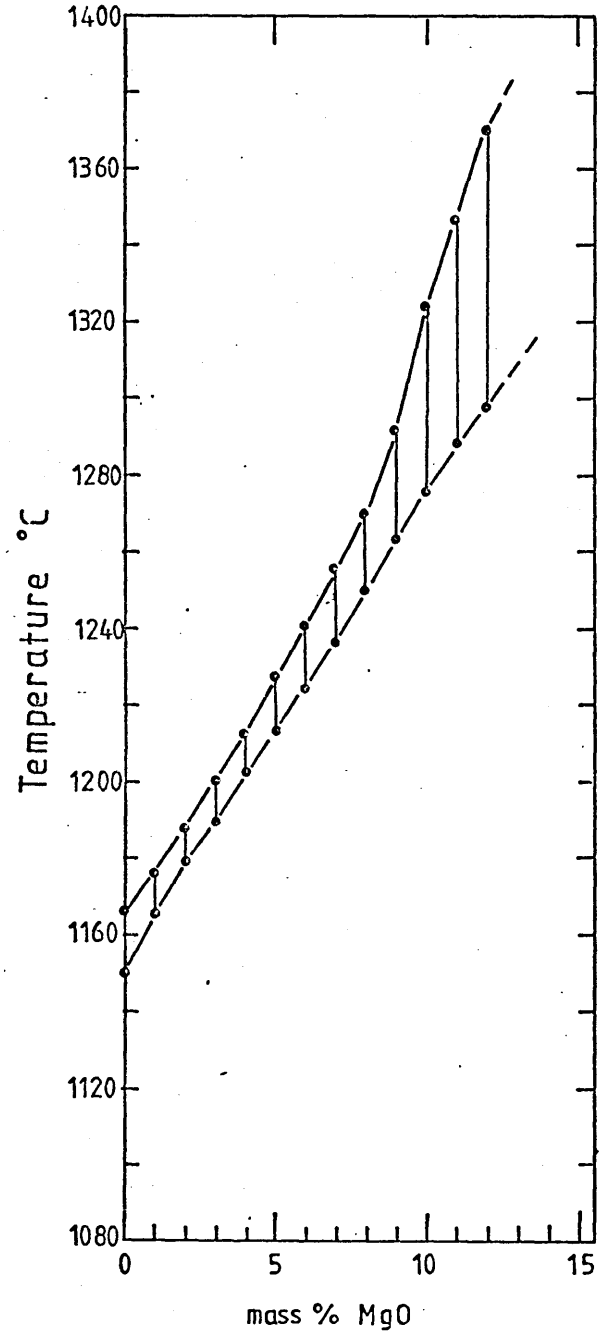

Fig 61 10 mass% – iron silicate

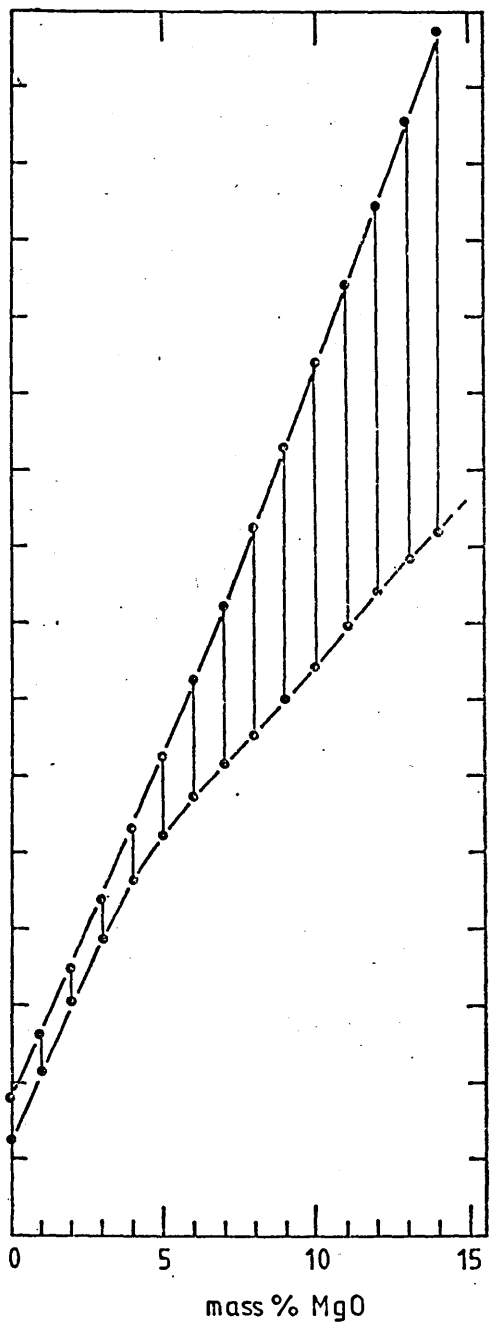

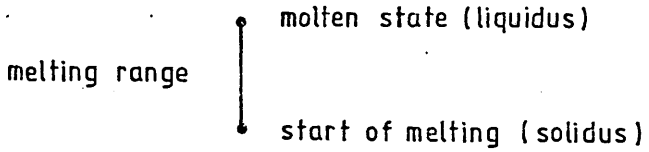

The influence of magnesia on the melting range of synthetic slags in the system $CaO-FeO-SiO_2$

Fig 62 15 mass % CaO-iron silicate

Fig 63 20 mass % CaO-iron silicate

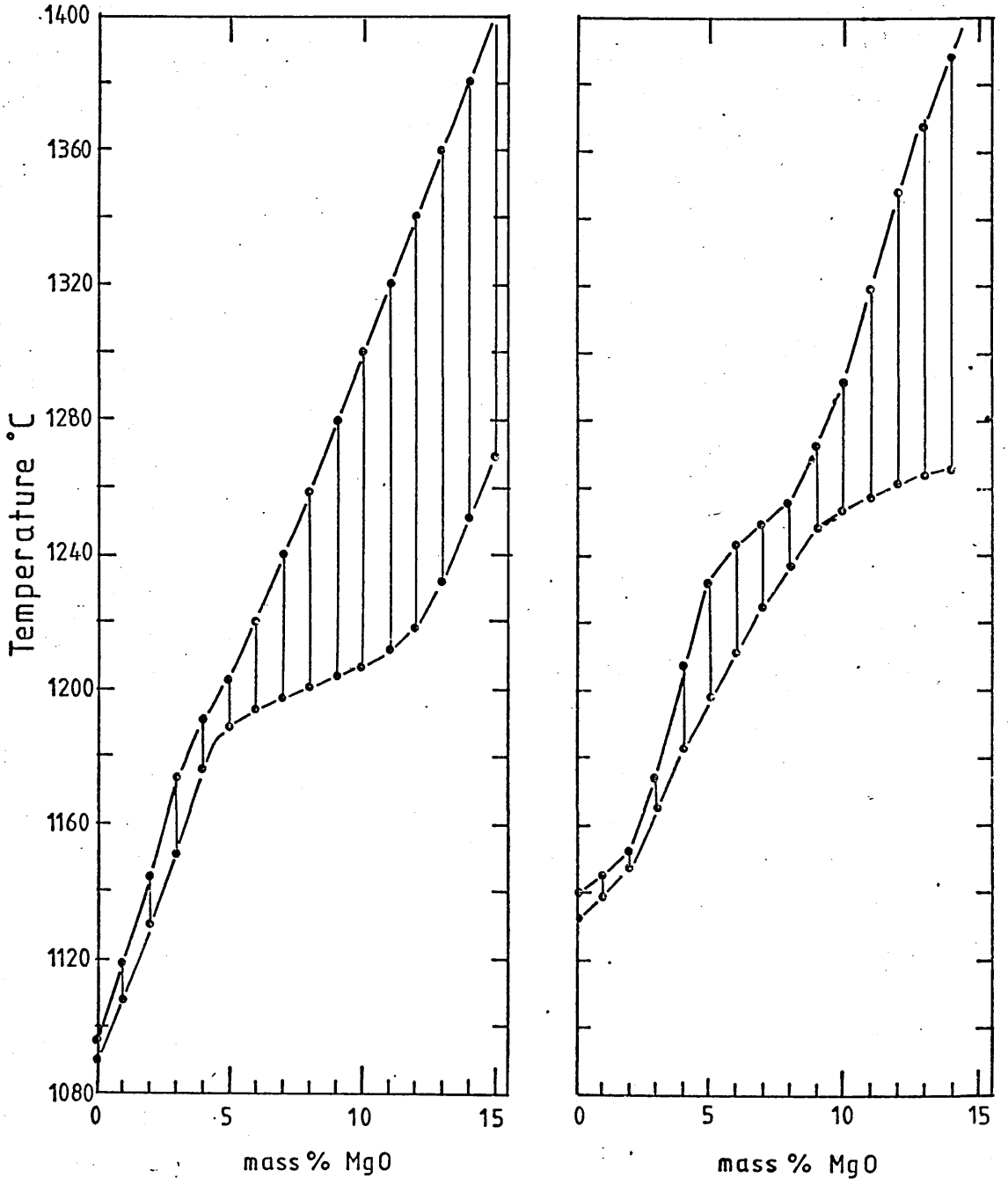

The influence of magnesia on the melting ranges of synthetic slags in the system $CaO-FeO-SiO_2$

Fig 64 30 mass % CaO-iron silicate

Fig 65 38 mass % CaO iron silicate

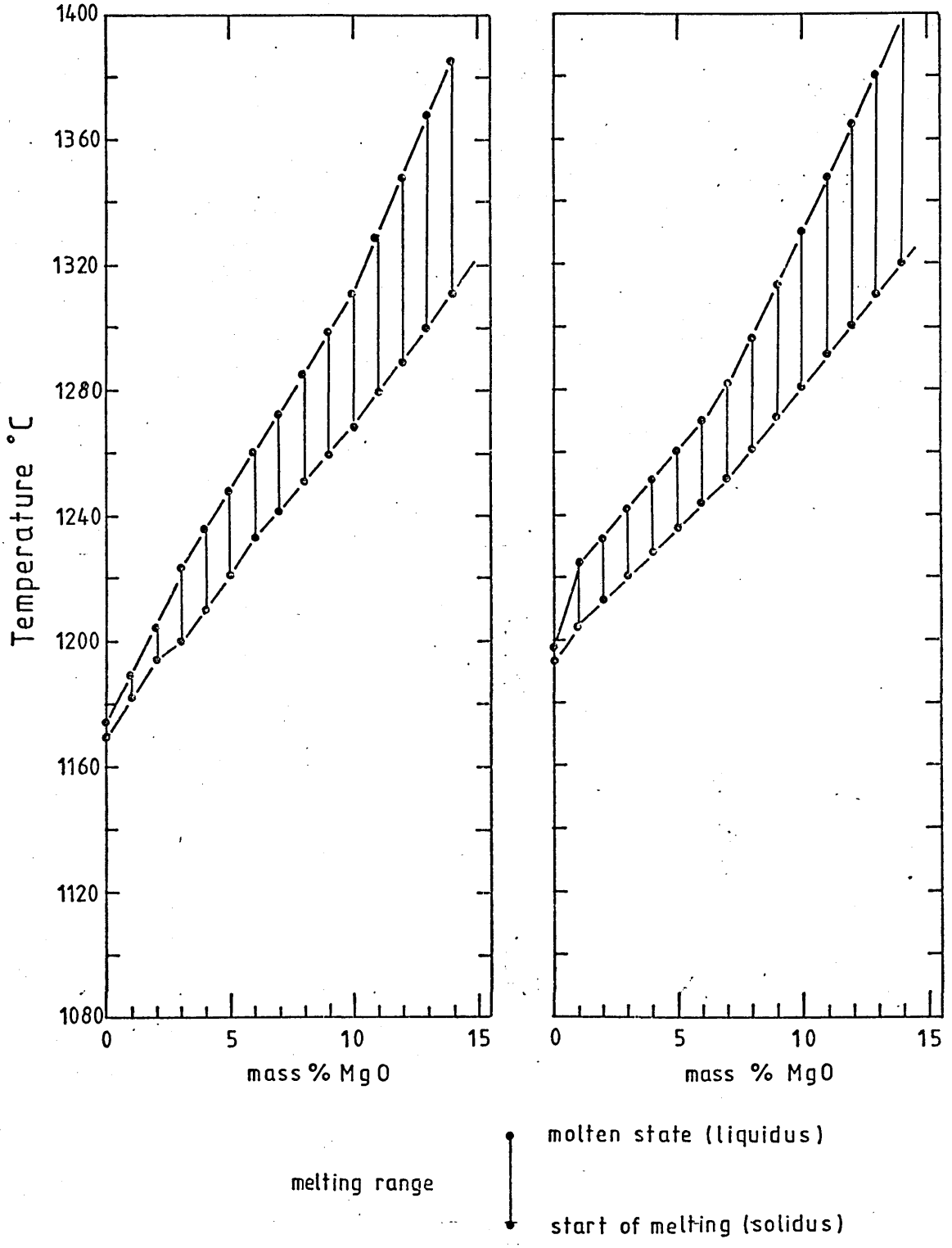

Plate 1 The assembled viscometer, used to measure synthetic slag viscosities within the system CaO - 'FeO' - SiO_2 - MgO.

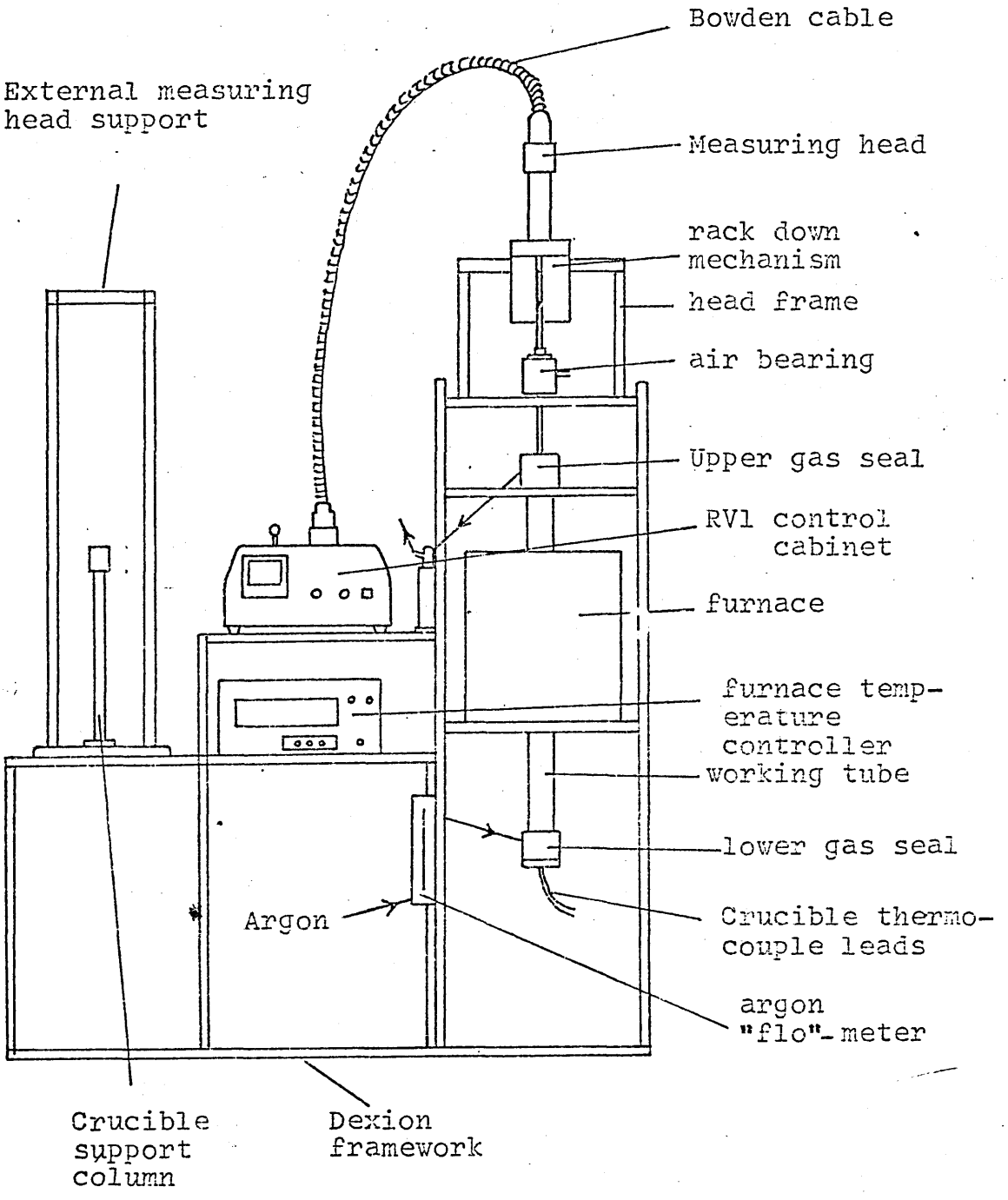

ltnrvr

^0681198

Plate 2.

The cone fusion furnace.

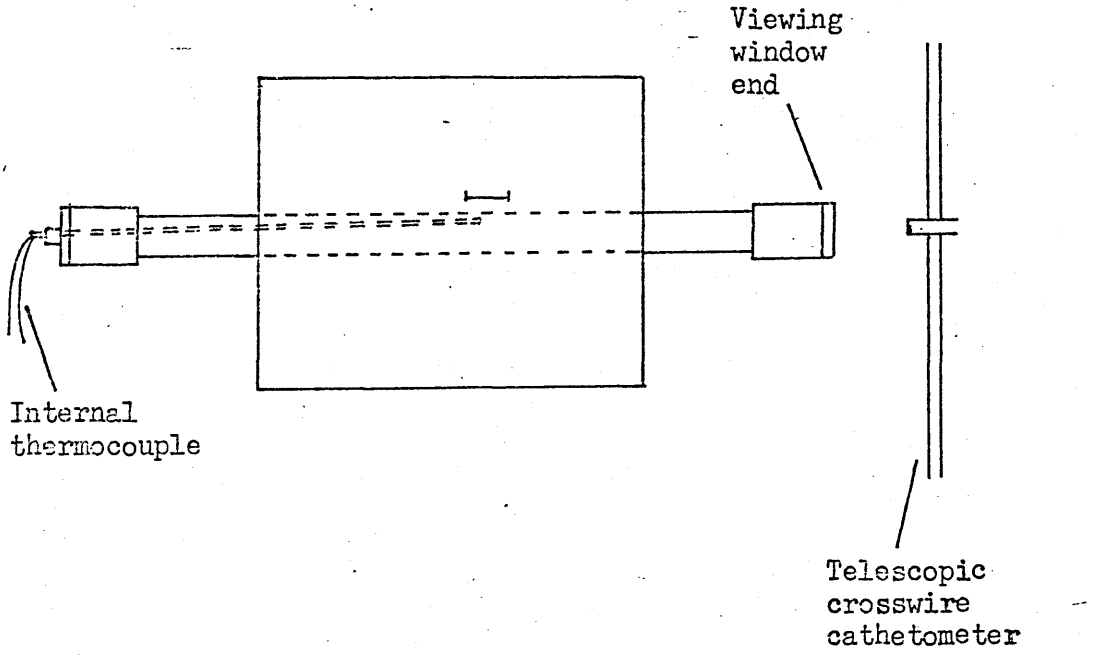

Plate 3

Iron crucible and measuring bob components used in the determination of synthetic slag viscosities. The longer crucible and measuring bob were replaced by the shorter components. All reported viscosity measurements were obtained with the short crucible and measuring bob assemblage.

Plate 4

An exploded view of the aluminium air bearing which was used to provide friction - free support for the viscometer shaft during the measurement of melt viscosity.

Plate 5 Detail of the measuring head, air bearing support clamp and rack-down mechanism.

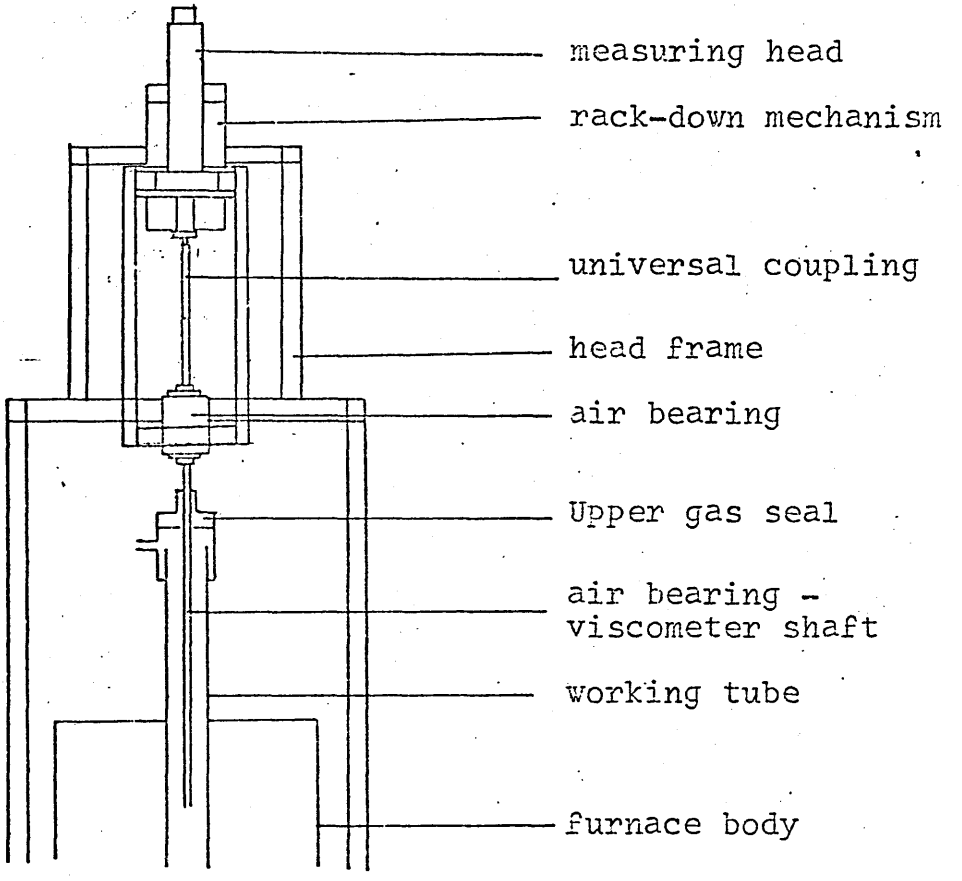

Plate 6

Crucible supports and graphite crucible holders.

Plate 7

The compressed air system used to maintain the air bearing under friction - free conditions.

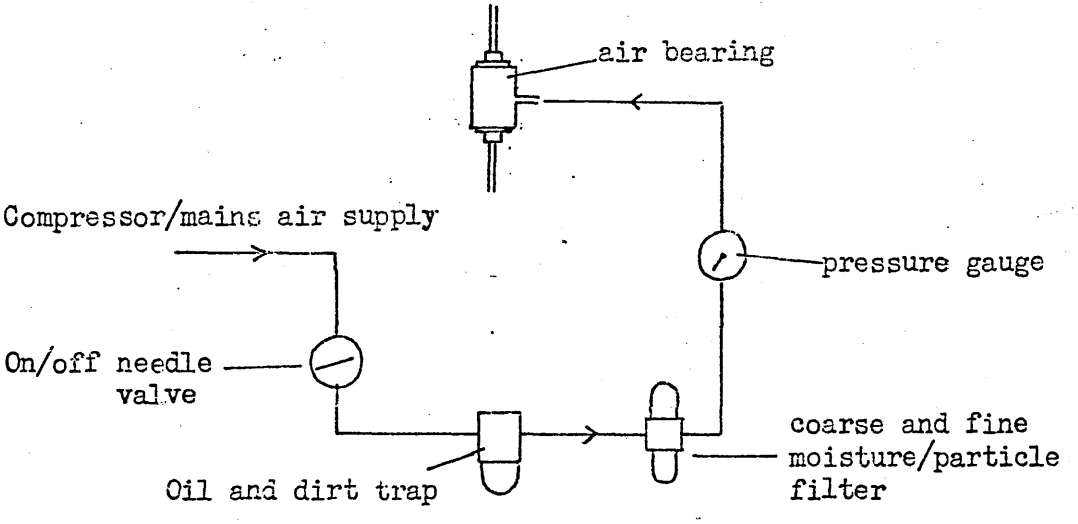

Plate 8

Green and calcined cylinder forms used in pill tests and immersion experiments.

1. Dolomitic limestone and dolomitic lime pill test cylinders.

2. Dolomitic limestone and dolomitic lime cylinders.

3. Limestone and lime cylinders.

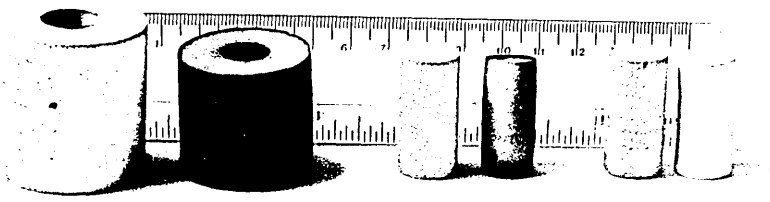

1 2 3

Plate 9

Cylinder support and crucible assembly used in the rotary immersion experiments.

Plate 10

The furnace head frame assembly used for rotational immersion experiments. A length of flexible polyethylene pipe was used to connect the motorised drive head to the spindle on the top of the cylinder support rod.

Plate 11

The energy dispersive x-ray spectrum for magnesium and silicon.

(a) The relative positions of the magnesium Kα and Kβ peaks, which give a combined x-ray count rate within the energy dispersive spectrum of magnesium.

(b) The half peak window width setting over part of the magnesium energy spectrum. The majority of x-ray counts will be recorded from the Mg Kα peak.

(c) The relative positions of the silicon Kα and Kβ peaks within the energy dispersive spectrum for silicon.

Q 79 1250EV K Z12 MG
Vs;5090 H5: 28EV/CH

2 1200EV 0C/S
VS:5000 HS: 20EV/CH

C 79 1740EV K Z14 SI
VS:5000 HS: 20EV/CH

Plate 12

A typical cone mounted on a fired alumina cement base and fixed with air dried C60 cement.

Plate 13

Cone at various stages of melting.

a. Initial stage

b. Intermediate stage

c. Collapse stage

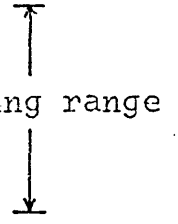

r a ’iM"" 8 n ^ r g r ^ T *1*f ir

7 . tie . ip ,210

Plate 14

The form of zirconia crucibles, which were used to contain synthetic melts before and after the completion of a viscosity determination. The expansion effect was produced after the crucible had furnace cooled from 1460°C to room temperature.

Plate 15

A 7.5 mass % MgO - iron silicate slag (melt 6) with an elongate and rectangular zirconia phase (pale grey). The zirconia phase also occurs as exsolution lamallae within the coarse, angular primary iron silicate phase (dark grey).

Mag. x 128

Plate 16

The interface between the wall of a zirconia crucible and a lime - magnesia - iron silicate melt (melt 7). Within the cooled slag, zirconia exists in a rounded and dendritic form, associated with dendrites of FeO (pale grey). The melt (dark grey) has produced well developed contraction cracks parallel to the crucible wall on cooling. The occurrence of zirconia dendrites suggests that this phase was partially soluble in the melt.

Mag. x 256

Plate 17

A polished specimen of dolomitic lime viewed under the SEM. Within the non-porous areas of the image, a magnesium oxide phase (dark grey) is beginning to recrystallise.

Cylinder Bd. 1780kgm^{-3}, P.app % 50.10

Mag. x 1200 approx.

Plate 18 Immersion time 420 s.

Recrystallisation of magnesia crystallites in the core of an unreacted dolomitic lime cylinder. Both the dark grey coloured magnesia and paler grey coloured lime matrix are adjacent to the pore network.

Mag. x 800

Plate 19a

Polished dolomitic limestone surface viewed under the SEM, revealing a sub-angular pore network.

Mag. x 700

Plate 19b

An SEM image of dolomitic crystals in macropores.

Mag. x 700

Plate 20a

Dolomitic lime fracture surface viewed under the SEM showing pore and particle size distribution.

P.app % 51.05
Bd 1740kgm^{-3} Mag. x 583

Plate 20b

A SEM image revealing the detail of pore development on the surface of relic dolomite crystals.

Mag. x 583

Plate 21

A SEM image of a dolomitic lime surface showing details of particle and pore sizes.

P.app % 51.05
Bd 1740kgm^{-3} Mag. x 2288 approx.

Plate 22

A SEM image of "DOLOMET" showing particle and pore size distribution.

Bd 1700 - 1750kgm^{-3} Mag. x 2500 approx.

, 10pm

Plate 23

Polished surface of limestone viewed under the SEM. A sub-angular pore structure is illustrated.

Mag. x 772

Plate 24

Polished surface of "hard" burnt lime viewed under the SEM. An extensive pore network is beginning to develop.
Bd 2340kgm^{-3}, P.app % 25.81

Mag. x 780

Plate 25

Polished surface of porous or "soft" burnt lime viewed under the SEM. An extensive pore network has developed and individual lime particles may be seen.
Bd approx. 1940kgm^{-3}, P.app % approx. 43

Mag. x 780

Plate 26

An SEM image of a broken "soft" burnt lime cylinder surface. A microporosity is visible within the coarser lime particles.
P.app % approx. 43

Mag. x 3520

Plate 27

A SEM image showing expansion cracks in the unreacted core margin of a dolomitic lime cylinder. Melt penetration is limited to the medium grey coloured phase in the left portion of the photograph.

Mag. x 4480 approx.

Plate 28 Immersion time, 15 s.

The reaction interface between an iron silicate melt and dolomitic lime. The reacted parts of the cylinder comprise of a dicalcium silicate phase (dark grey) and a magnesiowüstite phase (light grey). The globular wüstite phase (white) occurs at the melt (medium grey)-cylinder interface.

Mag. x 128

Plate 29 Immersion time, 15 s.

The occurrence of a globular wüstite zone (white) between the melt (pale grey) and dicalcium silicate cylinder interface (dark grey). A white dendritic wüstite phase occurs within the melt.

Mag. x 48

Plate 30 Immersion time, 180 s.

An irregular, globular wüstite phase (white) surrounding a partially dissolved dolomitic lime fragment. The wüstite phase occurs at the melt (grey) - cylinder reaction interface. The reacted cylinder contains dicalcium silicate (dark grey) and a magnesiowüstite (pale grey) phase assemblage.

Mag. x 96

Plate 31 Immersion time, 360 s.

A globular wüstite zone (white) occurs between the melt (light grey) and reacted dolomitic lime cylinder interface (dark grey). A dendritic form of wüstite occurs within the melt.

Mag. x 192

Plate 32 Immersion time, 15 s.

(a) A SEM image of the reaction interface between melt and dolomitic lime. The section was taken from near the top of the reacted cylinder and above the level of chilled surface melt. Unreacted dolomitic lime is enclosed by a "shadow" zone, which is adjacent to a dicalcium silicate - magnesiowüstite interface with the dark grey coloured melt. A globular wüstite (FeO) zone (pale grey) is visible within the melt.

Mag. x 300 approx.

(b) An x-ray distribution map of magnesium bearing phases.

(c) An x-ray distribution map of silicon bearing phases.

(d) An x-ray distribution map of calcium bearing phases.

(e) An x-ray distribution map of iron bearing phases.

(f) All element x-ray map revealing topographic depression on the specimen surface.

Plate 33 Immersion time, 15 s.

(a) A SEM image of the reaction interface between a dolomitic lime cylinder tip and an iron silicate melt. The melt (dark grey) contains globules of wüstite adjacent to magnesiowüstite (pale grey) and dicalcium silicate phases within the cylinder.

Mag. x 520 approx.

(b) An x-ray distribution map of magnesium bearing phases.

(c) An x-ray distribution map of silicon bearing phases.

(d) An x-ray distribution map of calcium bearing phases.

(e) An x-ray distribution map of iron bearing phases.

(f) An all element x-ray map.

Q

Plate 34 Immersion time, 15 s.

A SEM image revealing a narrow area of porous melt - cylinder interface. The area of melt (dark grey) contains rounded globules of wüstite. The lobate phase within the cylinder is magnesiowüstite (grey).

Mag. x 2500

Plate 35 Immersion time, 90 s.

A SEM image showing the maximum development of a meshwork lattice in the dicalcium silicate phase. The magnesiowüstite has a more globular appearance. The globular phase in the darker grey coloured melt is wüstite (pale grey).

Mag. x 2700

Plate 36 Immersion time, 120 s.

A SEM image indicating a closure of the dicalcium silicate at the melt cylinder interface.

Mag. x 2700

Plate 37 Immersion time, 360 s.

A SEM image showing the lobate magnesiowüstite phases (pale grey) at the melt cylinder interface. Thin stringers link the magnesiowüstite phase.

Mag. x 1485

Plate 38 Immersion time, 15 s.

A SEM image showing the detailed relationship between magnesiowüstite (medium grey) and dicalcium silicate (dark grey). The micrometre markers represent 1 μm divisions approximately.

Mag. x 3200 approx.

Plate 39 Immersion time, 90 s.

The presence of a third phase between rounded particles of magnesiowüstite (medium grey) and dicalcium silicate (dark grey) in a reacted dolomitic lime cylinder. The pale grey coloured phase was rich in iron oxide (FeO) and liquid at the reaction temperature (1300^{o}C).

Mag. x 640

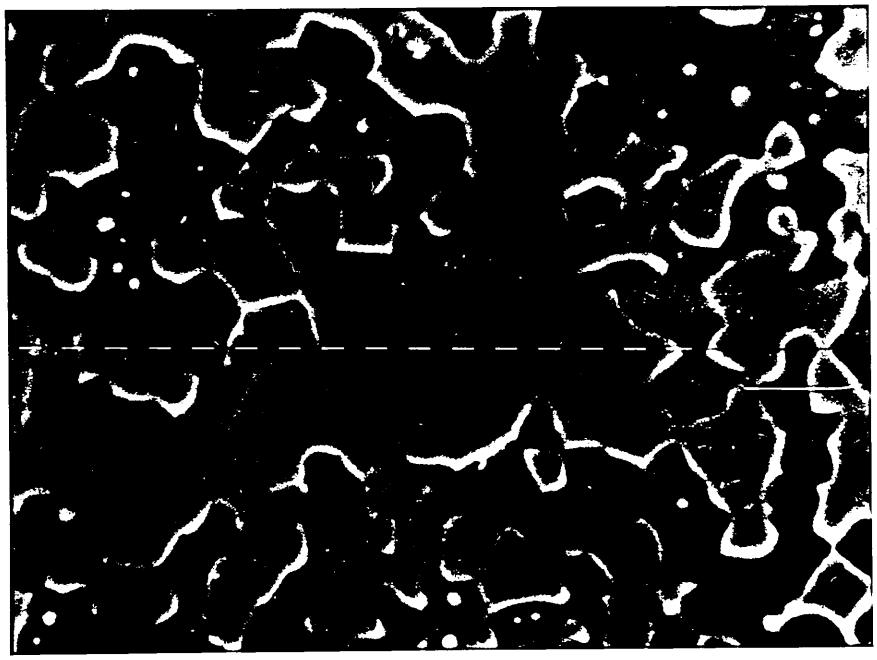

10 µm

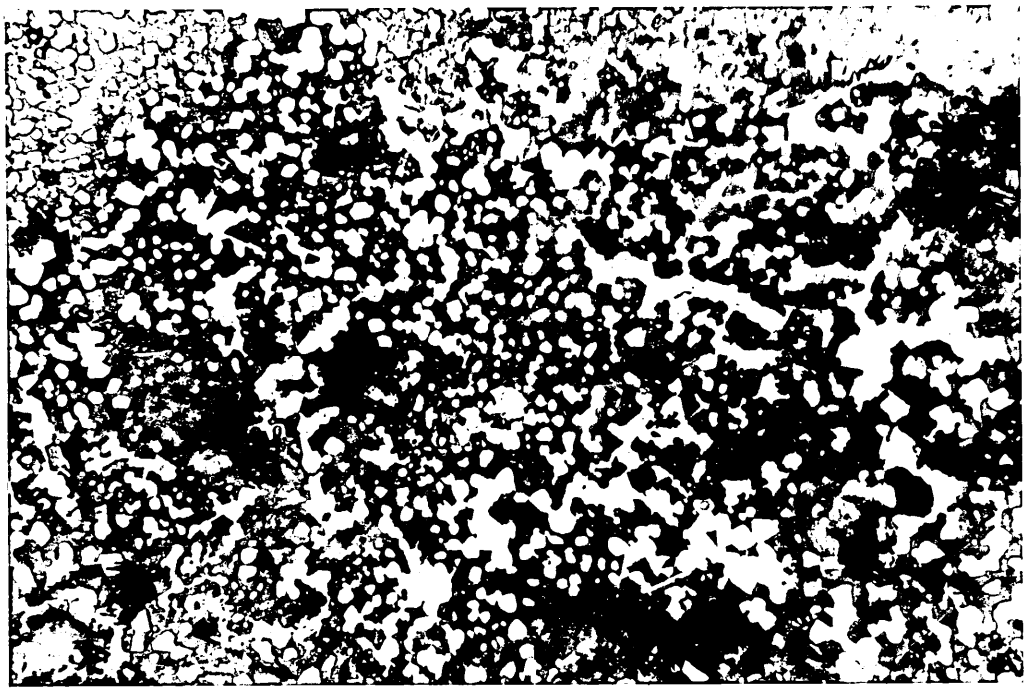

Plate 40 Immersion time, 360 s.

(a) Lobate magnesiowüstite phases (medium grey) straddle the melt - cylinder interface. The globular wüstites are represented by light grey coloured phases within the melt (dark grey).

Mag. x 600 approx.

(b) An x-ray distribution map of magnesium bearing phases. The magnesiowüstite phases are well defined and there is a melt - cylinder interface concentration of magnesium - rich phases.

(c) An x-ray distribution map of silicon bearing phases.

(d) An x-ray distribution map of calcium bearing phases.

(e) An x-ray distribution map of iron bearing phases.

(f) An all element x-ray distribution map.

Plate 41 Immersion time, 90 s.

The formation and nucleation of dendritic wüstite from the globular wüstite margin. Resorption of the globular wüstite margin by melt is occurring, the dendrites being precipitated by isothermal or athermal crystallisation.

Mag. x 256

Plate 42 Immersion time, 540 s.

The development of a granular magnesium - iron olivine phase (dark grey) adjacent to and within the globular wüstite zone (white). The margins of the cored crystals (pale grey) are similar in composition to the bulk iron silicate melt.

Mag. x 256

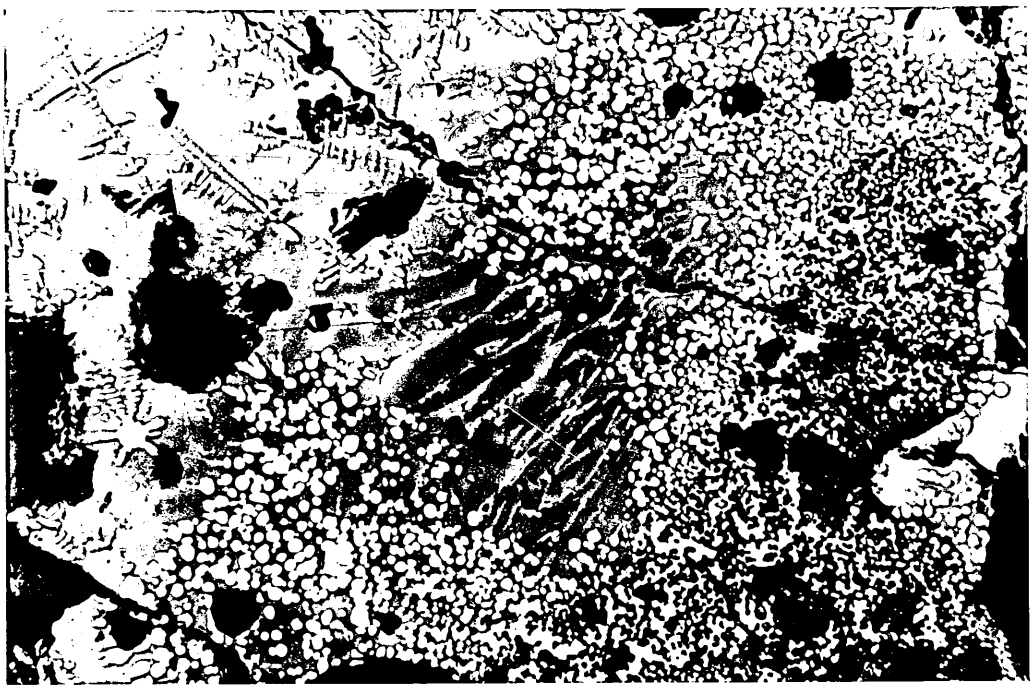

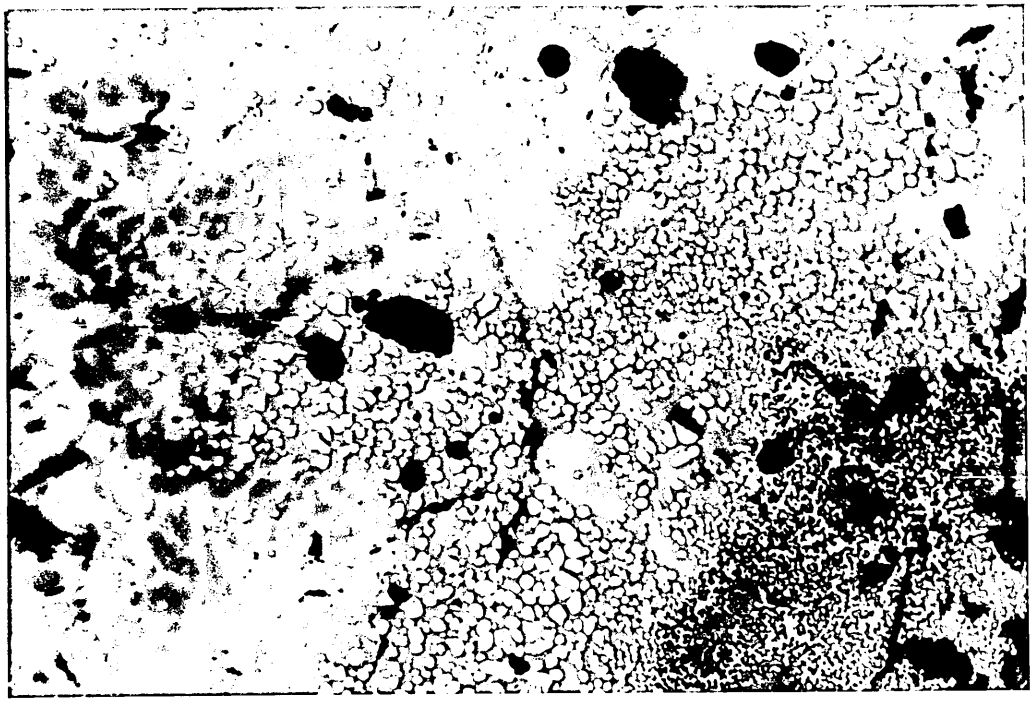

Plate 43 Immersion time, 420 s.

"Hard" burnt dolomitic lime P.app 36%

The development of cored magnesium - iron silicate crystals (dark grey) within the melt (pale grey) and globular wüstite zone (white). The cylinder contains dicalcium silicate (dark grey) and magnesiowüstite phases (pale grey).

Plate 44 Immersion time, 15 s.

Annealed at 1300°C for 1 hour.

Within the area of melt (medium grey) rounded particles of metallic iron (white phase) have precipitated. The once globular wüstite phases (pale grey) have developed a lobate morphology similar to that of the magnesio-wüstite associated with the dicalcium silicate phase (dark grey).

Mag. x 128

Plate 45 Immersion time, 15 s.

Annealed at 1300°C for 1 hour.

Detail of the interface between the iron silicate melt (pale grey) and the dicalcium silicate phase (dark grey) of the reacted dolomitic lime cylinder. Between the melt and the first dicalcium silicate - magnesio-wüstite interface, a second and later precipitated C_2S - MF interface has developed. The limited quantity of iron silicate available for reaction became saturated with lime from the earlier C_2S interface at the annealing temperature.

Mag. x 640

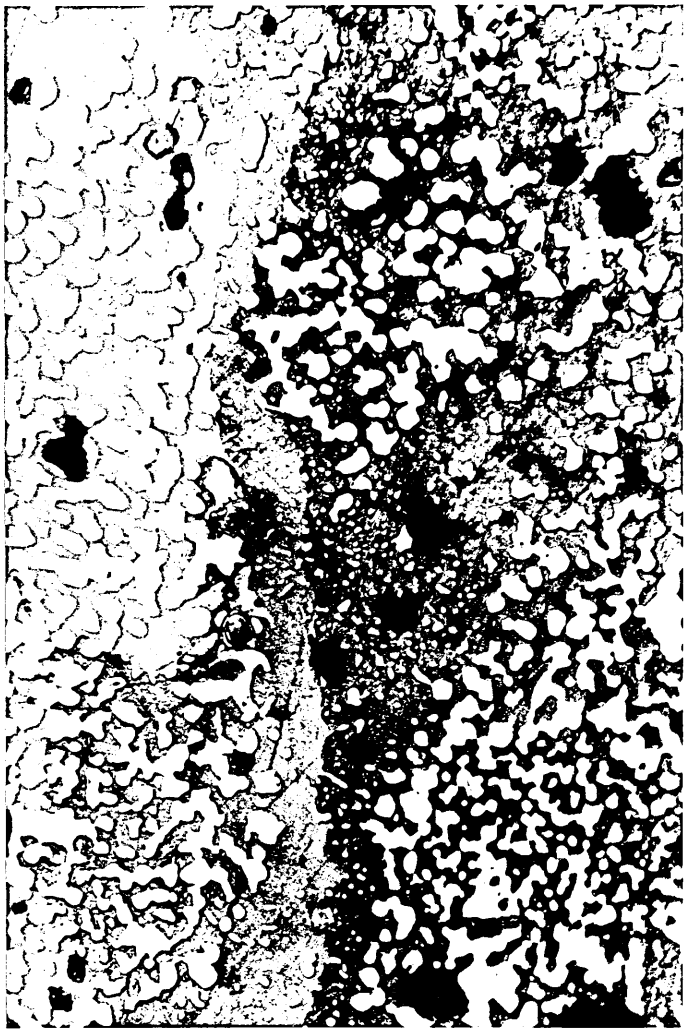

Plate 46 Immersion time, 60 s.

Rotated at 217 cm min^{-1} (50 r.p.m.)

Finger-like projections of melt (medium grey) penetrating into the reacted dolomitic lime cylinder now composed of dicalcium silicate (dark grey) and magnesiowüstite phases (pale grey). The globular wüstite zone (white) follows closely the melt - cylinder interface contour. Isolated and dissolved parts of the cylinder are indicated by clusters of globular wüstite.

Mag. x 64

Plate 47 Immersion time, 300 s.

Rotated at 217 cm min^{-1} (50 r.p.m.)

The development of a granular magnesium - iron olivine zone (dark grey), adjacent to the melt and globular wüstite interface. The cored olivine crystals persist up to the dicalcium silicate - magnesiowüstite interface of the cylinder.

Mag. x 128

Plate 48 Immersion time, 360 s.

Rotated at 217 cm min^{-1} (50 r.p.m.)

A SEM image recorded in the reflective mode with a negative potential applied to the grid. Atomic number contrasts are highlighted. The dark grey and grey coloured phases represent low atomic number magnesium and iron silicates. The globular wüstite phase appears as the white phase at the interface. The magnesium - rich olivine phases are virtually continuous at the melt - cylinder interface.

Mag. x 520

Plate 49

A cylinder of dolomitic lime after rotation in an iron silicate melt for 360 s. A pronounced erosion line occurs at the limit of submergence in the melt. The cooled melt present above the erosion line was lifted there by capillary suction.

Actual size

Plate 50

Dolomitic lime cylinders after static immersion at 1300°C in an iron silicate melt. The sectioned cylinder tips represent immersion times, from left to right, of 15, 90, 120, 180, 300, 360 and 540 seconds. Small patches of unreacted dolomitic lime occur as the white coloured areas within some of the mounted cylinders.

Plate 51

Dolomitic lime cylinder sections after rotation in an iron silicate melt at 50 r.p.m. (217 cm min^{-1}). The rotated cylinders were reacted isothermally with the melt at 1300°C and reading from left to right represent immersion times of 15, 60, 240, 360 and 540 seconds respectively.

Plate 52 Immersion time, 15 s.

Iron silicate melt + 5 mass % MgO.

A narrow but well developed zone of globular wüstite (white) at the melt (pale grey) - cylinder interface. The black amorphous phase within the reaction zone is unreacted dolomitic lime.

Mag. x 128

Plate 53 Immersion time, 360 s.

Iron silicate melt + 5 mass % MgO.

The development of a granular, magnesium - iron olivine zone (dark grey) which extends into the melt (pale grey). The globular wüstite zone (white) is reduced in thickness when in close association with the amorphous dolomitic lime cylinder (dark grey), which contains isolated patches of a dicalcium silicate - magnesiowüstite phase association.

Mag. x 256

Plate 54 Pill test.

A general view of the melt (grey) - cylinder wall reaction interface. Where there are small proportions of magnesiowüstite (pale grey), the interface of dicalcium silicate (dark grey) and melt is discernible. The black coloured amorphous phase represents the unreacted dolomitic lime cylinder side wall. The globules in the melt areas are metallic iron (white).

Mag. x 256

Plate 55 Pill test.

Detail of the melt - cylinder wall reaction interface. Dicalcium silicate (dark grey) contains a pale grey coloured magnesiowüstite phase with a lobate appearance. The actual melt - cylinder wall reaction interface is difficult to identify. Small patches of a globular wüstite phase (pale grey) occur.

Mag. x 640

Plate 56 Immersion time, 15 s.

"Dolomet" - iron silicate melt.

The reaction interface produced by the commercial slag conditioner "Dolomet" and an iron silicate melt. The reacted "Dolomet" is represented by dicalcium silicate (dark grey) and magnesiowüstite (pale grey) phases. The wüstite phase (white) is widely developed around the reaction interface. The melt also contains a dendritic wüstite phase.

Mag. x 128

Plate 57 Immersion time, 15 s.

"Dolomet" - iron silicate melt.

The development of metallic iron phases (white) within pockets of melt close to the main melt - cylinder interface. Black coloured patches of unreacted "Dolomet" occur within the phase association of dicalcium silicate (dark grey) and magnesiowüstite (pale grey).

Mag. x 256

mB

Plate 58 Immersion time, 15 s.

"Hard" burnt lime.

The reaction interface between an iron silicate melt and lime. An iron oxide rich phase (FeO)(light grey) occurs at the interface and within the pores of the subrounded lime particles. The lime particles are still well sintered together. A granular dicalcium silicate phase (dark grey) is beginning to precipitate between the melt (medium grey) and the FeO -rich liquid phase.

Mag. x 640

Plate 59 Immersion time, 15 s.

"Hard" burnt lime.

Detail of the melt - lime interface showing dicalcium silicate particles (dark grey) coalescing at the melt - FeO rich liquid boundary. Extensions of the FeO rich liquid (pale grey) are becoming isolated within the melt.

Mag. x 1280

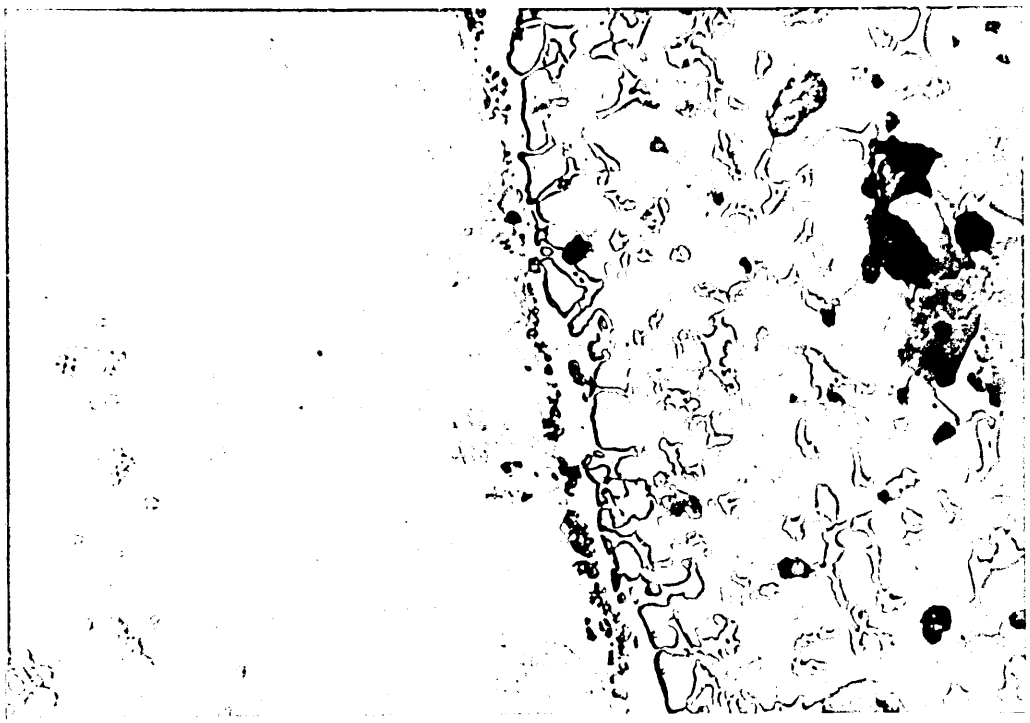

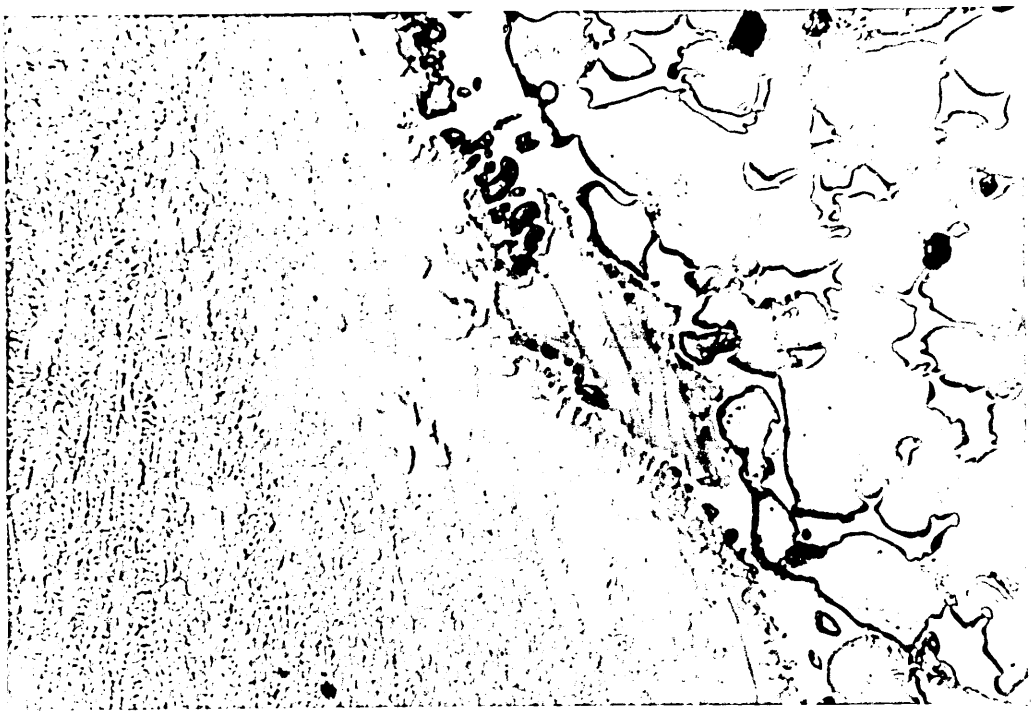

Plate 60 Immersion time, 120 s.

"Hard" burnt lime.

A continuous barrier of dicalcium silicate (dark grey) has formed at the interface of the melt (medium grey) and granular lime cylinder interface. A calciowüstite phase (white) has developed between the dicalcium silicate - lime cylinder interface and has also penetrated the cylinder pore network.

Mag. x 128

Plate 61 Immersion time, 240 s.

"Hard" burnt lime.

Thickening of the dicalcium silicate interface (dark grey) between the melt (pale grey) and lime cylinder. The dendritic wüstite phase was produced athermally within the melt. The black coloured areas denote mechanical damage.

Mag. x 256

Plate 62 Immersion time, 360 s.

"Hard" burnt lime.

An impermeable, continuous dicalcium silicate barrier (dark grey) has formed adjacent to the melt interface (pale grey). The dicalcium silicate (C_2S) phase which extends away from the melt - C_2S interface into the cylinder, has become granular and contains calciowüstite (white). Isolated fragments of lime exist on the periphery of the cylinder.

Mag. x 128

Plate 63 Immersion time, 360 s.

"Hard" burnt lime.

The calciowüstite phase (white) which was liquid at the reaction temperature of 1300°C, has penetrated into the lime cylinder where lime particles remain sintered together. Rectangular tricalcium silicate crystals (dark grey) have been precipitated in the liquid - filled voids between the sub-rounded particles of lime.

Mag. x 640

Plate 64 Immersion time, 15 s.

"Soft" burnt lime.

A granular dicalcium silicate phase - C_2S (dark grey) has been precipitated at the melt - cylinder interface. Calciowüstite (white) separates the C_2S barrier from the lime cylinder.

Mag. x 256

Plate 65 Immersion time, 120 s.

"Soft" burnt lime.

A narrow, convoluted boundary of dicalcium silicate - C_2S (dark grey) has developed at the melt - cylinder interface. An iron oxide - rich region (pale grey) has been established between the C_2S barrier and the cylinder. The periphery of the cylinder shows progressive dissolution and isolation of lime particles. A dissociated form of C_2S is forming behind the melt - C_2S interface adjacent to the reacted cylinder. Prismatic tricalcium silicate (C_3S) crystals (dark grey) occur within the FeO - rich phase penetrating the cylinder.

Mag. x 256

Plate 66 Immersion time, 15 s.
"Soft" burnt lime.

(a) A SEM image illustrating the reaction interface between an iron silicate melt (dark grey) and a lime cylinder. An irregular, granular dicalcium silicate (C_2S) phase (dark grey) separates the melt from an iron oxide rich liquid region and the lime cylinder.

Mag. x 600 approx.

(b) An x-ray distribution map for silicon bearing phases.

(c) An x-ray distribution map for calcium bearing phases.

(d) An x-ray distribution map for iron bearing phases.

(e) An x-ray distribution map for all elements.

f■ ?\r •r ' i ' V - '* £&S Kr.Jy ... -r

: .4^ ŷ> -O^V+m

; ~ • . ■■') '

,' V \ /

- H , V H- , Ir *: «} - : ; V / . • J

Plate 67 Immersion time, 540 s.
"Soft" burnt lime.

A narrow, convoluted dicalcium silicate (C_2S) layer (dark grey) separates the melt (medium grey) from the iron silicate - rich liquid region (white). A granular C_2S layer is beginning to precipitate in the proximity of the solid C_2S barrier. Angular shaped C_2S crystals are scattered through the FeO - rich region which also contains isolated particles of lime (medium grey) and rectangular crystals of tricalcium silicate (dark grey).

Mag. x 256

Plate 68 Immersion time, 540 s.
"Soft" burnt lime.

A SEM image revealing detail of the two-phase iron - rich region that penetrates the lime cylinder. The composition of the pale grey coloured phase is almost pure FeO whilst that of the dark coloured phase contains approximately 56 mass % FeO, 43 mass % CaO and 1 mass % SiO_2. The pear shaped phase is dicalcium silicate (dark grey).

Mag. x 3520

Plate 69 Immersion time, 540 s.

"Soft" burnt lime.

The penetration of iron oxide - rich liquid (pale grey) into the lime cylinder has dissolved and isolated particles of lime. Rectangular tricalcium silicate crystals (dark grey) have been produced as a product of the dissolution reaction. Micro - corrugations are visible on some of the lime particles.

Mag. x 256

Plate 70 Immersion time, 15 s.

"Soft" burnt lime.

The reaction between a 2 mass % MgO - iron silicate melt and a lime cylinder has produced an irregular, granular dicalcium silicate (C_2S) layer (dark grey) between the melt and the cylinder. The iron oxide - rich region (pale grey) separating the C_2S layer from the cylinder, contains prismatic crystals of tricalcium silicate - C_3S (dark grey).

Mag. x 640

Plate 71 Immersion time, 15 s.

"Soft" burnt lime.

The reaction between a 5 mass % MgO - iron silicate melt has produced a granular dicalcium silicate region (dark grey) extending into a zone of prismatic tricalcium silicate crystals.

Mag. x 640

Plate 72 Immersion time, 360 s.

"Soft" burnt lime.

The reaction between a "soft" burnt lime cylinder and a 5 mass % MgO - iron silicate melt has produced an extensive, disseminated dicalcium silicate (C_2S) region (dark grey) at the reaction interface. The projections of C_2S into the melt contain a calciowüstite phase (white) which at one point has ruptured the tenuous C_2S envelope. A zone of rectangular tricalcium silicate crystals (dark grey) occur in the calciowüstite zone between the C_2S - cylinder interface.

Mag. x 128

Plate 73 Immersion time, 360 s.

"Soft" burnt lime.

A SEM image of the 5 mass % MgO - iron silicate - lime interface showing a dispersed granular dicalcium silicate (C_2S) zone and the region of FeO - rich phase containing the prismatic tricalcium silicate crystals. The zone is approximately 100 μm wide and shows an increase in the sizes of the granular C_2S particles towards the lime cylinder.

Mag. x 520

Plate 74 Immersion time, 360 s.

"Soft" burnt lime.

A SEM image revealing the interface detail between a 5 mass % MgO - iron silicate melt and a lime cylinder. The granular dicalcium silicate (C_2S) particles at the melt interface do not form a continuous solid barrier around the reacted lime cylinder.

Mag. x 1040

Plate 75 Immersion time, 15 s.
"Soft" burnt lime.

(a) A SEM image of the reaction interface between a 5 mass % MgO - iron silicate melt and a lime cylinder. The dicalcium silicate interface is granular and contains an iron oxide - rich phase which was liquid at the reaction temperature of 1300°C.

Mag. x 260.

(b) An x-ray distribution map for magnesium bearing phases.

(c) An x-ray distribution map for silicon bearing phases.

(d) An x-ray distribution map for calcium bearing phases.

(e) An x-ray distribution map for iron bearing phases.

(f) An x-ray distribution map for all elements.

::V ^;Vf.'ryi';

Plate 76 Immersion time, 360 s.
"Soft" burnt lime.

(a) A SEM image of the reaction interface between a 5 mass % MgO - iron silicate melt and a lime cylinder. Within the reaction interface between granular dicalcium silicate and a FeO - rich phase, prismatic crystals of tricalcium silicate have developed.

Mag. x 260

(b) An x-ray distribution map for magnesium bearing phases.

(c) An x-ray distribution map for silicon bearing phases.

(d) An x-ray distribution map for calcium bearing phases.

(e) An x-ray distribution map for iron.

(f) An all element x-ray map.

Plate 77 Immersion time, 15 s.

A SEM image representing the interface between an iron silicate melt and a dolomitic lime cylinder. A globular wüstite phase (medium grey) is present between the melt and reacted cylinder. The numbers across the profile traverse line represent analysis points. The concentrations of oxide components have been plotted below the SEM photomicrograph. The profile analyses have been used to estimate the phases occurring across the reaction interface.

15 sec, immersion at 1300°C

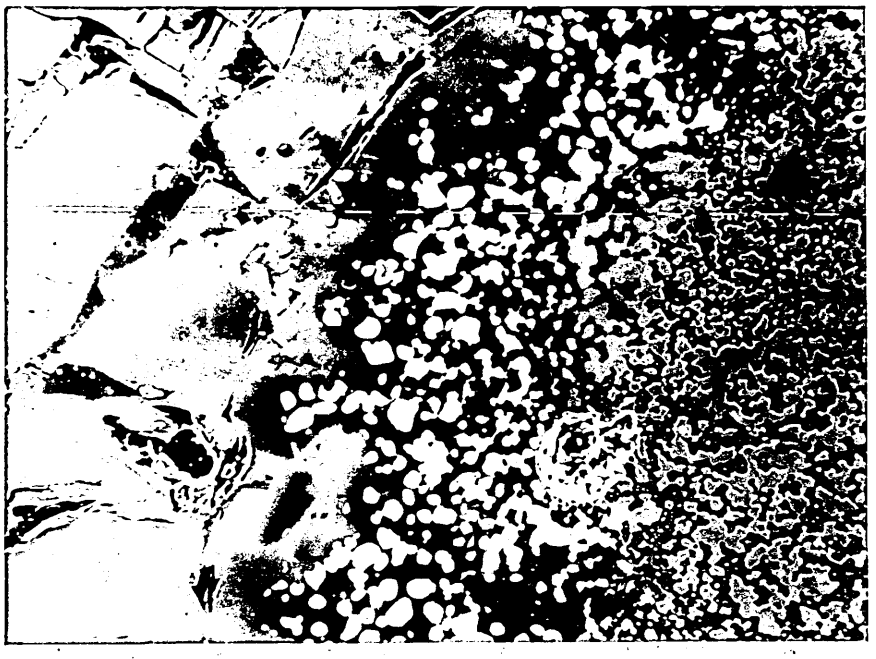

× 570

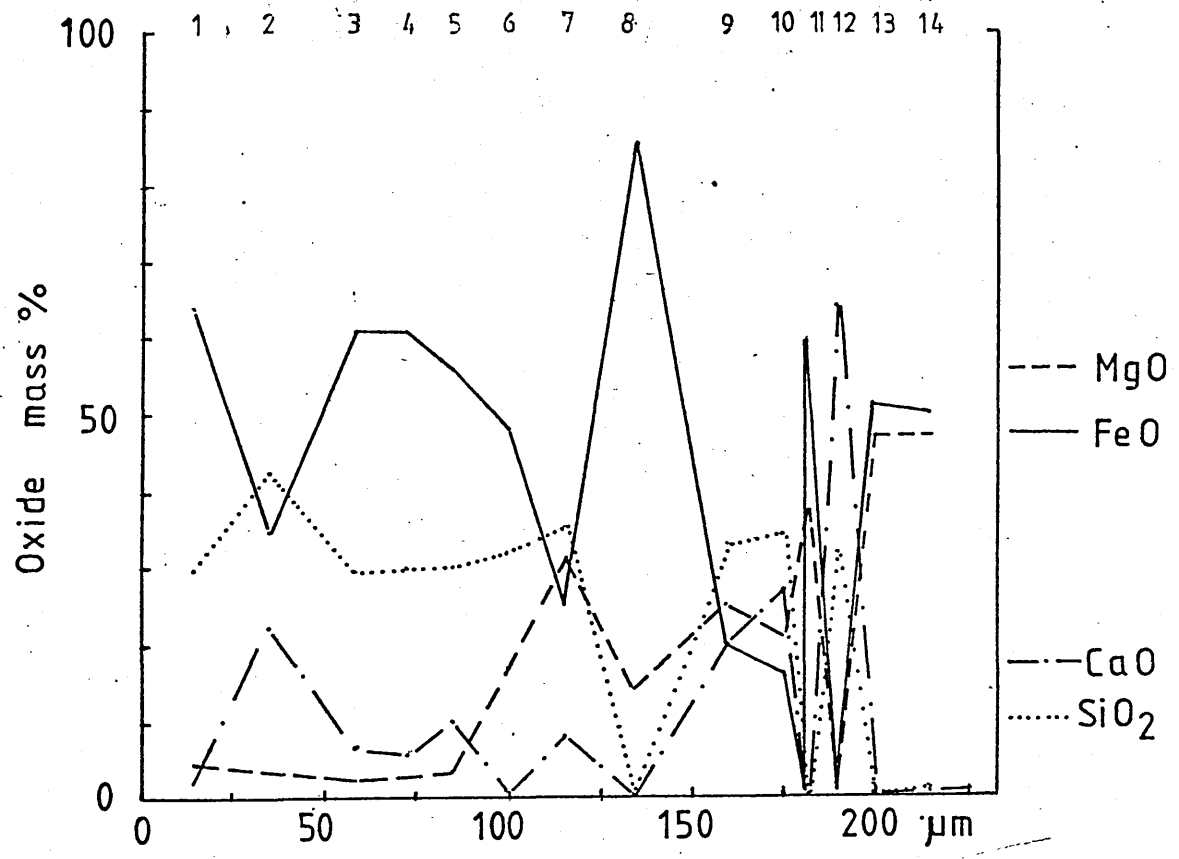

Melt		CYLINDER
F_2S (ℓ)	Globular F′ (s)	C_2S (s)
C-F-S olivine (ℓ)	Fo-Fa olivine (s)	MF′ (s)
	C-F-S olivine (ℓ)	

Plate 78 Immersion time, 120 s.

A SEM image representing the interface between an iron silicate melt and a static dolomitic lime cylinder. Numbers across the profile traverse line, denoted by the micrometre scale, represent analysis points. The concentrations of oxides in mass % across the reaction interface are plotted below the SEM photomicrograph. The profile analyses have been used to estimate the phase compositions occurring across the reaction interface.

120 sec. immersion at 1300 °C

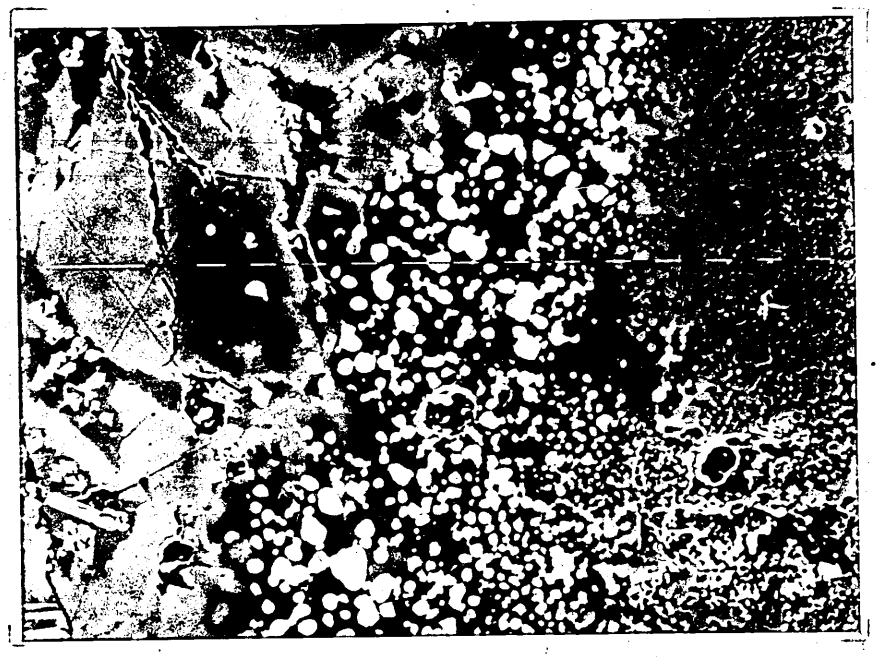

× 570

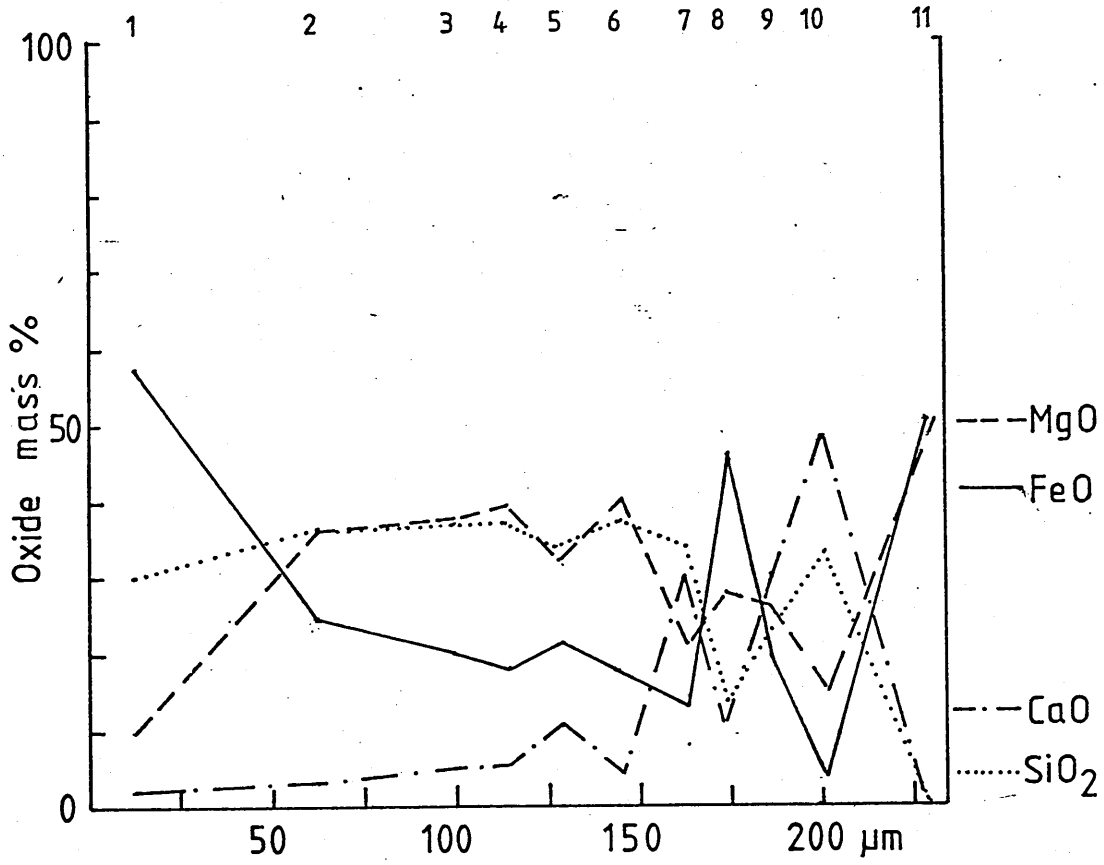

Melt		CYLINDER
F_2S (ℓ)	Globular F′ (ℓ)	C_2S (s)
C F S olivine (ℓ)	Fo-Fa olivine (s+ℓ)	M F′ (s)
dendritic F′ (s)	C-F-S olivine (ℓ)	

Plate 79 Immersion time, 360 s.

A SEM image representing the interface between an iron silicate melt and a static dolomitic lime cylinder. Numbers below the SEM photomicrograph refer to the analysis points which occur on the photomicrograph as black spots. The concentrations of oxides in mass % across the reaction interface are plotted below the Plate. The profile analyses have been used to estimate the phase compositions occurring across the reaction interface.

360 sec. immersion at 1300°C

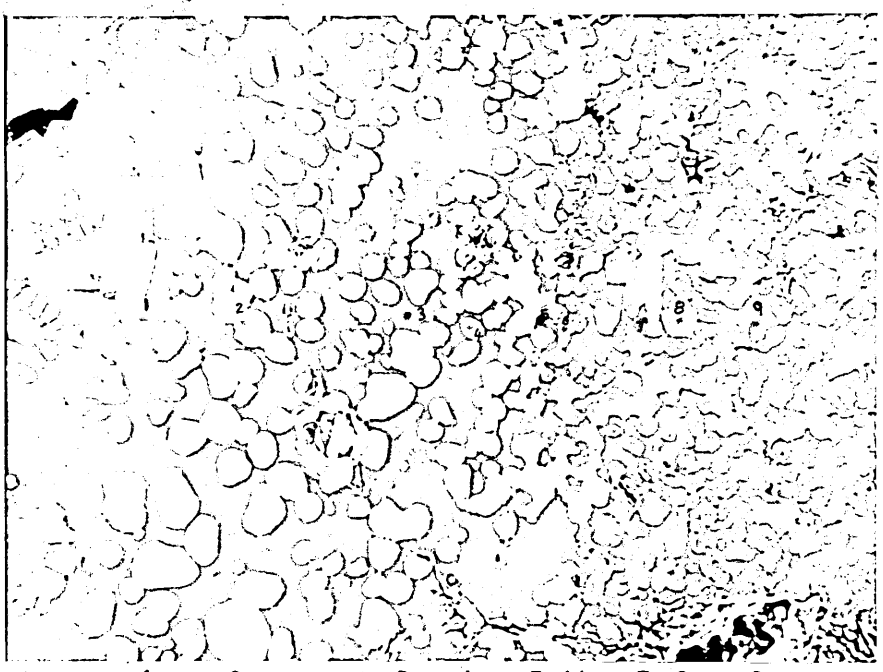

× 800

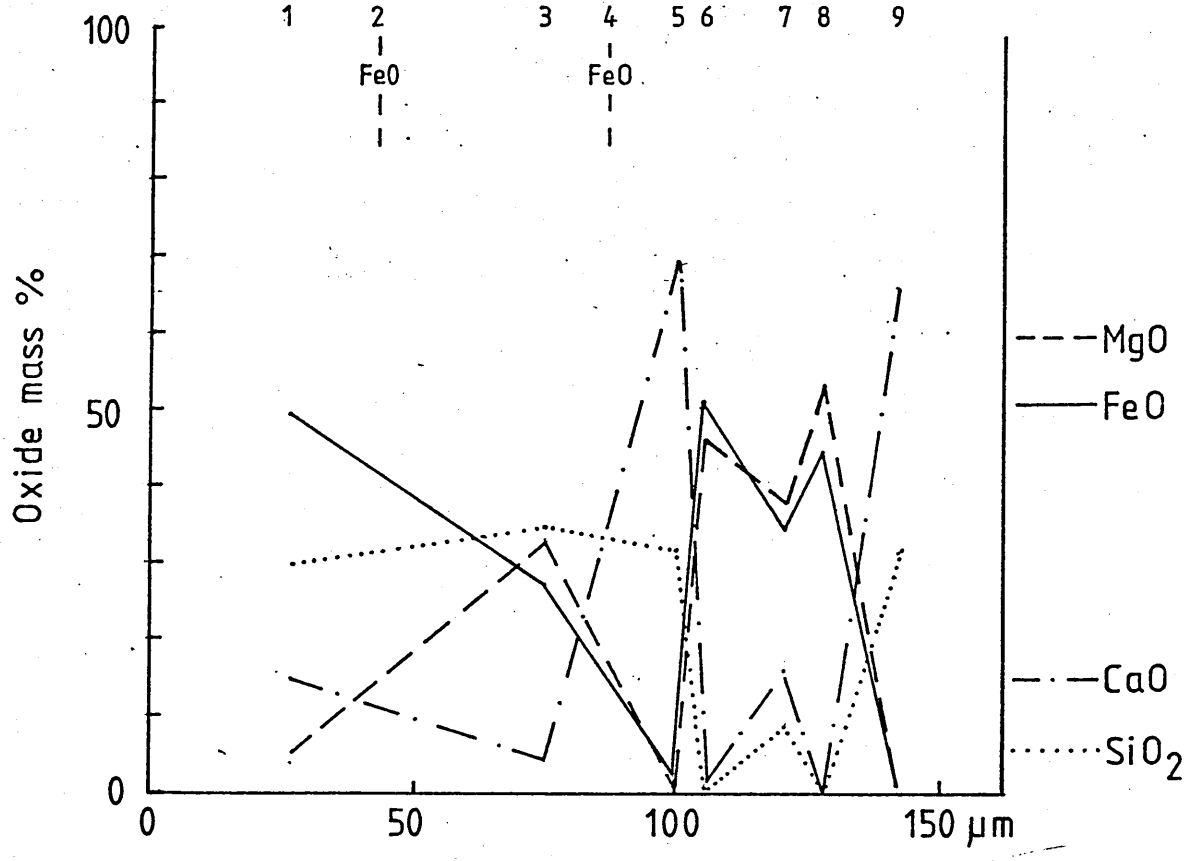

MELT		CYLINDER
C-F-S olivine(ℓ)	globular F´ (s)	C_2S (s)
Fo-Fa olivine	Fo Fa olivine (s+ℓ)	MF´ (s)
dendritic F´	C-F-S olivine (ℓ)	

Plate 80 Pill test.

A SEM image representing the interface between an iron silicate melt and dolomitic lime. Numbers on and below the photomicrograph refer to analysis points which appear as black spots. The mass % concentration of oxides across the interface are plotted below the Plate. The profile analyses have been used to estimate the phase compositions occurring across the reaction imterface.

Pill test. 25min. at 1300°C

Oxide mass%

■MgO

FeO

- CaO

- Si 0-

MELT | ^CYLINDER*

C-F-S olivines (I) I C2S (s)

Globular wustife(s) MF' (s)

Fo-Fa olivine (s+£)

Plate 81 Immersion time, 360 s.

5 mass % magnesia - iron silicate melt.

A SEM image representing the interface between an iron-silicate melt containing 5 mass % magnesia and a dolomitic lime cylinder. Numbers on and below the photomicrograph represent analysis points. The mass % concentration of oxides across the interface are plotted below the Plate. The profile analyses have been used to estimate the phase compositions occurring across the interface.

360 sec. immersion at 1300 °C

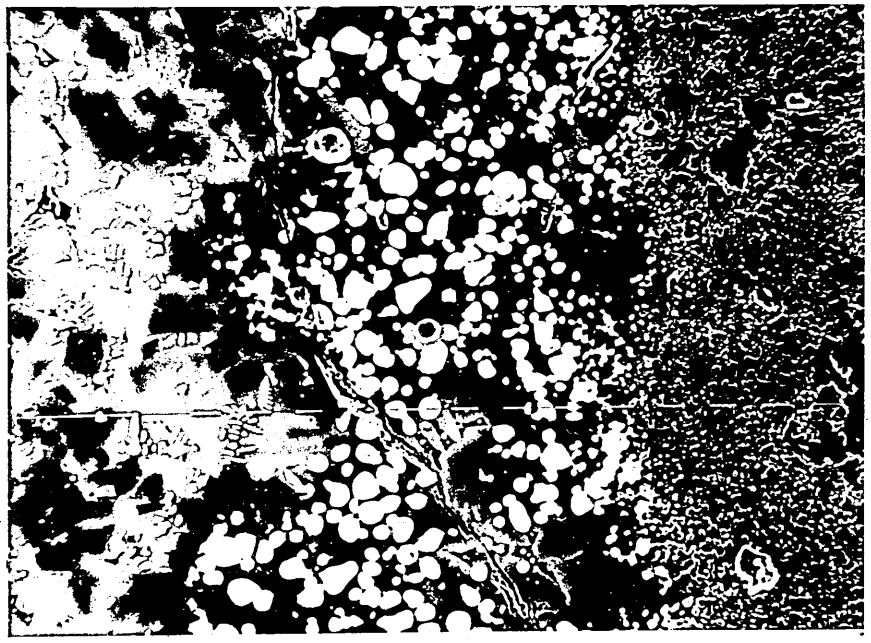

× 400

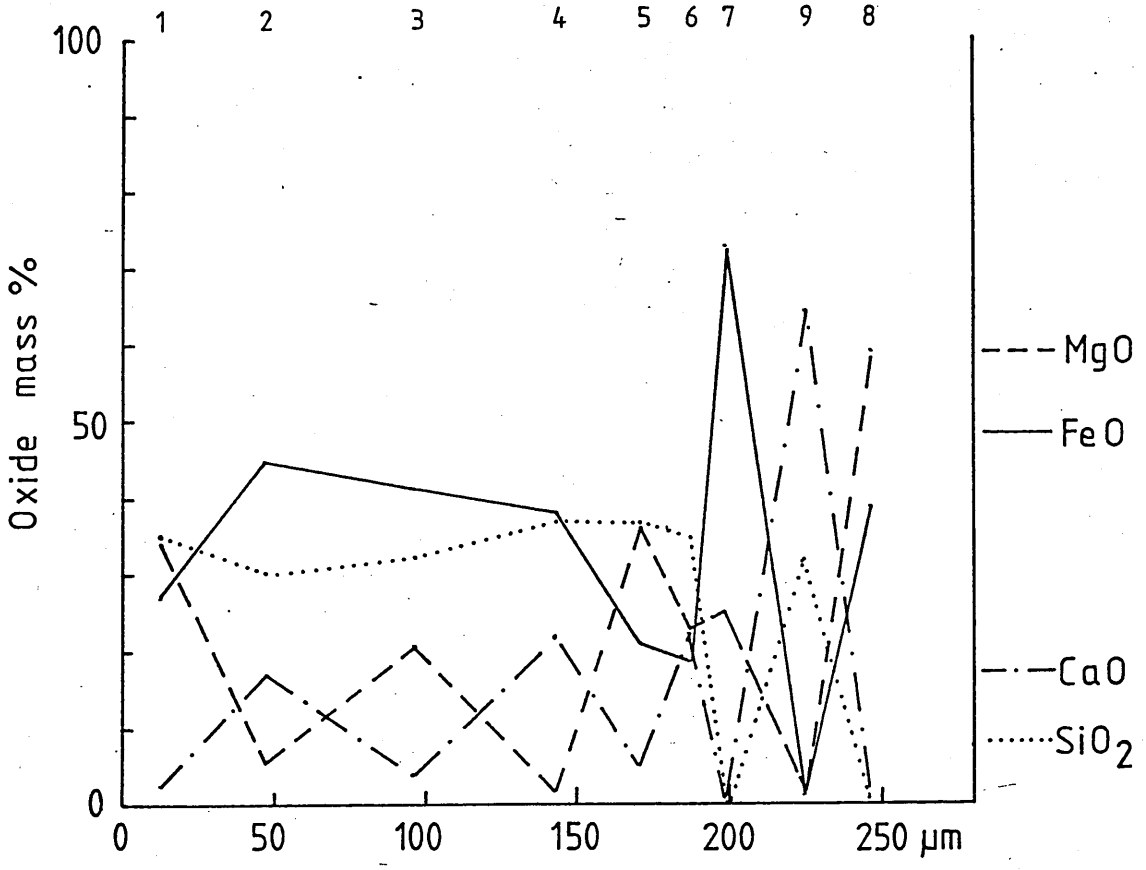

Melt		CYLINDER
C F S olivine (ℓ)	globular F´ (s)	C_2S (s)
Fo-Fa olivine (s+ℓ)	Fo-Fa olivine (s+ℓ)	M F´ (s)
dendritic F´ (s)		

Plate 82 Immersion time, 420 s.

"Hard" burnt dolomitic lime.

A SEM image representing the interface between an iron silicate melt and a "hard" burnt dolomitic lime cylinder. Numbers on and below the photomicrograph represent analysis points. The mass % concentration of oxides across the interface are plotted below the Plate. The profile analyses have been used to estimate the phase compositions occurring across the interface.

Hard burnt dolomitic lime
420 sec. immersion at 1300°C

x 880

Oxide mass %

CaO

SiO2

150 jjm

MELT

CYLINDER

C-F-S olivine (I)

globular F (s)

C2S (s)

Fo-Fa olivine (s+jl)

Fo-Fa olivine (s+2)

MF' (s)

F2S (l)

Plate 83 Immersion time, 15 s.

"Soft" burnt lime.

A SEM image representing the reaction interface between a lime cylinder and an iron silicate melt. The numbers below the photomicrograph represent analysis points which have been used to estblish the concentration profiles of oxides across the interface. The profile analyses have been used to estimate the compositions of phase assemblages.

15 sec immersion at 1300°C

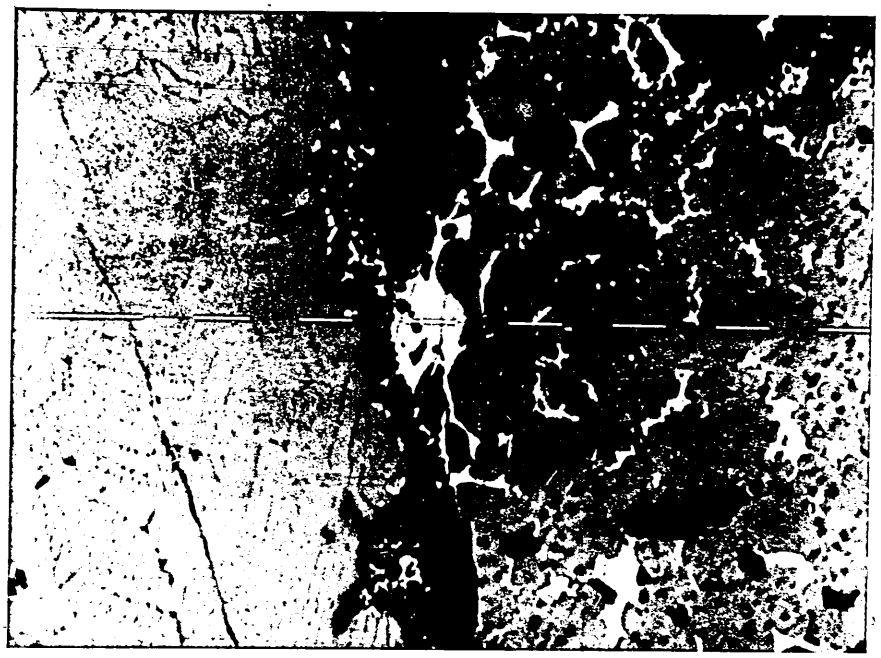

× 800

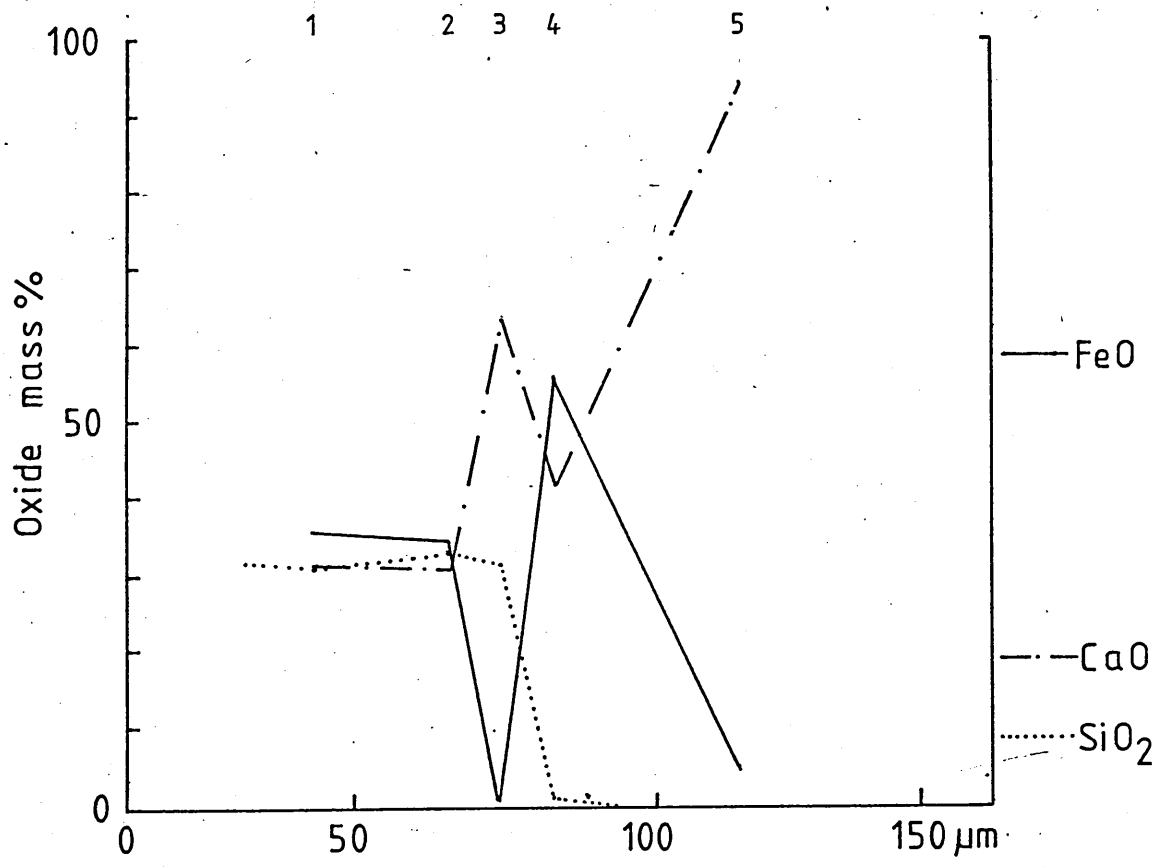

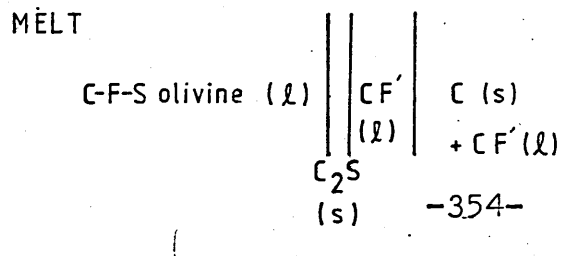

Plate 84 Immersion time, 540 s.

"Soft" burnt lime.

A SEM image representing the reaction interface between a lime cylinder and an iron silicate melt. The numbers below the photomicrograph represent analysis points which have been used to establish the concentration profiles of oxides across the reaction interface. The profile analyses have been used to estimate the compositions of phase assemblages.

540 sec. immersion at 1300 °C

×440

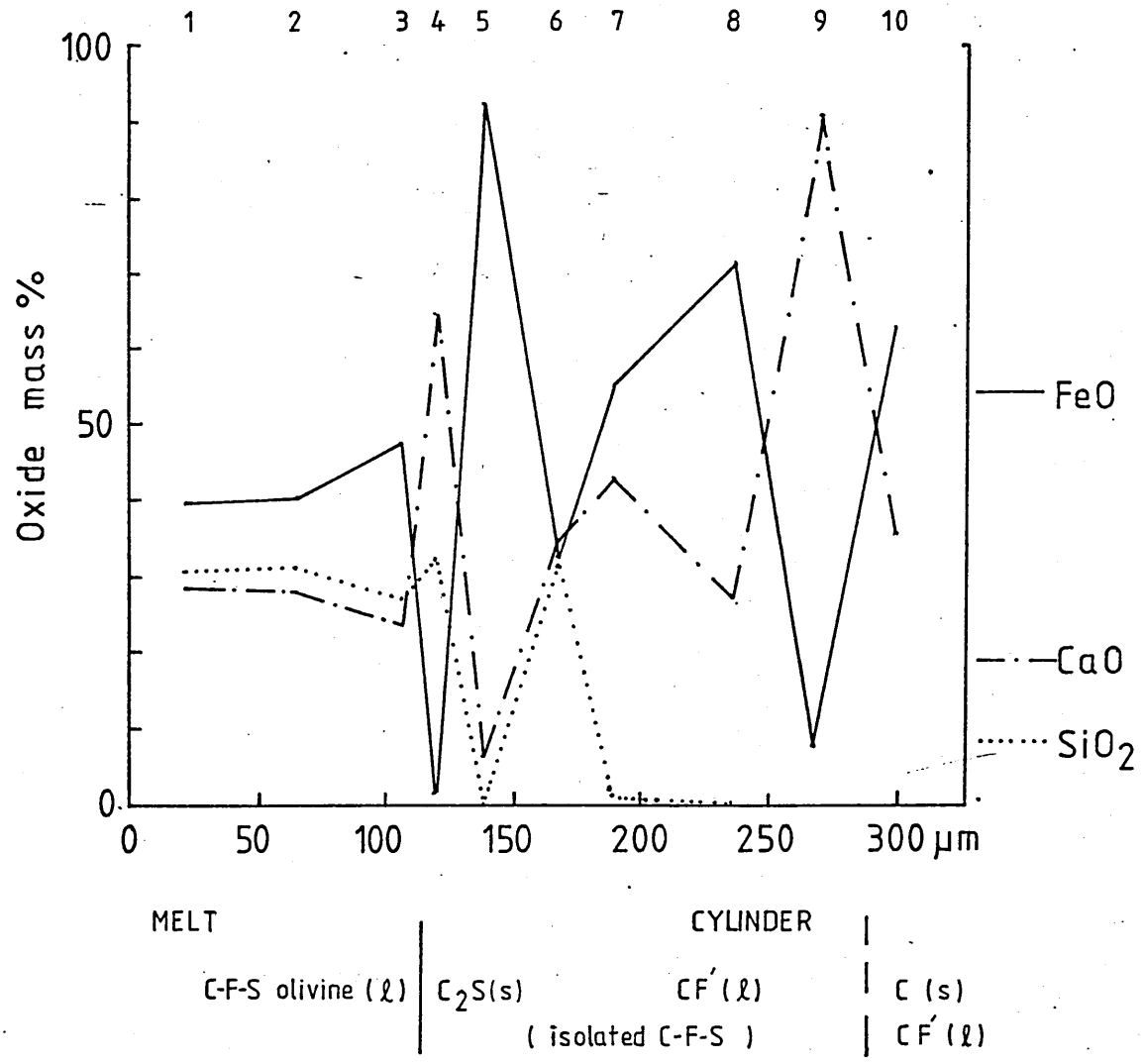

MELT | CYLINDER

C-F-S olivine (ℓ) | C_2S(s) CF′(ℓ) (isolated C-F-S) | C (s) CF′(ℓ)

Plate 85 Immersion time, 15 s.

"Soft" burnt lime.

A SEM image representing the reaction interface between a lime cylinder and a 5 mass % MgO - iron silicate melt. The numbers below the photomicrograph represent analysis points which have been used to establish the concentration profiles of oxides across the reaction interface. The profile analyses have been used to estimate the compositions of phase assemblages.

15 sec immersion at 1300

x 1320

Oxide mass

Fe0

Si 0

MELT **CYLINDER**

C F S olivine II) I C2S (sI C (s)

C3S($) CF'U)

F' dendrites C?'I 1)

Plate 86 Immersion time 360 s.

"Soft" burnt lime.

A SEM image representing the reaction interface between a lime cylinder and a 5 mass % MgO - iron silicate melt. The numbers below the photomicrograph refer to analysis points which have been used to establish the concentration profiles of oxides across the reaction interface. The profile analyses have been used to estimate the compositions of phase assemblages.

360 sec immersion at 1300°C

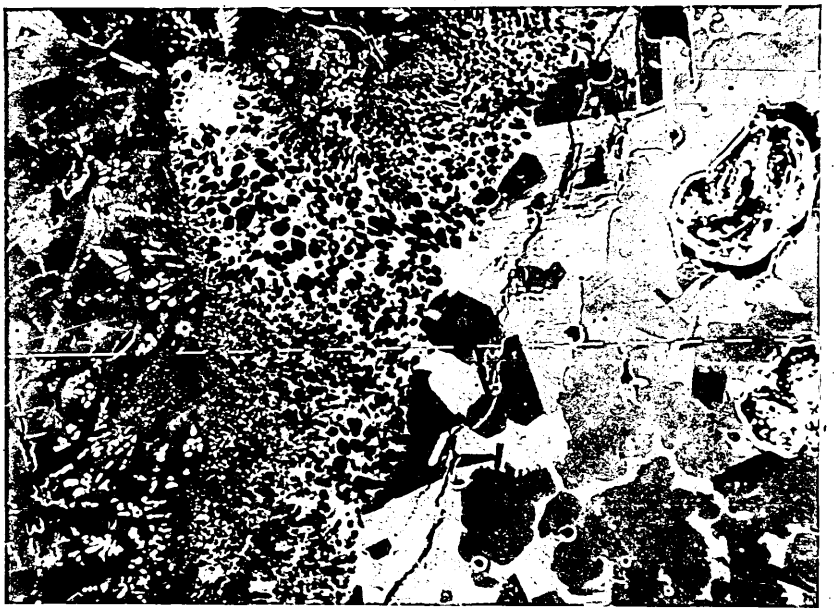

×440

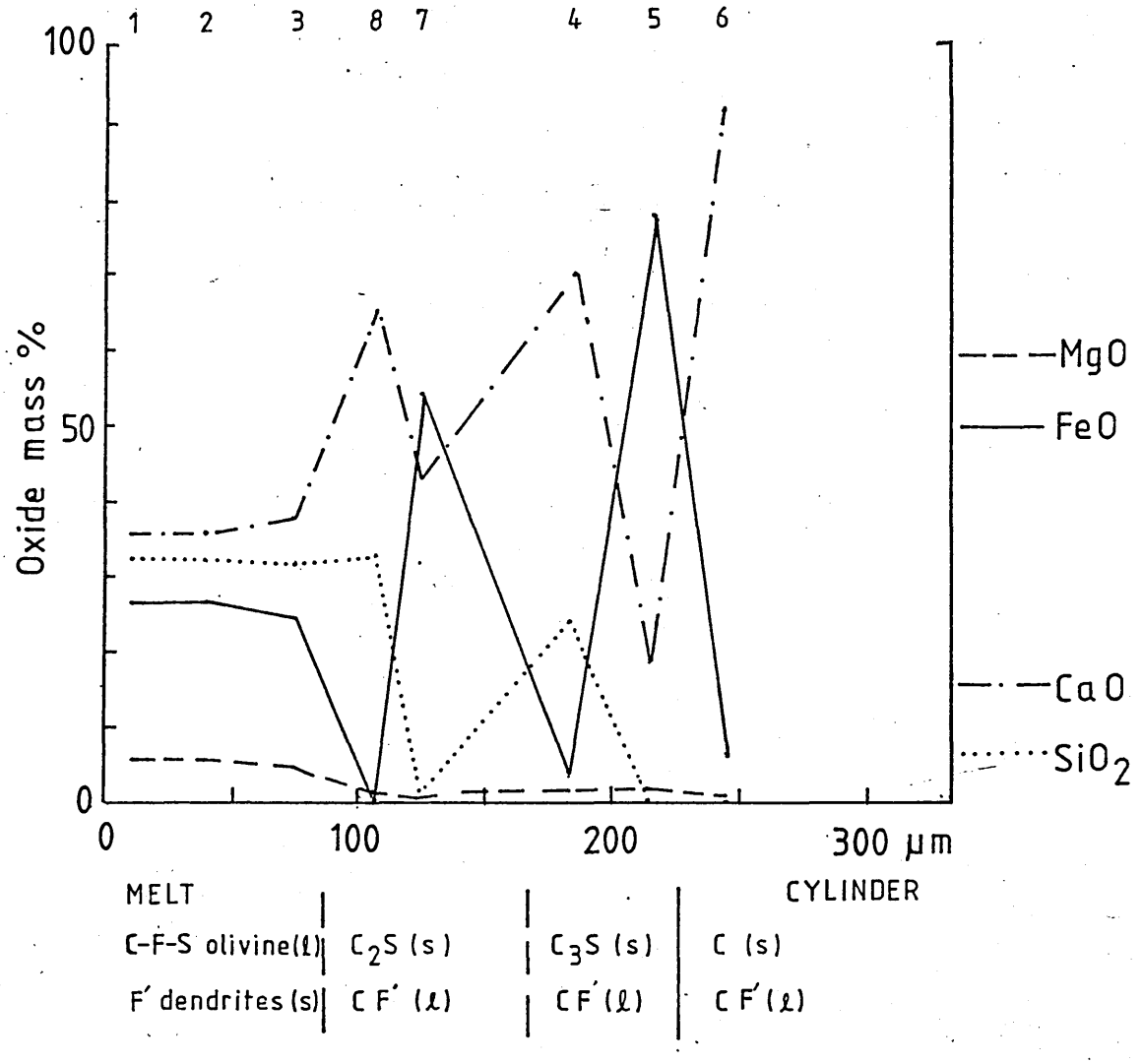

Plate 87

A 15 mass % MgO - 13 mass % CaO - iron silicate melt quenched from 1342°C into water. The globular phase represents a sub-liquidus phase (pale grey) which has acted as a nucleation site for the athermally cooled liquid from which dendritic wüstite precipitated. The matrix comprises of a calcic - olivine (dark grey) showing slight prismatic habit and zoned margins. There is no visible evidence of undissolved magnesia.

Cone sample 15MCF13 (Table 35 p. 258)

Mag. x 170

Plate 88

A 10 mass % MgO - 20 mass % CaO - iron silicate melt quenched from 1342°C into water. Only a small proportion of solid globular wüstite phase is present within a generally homogeneous liquid melt which has athermally cooled to crystallise dendritic wüstite (pale grey) and calcic - olivine (dark grey). The white globules associated with globular wüstite are metallic iron. The matrix has a lathe-like habit (dark grey).

Cone sample 10MCF20 (Table 35 p. 258)

Mag. x 170

Plate 89

A 15 mass % MgO - 32 mass % CaO - iron silicate melt quenched from 1342°C into water. An essentially sub-liquidus phase assemblage is illustrated. The clusters of globules represent a magnesiowüstite -solid solution (pale grey).

Cone sample 15MCF32 (Table 35 p. 258)

Mag. x 170

8. The case study for Ph.D in Industrial Metallurgy:-

To assess the feasibility of the use of dolomitic lime in addition to calcitic lime in the LD process. The factors influencing the feasibility will include the supply of suitable materials, the efficiency of the process and the overall economics.

Introduction

Iron ore used in the United Kingdom contains typically 25 pct iron for local ores and 62 pct iron for imported ones.[1] After reduction in the blast furnace, phosphorus is retained in the pig iron in addition to sulphur, carbon, manganese and silicon. Conventional steelmaking requires that the unwanted metalloids are oxidised and removed via a slag phase which is liquid at steelmaking temperatures, easily removed at the end of the steelmaking process and is compatible with the refractory lining of the furnace. The lining life of a steelmaking furnace will ultimately determine the overall availability and possible economic viability of a process. The desired aim being to produce more or less continuously the correct grades of steel with a minimum of furnace downtime.

Over 50 pct of current U.K. steel production is produced by the top blown oxygen converter or LD process.[1] Oxygen being used to initiate the largely exothermic oxidation reactions of the metalloids within the bath through the transfer of O^{2-} anions from FeO generated within the slag phase. Examination of a standard free energy - temperature diagram for oxides, Fig. 1, illustrates that there would be a likelihood of converting much of the iron charge within the bath to FeO whilst attempting to oxidise phosphorus to P_2O_5. This problem is overcome by using a basic slagmaking phase, consisting primarily of burnt lime (CaO) which produces a marked lowering of the activity of P_2O_5 within the slag.[2] The presence of a basic slag also favours the partition

of sulphur from the bath to the slag [3,4] whilst the rapid oxidation of silicon forms stable calcium silicates in the presence of CaO as indicated by Fig. 2.[4] Compatibility between the slag and refractory lining is achieved by using either doloma or doloma-magnesia refractories. In order to improve vessel lining lives and process control, improvements have been made to hot metal and scrap qualities, refractory linings, lance practices and slag chemistry. It is against the background of slag chemistry that the feasibility of dolomitic lime usage has been developed.

The Steelmaking Plant

Since the early 1970's the oxygen or LD converter has become the major production route for tonnage steel.[1] Large LD shops in four or five main centres are likely to produce the required tonnages. As a framework for discussion it has been assumed that a 3 x 300 T vessel shop is about to come on stream and has to consider a choice of refractory lining materials and slagmaking practices. To derive certain figures necessary to the discussion a schematic production route has been drawn up offering a choice of heats per vessel per day, an annual target production figure per vessel and a selection of lining and slag-making materials Fig. 3.

If a 300 tonne vessel is operated continuously for one year, the maximum tonnages of steel produced at 10, 15 or 20 heats per vessel per day would be 1.1, 1.64 and 2.2 million tonnes, respectively. Using the theoretical values and setting annual production targets of 0.75, 1.125 and 1.5 million tonnes per vessel respectively, an

estimation may be made of the maximum number of relines permitted to achieve these target figures. This may be done by using a particular reline-downtime period. For a small vessel (100 T), Hardy [5] has indicated that approximately 8 days are required to fulfill the following reline operations.

	Operation	relative percentage of time taken
(a)	Cool down	9%
(b)	Tear out	7
(c)	Reline	80
(d)	Burn in	4

For a 300 tonne vessel the above sequence of operations is chosen to be 10 days. For each reline period there will be a potential production loss on the number of daily heats specified amounting to 30000, 45000 and 60000 tonnes of steel respectively. By plotting the number of relines against theoretical and target tonnages, an estimate of the heats required from the vessel lining can be extrapolated. Figure 4 illustrates these various plots and indicates that for the operations A, B and C, 12 campaigns are required to achieve production targets. This may be translated to heats required of the lining as follows;

	Operation	heats required from lining	with 5 pct safety factor
A	20 heats/vessel/day	416	415
B	15 " " "	312	312
C	10 " " "	200	190

The plant management could then conceivably be faced with two courses of action.

(a) How to increase target steel production.

(b) How to increase overall vessel availability as a means of reducing costs on existing levels of production.

A reduction of tap to tap times would allow more heats per vessel per day to be made but would reduce the campaign period. This may compromise relining operations especially if a vessel was taken off through premature lining failure. Running a 2 from 3 vessel operation may even become impossible. Alternatively, the lining life could be extended by the selection of a relevant refractory material or through a slagmaking practice that reduced the refractory consumption per tonne of steel produced.

For any of the specified A, B or C operations, it will be self evident that either an increase in lining life or decreased reline downtime will lead to a potential increase in vessel availability. However, there will be a practical limit to the amount of reduction in reline downtime. No such constraint is placed on an increase in lining life.

The lining of a LD vessel is limited by four properties [6]

(i) Resistance to impact in the charge pad area

(ii) Resistance to thermal stress

(iii) Resistance to early silica-rich slags

(iv) Resistance to early ferruginous slags.

A typical wear pattern of an LD vessel is illustrated in Fig. 5. The trunnion areas are prone to wear through mechanical stresses set up during vessel manoeuvres. The charge pad has to withstand the impact and

mechanical abrasion from charged scrap whilst the tap hole suffers high temperature wear from liquid steel plus additional attack from slag residue which may remain on completion of tapping. In the United Kingdom, LD vessel linings are fabricated from either tempered doloma or tempered magnesia enriched doloma[7]. Figs.6 and 7 illustrate typical U.K. LD lining practices. The lower barrel section is often reinforced at the slag line as illustrated to compensate for the increased wear rate through slag attack at this particular point, producing an even, overall refractory wear pattern. Composite linings utilising varying brick compositions can be used as an alternative method of increasing refractory life [8], Fig. 8. Typical lining lives and refractories consumption for LD vessels may be estimated from Figs.9 and 10. For doloma refractories a lining life between 200 and 320 heats could be considered typical for large vessels. Figure 9 suggests that 290 heats per lining would be an average figure with a refractory consumption of 6 kg/tonne steel (Fig.10). A composite lining would give about 420 heats with a refractory consumption of 5 kg/tonne steel. Magnesia linings, although relatively uncommon may produce 700 or more heats per lining with a refractory consumption of 3.2 kg/tonne steel. The apparent lack of popularity of magnesia based linings could be due to the fact that through limited hot metal supply and reduced steel output, cheaper linings are more than able to cope with demand. A comparison of relative refractory brick costs may be made with reference to Fig. 11. The change of slope of magnesia refractory costs as opposed to doloma suggests that current

price indexes will be between 3 and 4 for magnesia types compared to 1 for doloma if relative prices are calculated from the 1975 upturn. Tempered magnesia rich doloma would be approximately 1.8 to 2.4 on this index, depending upon the degree of magnesia enrichment. Having derived some estimations on refractory lining lives and relative costs it should be possible to predict the behaviour of these linings whilst in contact with typical LD slags at steelmaking temperatures.

The Resistance of LD Refractories to slag attack

The composition of LD steelmaking slags is such that they may be discussed either in terms of the $CaO-Fe_2O_3-SiO_2$ system in air or the system $CaO-FeO-SiO_2$ in contact with metallic iron.[3][8] Slag turndown temperatures are also in the region of 1620 to 1630°C so that it is possible to study the solubility of basic bricks with reference to the 1600°C isotherm for the system MgO-CaO-FeO in contact with metallic iron. A notional pseudo ternary-type diagram of the MgO-CaO-FeO system can be constructed from the binary systems CaO-MgO, MgO-FeO and FeO-CaO [8], Fig. 12. A plant operating a low carbon, dead mild steel practice would have a turndown slag containing between 41 to 50 pct CaO, 18 pct FeO and 12-13 pct SiO_2. The CaO, FeO composition may be scaled up in relative proportions to fit the CaO-FeO side of the diagram and be represented by the point S. In weight pct terms, doloma bricks have a composition close to 40 wt pct MgO and 60 wt pct CaO [6] and would be represented by point D in Fig. 12. A magnesia brick is assumed to have a composition indicated by M on the apex of the triangular diagram. The solubility

of a particular brick type or relative resistance to slag attack can be determined by constructing tie lines from M and D to S, to intersect the 1600°C isotherm at points A and B respectively. The solubility when expressed as a percentage is illustrated by reference to the simple sections in Figures 13A and 13B. From a refractories selection viewpoint for the plant in question, magnesia linings should be approximately three times as resistant to slag attack as doloma bricks at the corresponding temperatures of 1600°C. Raw materials impurities within the various brick types could affect this comparison to a limited extent. In practice, the lining life of a magnesia refractory may only be twice that of a doloma one.(6) Bearing in mind the three times higher cost of a magnesia lining, the cheaper doloma lining could be more cost effective if a limited quantity of steel is produced. Magnesia enriched doloma bricks would give a corresponding decrease in brick solubility if the above exercise was applied. However, as a doloma brick suffers slag attack through the dissolution of the lime phase it is difficult to imagine how any additional magnesia grain could retard solution.(7) Dissolution of the lime containing matrix would allow the "grains" of magnesia to be "washed" out into the slag. Resistance to slag attack for tar bonded bricks can be related to data derived on LD lining lives which gave the following type of relationships when tar bonded doloma was taken as unity.(7)

Tar bonded doloma	1
Tar bonded magnesia enriched doloma (60-65pctMgO)	1.3
Tar bonded magnesia	1.5-2.0

Tar impregnated fired high purity magnesia (low B_2O_3), >3-4.

The solubility of magnesia in LD steelmaking slags.

The rapid formation of an LD slag is largely dependant upon the generation of FeO to flux or dissolve the lime charge. The rate of solution of lime has been shown to vary throughout an LD blow.[9][10] The marked decrease in the lime solution rate during the first 20pct of the blow is due to the formation of a solid dicalcium silicate cortex around the lime particles. A flux such as fluorspar is added to accelerate lime dissolution by modifying the morphology or lowering the melting point of the dicalcium silicate cortex. Since silicon is oxidised into the slag very rapidly[3], the early formed slag becomes relatively siliceous once the lime-dicalcium silicate saturation limit has been reached. These early formed slags will therefore become potentially aggressive towards basic linings due to the large chemical gradient between magnesia from the refractory and the slag. Under equilibrium conditions, the solubility of magnesia in $CaO-FeO-SiO_2$ slags has been determined at 1600°C.[11][12] By superimposing a series of slag paths such as those proposed by Baker[10] onto the magnesia solubility diagram, it becomes possible to assess magnesia solubility as a function of the lime to silica ratio. The lime to silica or V-ratio may be used as a measure of blowing progress during an LD heat. Figure 14 illustrates such a diagram with the desired slag end point indicated by the dashed circle. If a good slag path is achieved, the developing slag will bring about the required amount of dephosphorisation and desulphurisation. The solid line in Fig. 14

represents a dry slag path where FeO values are low and slag basicities correspondingly unsatisfactory for phosphorus removal. The short dotted line represents a slag path high in iron oxide (FeO) which produces fluid slags that slop heavily during the decarburisation period. Slopping conditions result in varying losses of metallic yield. By plotting the intersection of each slag path with magnesia iso-solubility lines, each point can be fixed by reference to a particular slag V-ratio. The magnesia solubility can then be plotted against the V-ratio as in Figure 15. At a low V-ratio all the slags will be very aggressive towards a basic (magnesia) lining even in the absence of a true brick-slag equilibrium. It is apparent from Fig. 15 that the relative solubility of magnesia decreases rapidly during the blow as more lime is dissolved and the V-ratio increases. A typical LD turn down slag has a V-ratio of 3 to 3.2 and a magnesia content of 4 to 6 wt pct could be expected. Workers [13] have indicated that the specific aggressiveness of the slag towards the lining is very high in the first 12 pct of the blow. In the latter part of the blow, an increase was observed again due to an increase in the FeO content occurring after the main decarburisation period.

To reiterate some of the above points, the selection of a particular refractory lining will depend upon the required rates of steel production or vessel availability. Magnesia linings should have about three times the resistance to slag attack as doloma linings. Magnesia linings are in addition three times as costly as doloma linings yet in service may give only twice the required lining

life. The solubility of magnesia in LD slags at 1600°C is potentially very high during the early part of an LD blow and the turn-down slag may contain between 4 to 6 wt pct because of this. Clearly, the next logical step would be to reduce the wear of basic refractories by pre-doping the early formed slag with magnesia. The simplest method of doing this is to modify the slag practice by replacing some of the lime charge with dolomitic lime. What this means in terms of cost effectiveness will be examined in the next section.

Slag practices.

With reference to Fig. 3, three slag practice alternatives can be considered.

(a) Lime + spar practice

(b) Lime + dolomitic lime + spar practice

(c) Lime + dolomitic lime practice

Gunning is an additional possibility for any of the practices either from an emergency or programmed point of view. However, to simplify the slag practices from a materials cost aspect, gunning will be considered separately. Slag materials costs can be added to refractory costs to estimate and compare the relative feasibility of each practice. Refractory costs will be based upon the lining cost divided by the total metal throughput. The total metal throughput may be derived in terms of lining lives multiplied by the quantity of good ingot tonnes of steel produced. For a particular slag and refractory practice the cost per tonne of steel can be worked out from a simple relationship such as:

$$Rc = \frac{Lc}{Ll.M.} + Sp.$$

where

Rc = Total cost of refractory and slagmaking practice

Lc = lining cost

Ll = lining life

M = average tonnage of steel produced (good ingot yield) per cast

Sp = slagmaking costs

Trials carried out at Port Talbot from 1971/2 have used the above approach whilst comparing various types of slag practice [14]. The economic break even point was established when

$$\frac{Lc}{Ll \times M} + Sp = \frac{Lc}{Ll^N \times M} + Sp^N$$

Standard practice New practice

A brief resume of the Port Talbot trial will be outlined as follows:

Flux costs	1972 (as delivered)
Lime	£6.07 per ton
Dolomitic lime	12.30 " "
Fluorspar	13.92 " "
Average hot metal Si	0.85 pct
Average good ingot yield per cast	300 ton.

Lime addition calculated from hot metal analysis was reduced by 0.46 x weight of dolomitic lime used.

	Practice	Quantity (Tons)	value (£)
(a)	Lime + fluorspar	Total lime 22.2	134.89
		spar 0.61	8.49
			143.38
	Cost per good ingot ton		0.48

(b) Lime + dolomitic lime + fluorspar

Total lime	20.3	123.34
Dol-lime	4.0	45.20
spar	0.61	8.49
		181.03
Cost per good ingot ton		0.60

The use of soft burnt dolomitic lime as a partial replacement for lime at a rate sufficient to give 4 to 5 pct MgO in the turndown slag had improved converter lining life at Port Talbot by 30 pct [14]. To ensure satisfactory sulphur and phosphorus removal within the standard blowing time, fluorspar additions were maintained at past levels (2 kg/t.s.). From a materials cost basis dolomitic lime additions involved an increase in cost from £0.48 to £0.60 per ton of steel. However, the increased cost was offset by a corresponding increase in the lining life of the vessel.

A similar approach to that used above can be done to assess the feasibility of dolomitic lime usage in respect of the alternative practices outlined in Fig. 3 but using current prices of slagmaking raw materials. Although prices may vary through delivery costs the prices of slagmaking materials are approximately as follows:

Lime	£20	per tonne	
Dolomitic lime	£30	" "	
Fluorspar	£30[15]	" "	75 pct CaF_2

Dolomitic lime is supplied under the trade name "Dolomet" and has a specification as follows; CaO 57 pct, MgO 39 pct, SiO_2 1.0 pct, S 0.05 (max), Fe_2O_3 1.35 pct. For the estimation of total lime in the slag practice, the composition

of Dolomet will be taken as 40 pct MgO and 60 pct CaO. For a plant operating under condition C (Figs. 3,4) the hot metal silicon content is assumed to be similar to that of Port Talbot's i.e. 0.85 pct Si, so that the same slag charge tonnages can be used. The slagmaking operation costs may be determined as before.

Practice	Quantity (Tonnes)	cost £
(a) Lime - fluorspar		
Total lime	22.2	444
spar	0.61	18.3
		462.3
Cost per good ingot tonne		£ 1.54
(b) Lime + spar + dolomitic lime		
Total lime	19.8	396
Dolomitic lime	4.0	120
spar	0.61	18.3
		534.3
Cost per good ingot tonne		£ 1.78

Assuming that practice C gives 190 heats on a standard practice and is lined with doloma costing £35000 per lining, it becomes possible to plot a series of cost curves for a standard and dolomitic lime practice, Fig. 16. The curves are derived by plotting the refractory and slagmaking costs against the lining life. To achieve a materials break even cost the lining life would have to be extended from the standard practice of 190 heats to 316 heats using dolomitic lime. This would represent a 66 pct increase in terms of lining life and is far above the 30 pct increase described at Port Talbot [14]. If the distance x in Fig. 16 represents the average increase in

lining life extension due to dolomitic lime addition, the "extra cost" of this slagmaking practice will be materials and refractory costs used in 69 heats. Taking an average cost of £2.20 for the refractories and slagmaking materials used per tonne of steel, the "extra cost" in using dolomitic lime would be £45540. However, the 30 - 33 pct increase in lining life through dolomitic lime usage requires only 10 relines per year to meet the 0.75 million tonnes of steel production target. The savings in actual refractory costs will then amount to £70 000. This more than covers the additional dolomitic lime slagmaking costs. In addition, the gaining of 20 days production through decreased downtime allows either an extra 60000 tonnes of steel to be produced or a greater safety margin in bringing vessels back on stream in 2 or 3 vessel operations. With the above particular practice it would be a short-sighted view if materials costs were used solely to judge the feasibility of a dolomitic lime practice.

Additional benefits of dolomitic lime practices may be found in the literature but there is no obvious way of assigning a cost figure to them. The possible effects of dolomitic practices may be considered briefly under three main headings;

(i) Factors affecting lining life.

(ii) Factors that affect the refining character of LD slags.

(iii) Factors that have led to a saving in lime fluxes.

(i) Factors affecting lining lives.

(a) The addition of dolomitic lime reduces the chemical gradient between the slag and refractory lining.

(b) Dolomitic lime addition may increase slag viscosity thereby reducing slag penetration into the refractories especially at low slag V ratios.[16]

(c) Dolomitic lime acts as a lime flux by increasing the rate of lime solution, resulting in a decreased acid slag/refractory contact time.[17][18]

(d) The increased MgO component of the slag could reduce the iron - oxygen equilibrium such that the iron oxide content is reduced.[16] An increase in metallic yield would be the result.

(e) At 5 to 7 pct MgO in the slag, lower slag fusion temperatures may result and through decreased slag viscosity, increase the slag development rate.

(f) Dolomitic lime may retard dicalcium silicate formation on lime particles.[19]

(ii) Factors affecting the refining character of LD slags.

(a) Difficulties in meeting sulphur specifications have been reported in some American practices.[20] At the moderate MgO concentrations used in this country, 6 - 7 pct, no adverse problems have been reported.

(b) With high hot metal phosphorus heats problems were met with end point P values when dolomitic lime was used in the slag charge.[16] Plant trials suggest that with normal hot metal phosphorus charges, loss of efficiency in P removal occurs only above 8 pct MgO in the turndown slag.[21]

(iii)Factors that have led to a saving in lime fluxes.

Magnesia has the apparent ability to flux lime, and modify or even depress the formation of calcium silicates around the lime particles, allowing a considerable saving

in fluorspar and other fluxes to be made. It has generally been established that dolomitic lime can reduce fluorspar consumption by 30 to 60 pct[17,18] whilst some practices have been able to replace fluorspar additions totally with dolomitic lime.[21][22]

The role of fluorspar as a metallurgical flux has changed over previous years through increased prices and environmental factors connected with fluorides. The decrease in fluorspar consumption since 1970 may be illustrated as follows;[23]

5 to 6 kg / tonne steel 1970

3 to 4 kg / " " 1975

± 2 kg / " " currently

No fluorspar practice in Japan.

The above trend is probably due to improved process control and possibly to the increase in dolomitic lime usage. Recent demand for 80 - 85 pct CaF_2 metspar grades will undoubtedly increase fluorspar raw material costs. From a fluorspar flux substitute aspect, dolomitic lime appears to be a logical choice.

Gunning costs.

Scheduled or programmed gunning has been described as another method of increasing vessel availability.[6] However, continuity of production may be interrupted for between 25 - 35 minutes to allow for cooling down and the actual gunning process. Doloma linings may be increased by 18 to 30 pct at very little extra cost[6], although dolomitic lime would be a cheaper way of increasing the MgO slag content as it costs approximately 5 times less than that of gunning material. Gunning is apparently

more successful with the expensive magnesia linings, and if used in conjunction with a dolomitic lime practice, appears to adhere much easier onto the sidewalls of the vessel (Quin, J. private communication). Consumption of gunning material is between 0.29 and 0.3kg per tonne of steel. Tempered and fired magnesia refractory campaigns are currently underway with programmed gunning and a dolomitic lime practice of 18 - 20 kg/tonne steel. Lining life has been increased using this joint practice but no information regarding campaign life or refractory costs has been released.

American dolomitic lime practices.

In the U.S.A. the high degree of utilisation of magnesia refractory LD linings compared with Western Europe has generally been associated with a price ratio less favourable to doloma and also to the problems of doloma transport over large distances.[24] As a means of reducing the refractory wear rate, soft burnt dolomitic lime has been used in most operations since 1963. The proportion of dolomitic lime charged has ranged from 10 to 35 pct of the flux charge up until 1970[16]. From 1970 the consumption of dolomitic lime has stabilised at 20 to 25 kg/tonne of steel. Fixed slag weight additions of dolomitic lime were made initially through statistical studies on lining lives[10]. A typical magnesia and lime mass balance in the slag is illustrated in Table 1. Utilizing this approach, it was found that MgO in the slag reaches a maximum of 7.4 pct at a $^{D}/_{B}$ (dolomitic lime/lime ratio) of 0.36 and that MgO pick up from the refractory is countered by that of dolomitic lime addition. Using this

scheduled dolomitic lime addition an increase in lining life of 40 pct was reported. A study of dolomite additions required to saturate LD slags with MgO has been carried out by Leonard and Herron[12]. The equilibrium solubility data indicated that the addition of MgO to the furnace in amounts equal to between 4 and 6 pct of the liquid top slag weight will provide sufficient MgO to saturate the slag throughout the blow. Differing slag weights for various grades of steel led to variable percentages of MgO levels in the top slag which meant that optimum magnesia charges were impossible to determine. An empirical formula was developed that allowed the maximum weight of liquid slag to be determined and ultimately the weight of dolomitic lime required in the charge. These formulas were:

1) $$\frac{\text{CaO lb} + \text{SiO}_2\text{ lb}}{100\% - \%\ \text{oxides} - \%\text{FeO}} \times 100 = \text{Max total liquid slag lb}$$

2) $$\frac{\text{Max Total liquid slag lb} \times \text{desired MgO\%}}{\text{MgO in dolomitic lime}} = \text{Dolomitic lime charge lb}$$

It was assumed that the liquid portion of the slag would seldom exceed a lime - silica ratio of 3, and that the sum of the oxides, other than CaO, SiO_2 and FeO remained constant at 12 pct for this ratio. To calculate the estimated maximum liquid slag weight the hot metal weight, silicon level and slag FeO levels were required. Balla and Beechan[25] developed the above approach for the efficient use of dolomitic lime in LD operations at Bethlehem steel. The hot metal weight and silicon levels were known and a study of slag analyses obtained over a six month period showed variable slag FeO levels which could be correlated with the carbon level in the steel. Maximum FeO levels

were therefore used for a range of aim carbons and these are illustrated in Table 2. An example of a dolomitic lime-type calculation may be illustrated using the 0.07 — 0.12 pct C practice assumed for the 2 from 3 vessel plant operation in Fig. 3. The dolomitic lime requirements have been calculated to provide a 6 pct magnesia level in the liquid slag, Table 3. The value of 4.2 tonnes of dolomitic lime is similar to the value used in the slag materials cost study discussed in an earlier section. Charging dolomitic lime according to this method reduced variations in magnesia additions at the Bethlehem shop and enabled maximum life to be achieved at lower cost. A comparison of lining performances at selected magnesia charge levels also showed that MgO levels greater than 6 pct of the maximum liquid slag weight did not improve lining performance and was therefore not economically justified.[25] Investigation of the effects of other operating or flux practice charges revealed that spar practice and the charge lime - silica ratio were more significant in terms of effect on LD lining performance than MgO levels higher than 6 pct.

At the U.S. Steel Corp. South Works LD shop, production rate, dolomitic lime usage and hot metal silicon were found to be significant towards lining life[26]. Low heats decreased the lining life through spalling and oxidation of the brickwork during the holding period between heats. With high production rates (25 heats per day) the lining life was extended since spalling and oxidation were kept to a minimum. Lining life was also found to decrease when dolomitic lime usage increased slag viscosity and slag MgO

levels promoting a build up on the inside of the furnace which then acted as a shield towards the lining. Investigations indicated that there was a relationship between the actual slag MgO and the theoretically charged MgO. This relationship is illustrated in Fig. 17. Generally, the actual slag MgO levels were greater than theoretically possible when less than 50lb per ton (23kg) of dolomitic lime was used, suggesting refractory wear was occurring. Conversely, the slag MgO levels are lower than theoretically possible when greater than 50lb per ton was charged, suggesting that refractory build up by the slag was occurring. Excessive dolomitic lime usage promoted heavy bottom build up, increased slopping and skulling. Slag build up on the furnace lining was achieved at low silicon levels but was removed at higher silicon levels and therefore indirectly affected lining performance. Through the improved practice, lining lives on the tar bonded and tempered magnesia and periclase linings averaged 2,582 heats.

Japanese Practices.

In Japan the Kimitsu plant has achieved record lining performances of 5,000 and 10,000 heats on vessels operating with dolomitic lime and programmed gunning[21]. Refractory qualities ranged from 60 pct MgO content in the cone above the charging side to 86 pct MgO at the centre and lower barrel. The refractory brick thickness ranged from 810mm on the charge pad to 500mm in the cone. The plant trials involved 3 steps according to dolomitic lime consumption;

(a) 1st step 5-7 kg/T.S. - 3 pct MgO in slag

(b) 2nd step 13-15 kg/T.S. - 5-6 pct MgO in slag

(c) 3rd step 20-40 kg/T.S. - 8pct MgO (saturation).

Fig. 18 shows how each step was developed and the effect of each different step and slag MgO content on lining life. The 3rd step gave the greatest number of heats with slags saturated in MgO. The use of non tilting operations and a sub-lance was probably a major factor in extending lining life during the 3rd step. An extensive gunning campaign was also undoubtedly important in maintaining the service life of the refractories. If the weight of MgO, charged as dolomitic lime, was subtracted from the weight of magnesia in the slag, it becomes possible to measure the amount of magnesia eroded per heat ΔMgO. Plotting this value against dolomitic lime consumption indicated a linear relationship, the straight line crossing the horizontal axis at about 20 kg/tonne steel, Fig. 19. This diagram implies that above the 20 kg/tonne level, magnesia is being deposited in the vessel i.e. ΔMgO becomes negative. A similar plot against slag MgO intersects the line at 6 pct MgO Fig. 20. This result compares favourably with the approach used to determine the magnesia saturation limits in Fig. 14. At magnesia levels attributed to step 3 (saturation), a decrease in the dephosphorising and desulphurising power of the slag was reported.[21] This may be a practical confirmation that MgO is less basic than CaO.

Raw Materials Supply.

Dolomite is the double carbonate of calcium and magnesium and it is a compound rather than a mixture of calcite and magnesite. Theoretically, pure dolomite contains 45.7 pct $MgCO_3$ (21.85pct MgO) and 54.3 pct $CaCO_3$

(30.4 pct CaO) and has the chemical formula $CaMg(CO_3)_2$. The composition of commercial dolomites may vary considerably but for refractory and chemical purposes they may be termed dolomitic limestones after the classification of Pettijohn[27]. A dolomitic limestone is composed of 10 to 50 pct $MgCO_3$ and 50 to 90 pct $CaCO_3$. In the U.K. such dolomitic limestones contain between 38 pct and 42 pct $MgCO_3$.

The largest U.K. producer is the Steetley Company Ltd., which operates quarries in Durham, South Yorkshire, North Nottinghamshire, Shropshire and Glamorgan. Almost 3 million tonnes of dolomitic limestone was mined during 1978[28], principally by the Steetley Company for use in the refractories and chemical industry. Outcrops of dolomitic limestone lie close to all the major steel producing centres of the U.K. so that haulage costs remain reasonable. Fig. 21 illustrates the geographic locations of iron and steel works in the United Kingdom, excluding Northern Ireland[29]. The principal source areas for dolomitic limestone, which is burnt to form dolomitic lime, have been superimposed onto Fig. 21 to illustrate in a similar manner the geographical relationships with major steel producing centres. Fig. 22 summarises oxygen steelmaking plants which were still in existence at the end of 1977[1] and which consume the bulk of the dolomitic lime produced in this country.

Geological Occurrences.

Dolomitic lime occurrences of economic importance are restricted to Lower Carboniferous lithologies of South Wales and to the Permian, Lower Magnesian Limestone Stage

of North Nottinghamshire, South Yorkshire and County Durham. They originated as secondary diagenetic deposits after calcite which became permeated by magnesian solutions[30]. Only within the subdivision of the Laminosa Dolomite of South Wales is dolomite considered of primary origin[31].

(a) Dolomitic limestone occurrences in South Wales.

In the south eastern rim of the South Wales Coalfield, Carboniferous Limestone outcrops on a general WSW - ENE strike, diminishing in width from a mile in the vicinity of Pontyclun to less than half a mile on the Cefn Onn ridge to the north of Cardiff. On the western side of Taffs gorge, near Taffs Well, massively bedded dolomitic limestones make up practically the full thickness of the Main Limestone Group. The dolomites reaching their maximum thickness of around 1200 feet. Borehole evidence indicates that at the western side of Taffs gorge, thrust faulting aligned roughly parallel to the strike of the formation may pose a limit to mineable material. Material mined at the Taffs Well quarry is used mainly for fluxes at the Llanwern and Port Talbot steelworks at a rate predicted at 10000 tons per week. Workable reserves on the western part of Taffs gorge and part of Garth Wood have been estimated at more than 10 million tonnes, averaging 40 to 41 pct magnesium carbonate[31]. Dolomite burning at Taffs Well has recently ceased through high costs and dolomitic lime flux is transported from the Steetley Company's Whitwell quarry near Worksop in Nottinghamshire.

(b) Dolomitic limestone occurrences in England.

The major sources of dolomitic limestone are mined

from outcrops of the Permian System which extends southwards from County Durham, through Yorkshire to North Nottinghamshire. Dolomitic limestones occur in flat-lying, buff-coloured Lower Magnesian Limestone lithologies. The rock has a sandy appearance partly due to recrystallized rhombs of secondary dolomite within matrix pores. The Steetley Company operates two open pit operations at Whitwell near Worksop, Nottinghamshire and Thrislington, County Durham. South of Thrislington Hall, enormous reserves are limited only by the overburden of Middle Magnesian Limestone to the east(32).

A variety of burnt dolomitic limestone products are produced by both quarries. At Whitwell, two 120m long by 3.4m diameter rotary kilns are able to manufacture various product types. Firing is by pulverised coal which when burnt with high temperature secondary air from the grate coolers can generate temperatures in excess of 1900°C. Dolomitic lime is sold under the trade name "Dolomet" and is produced by firing dolomitic limestone at 1400°C to produce a soft burnt, porous product. A small amount of ferric oxide is added to aid sintering and material within the size range -40 to +5mm is produced for LD slag additives. The specification for "Dolomet" is obviously as important as that for lime and a typical specification is given in Table 4. The storage life is greater than that of burnt lime and may be stored for up to one month in normal steelworks bunkers. Dolomitic lime additions should be added with the normal lime charge as early in the blow as possible in LD operations.

An estimation can be made on the actual tonnages of

dolomitic lime required by Oxygen Steelmaking processes. Assuming that the 10.8 million tonnes of steel produced by such processes[1] uses 18 kg/tonne steel of dolomitic lime, then an annual production of 195000 tonnes is required. On a weekly basis this is 3750 tonnes of dolomitic lime. The Whitwell plant alone has the capacity to produce in excess of this figure so there should be no problems in meeting the dolomitic lime requirements of the steel industry. Although transport costs will continue to rise, the use of coal fired kilns should help to maintain the competitiveness of dolomitic lime as a slag additive since increasing oil prices will effect future calcined soft burnt lime products.

Discussion.

There are obvious large differences between the lengths of campaigns obtained by American and Japanese practices and those of Europe and the U.K. The development of basic linings through a dolomitic route may be partly the reason for this, although there are indications that magnesia enrichment and magnesia refractories will become dominant in the linings of LD vessels. Spencer[33] has forecast that by 1990, 85 pct of LD raw materials will be derived from magnesia, Fig. 23. With this lining trend it is difficult to imagine a reduction in dolomitic lime consumption from its present 15 to 18 kg/tonne steel levels[17]. The economic assessment for dolomitic lime usage discussed in an earlier part of the case study still appears valid when reviewing vessel availability and overall cost reduction rather than specific lining wear and slagmaking costs.

By applying cost curve relationships to a lime - spar,

lime - dolomitic lime - spar and a lime - dolomitic lime practice at the 18 kg/tonne level, the effect on the break even materials cost for a pitch bonded tempered magnesia lining is different from that of doloma. If it is assumed that the magnesia lining gives 700 heats for a standard lime practice and the cost index is 3 times that of doloma ($\pm$ £100000), then lining lives utilizing either dolomitic lime practice will have to double or treble before a materials break even point is reached, Fig. 24. For slag practices designated 2 and 3 in Fig. 24 the refractory/slagmaking cost break even point of £2.2/tonne steel will be attained only at 1540 and 2000 heats respectively. An increase in lining life due purely to the dolomitic lime addition can be inferred but probably only by as much as 30 to 40 pct. Therefore, additional factors such as the reduction in the number of campaign relines and increased vessel availability would have to be taken into consideration to truly assess whether the slag practice was economic or not. At dolomitic lime additions greater than saturation MgO levels, (20kg/t.s.), problems associated with bottom build up or reduced phosphorus and sulphur efficiency have been predicted. Reduction of vessel volume through viscous slag build up is believed to cause slopping and ejection of metal from the vessel. However, Quin (private communication) has indicated that the use of a dolomitic lime practice has enabled one particular U.K. shop where slopping commonly occurred, to reduce the lining thickness and increase vessel volume to contain the slopping tendency. As a result, the increase in metal yield has more than compensated for the extra slagmaking cost.

This example again illustrates the difficulty in assessing the benefits of a dolomitic lime practice if a purely economic approach is applied.

With the exception of the Port Talbot flux trials[14], no U.K. plant has reported trials similar to those discussed under American practices which have tried to isolate the major variables specifically relating to lining performances. To establish economic and practical limits to dolomitic lime practices a programme of trials might have to be undertaken on lines similar to those proposed below;

(a) Selecting a particular refractory lining arrangement, operate a lime plus spar practice which achieves optimum phosphorus and sulphur removal.

(b) Operate a dolomitic lime - lime plus spar practice in an adjacent vessel with similar refractories.

(c) Gradually increase dolomitic lime addition at the expense of spar up to slag saturation levels.

(d) Carefully monitor turndown slag compositions and aim sulphur and phosphorus end points.

(e) Ensure that blast furnace slag carry over and hot metal silicon levels remain within defined limits.

(f) Maintain an equivalent number of normal and concast heats between the vessels.

The true economic costs of using a dolomitic lime practice as a substitute for a lime flux are open to many imponderables and an economic approach based simply on materials costs cannot be justified. This case study has tried to develop logically the reasons why dolomitic lime is used as a slag-making additive in the U.K. and other LD steelmaking practices. The direct and indirect benefits

of its use have been noted. The decision, economic or otherwise, to reduce or maintain levels of usage can only be based on information which currently may not have been determined or has not been reported on.

REFERENCES

1. B.S.C. Annual Statistics 1978

2. Ward, R.G. — The physical chemistry of iron and steelmaking. Arnold, 1962

3. Walker, R.D. and Anderson, D. — Reaction mechanisms in basic oxygen steelmaking.
Iron & Steel June 1972 Pt 1 p.271
" " " Aug. 1972 Pt 2 p.403
" " " Oct. 1972 Pt 3 p.409

4. Richardson, F.D. — Physical chemistry of melts in metallurgy. Vol.I. Academic Press 1974

5. Hardy, C.W. — Refractories Journal 1972 Nov

6. Hardy, C.W. and Owen, A.J. — Metals Society Conference May 1978 p.15

7. Spencer, D.R.F. — Developments in LD Refractories. Ref. Jnl. Nov/Dec 1978 p.8

8. Muan, A. and Osborn, E.F. — Phase Equilibria among oxides in steelmaking. Addison-Wesley 1965.

9. Baker, R. — Desirable slag composition paths and method of control in the LD process. B.S.C. rpt. CAPL/SM/A/31/74. 1974

10. Iyengar, R.K. and Petrilli, F.C. — Statistical analysis of BOF lining life. Journ. Metals 1972 March p.46

11. Fetters, K.L. and Chipman, J. — Equilibria of liquid iron and slags of the system CaO-MgO-FeO-SiO_2. Trans. AIME 1941 145 p.95

12. Herron, R.H. and Leonard, R.J. — Dolomite additions required to saturate BOF slags with MgO. Conference Proc. AIME April 17-20, 1977

13. van Hoorn, A.I. et al — Evolution of slag composition and weight during the blow. McMaster Symposium May 1976

14. Latty, C.W. — Assessment of flux practices at Port Talbot. 1972 B.S.C. report.

15. Ind. Minerals — 1979 August

16. Snyder, E.B. — High calcium lime, dolomitic lime and other fluxes for steelmaking furnaces. I.& S.M. 1976 1 p.11

17. Green, J. and Quin, J. — The influence of MgO on BOF slag fluidity and its correlation with BOF refractory wear rate. Basic Open Hearth Proc. Conf. April 1978

18. Yarashenko, N.I. — Steel in the USSR 1971.

19. White, J. — Iron & Steelmaking (Qtrly) 1974 no.2 p.115

20. Harhai, J.G. and Dukelow, D.A. — Factors affecting sulphur removal in the basic oxygen process. Journ. Met. 1966 July p.833

21. Obinata, T. — High magnesia slag operation in BOF. McMaster Symposium Ed.W-K Lu 1976

22. Nashiwa, H. et al — Effective use of returned LD slag and dolomite and operation with sublance system. Ironmaking & Steelmaking 1978 No.3 p.95

23. Ind. Min. — 1978 February

24. Leonard, R.A. — Refr. Jnl. 1977

25. Balla, D.M. and Beechan, C.R. — Development of a guideline for the efficient use of dolomitic lime in BOF operations. I. & S.M. July 1977

26. Rodal, D.B. and Calanog, E.M. — Operating factors affecting South Works BOF lining life. I. & S.M. May 1977 p.38

27. Hatch, F.H. and Rastall, R.H. — Petrology of the sedimentary rocks. 1965 4th Edn. Allen & Unwin

28. United Kingdom Mineral Statistics 1978 H.M.S.O.

29. Pounds, N.J.G. — Geography of iron & steel. 1971 5th Edn. Hutchinson Univ. Lib.

30. Wells, A.K. and Kirkaldy, J.F. — Outline of Historical Geology 1966 5th Edn. Allen & Unwin

31. Thomas, T.M. — The mineral wealth of Wales and its exploitation. 1961 Oliver & Boyd

32. Memoir Geol.Survey — The Geology between Durham and West Hartlepool

33. Spencer, D.R.F. — Refractories in the Eighties Refr. Jnl. 1979 May/June p.12

TABLE 1 MgO and CaO in Slag. (after Iyengar et al [10])

(Hot metal Si 1.10 to 1.35 pct)

A mass balance for MgO and CaO in the flux charge gives

Burnt lime	90 pct CaO,	2 pct MgO	
Dolomitic lime	60 " " ,	40 " "	
B.F. slag	40 " " ,	14 " " ,	9 pct Al_2O_3.

lbs of MgO in LD slag. = lbs of MgO from dolomitic lime
+ lbs MgO from B.F. slag
+ " " " burnt lime
+ " " " Refractory wear.

* pct MgO x wt $\frac{LD}{100}$ slag = 0.4 wt dol. lime
+ 0.14 wt BF slag
+ 0.02 wt burnt lime
+ wt MgO from refractories

* Assumed that Al_2O_3 in LD slag above 0.3 pct comes from BF carry over and by using an average BF slag chemistry as above,

$$\text{wt of BF slag} = \text{wt LD slag} \frac{\frac{(Al_2O_3 - 0.3)}{9}}{100}$$

Substituting

A $\frac{\text{wt LD slag}}{100} (MgO - \frac{14}{9} (Al_2O_3 - 0.3)) = 0.4$ Dolime
+ 0.02 B.lime
+ MgO ref.

A mass balance for CaO gives

B $\frac{\text{wt LD slag}}{100} (CaO - \frac{40}{9} (Al_2O_3 - 0.3) = 0.6$ Dolime
+ 0.9 burnt lime

Dividing A by B

$$\frac{MgO - \frac{14}{9} (Al_2O_3 - 0.3)}{CaO - \frac{40}{9} (Al_2O_3 - 0.3)} = \frac{0.4\ D/B + 0.02 + MgO\ ref/B}{0.6\ D/B + 0.9}$$

$$D/B = \frac{\text{Dolomitic lime}}{\text{Burnt lime}}$$

Table 2–Dolomitic lime requirements to provide a 6% magnesia level for estimated maximum liquid slag weights determined using different FeO's (aim carbons) and two silicon levels

Aim Carbon, %	Maximum FeO, %	Estimated Slag Weight, lb		Ibint Dolomitic Lime* for 6% MgO	
		@0.90% Si	@ 1.50% Si	@0.90% Si	@ 1.50% Si
.00 to .04	35	73,600	121,000	37	61
.05 to .09	30	66,000	111,000	33	55
.10 to .14	25	61,000	102,000	31	51
.15 to .20	20	57,000	94,000	29	47
.21+	15	53,000	88,000	27	44

*This is a 40% MgO dolomitic lime.

(after Balla and Beechan[25])

TABLE 3. Dolomitic lime requirements to provide a 6 pct MgO level in a 0.07 to 0.12 carbon steel.

Hot metal charge 0.7 x 300000 = 210,000kg.

Hot metal Si = 0.9 pct.

Utilizing information from Table 2

The maximum FeO level for a 0.05 to 0.09 Carbon slag level will be 30 pct for the dead mild steel practice.

The estimated slag weight at 0.9 pct Si is 66000kg.(Table 2)

Calculation

The weight of silica in the slag will be

$$210{,}000 \times 0.009 \times 2.14 = 4045\text{kg } SiO_2$$

With 3 as the maximum lime-silica ratio

$$4045 \times 3 = 12135\text{kg CaO}$$

Total mass of $CaO + SiO_2$ = 16180kg

It is assumed that at a V-ratio of 3, the sum of the oxides contained in the slag is equal to 12 pct of the slag mass.(12) (25)

i.e. $CaO + SiO_2$ will be 100% - (12% + FeO %).

Mass of liquid slag will be

1)
$$\frac{CaO\,kg + SiO_2\,kg}{100\% - \%\{\text{oxides} - \%\,FeO} \times 100 = \text{Maximum total liquid slag kg.}$$

$$\frac{16180\ CaO + SiO_2\,kg}{100 - 12 - 30} \times 100 = \underline{\underline{27897\ kg}}$$

2) Mass of MgO required at 6 pct level

$$\frac{\text{Maximum total liquid slag kg} \times \text{desired MgO\%}}{\text{MgO in dolomitic lime}} = \text{Dolomitic charge kg}$$

$$\frac{27897 \times 6}{100} = 1673 \text{ kg MgO}$$

or $$\frac{1673}{*40} \times 100 = \underline{4183 \text{ kg dolomitic lime}}$$

* % MgO in dolomitic lime.

TABLE 4 Typical 'Dolomet' composition.

CaO	-	57.0 %
MgO	-	39.0 %
SiO_2	-	0.75%
Fe_2O_3	-	1.35%
Al_2O_3	-	0.40%
S	-	0.05% (max)
Mn_2O_3	-	0.22%
CO_2	-	0.50%

Bulk density :- 1.50/1.70

Size grading :- $1\frac{3}{4} - \frac{3}{16}$ (approx. similar to calcimatic lime)

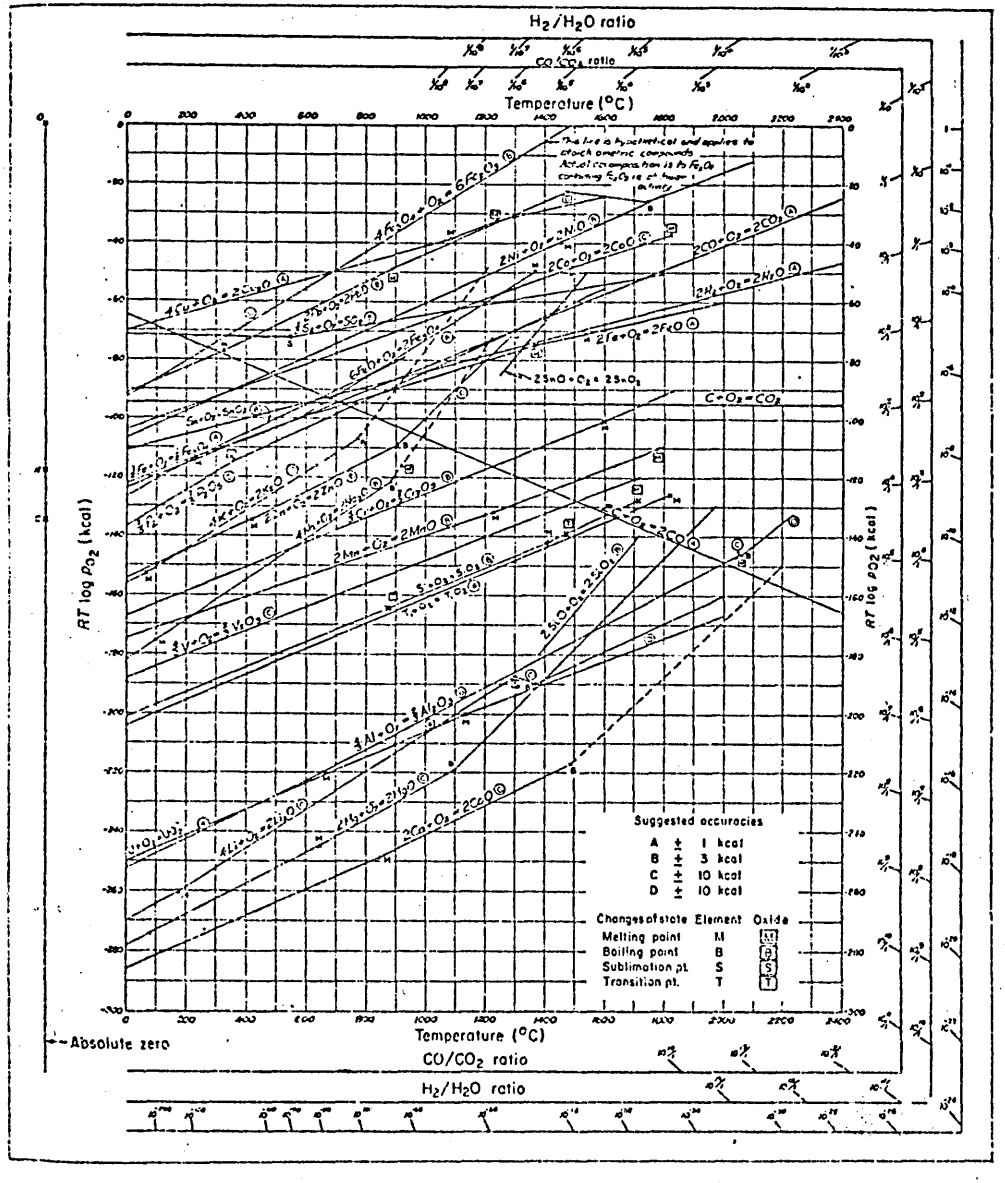

Fig 1. A standard free energy diagram for oxides.

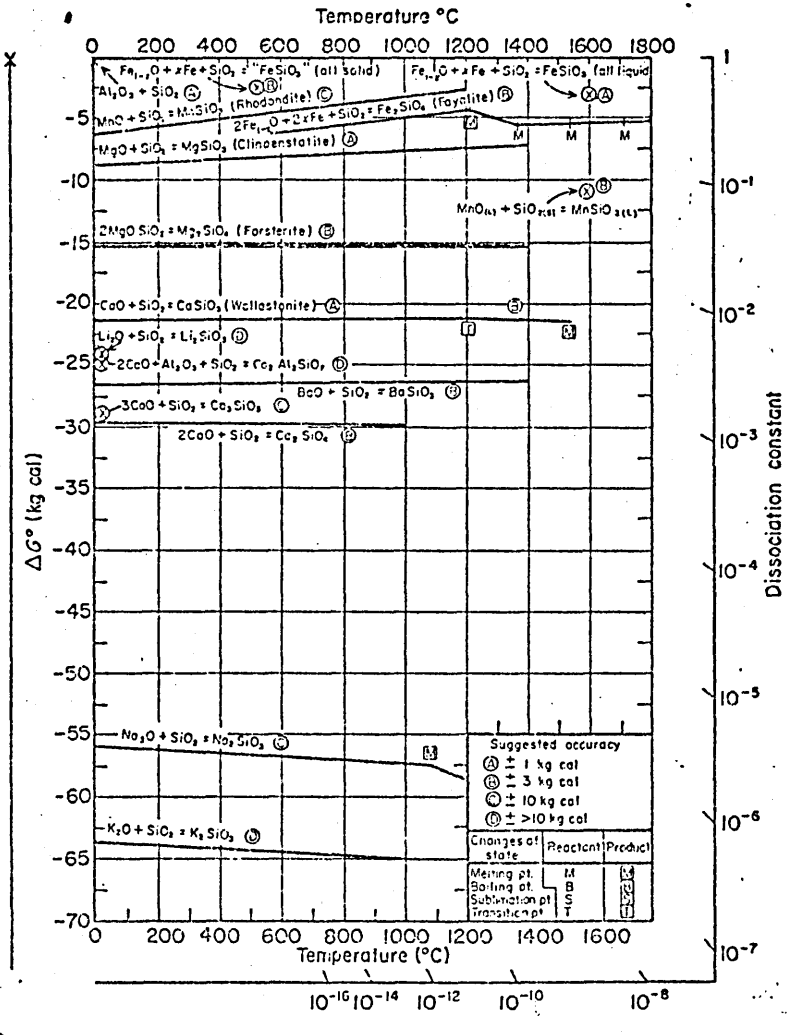

Fig 2. Free energies of formation of pure crystalline silicates from their compone oxides.

(after Richardson [4])

Fig 3 PRODUCTION TARGETS AND LINING AND SLAG PRACTICE SELECTIONS FOR A HYPOTHETICAL LD SHOP.

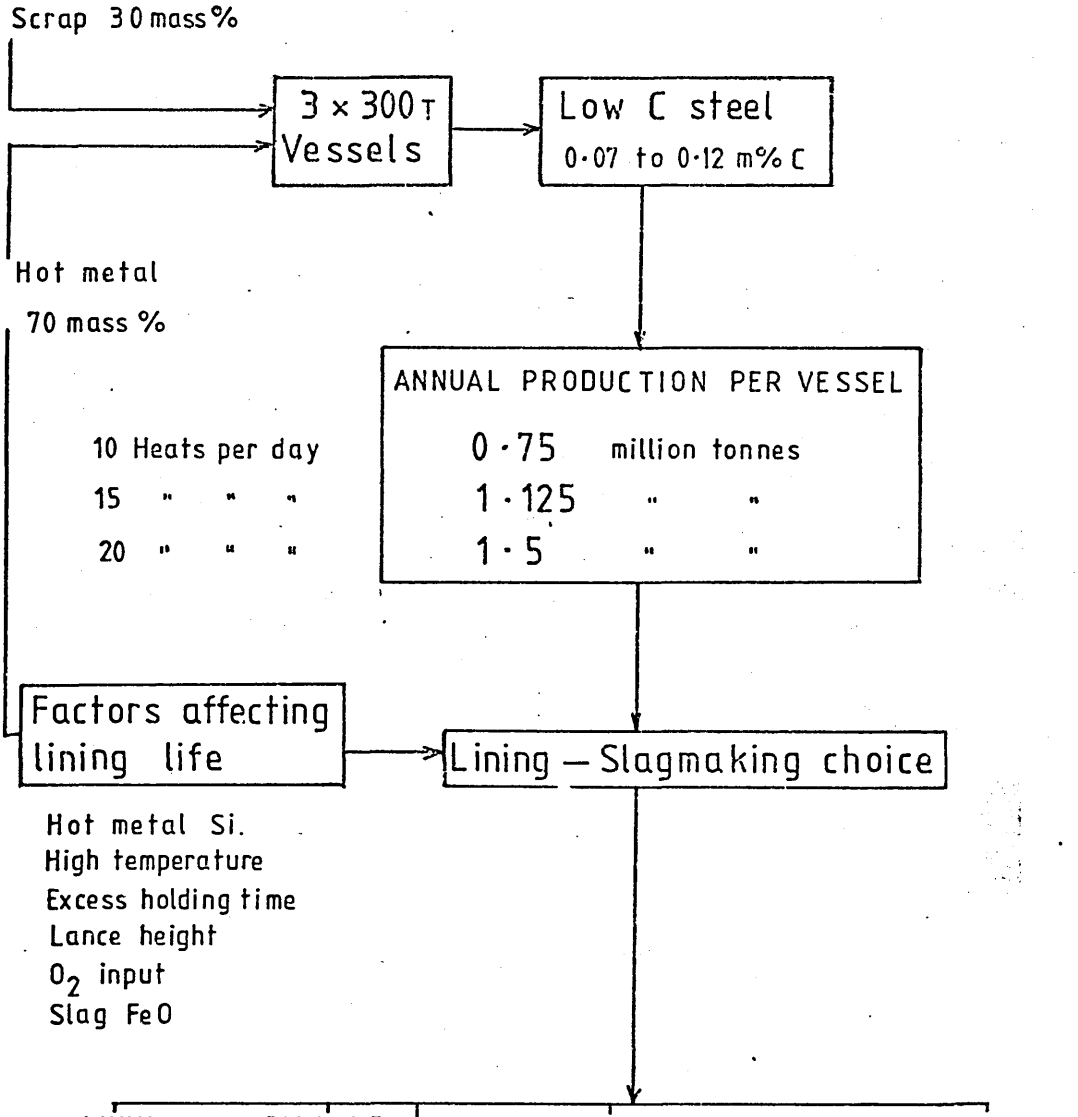

LINING	RELATIVE COST	SLAG PRACTICE	RELATIVE COST
Doloma	1	(a) Lime + spar + (gunning)	1 + 1·5 + (8)
Dol-mag	1·8	(b) Lime + spar + dolomitic lime	1 + 1·5 + 1·5
Mag-dol	2·4	(c) Lime + dolomitic lime	1 + 1·5
Magnesia	> 3 – 4	(d) Lime dolomitic lime (gunning)	1 + 1·5 + (8)

Fig 4 Extrapolated lining life requirements from a 300T Converter operating at 3 choices of output.

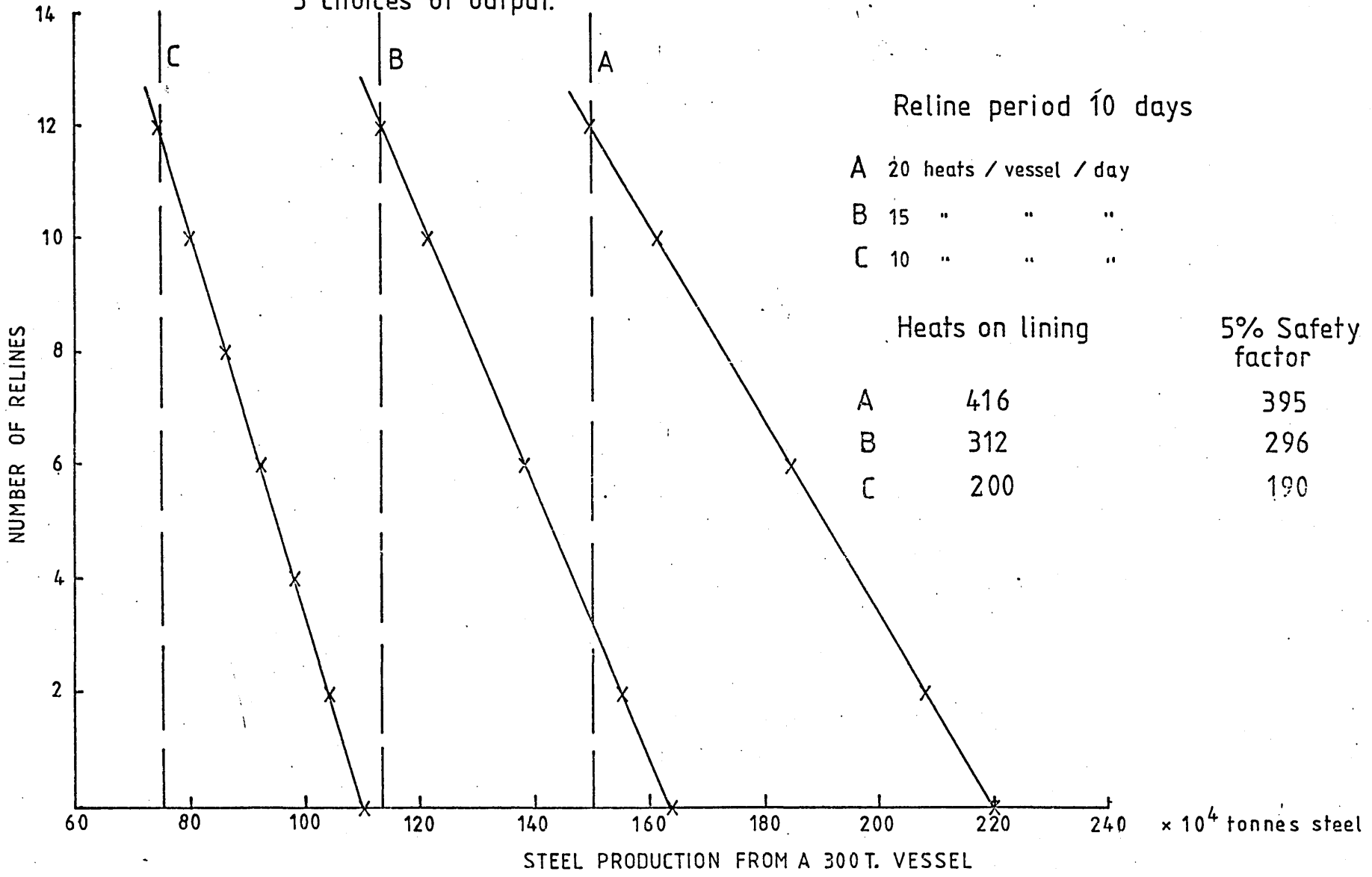

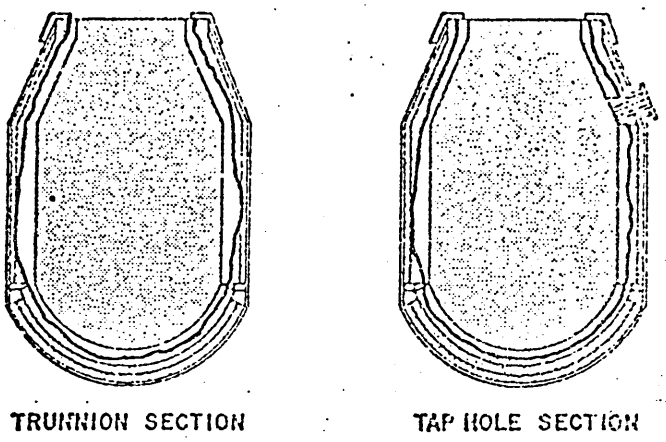

FIGURE 5

Typical Wear Pattern in BOF Lining.
Trunnion areas are major wear spots followed by charging pad area. (Limes. J. Brit. Ceram. Soc 1975)

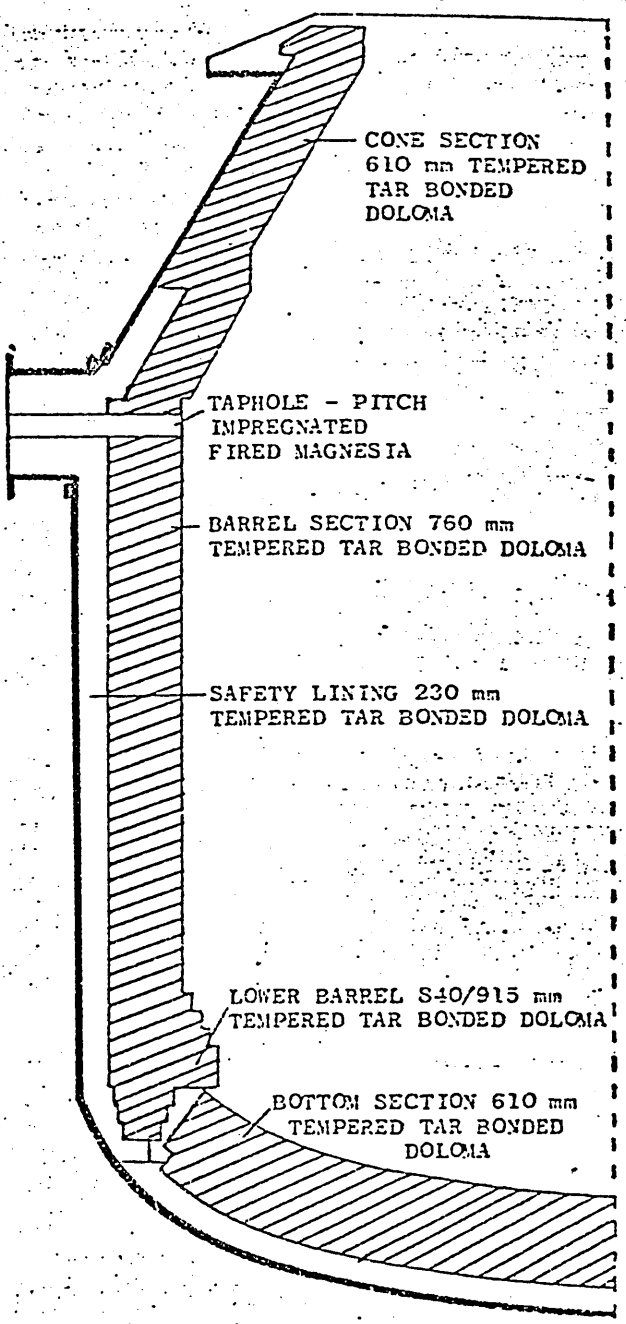

Fig 6. : Typical UK LD vessel lining design based on tempered doloma

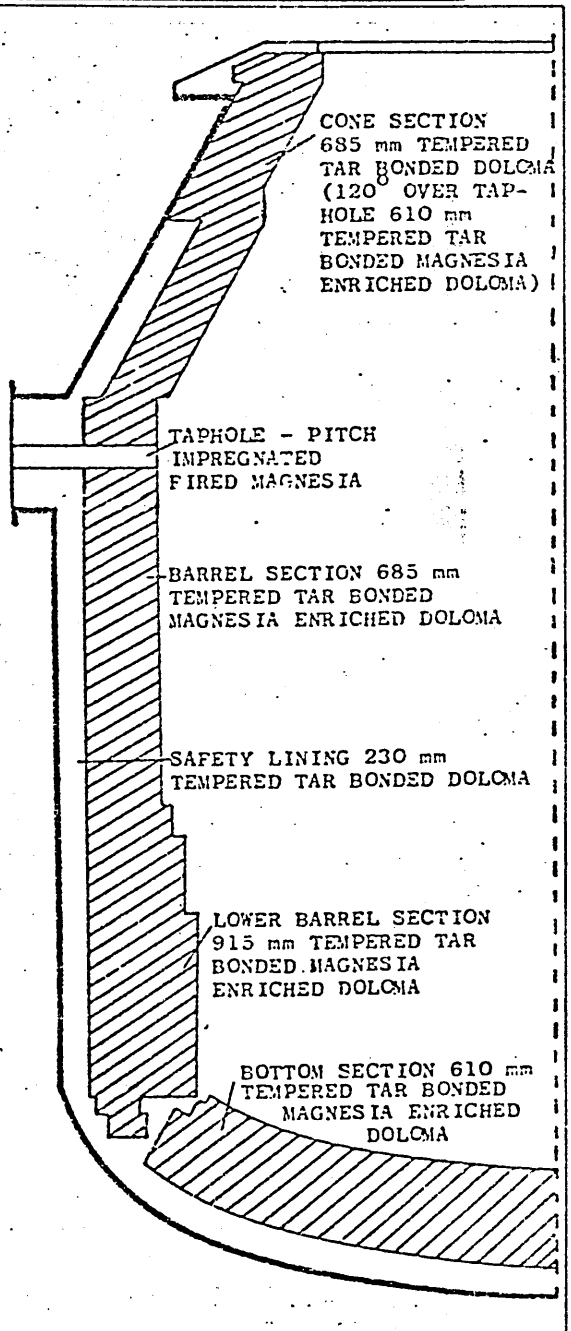

Fig 7. : Typical UK LD vessel lining design based on tempered magnesia enriched doloma (after Spencer[7])

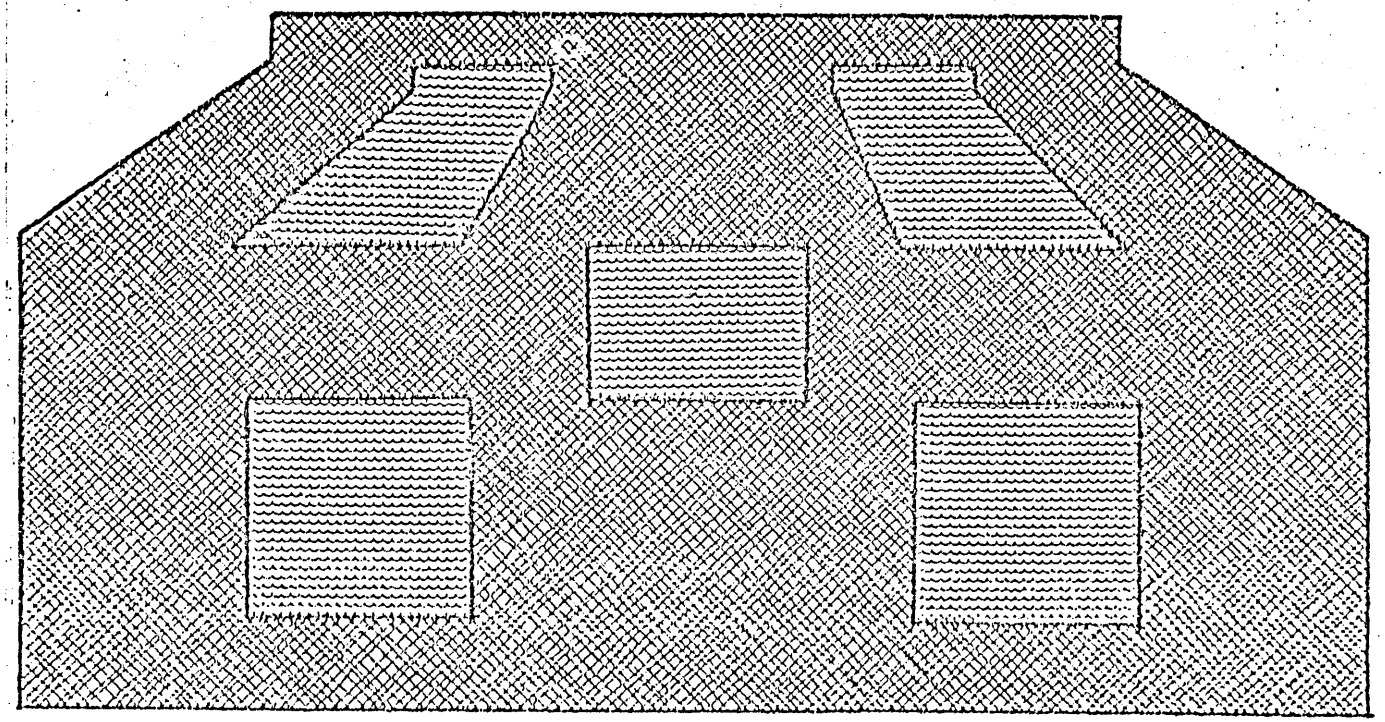

tar bonded & tempered enriched dolomite

tar bonded & tempered magnesite

Fig 8 TYPICAL COMPOSITE LINING (after Hardy and Owen [6])

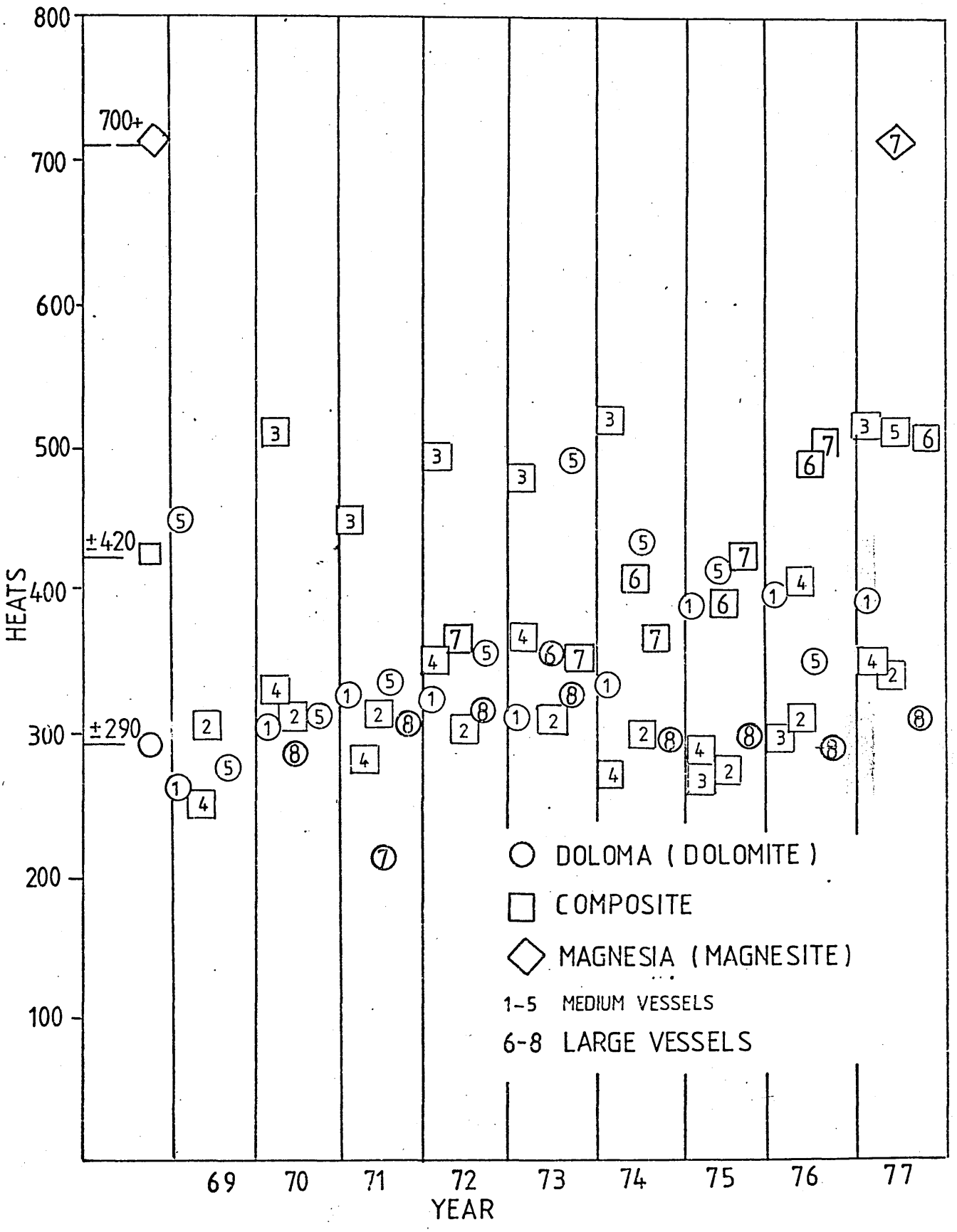

Fig 9. Average Yearly Lining Lives

(after Hardy and Owen [6])

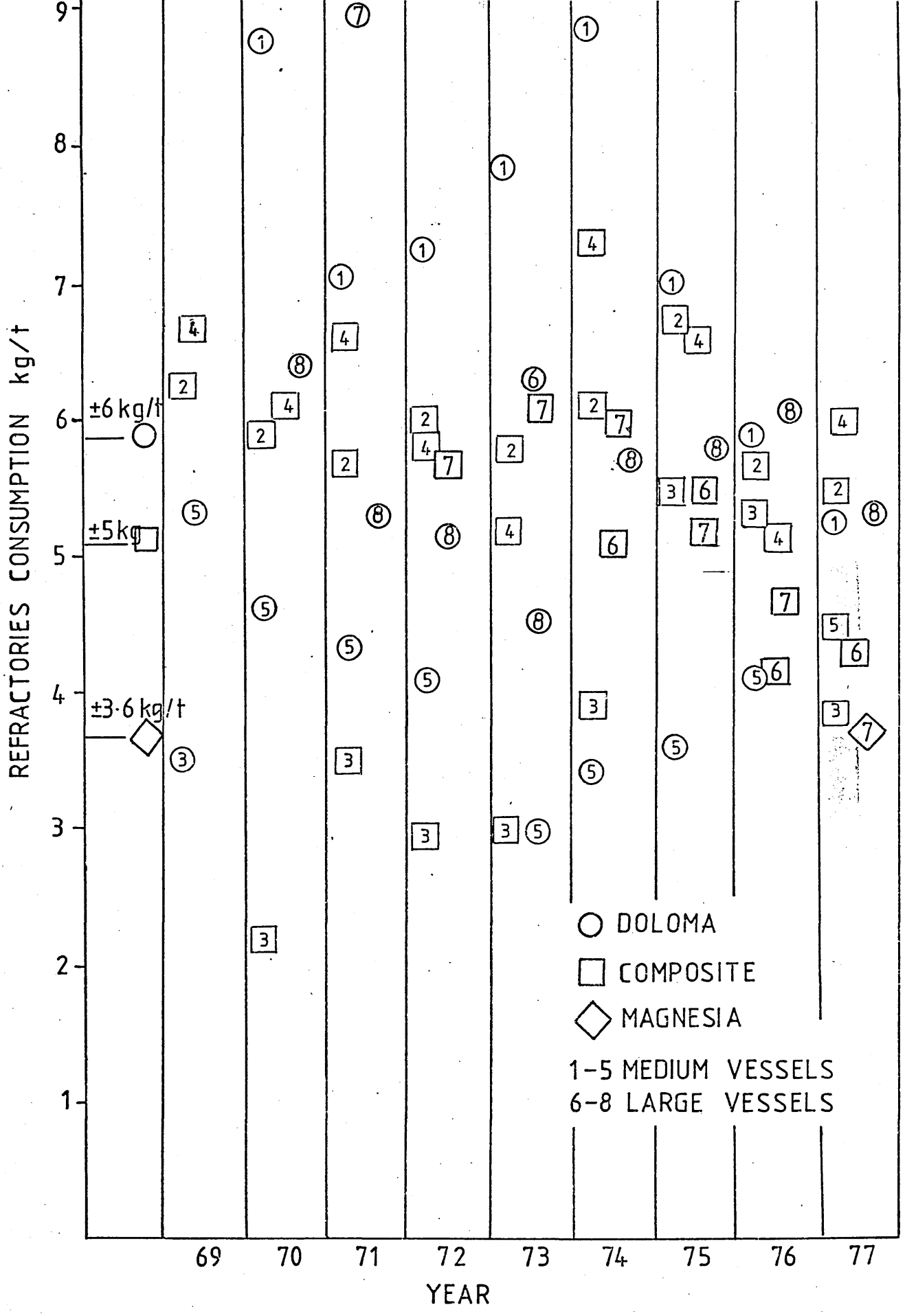

Fig 10 Average Yearly Refractories Consumption

(after Hardy and Owen [6])

Fig 11 Trends in the UK prices of LD refractories

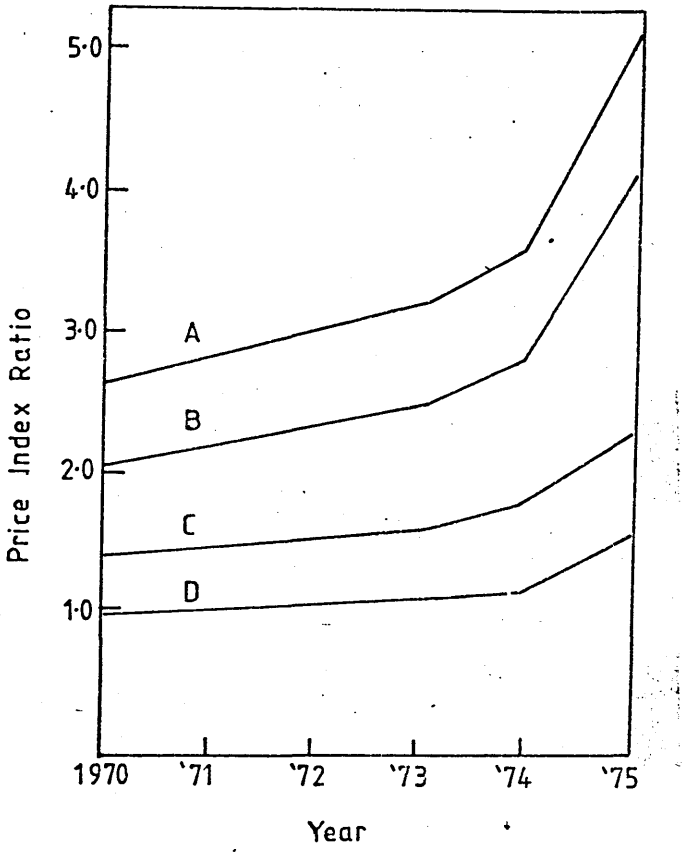

A Fired tar impregnated Magnesia

B Tempered 100% Magnesia

C Tempered Magnesia enriched Doloma

D Tempered 100% Doloma

(after Spencer [7])

Fig 12 Notional pseudo-ternary of the CaO-MgO-'FeO' system

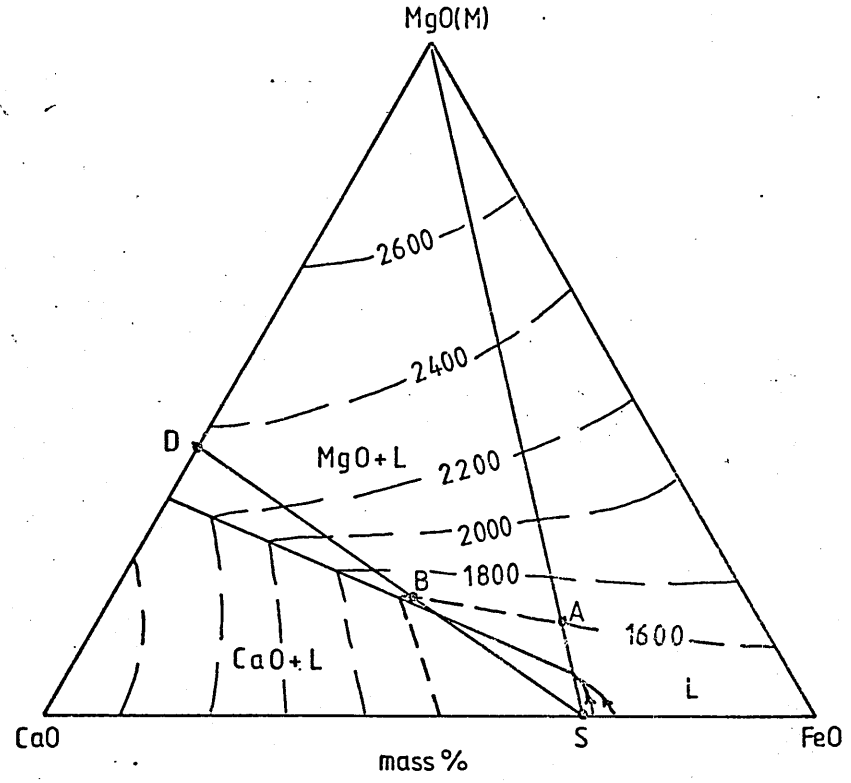

Fig 13 The solubility of doloma and magnesia in ferruginous slags

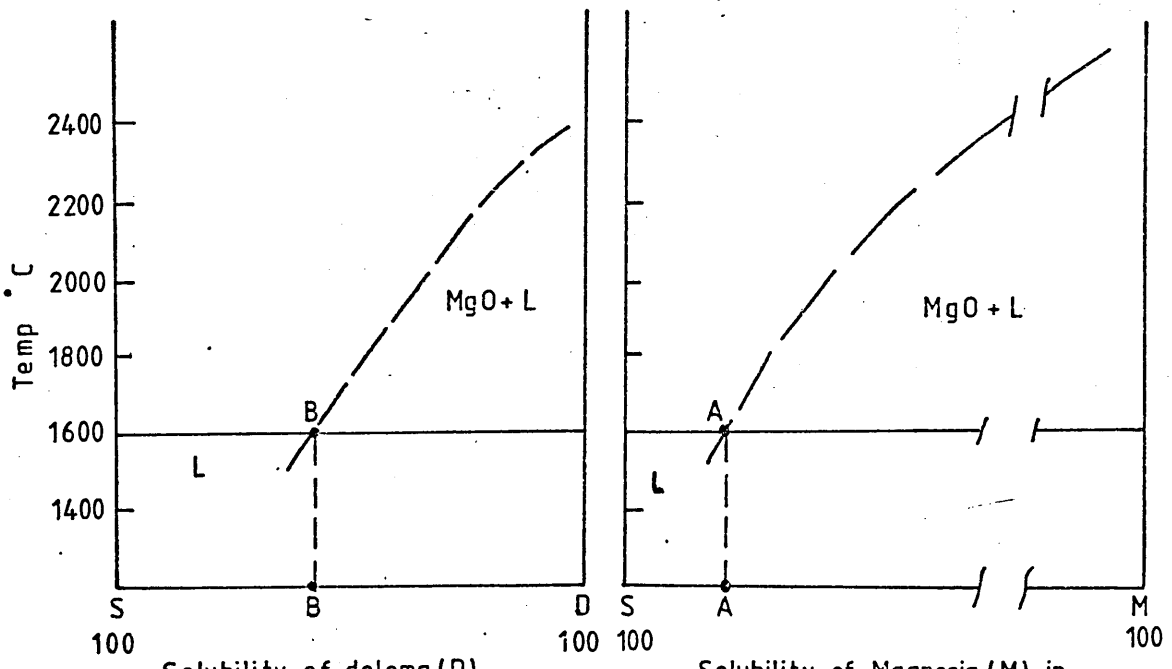

$$sol\% = \frac{SB}{SD} \times 100$$

$$sol\% = \frac{42}{100} \times 100 = \underline{42\ \%}$$

$$sol\% = \frac{SA}{SB} \times 100$$

$$sol\% = \frac{14}{100} \times 100 = \underline{14\ \%}$$

Fig 14 The solubility of magnesia in CaO-FeO-SiO_2 slags at 1600°C superimposed on slag-path trajectories

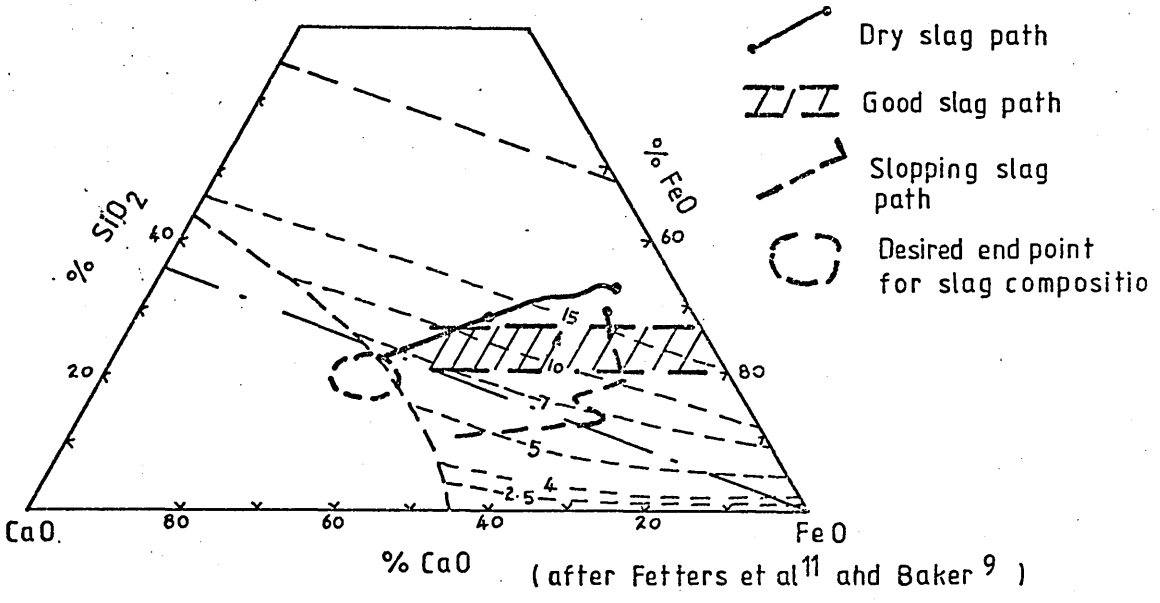

(after Fetters et al[11] and Baker[9])

Fig 15 Estimated solubility of MgO in LD-type slags at 1600°C

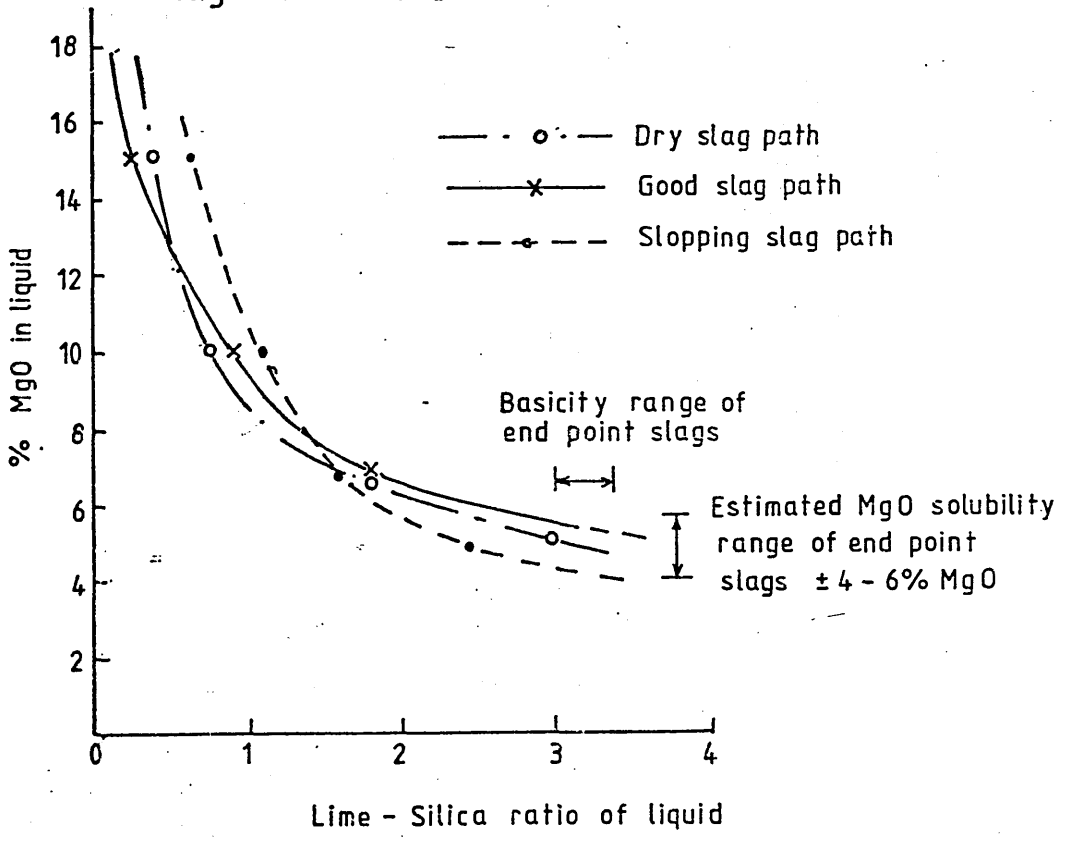

Fig 16 Cost curves for standard and dolomitic lime slag practice

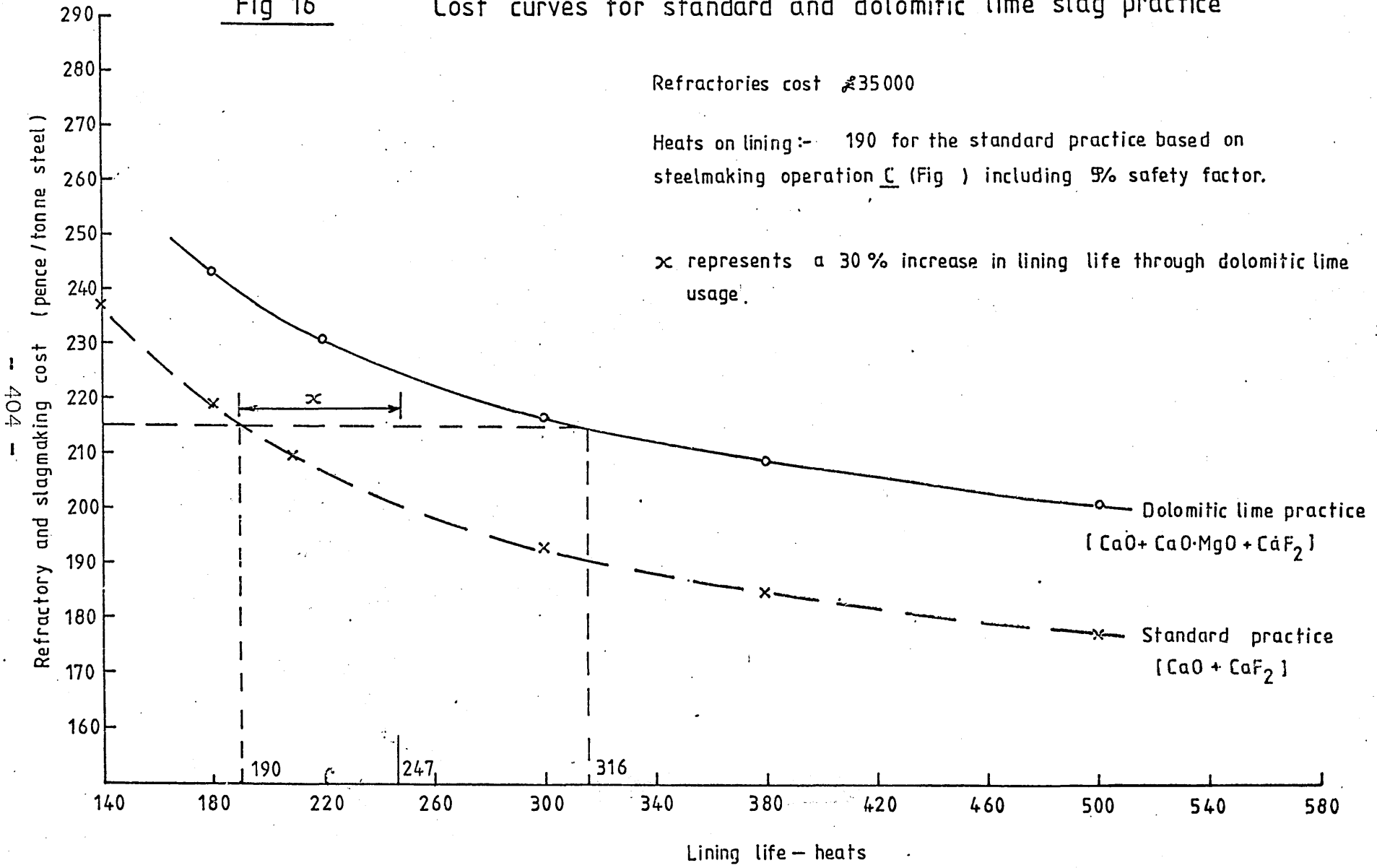

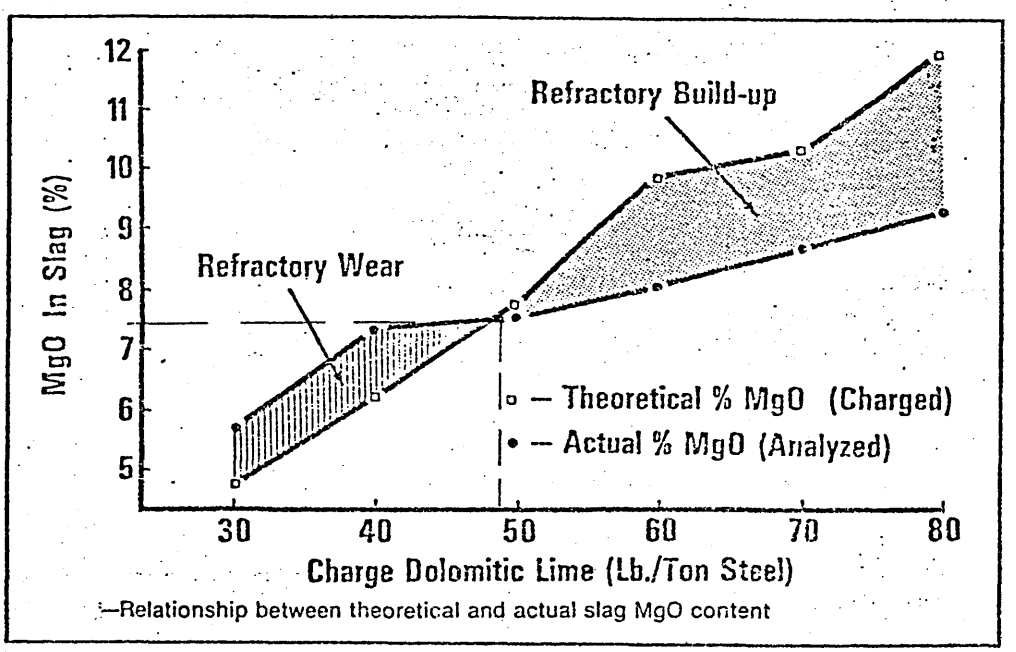

—Relationship between theoretical and actual slag MgO content

Fig 17 (after Rodal et al[26])

Fig 18

Lining Life at BO Plant Kimitsu (ex. Obinata-McMaster).

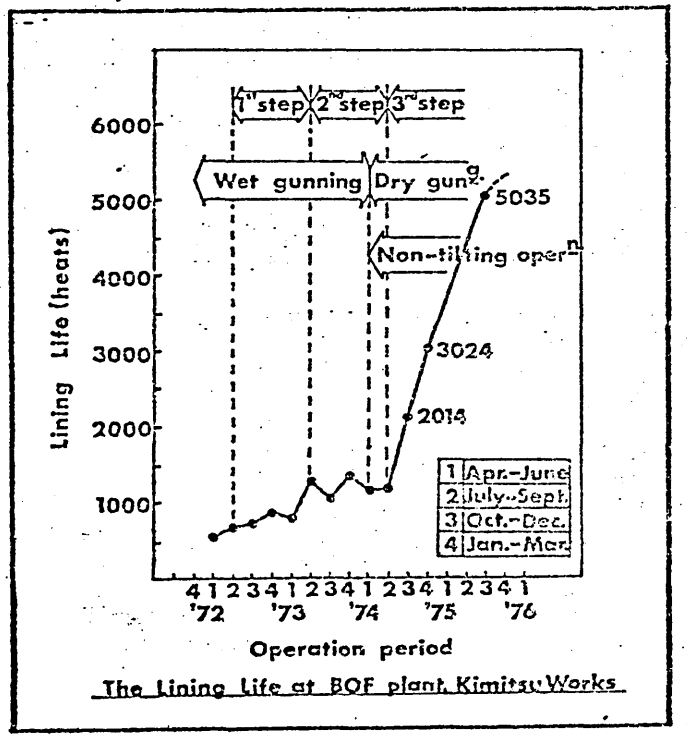

The Lining Life at BOF plant, Kimitsu Works

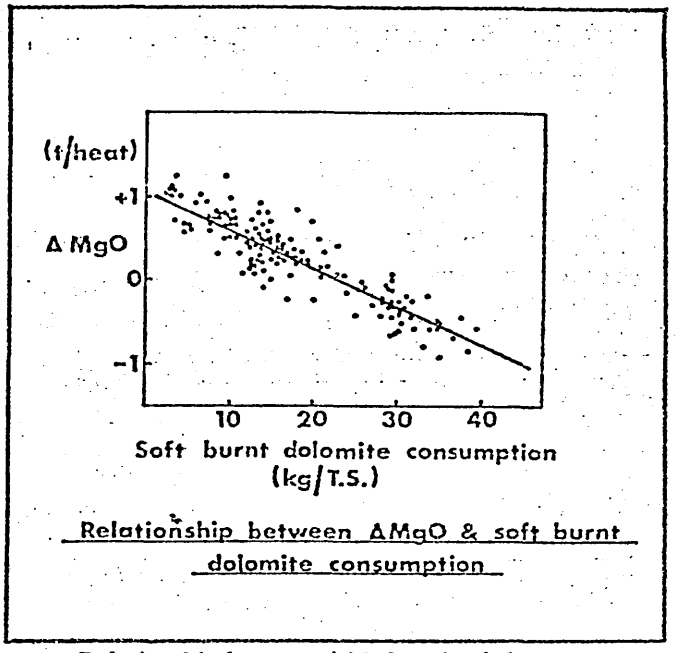

Fig 19 : Relationship between Δ MgO and soft burnt dolomite consumption (ex Obinata-McMaster). (21)

Fig 20 : Relationship between MgO in BOF slags and brick erosion (ex. Obinata-McMaster). (21)

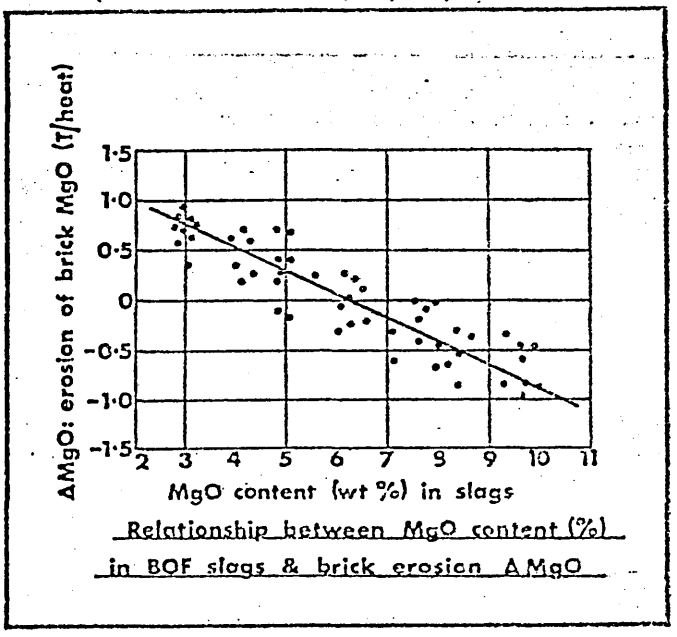

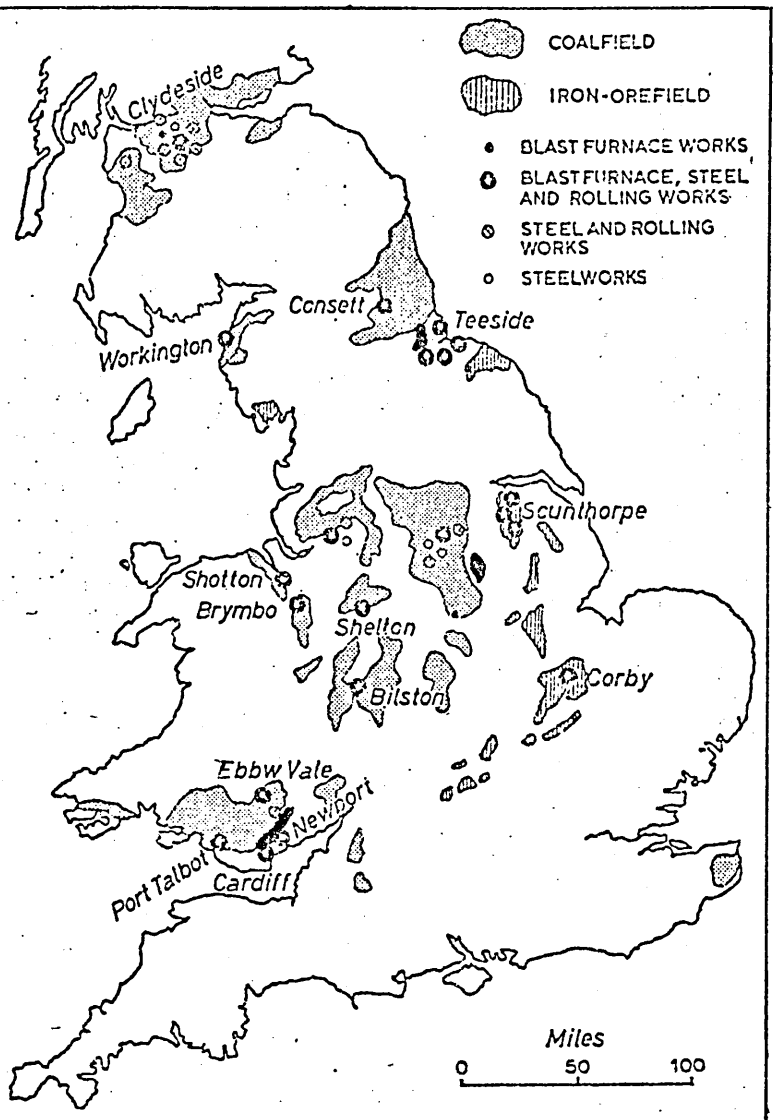

Fig 21 Iron and steel works in the United Kingdom, excluding Northern Ireland (modified after Pounds (29))

Fig 22 **OXYGEN CONVERTERS** Plants in Existence at end of 197

Name	Location	Type	Number	Capacity per Vessel *Tonnes*
North				
British Steel Corporation				
Consett	Consett	L.D.	2	132
South Teesside	Middlesbrough	L.D.	3	258
Total			5	
Yorkshire and Hmuberside				
British Steel Corporation				
Appleby Frodingham	Scunthorpe	L.D.	3	300
Normanby Park	Scunthorpe	L.D.	2	86
Total			5	
East Midlands				
British Steel Corporation				
Corby	Corby	L.D.	3	134
West Midlands				
British Steel Corporation				
Shelton	Stoke on Trent	Kaldo	2	68
Wales				
British Steel Corporation				
Llanwern	Newport	L.D.	3	182
Port Talbot	Port Talbot	L.D.	2	329
Total			5	
Scotland				
British Steel Corporation				
Ravenscraig	Motherwell	L.D.	3	129
GRAND TOTAL 1977			23	
1976			23	

From B S C annual statistics 1978.(1)

Fig 23 Comparison of the usage of magnesia and doloma raw materials in LD vessel linings in the UK

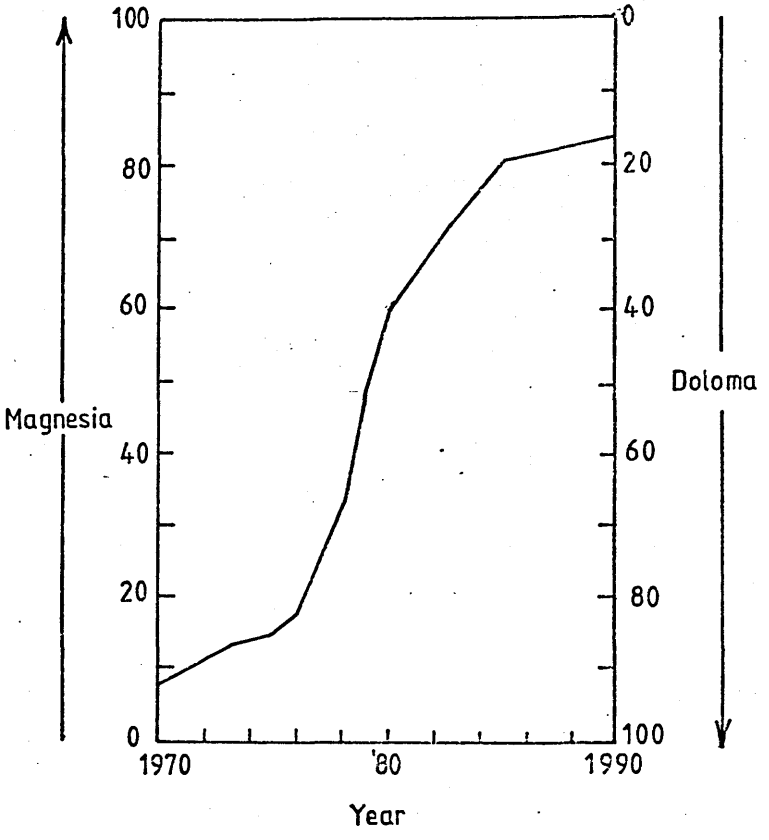

(after Spencer [33])

Fig 24 Refractory and slagmaking cost curves